

**POLARIMETRIC DATA FOR TROPICAL FOREST
MONITORING.
STUDIES AT THE COLOMBIAN AMAZON**

CENTRALE LANDBOUWCATALOGUS



0000 0912 4625

Marcela Quiñones Fernández
Polarimetric data for tropical forest monitoring. Studies at the Colombian Amazon

Doctoral Thesis, Wageningen University – with references – with summaries in English, Spanish, and Dutch.

ISSN: 1383-6811
ISBN: 90-5808-750-6 (thesis edition)
90-5113-061-9 (Tropenbos edition)

©Tropenbos International, 2002

The opinions expressed in this publication are those of the author and do not necessarily reflect the views of Tropenbos International

All rights reserved. No part of this publication, apart from bibliographical data and brief quotations in critical reviews, may be reproduced or published in any form including print, photocopy, microfilm, electronic or electromagnetic record without written permission

Cover: AirSar Image, Scene 336-b of the Araracura study area with three different classified maps. Flooded Map (top right), Structural Type Map (bottom, left) and Biomass Map (bottom right).

Printed by: Ponsen & Looijen, Wageningen, the Netherlands
Distribution: Tropenbos International, Wageningen, the Netherlands

WNO8201, 3297

**Propositions belonging to the thesis:
Polarimetric Data for Tropical Forest Monitoring Studies at the
Colombian Amazon
by: Marcela Quiñones Fernández.**

1. People have the right to get accurate information about the condition of the land, the ocean and the atmosphere in order to make their political choice.
2. The incidence angle effects on the radar return values are too important to be ignored in future studies. (This thesis, Chapter 3)
3. The use of multi-frequency data contributes more to the classification accuracy of tropical forest than multi-temporal or polarimetric observations. (This thesis Chapters 2 and 6).
4. The structure of tropical vegetation is too complex to be described accurately by remote sensing interaction models. (This thesis, Chapter 5)
5. Multi-frequency polarimetric coherence signatures can be physically associated with forest types. (This thesis Chapter 3).
6. Mapping of vegetation structure is required prior to mapping of biomass in the tropics. (This thesis, Chapter 4)
7. I strongly believe that we must consciously develop a greater sense of universal responsibility, which is the best foundation both for our personal happiness, for world peace, the equitable use of our natural resource and the proper care for the environment (H.H. Dalai Lama).
8. We must learn to work not just for our own individual self, family or nation, but for the benefit of all mankind (H.H. Dalai Lama).
9. Scientists are very busy publishing articles to survive the competition rather than addressing the urgent needs of mankind.
10. Dutch people like to eat 'frietjes' as much as Colombian people like to go 'salsa', that is once a week.

7626, 10280NM

ERRATA "Polarimetric Data for Tropical Forest Monitoring. Studies at the Colombian Amazon"

Page 24, line 18. Reference in square brackets should read **Tought *et al*, 1995** instead of 15

Page 26, line 15. Reference in square brackets should read **Press *et al*, 1994** instead of 20.

Page 93, Figure 4.11. Missing forest profile label should read **Ara 13**.

Page 154. Last sentence should be omitted.

1002701.13075

**POLARIMETRIC DATA FOR TROPICAL FOREST
MONITORING.
STUDIES AT THE COLOMBIAN AMAZON**

Marcela Quiñones Fernández

Proefschrift

Ter verkrijging van de graad van doctor

Op gezag van de rector magnificus

Van Wageningen Universiteit

Prof. dr. ir. L. Speelman

In het openbaar te verdedigen

Op maandag 4 november 2002

Des namiddags te 16.00 uur in de Aula, Wageningen

157. 1002701.13075

Promotor: **Prof. dr. ir. R.A. Feddes**
Hoogleraar in de bodemnatuurkunde, agrohydrologie en het
grondwaterbeheer, Wageningen Universiteit.

Co-promotor: **Dr. ir. D.H. Hoekman**
Universitair hoofddocent bij het Departement
Omgevingswetenschappen,
Wageningen Universiteit

Samenstelling promotiecommissie:

Prof. ir. P. Hoogeboom, Microwave Laboratory, Technische
Universiteit, Delft

Prof. dr. A. Cleef, Wageningen Universiteit

Prof. dr. F.J.J. Bongers, Leerstoelgroep Bosteelt en bosecologie,
Wageningen Universiteit

Dr. Y. Hussin, International Institute for Aerospace Survey and
Earth Sciences

**POLARIMETRIC DATA FOR TROPICAL FOREST
MONITORING.
STUDIES AT THE COLOMBIAN AMAZON**

Marcela Quiñones Fernández

Tropenbos International
Wageningen, the Netherlands
2002

TROPENBOS SERIES 21

The Tropenbos Series presents the results of studies and research activities related to the conservation and wise utilisation of forest lands in the humid tropics. The series continues and integrates the former Tropenbos Scientific and Technical Series. The studies published in the series have been carried out within the international Tropenbos programme. Occasionally, this series may present the results of other studies, which contribute to the objectives of the Tropenbos programme. Other publication series published by Tropenbos present results of studies related to specific regions. For a full overview of all Tropenbos publications: www.tropenbos.nl

ISSN 1383-6811

*To the earth,
For standing the impact of our presence,
For maintaining the greenness of the forests
And the creative force of the sea.*

ABSTRACT

Polarimetric Data for Tropical Forest Monitoring. Studies at the Colombian Amazon.

Doctoral Thesis, Wageningen University, The Netherlands.

An urgent need exists for accurate data on the actual tropical forest extent, deforestation, forest structure, regeneration and diversity. The availability of accurate land cover maps and tropical forest type maps, and the possibility to update these maps frequently, is of great importance for the development and success of monitoring systems. For areas like the Amazon the use of optical remote sensing systems as the source of information, is impeded by the permanent presence of clouds that affect the interpretation and the accuracy of the algorithms for classification and map production. The capabilities of radar systems to acquire cloud free images and the penetration of the radar waves into the forest canopy make radar systems suitable for monitoring activities and provide additional and complementary data to optical remote sensing systems. Information regarding forest structure, forest biomass, and vegetation cover and flooding can be associated with radar images because of the typical wave-object interaction properties of the radar systems.

In this thesis new algorithms for the classification of radar images and the production of accurate maps are presented. The production of specific maps is studied by applying the developed algorithms to two different study areas in the Colombian Amazon. The first site, San José del Guaviare, is a colonisation area with active deforestation activities and dynamic land cover change. The second area is a pristine natural forest with high diversity of landscapes.

A detailed statistical description of the polarimetric AirSAR data is made in terms of backscatter (gamma values), polarimetric phase difference and polarimetric correlation. This approach allows a better interpretation of physical backscatter mechanisms important for interpretation of images in relation to ground parameters. Theoretical cumulative probability density distributions (pdf) are used to describe the mean field values and the standard deviation for a class. A Gaussian distribution is used to describe the field average gamma values; a circular Gaussian distribution is used to describe the field average HH-VV phase difference and a Beta distribution is used to describe the field average HH-VV phase correlation. The accuracy of the estimation of the field-averaged values depends on the level of speckle, i.e. number of independent looks. This effect is included in the calculation of the pdf's and therefore can be simulated.

For the Guaviare site the classification algorithm is used to assess the AirSAR data in the production of a land cover type map. Classification accuracies are calculated for different combinations of bands and level of speckle. An accuracy of 98.7% was calculated for a map when combining L-HV and P-RR polarisations. Confusion between classes are studied to evaluate the use of radar bands for monitoring activities, e.g. loss of forest or detection of new deforested areas. In addition a biomass map is created by using the empirical relationship between the combination

of the same radar bands and the biomass estimations from 28 plots as measured in the field. The agreement of the biomass map with the land cover map is used to evaluate the biomass classification.

For the Araracuara site the classification algorithm is used to assess the use of polarimetric data for forest structural type mapping and indirect forest biophysical characterisation. 23 field-measured plots used for forest structural characterisation are used to assess the accuracy of the classification. A new SAR derived legend is more suitable for the SAR map allowing better physical interpretation of results. A method based on iterated conditional modes is introduced to create maps from the classified radar images, increasing in most of the cases the accuracy of the classification. The structural type map with 15 classes can be classified with accuracies ranging from 68% to 94% depending on the classification and the mapping approach. The relationship between forest structure and polarimetric signal properties is studied in detail by using a new decomposition of polarimetric coherence, based on a simple physical description of the wave-object interactions. The accuracy of the complex coherence is described using the complex Wishart distribution. In addition for the same area, a biomass map is created using the previous structural type characterisation as the basis for the classification, overcoming problems as the well know radar signal saturation.

The possibilities and restrictions of creating biomass maps with AirSAR polarimetric images are deeply investigated. Two different approaches are proposed depending on the terrain conditions. A theoretical exploration on the physical limits for radar biomass inversion is made by using a new interface model, called LIFEFORM that describes the layered tropical forest in terms of scatterers. The UTARTCAN scattering model is used to analyse the effect of flooding, forest structure and terrain roughness in the biomass inversion.

FOREWORD

I came to Holland to learn about applications of remote sensing and geographical information systems for forestry. My intention was specifically to learn vegetation mapping for further applications in the Colombian Amazon, territory that is being on my heart since the first time I saw the green immensity from the window of the plane that brought me to the middle Caquetá river in 1985.

My initial works in tropical forest remote sensing interpretation were made as a student of ITC (International Institute for Aerospace Survey and Earth Sciences), where I learned to use optical and aerial photography for vegetation mapping. It didn't take long to realise that image interpretation in this remote sensing images was affected by presence of clouds and therefore incomplete observations and inaccurate classifications were made. The problem was more pronounced in the tropical regions where it was very hard to get cloud free images. For that reason, I started to think about the possibility of learning about radar remote sensing and its applications in the tropical forest. In a coffee break at ITC, I met Wietske Wijker, at that time a Dutch PhD student who was working in the application of ERS-1 radar data for monitoring the Colombian Amazon. She introduced me to Dr. Dirk Hoekman of Wageningen University, who was working as one of NASA's principal investigators for AirSAR polarimetric data, being that my first acquaintance with one of the most complete sets of polarimetric data existing at that time. When I first saw the AirSAR images in 1994, as part of my MSc thesis at ITC, I thought that they were beautiful!, the colours and the texture were revealing the tropical forest as I had never seen before. I could almost "walk" through the images. Immediately lots of questions about their possible use and application arose in my mind and I started to study carefully the principles of radar, so different from the already learned optical systems. My first attempts to understand and use the images are consigned in my MSc thesis. But my work with the images was far from complete.

The understanding of the radar principles allowed me to design an appropriate field methodology that could help me with the interpretation of the images. When I understood a little about them and realised the potential amount of information that they could contain it became a challenge for me to extract as much information as possible, in order to create accurate maps of the Amazon. Of course the job was not easy, because the interpretation, description, classification and mapping of radar images is not a straightforward process. It requires a precise understanding of the physics involved between the interactions of the radar waves and the forest and a complete new terminology in mathematics and physics had to be introduced and learned. My specific contribution to this kind of studies, as presented in this thesis, is precisely to assess polarimetric radar images of the AirSAR system in the production of specific maps for the management of the tropical forest, specifically the Amazon forest.

During this work my expertise over tropical forest structure and ecosystems were complemented by the expertise in physics and efficient computing skills of Dirk Hoekman and Martin Vissers from whom I learned a lot about radar. The co-

ordinated efforts between us, from different disciplines, allowed the development of ideas and products that without joining our expertise could not have been done. At that respect I have to say that a PhD research was more than an interesting job, was to build a bridge between different branches of science, was to promote the use of a common language in the search of one objective, in this case accurate tropical forest mapping.

I hope that this thesis will contribute in fulfilling the information needs, reducing our ignorance about the tropical forest and benefit the conservation and the management of the tropical forest.

ACKNOWLEDGEMENTS

I would like to express my special gratitude to my co-promotor, Dirk H. Hoekman for his permanent advice and for helping me in the development of ideas always enthusiastic and supportive. I feel it was a privilege to count always on his scientific expertise. To my promotor Dr. Prof. Reinder Feddes, for unconditional support, for believing in the quality of my work and for his accurate comments in the final stage of this work. Special thanks to Martin Vissers, for all the time devoted in the development of necessary research tools. The interactive work with him and Dirk Hoekman allowed me to answer most of the questions of this research.

To Dr. Prof. Antoine M. Cleef, for his permanent interest and support in my research even during the most difficult periods. To Dr. Carlos Rodriguez, actual director of TROPENBOS Colombia, for devoting time and resources for the translation and publication of part of this work in Spanish in order to make accessible the new technology in our country. To the Colombian Institute for Amazon Research (SINCHI) and TROPENBOS Colombia, for logistic support during the fieldwork periods.

Without the support of people in the field it would have been impossible for me to acquire the necessary data. Therefore I sincerely like to thank Leonel Martinez, Armando Lucena, Marco Aurelio Grajales, Anibal Matapi and Elisa Payeu for hard working hours in the field, which for me was also time to discover the beauty of the Amazon forest.

To the Nuffic Huygens Fellowship Program which supported my work in the last ten months and to TROPENBOS, The Netherlands for the publication of this thesis.

To Marcela Santamaria, Citlali Lopez, Edwin Keizer, Kasper Kok and Joost Wilms for their friendship and support during hard times and for the conversations over life, environment and science that with no doubt encouraged me to continue with this research. To class-mates, friends and house-mates in Wageningen, for good time and nice dinners, sharing opinions about the world, learning from each others cultures, for the parties, the cooking, the flamenco dance, the Tai-chi and the Dutch lessons, for me very important aspects to develop as a person.

To my father for bringing me to the Amazon when I was a kid, for showing me the beauty of the *Victoria regia* symbol of the amazon magic. To my mother for teaching me how to work hard and enthusiastically for what I believe in. To my grandmother for teaching me to go through life with courage and humour. To my brother and sister for their company and support. To "mi chico" Lorenzo Ganzeveld for his love and long walks in the Dutch forest and for translating the summary in Dutch. To his parents Roel and Klaas for making my time in the Netherlands very special, feeling like at home, understanding and helping me to overcome the differences between our cultures

Thanks to all.

LIST OF FREQUENTLY USED SYMBOLS

SYMBOL	UNIT	DESCRIPTION
$C(..)$	-	circular Gaussian distribution
E_h	$V\ m^{-1}$	horizontal component of electric field strength
E_v	$V\ m^{-1}$	vertical component of electric field strength
f_1	-	relative strength of the vegetation layer
f_2	-	relative strength of the ground surface
f_3	-	relative strength of the trunk-ground interaction component
\hat{K}	-	Kappa statistic
$li_{i,c}$	-	likelihood of a pixel i belonging to class c
$mli_{i,c}$	-	ICM modified likelihood of a pixel i belonging to class c
N	-	number of radar looks
$N(..)$	-	normal or Gaussian distribution
$P_\gamma(..)$	-	marginal distribution for intensity
$P_\phi(..)$	-	marginal distribution for polarimetric (HH-VV) phase difference
$P_{ \rho }(..)$	-	marginal distribution for coherence magnitude
S_{hh}	-	scattering matrix element for HH polarization
$u_{i,c}$	-	number of neighboring pixels of pixel i having class c
P_c	-	relative occurrence of class c
$R_{i,c}$	-	relief factor for pixel i and class c
S	-	scattering matrix
$T_{i,c}$	-	texture factor for pixel i and class c
Tm_c	-	mean of the textural coefficient of variation for class c
Tv_c	-	variance of the textural coefficient of variation for class c

r_1	-	HHVV coherence magnitude of the vegetation layer
r_2	-	HHVV coherence magnitude of the ground surface
r_3	-	HHVV coherence magnitude of the trunk-ground interaction component
α	m^{-1}	complex attenuation factor for HHVV coherence magnitude
$ \alpha $	m^{-1}	magnitude of complex attenuation factor ($\alpha = \alpha \exp(i\phi_\alpha)$)
γ	$m^2 m^{-2}$	differential radar cross section per unit projected area ($\gamma = \sigma^0 / \cos(\theta_i)$)
γ_i	$m^2 m^{-2}$	differential radar cross section per unit projected area for field i
$\Delta \hat{K}$	-	test statistic
θ_i	°	incidence angle
$ \rho $	-	polarimetric coherence magnitude or polarimetric correlation
$ \rho_i $	-	polarimetric coherence magnitude for field i
σ^0	$m^2 m^{-2}$	differential radar cross section
$\hat{\sigma}_\infty^2 [\hat{K}]$	-	large sample variance of \hat{K}
ϕ	°	polarimetric (HH-VV) phase difference
ϕ_α	°	phase shift caused by propagation through the vegetation layer
ϕ_i	°	polarimetric (HH-VV) phase difference for field i
ϕ_1	°	HHVV coherence phase of the vegetation layer
ϕ_2	°	phase of the HHVV coherence of the ground surface
ϕ_3	°	phase of the HHVV coherence of the trunk-ground interaction component

TABLE OF CONTENTS

ABSTRACT	ix
FOREWORD	xi
ACKNOWLEDGEMENTS	xiii
LIST OF FREQUENTLY USED SYMBOLS	xv
1. INTRODUCTION	1
1.1 PROBLEM DEFINITION	1
1.2 BASIC INFORMATION OVER RADAR SYSTEMS	4
1.3 REVIEW ON THE USE OF RADAR IN TROPICAL FOREST STUDIES	6
1.4 OBJECTIVES	8
1.4.1 General	8
1.4.2 Technical Aspects	8
1.4.3 Regarding Applications	9
1.5 AirSAR DATA ACQUISITION AND STUDY SITES	10
1.6 NEW DEVELOPMENTS INTRODUCED IN THIS THESIS	12
1.7 OUTLINE OF THIS THESIS	13
2. LAND COVER TYPE AND BIOMASS CLASSIFICATION USING AirSAR DATA FOR EVALUATION OF MONITORING SCENARIOS IN THE COLOMBIAN AMAZON	
2.1 INTRODUCTION	17
2.2 BRIEF DESCRIPTION OF THE GUAVIARE TEST SITE	18
2.3 DATABASE	19
2.4 APPROACH	21
2.4.1 Variation with incidence angle	21
2.4.2 Statistical description of data	21
2.4.3 Simulation of pixel classification	25
2.5 RESULTS	27
2.5.1 Land cover type classification	27
2.5.2 Biomass classes	30
2.5.3 Comparison with other results	32
2.6 APPLICATION OF RESULTS	33
2.7 CONCLUSIONS AND RECOMMENDATIONS	36
3. BIOPHYSICAL FOREST TYPE CHARACTERIZATION IN THE COLOMBIAN AMAZON BY AIRBORNE POLARIMETRIC SAR	
3.1 INTRODUCTION	41
3.2 TEST SITE DESCRIPTION	43
3.3 RADAR EXPERIMENT	44
3.4 FIELDWORK AND LEGEND	47
3.5 CLASSIFICATION SIMULATION	51
3.6 IMAGE CLASSIFICATION, VALIDATION AND AGGREGATION	52

3.7	POLARIMETRIC MODELLING	57
3.8	CONCLUSIONS	65
4.	BIOMASS MAPPING USING BIOPHYSICAL VEGETATION CHARACTERIZATION DERIVED FROM SAR IMAGES. EXPERIMENTAL ANALYSIS IN THE COLOMBIAN AMAZON	
4.1.	INTRODUCTION	69
4.2.	BRIEF DESCRIPTION OF TEST SITES	70
4.3.	DATA BASE	71
4.4.	APPROACH	72
4.5.	RESULTS	77
4.5.1	Direct approach using empirical relationship with backscatter	77
4.5.2	Indirect approach using forest structural type classification	82
4.5.3	Field data analysis	86
4.6.	CONCLUSIONS AND RECOMMENDATIONS	92
5.	THEORETICAL EXPLORATION OF PHYSICAL LIMITS FOR RADAR BIOMASS INVERSION	
5.1.	INTRODUCTION	97
5.2.	APPROACH	98
5.2.1	The UTARTCAN Backscatter Model	98
5.2.2	Field data for model validation	100
5.2.3	The LIFEFORM interface model	103
5.2.4	Biomass inversion algorithm	105
5.3.	UTARTCAN VALIDATION	105
5.4.	HYPOTHETICAL FOREST PLOTS	110
5.5.	RESULTS	111
5.5.1	Effect of tree density	111
5.5.2	Effect of soil surface roughness and moisture	116
5.5.3	Effect of DBH	119
5.5.4	Effect of layering	119
5.5.5	Theoretical inversion results	121
5.6.	CONCLUSIONS AND RECOMMENDATIONS	122
6.	ASSESSMENT OF SUITABLE RADAR PARAMETERS FOR TROPICAL FOREST MAPPING APPLICATIONS.	
6.1	INTRODUCTION	127
6.2	STUDY AREA	129
6.3	DATABASE AND APPROACH	131
6.4.	RESULTS	132
6.4.1	Maps and Legend	132
6.4.2.	Simulation of map accuracy for different band and polarisation combinations.	135
6.5	CONCLUSIONS	138
7.	GENERAL DISCUSSION AND RECOMMENDATIONS	
7.1	TECHNICAL DEVELOPMENTS	143
7.1.1	New developed classification algorithms	143

7.1.2	New decomposition of polarimetric radar coherent elements in relation with forest structure	145
7.1.3	Assessment of scattering models as tool for inversion	146
7.1.4	New mapping techniques	147
7.2	APPLICATIONS	147
7.2.1.	Monitoring system	147
7.2.2.	Land cover map	148
7.2.3.	Structural type map	149
7.2.4	Flooding map and forest type map	151
7.2.5.	Biomass map	152
7.3.	AN IDEAL SYSTEM FOR TROPICAL FOREST MONITORING?	153
7.4.	FUTURE CAMPAINGNS?	154
	SUMMARY	163
	RESUMEN	167
	SAMENVATTING	173
	CURRICULUM VITAE	179
	COLOUR PLATES	183

1. INTRODUCTION

1.1 PROBLEM DEFINITION

Tropical rain forests cover, nowadays, six percent of the earth land surface (8.5 million square kilometres) which is just over half of the cover existing not long ago (14 million square kilometres). The deforestation rate in the last few years is been calculated at around 142.000 square kilometres per year [FAO, 2001]. The rapid decrease of the tropical cover into secondary forest or pastures or into degraded forest is of great concern for environmentalist, for the countries and for the local inhabitants. The great extensions of tropical forest with high diversity of soils, landscapes, niches and biological species attacks the attention not only of naturalists, but also of logging and mining companies which extract resources, changing the cover and the soils forever.

The tropical forest is an integral part of the Earth's life support system and plays an important role in the regulation of climate, hydrological and carbon cycles and in the maintenance and conservation of tropical soils. The rain forest with complex root and canopy structures is able to regulate water supplies and to regulate local and global climate. In addition, tropical rain forests are among the Earth's most complex ecosystems and have large bio-diversity. The functioning of this ecosystem and the significance of its genetic resources are still not well understood. In terms of bio-diversity Latin America is perhaps the richest region in the world followed by Southeast Asia. For instance Colombia possesses an estimate of 25.000 plant species, which is the same number found in Southeast Asia in an area four times larger than the Colombian territory [Beazley, 1995]. The ecosystem is the result of the complex interactions of species occurring in different densities, creating a delicate balance that once broken can lead to extinction of many of the living links. Another important characteristic of the tropical rain forests is the large economic value as a major source of timber and non-timber products, and as a source of land. Large areas are converted into forest plantations, arable land and pastures or are part of transmigration programs of the tropical countries. In addition illegal and legal logging activities are far from being controlled despite the efforts of international agreements and environmental politics.

The Amazon is the greatest extension of tropical forest existing on earth. Covering more than one third of the South American region (six million square kilometres) is crossed by the Amazon river with more than 1000 tributaries holding more than one fifth of the earth's fresh water. It is more than an immense tropical forest. It is a living entity that interacts with the atmosphere and has a very important role in the water and carbon cycles of the region. We know so little about the complex interactions going on in that immense biophysical net, that much more energy must be placed into the understanding of those processes and their relevance on global climate. In addition we know that at local and regional level the proper management of the Amazonian forest will assure the maintenance of the bio-diversity, of fresh

water supplies and of timber and non-timber forest products. The proper management of the area is of great importance in the economy of many local communities and in the economy and development of the Amazonian countries.

Each Amazonian country faces different problems but in general all countries face colonisation-settlement processes accompanied by unsupervised cattle ranching and agricultural activities, in many cases of illegal crops. In the Colombian Amazon an annual deforestation rate of about 6000 km² per year has been calculated, especially in the forest near to the Andes mountains, in general as a consequence of the increasing agriculture for illegal crops followed by extensive cattle ranching. Important world natural treasures like the Macarena Mountains or the Andean-Amazonian forest at the foot slopes of the Andes are in permanent threat. The rapid change of forested lands into pastures and later into bare degraded soils is changing the ecosystems and loosing unspeakable biological resources that will be gone forever. Before we will understand the relevance and richness of the Amazon territories, it will be destroyed for the short-term profit of few, loosing the social benefits for the humanity and the balance of the earth ecosystems, forever. At present the conservation of pristine areas is happening only in the few Amazonian Natural Parks and hopefully will represent the vast bio-diversity in that land.

Ignorance, over the land and the ecosystems, is one of the important causes for the bad management and mistreating of the forest, allowing people and governments to take sometimes very imprecise decisions. Areas so extensive and poorly accessible like the Amazon basin seem to be remote and inhabited for people at the central governments. They see that vastness as empty territories full of resources that can be the short-term solution for social problems like poverty and unequal land ownership that affects great part of the so called 'third world' countries. A direct consequence of these problems is the lack of agricultural land for great part of the population forcing people to move and colonise the forest, using, in most of the cases, inappropriate and unsustainable techniques that destroy the ecosystems forever. Once the trees have been cut down and the soil has been eroded there is little chance that the forest will regenerate satisfactory. Instead degradation processes start which are the beginning of extensive ranching activities that end up in desertification processes.

In addition the increasing demand for tropical timber and the intensive demand for beef cattle, by industrialised countries, puts a lot of pressure and force the tropical countries to overexploit their natural resources in order to pay the increasing international debts. If countries, governments and local entities get more conscious of the importance of the tropical forest ecosystem and get to know more about its effect on global climate processes, diversity and fragility, perhaps in common accordance with the actual inhabitants, they will reach levels of understanding and make proper decisions over the management.

The lack of accurate updated spatial information over the extended territories is a cause for misinterpretation and bad management. Maps, if available, are usually two or three decades out of date and large changes in the land cover can hardly be detected on time. The permanent availability of spatial information regarding ecosystem distribution, bio-diversity distribution, seasonal flooding, areas of deforestation, areas of regeneration, extension of grassland boundaries, penetration roads, and mining activities for instance, can help in the development of management plans and can help the enforcement of laws and regulation over the forest. The importance of the establishment of monitoring systems at regional or national level could help the governments to take more rational and adequate actions and decisions over the ecosystems.

Due to the actual deforestation and degradation occurring in the tropical forest, accurate updated data on the complexity, extent, and cover changes occurring is needed for several purposes:

- 1) As an input for climate and water balance studies and modelling.
- 2) For selection and monitoring of forest reserves and of environmentally sensitive areas, the latter related to mining and selective logging activities in areas under sustainable management.
- 3) In new settlement or colonisation areas data on land cover (change) and land degradation processes are needed for land use planning and development of sustainable land use management.

Hence, an urgent need exists for accurate data on the actual tropical forest extent, deforestation, forest structure, regeneration and diversity. The availability of accurate land cover maps and tropical forest types, and the possibility to update these maps frequently, is of great importance The development and success of monitoring systems will depend in great part on the accuracy and temporal resolution of the produced maps. For areas like the Amazon the use of optical remote sensing systems as the source of information is impeded by the permanent presence of clouds, which affect the interpretation and the accuracy of the algorithms for classification and map production. In recent years much research focused on the use of Synthetic Aperture Radar (SAR) to study tropical rain forest has been done. The capabilities of radar systems to acquire cloud free images and the penetration of the radar waves into the forest canopy make radar systems suitable for monitoring activities and provide additional and complementary data to optical remote sensing systems. Information regarding forest structure, forest biomass, vegetation cover and flooding can be associated with radar images because of the typical wave-object interaction properties of the radar systems.

In this thesis new algorithms for the classification of radar images and the production of accurate maps are presented. The production of specific maps is studied by applying the developed algorithms to two different study areas in the Colombian Amazon. The first one is the area of San José del Guaviare, located at the boundary between the natural savannas and the Colombian Amazon.

Colonisation processes had occurred in the area since the late 50's and changes in the land cover are very dynamic. The encroaching into the forestland is being promoted by the increasing cultivation of illegal crops followed by extensive ranching. The second area corresponds to a 'pristine' natural forest located in the middle Caquetá river, inhabited by indigenous tribes that since recent times have the legal control over their lands. The diversity of landscapes in this area makes it a very interesting one to study the variety of ecosystems possibly occurring in the Colombian Amazon.

1.2 BASIC INFORMATION OVER RADAR SYSTEMS

Radar is an active remote sensing system that transmits its own electromagnetic wave signal in a narrow beam in a direction of interest. Objects occurring in the area illuminated by the radar, depending on their size, shape and orientation relative to the wavelength and look direction of the beam, interact with the wave and produce multiple reflections, changing the properties of the incidence wave. Part of the incident energy, after interaction with the objects, returns to the system (backscattered waves) and is recorded. In that case the object of interaction is said to be detected. Table 1.1. shows technical specifications of the transmitted radio waves.

Table 1.1: Radar bands for earth observation with corresponding wavelength and frequency.

Band denomination	Wavelength (cm)	Frequency (Hz)
X	3.0	10 GHz
C	5.6	5.3 GHz
L	24	1.25 GHz
P	65	440 MHz

A system can transmit and record single polarisation or can be a polarimetric system. Single polarised systems transmit and receive vertically (V) or horizontally (H) polarised electromagnetic energy and record the amplitude of the corresponding polarised component. Transmitted and received waves can be of the same or different type and then are referred to as a like or as a cross-polarised system. Conventionally a radar system transmitting V-polarisation and receiving H-polarisation will be noted as radar with HV polarisation. Polarimetric radar systems transmit both H- and V- polarised waves and record the amplitude as well as the phase of the received H- and V- polarised component.

As expected the resulting SAR data files are large sets of raw data, therefore special compact formats must be designed to transfer the information to the users. For instance the Jet Propulsion Laboratory (JPL) of NASA processes the polarimetric images in the so-called Stokes matrix format. Polarimetric properties of targets can be described in terms of parameters (or extractions) from the elements of that matrix. These parameters can be of two types. The incoherent parameters (power or

intensity measurements) and the coherent parameters (those that require information on the phase [Boerner *et al.*, 1998]).

The capacity of isolated objects to reflect radar waves is expressed by an incoherent parameter known as the radar cross section (σ), which is a function of the radar wavelength and the object characteristics (size, shape, orientation and composition). For distributed objects (i.e. land surface), σ depends on the resolution cell, larger cells may give more backscattered power. The parameter that describes the reflectivity of homogeneous land areas independent of the area of resolution is called the 'differential radar cross section' (σ^0). An associated measure is the 'radar cross section per unit projected area' (γ). These are known as the intensity parameters [Hoekman, 1990].

The descriptions of the coherent parameters include information contained in the relative phase of the scattering matrix elements and in the correlation between the elements. A commonly used parameter is the complex co-polarised correlation coefficient (ρ_{HH-VV}) from which two parameters can be derived: the coherence magnitude and the polarimetric phase difference. Detailed descriptions can be found in [Boerner *et al.*, 1998].

Another important technical inherent characteristic of a radar system is the image speckle. Speckle is the result of the coherent illumination (transmission of electromagnetic waves with the same frequency and phase) of the SAR systems. Speckle gives the images the so-called 'salt and pepper' or 'grainy' appearance. Speckle is caused by the interference among backscatter waves of the individual scattering elements (scatterers) that are present within one resolution cell. Interference between echoes produced by the scatterers can be constructive or destructive depending on the phase and the amplitude and therefore result in a higher or lower overall backscatter. Speckle obstructs the measurements of a single resolution cell. In order to characterise objects with radar it is important that measurements are accurate estimates of either the mean power or the mean amplitude. The measurement of a single resolution cell is called a look. The accuracy of the radar measurements can be improved by the linear averaging of measurements corresponding to cells adjoining in the azimuth direction (direction of flight). An image with averaged adjoining cells is called a multi-look image. In general it can be said that multi-look images have less backscatter fluctuations and therefore the effect of speckle is less evident. The accuracy of the mean amplitude or power estimations will increase with an increase in the number of looks. A large number of looks reduces the fluctuations in the radar measurements and improves the radiometric resolution [Hoekman, 1990; 1991].

The interactions of the radar waves with the objects result in changes in the amplitude and/or phase of the returned waves and may be object specific. Therefore the study of the wave characteristics like power, amplitude and phase is of great importance in the interpretation of the radar images. The processes involved in the interactions of the waves with the object (i.e. forest) are mainly transmission,

reflection (scattering) and absorption. The reflection and the transmission of radar waves into a medium like the forest are repetitive and finite processes since there is a loss of power in the direction of propagation. The amount of power transmitted, reflected and absorbed is a function of the dielectric constant of the objects present in the media. Radar backscatter increases as a function of water content. Backscatter also depends on wave parameters such as wavelength, polarisation, incidence angle and orientation of the objects and on terrain parameters such as soil roughness, soil moisture content and vegetation structure. Within the parameters on the vegetation structure that affect the radar return one can consider the dielectric properties of individual components (i.e. leaves, trunks, branches), orientation distribution, shape, size and density of the individual components and the openness and thickness of the canopy. For more specific information see [Hoekman, 1990; Lillesand and Kiefer, 1994; Van der Sanden, 1997].

Theoretical models describing the interactions of radar waves with the forest have been developed and are still a topic of research. These models consider the effects of general canopy characteristics, and terrain characteristics to predict radar return values. These models describe the forest as a set of continuous horizontal layers and a soil surface and model tree trunks and branches as dielectric cylinders and the needles and leaves as dielectric ellipsoids or discs. In this models the scattering behaviour of the waves is decomposed according to wave object interaction models. The most common interaction processes, according to [Ulaby *et al.*, 1990], are:

- 1) Surface and volume scattering from the forest canopy.
- 2) Surface scattering from the ground.
- 3) Surface scattering from the tree trunks.
- 4) Trunk to ground and ground to trunk interactions (double bounce) and
- 5) Ground to crown and crown to ground interactions.

Different types of models have been developed and validated using SAR data collected in different locations. But because of the high degree of complexity in the interaction, inversion of scattering models for estimations or predictions of specific forest parameters, such as biomass, is still not possible. Nevertheless models are interesting tools to enhance the understanding of the complex interactions occurring between the forest and the radar waves. A complete review on radar models can be found in [Simonett *et al.*, 1987; Richards, 1990]. Example of scattering models are e.g. the Michigan Microwave Canopy Scattering model (MIMICS) [Ulaby *et al.*, 1990] and the University of Texas at Arlington Radiative Transfer CANopy model (UTARTCAN) [Karam *et al.*, 1992].

1.3 REVIEW ON THE USE OF RADAR IN TROPICAL FOREST STUDIES

Many studies have assessed the use of different systems for diverse applications for tropical forest management. A review on the use of radar for ecological applications presents specific algorithms and classification procedures for land cover

classification, measuring above ground biomass and delineation of wetlands and flooding, is given by [Kasischke, *et al.*, 1997]. A detailed analysis of radar data to support tropical forest management in the Guyana forest, using polarimetric and textural information to assess images for specific information requirements at global, national and local scales is given by [Van der Sanden, 1997].

At continental scale, mosaics of tropical rain forests have been recently created using JERS-1 SAR images [De Grandi *et al.*, 1999; Siqueira *et al.*, 2000; Rosenqvist *et al.*, 2000]. At a larger scale researchers have focused their studies on the development of inversion algorithms, segmentation and classification techniques for polarimetric and interferometric SAR images and created a variety of types of tropical rain forest maps [Oliver, 2000; Hoekman and Quiñones, 2000; Hoekman and Varekamp, 2001; Varekamp and Hoekman, 2001]. In addition new models for the decomposition of polarimetric signals of forest vegetation were developed [Freeman and Durden, 1998]. An overview of decomposition theories was presented by [Cloude and Portier, 1996].

The use of radar images in the Colombian Amazon date from 1973 when the X-band Synthetic Aperture Radar GEMS (Goodyear Electronic Mapping System) surveyed the extensive territory. The PRORADAM project created for the first time geological, soil and forest type maps, scale 1:500,000 of the Colombian Amazon. The extended legend and maps constituted one of the first sets of information ever available for the Colombian Amazon [PRORADAM, 1979]. In recent years images from the South American Radar Experiment (SAREX-92), the AirSAR South-American deployment, the SIR-C Radar Shuttle Mission, and from the ERS-1 and JERS-1 systems have been taken over the Colombian Amazon. A systematic study on the use of ERS radar data for implementing a monitoring system shows that ERS data can be used to detect changes on vegetation cover types and to some extent mapping land cover types. Classification accuracies obtained in that study range from 40% for secondary vegetation to 80-90 % for pastures [Bijker, 1997].

At present, spaceborne SAR systems of different bands and polarisations like ERS-1 (C-VV), ERS-2 (C-VV), JERS-1 (L-HH) and RADARSAT (C-HH) have been successfully deployed and have taken images over the globe. New additional satellite systems with new bands and polarisations are being developed and are expected to be operationally very soon like RadarSAT-2 (C-band polarimetric), ALOS-PALSAR (L-band polarimetric) and EnviSAT (C-band multi-polarisation). In addition a P-band satellite is being assessed for applications on biomass mapping and is still under assessment for future systems. Considering that new band and polarisations are entering the picture of the applications and that a large amount of data will be available in the future it is of great interest to continue the development of the radar decomposition and classification algorithms for specific applications.

A multi-frequency polarimetric system like the AirSAR (C-, L- and P-band fully polarimetric), allows the evaluation of radar characteristics. Wavelength parameters, speckle and intrinsic polarimetric characteristics such as the polarimetric phase

difference can be used as experimental data to assess the capabilities of the polarimetric radar for specific applications. In addition a system like AirSAR (with effectively 15 independent channels) is ideal to simulate results as produced by simpler systems.

1.4 OBJECTIVES

In the initial stages of this research existing decomposition algorithms were applied to the images to relate the information to available field data. In general the decomposition algorithms did not reflect all the variation observed in the field especially in the areas of pristine forest. Problems were specially related to the fact that display of decomposed images can not show all the available variation. It was necessary to have a classification algorithm to combine all the information existing in the 15 channels. Speckle was found in the literature as a factor affecting the classification. According to the characteristics of the speckle it is expected to be a relevant factor to consider in a classification algorithm. In addition the comparison of field derived vegetation structure data and the signatures of the polarimetric system was expected to give further insights in the wave-forest interaction models. The application of the developed algorithm to the AirSAR C, L P polarimetric images at two study sites in the Colombian Amazon would allow the assessment of the images for specific applications.

1.4.1 General

- *Assessment of polarimetric C, L and P radar data to create accurate maps for monitoring and resources assessment of tropical rain forest.* In general new and robust decomposition, classification and mapping algorithms for radar systems are needed.

1.4.2 Technical Aspects

- *Development of classification algorithms to classify polarimetric images* The statistical description of polarimetric images in terms of backscatter γ , polarimetric phase difference ϕ , and polarimetric correlation $|\rho|$, allow better interpretation of the images in terms of backscatter physical mechanisms. A new classification algorithm that used the above mentioned polarimetric parameters is expected to combine the information contained in the available C, L and P polarimetric images and allow the maximum differentiation between classes. The effect of the speckle is included in the classification and its effect on the classification accuracy of images can be evaluated.
- *Development of mapping (image processing) algorithms to create maps of natural tropical forest, out of classified polarimetric images.* In radar images the presence of speckle, texture, relief and drainage patterns may have a strong effect on the classification of an image. Including the effect of these parameters in the classification and mapping of the radar images can be one way of

overcoming the negative effects. Previous existing segmentation processes like the one proposed by [Oliver and Quegan, 1998] fail to generate appropriate boundaries in areas of natural tropical forest where transitions between two forest type are not very clear, which is a common natural state in regenerating forest. In addition texture analysis also does not seem to be appropriate in areas where texture is almost homogeneous, being the case of many natural tropical forest areas [Van der Sanden, 1997].

- *Assessment of physical scattering models to explain classification capabilities based on theoretical scattering mechanisms* So far an unsupervised classification of scattering behaviour in radar polarimetric data is being associated with certain vegetation structures [Van Zyl, 1989]. Information contained in the complex coherence has not been completely explored in relation to forest structure. In this study a detailed analysis of the complex coherence elements in relation to forest structural parameters and terrain conditions will be made. Conclusions are expected to bring new insights. The effect of speckle in the accuracy of the complex coherence parameters will also be studied. So far this characteristic has been ignored in the literature.

1.4.3. Regarding Applications

Tentatively, it may be assumed that the AirSAR system may fulfil information needs at a scale of 1:50,000. The usefulness of certain combinations of frequency bands and polarisation, polarimetry, the effect of incidence angle θ_i and the effect of speckle have to be evaluated for different types of information needs. Though spaceborne SAR may well be capable of providing relevant information in the near future, it is not yet clear how such a SAR should be designed in terms of, for example, wave parameters and resolutions. Clearly the optimal design will depend on specific priorities in information needs. AirSAR images acquired over two study sites at the Colombian Amazon were used to test the developed algorithms for different types of applications.

- *Application of developed algorithms for land cover types mapping and cover change monitoring.* For the colonisation area of San José del Guaviare the classification algorithms differentiate four land cover classes. Classification accuracies using field observed plots are used to assess the performance of the algorithm.
- *Application of developed algorithms to map forest structural types, forest types and flooding conditions. Study the relation between forest structure and radar signals.* For the pristine tropical forest area of Araracuara where there is a high diversity of forest types, the existing landscape ecological map [Duivenvoorden and Lips, 1991] is used for interpretation and study of radar images. Algorithms are tested in order to generate forest type and forest structural maps (units combining flooding, soil and forest structure). The capabilities of the radar can also be assessed to distinguish flooded areas from non-flooded areas. Field measured plots are used to assess the performance of the classification.

- *Application of developed algorithms for biomass classes mapping* Direct inversion of radar data for biomass estimations is restricted to certain biomass levels due to saturation problems and is affected by terrain conditions and forest structure [Imhof, 1995]. In this thesis the effect of forest structure on the relationship between radar values and biomass is studied. Radar data corresponding to field-measured plots of different forest structure and terrain condition are analysed. For a systematic analysis of the effect of terrain conditions (flooding and terrain roughness) and forest structure on biomass estimations, use is made of the existing UTARTCAN (radiative transfer) scattering model [Karam *et al.*, 1992]. Results are expected to give alternatives for accurate biomass mapping.
- *Assessment of existing radar spaceborne systems for specific applications and generation of insights on system characteristics required for the design of new SAR system according to information needs.* The need to develop new dedicated spaceborne SAR systems will not be very high when sensors already planned for new spaceborne SAR missions, such as the C-band ASAR on ENVISAT, RADARSAT-2 or the polarimetric L-band 'ALOS PALSAR', can satisfy the information needs cost-effectively.
- *Evaluation of the performance of P-band.* The use of P-band SAR has been proposed for its supposedly superior capabilities for biomass assessment and deforestation mapping. Most study results to date indicate P-band's capability, notably the HV-polarisation, to estimate biomass levels up to 150-200 ton/ha (Le Toan *et al.*, 1992, Ranson and Sun, 1994; Kasischke *et al.*, 1995; Dobson *et al.*, 1992; Ranson and Sun, 1997). By combining P-band data with L- and/or C-band data even higher biomass levels may be reached for certain forests. The capabilities of P-band can also be evaluated for other applications considered in this study.

1.5. AirSAR DATA ACQUISITION AND STUDY SITES

In the period of 25 May until 17 June 1993 NASA executed an airborne radar data acquisition campaign in Central- and South-America with the AIRSAR system. This campaign was named the "AIRSAR South American Deployment". The AIRSAR is a C-, L- and P-band fully polarimetric system. It is operated from the NASA/Ames DC-8 aircraft at an altitude of roughly 8000 m. More detailed system specifications can be found in literature (e.g.: van Zyl *et al.*, 1992). The main objectives of the AIRSAR deployment were, as in previous campaigns, the support of scientific research and, in particular, coverage of SIR-C/X-SAR sites.

The campaign was executed in a large number of countries. In the original plan Brazil was included, however, necessary clearances could not be obtained in time. Since no data could be acquired over Brazil then the study sites of the TROPENBOS foundations in Colombia and Guyana were the only ones to represent the tropical rain forest of the Amazon basin. The present study makes use of the two selected

areas in the Colombian Amazon. Radar studies on the Guyana site can be found in previous research [Van der Sanden, 1997].

Out of 7 recorded tracks in the Colombian Amazon, five AirSAR images [Van Zyl *et al.*, 1992] have been processed for each of the study sites. Scenes from three tracks were selected for processing. Table 1.2 shows the specific information over the tracks and the processed frames. The data were processed on the JPL frame processor version 3.56, which includes absolute calibration. The image frames were received in a 16-look compressed Stokes matrix format. Pixel spacing of the imagery is 6.66 m in range and around 8.20 m in azimuth. The incidence angle varies from about 20° to 60° . It is noted that the data quality and in particular the absolute calibration were not in accordance with well calibrated data. As an example of these problems backscatter levels for tropical rain forests in C-band with VV-polarisation are in the range of -3 to -5 dB for AirSAR, while the ERS-1 windscatterometer, a well-calibrated instrument, shows a very stable level in the range of -8 to -9 dB for Amazonian rain forests for this incidence angle range [Wismann *et al.*, 1996].

The first study site is San José del Guaviare, a colonisation area in the northern border of the Colombian Amazon forest with the natural savannahs (2.5° N, 72.5°W), south of the Guaviare river. In this area the natural cover is a mosaic of tropical forest of intermediate biomass and natural edaphic savannahs. Continuous changes in the vegetation cover occur due to the colonisation process and to the increase in agricultural activities and extensive cattle ranching. Natural forest also suffers from degradation and decrease in standing biomass due to selective cutting activities. A more detailed description of the processes occurring in the area can be found in Chapter 2.

The second study site corresponds to a pristine natural forest in the middle Caquetá river (0°40'S, 72°15'W). It is a region of high landscape diversity and therefore very rich in terms of species bio-diversity. In this area the forest is in relatively good condition with only few human activities mainly in areas near the river where traditional local indigenous communities practise shifting cultivation. Extensive description of the study area can be found in Chapter 3.

In both study areas detailed field observations were made For the area of Guaviare field observations on vegetation and terrain characteristics were made at 123 locations in the AirSAR images. With the help of the land cover map, aerial photography acquired in 1990, airborne radar data acquired during the SAREX campaign of ESA in 1992 [Hoekman and Van der Sanden, 1994; Wooding and Attema, 1994] and terrain knowledge, a total of 778 areas of at least 50 pixels could be delineated, covering the four main land cover classes. In addition detailed measurements of structural and physiognomic characteristics were made for 13 plots of primary forest and 10 plots of secondary forest, each 1,000 m² in size.

Table 1.2 Overview of AirSAR recorded tracks in the Colombian Amazon, dates of acquisition and processed images.

Flight date	Run name	HDDC number	Location	Processed frames
31may93	SJ-Guaviare-123-1	93018/3	Guaviare	
31may93	SJ-Guaviare-303-1	93018/3	Guaviare	303-1(A) 303-1(B) 303-1(C) 303-1(D) 303-1(E)
31may93	SJ-Guaviare-123-2	93018/3	Guaviare	
31may93	Araracuara-156-1	93018/3	Araracuara	
31may93	Araracuara-336-1	93018/3	Araracuara	336-1(A) 336-1(B) 336-1(C) 336-1(D)
31may93	Araracuara-048-1	93018/3	Araracuara	048-1(A)
31may93	Araracuara-228-1	93018/3	Araracuara	

For the area of Araracuara the fieldwork was designed to capture the variation found in the landscape ecological map, existing for the area [Duivenvoorden and Lips, 1991], as well as in the radar data. Consequently, selected plot locations cover a wide range of forest structure and flooding conditions. Detailed field observations were made at 23 plots in the 27°-60° incidence angle range. With the help of the landscape ecological map, aerial photography acquired in 1987 and terrain knowledge, a total of 878 additional areas could be delineated, representing 15 classes. These well represent all main forest types and the variation in flooding, drainage and soil characteristics in a 24°-61° range of incidence angles. Detailed measurements of structural and physiognomic characteristics were made at 23 plots of primary forest, each 1,000 m² in size, using the same methodology as for the Guaviare site. A detailed description of that methodology can be found in Chapter 5.

A database of averaged Stokes scattering elements was created from the radar data extractions from delineated areas over specific land cover and forest types classes. These areas can be grouped according the legend of the map to be produced.

1.6 NEW DEVELOPMENTS INTRODUCED IN THIS THESIS

In this thesis a new fully polarimetric multi-band approach for classification is introduced. The method introduces probability density functions (pdf) for multi-look samples of a certain class, for intensity, phase difference as well as coherence magnitude. The effect of speckle is introduced in the simulated classification by using the field averaged values and random derived samples from the theoretical distributions, increasing the number of samples to be classified and resulting in wider distributions. The Kolmogorov-Smirnov tests of fit can be used to test the deviations from the model of the new speckle included distributions. The likelihood

classification of an observation to be classified as a certain class is the product of the joint Gaussian distributions of the backscatter multiplied by the likelihood of the phase difference values and the likelihood of the correlation values. The confusion matrix, the overall classification accuracy and the confusion between pairs of classes can be calculated for each simulated classification. The evaluation of the simulated classifications is discussed in the context of the appropriateness of certain mission characteristics to meet current or foreseen information needs, considering the presently operational and proposed satellite radar systems.

A new approach is proposed to interpret multi-frequency complex coherence numbers, how to link it with concepts of scattering mechanisms, physical backscatter models and number of independent samples.

Problems related to radar data, such as speckle, texture and relief have to be considered in the radar classification and mapping. *A new method based on iterated conditional modes (ICM) [Besag, 1986] is introduced to yield radar-derived maps* The software developed to classify and create maps allows the user to change and adapt these variables according to the type of application and the system characteristics.

The above mentioned new techniques are used in this thesis to assess the AirSAR images for different kinds of applications. The 15 channels of the polarimetric C-, L- and P-band AirSAR images are used to assess the performance of different bands and polarisation combinations for the different applications. The calculation of the accuracy of the maps is considered of great importance for the establishment of a monitoring system. Each classification or map should be accompanied by an accuracy calculation in order to give a range of confidence, not only for scientific reasons but also for political and economical purposes. Global agreements like the Kyoto Protocol can benefit from accurate calculations or at least from results that can be handled with a certain level of accuracy.

In this study four different types of maps are considered of importance for integrating in a monitoring system of the tropical forest A vegetation cover map, a flooding map, a forest structural map and a biomass map. Technical considerations and restrictions to create these maps, using radar images, are included.

1.7. OUTLINE OF THIS THESIS

This thesis is a compilation of articles published in, accepted by or submitted to high standard scientific journals. The first two articles contain the technical developments. Application of these developments can be seen in all the papers. Each paper includes a relevant introduction and background, depending on the specific subject and the corresponding conclusions. The different applications are expected to fulfil information needs over the Amazon and be useful for future applications.

In Chapter 2 a detailed description of the polarimetric classification algorithm is presented. A detailed study of the AirSAR images of the Guaviare site is made. Aspects like incidence angle dependence for each radar channel, considering the studied land cover types and the statistical description of the images according to the presented algorithm, are studied. The algorithm is applied to the Guaviare data and assesses the production of a land cover type map. Accuracies for this map are calculated for different combinations of bands and polarisations and different levels of speckle. In addition a biomass map is created by using the empirical relationship between radar values and biomass, and related to the land cover map to assess its accuracy. The section on application of results assesses the different combinations of bands for the distinctive pairs of land cover classes as examples of possible scenarios for land cover monitoring. This paper is already published [Hoekman and Quiñones, 2000]

In Chapter 3, the radar images of the Araracuara site are investigated. Incidence angle dependence of the backscatter parameters are studied for all classes, bands and polarisations. In addition the calculation of accuracies for complex coherence is introduced for different levels of speckle. A SAR derived legend for the structural forest type map is presented and explained in relation to the existing landscape ecological legend available for the area. The polarimetric algorithm is tested in the Araracuara site for the classification of structural types, flooding and forest structure according to the developed legend. Field observations and the available landscape ecological map for the area are used to simulate accuracies of classification. The Iterated Conditional Modes (ICM) method [Besag, 1986] is introduced as a mapping algorithm for radar images. Effects on the accuracy calculations after the application of the ICM method are presented. Also in Chapter 3 a new and complete description of the complex coherence is introduced. The new model describes the multi-frequency complex coherence making links with scattering mechanisms, physical backscatter models and number of independent samples (looks). This paper is already published [Hoekman and Quiñones, 2002].

In Chapter 4 the possibilities and restrictions of creating biomass maps with AirSAR polarimetric images is investigated. Two approaches are proposed depending on the terrain conditions. For the Guaviare site an empirical relationship between biomass and radar data is presented. The second approach uses the already available forest type classification of the Araracuara site for the creation of a biomass map. Accuracies for different combinations of bands and polarisations are calculated for this new approach. The effects of flooding forest structure and biomass level are extensively analysed, using the complex multi-frequency coherence and the backscatter multi-frequency signature. This paper was presented at a conference [Quiñones and Hoekman, 2002a] and submitted [Quiñones and Hoekman, 2002b].

In Chapter 5 a theoretical and systematic study of the effects of flooding, terrain roughness and forest structure on biomass estimations is done using a scattering model (UTARTCAN). In order to evaluate the performance of the multi-layer

scattering model to predict backscatter values over tropical forest, use is made of the experimental data in both study sites. An interface model, called LIFEFORM is introduced for describing the layered tropical forest in terms of scatterers, as input for the UTARTCAN model. The analysis of the field data reveals some of the limitations of the scattering model to simulate radar values for the tropical forest. Nevertheless, despite the restrictions, simulations may still be used to evaluate systematically the effect of terrain conditions in biomass estimates. In order to evaluate the effect of terrain conditions on radar inversion for biomass estimations a theoretical inversion is done using the simulated radar data, including the effect of speckle. This paper is submitted [Quiñones and Hoekman, 2002c].

In Chapter 6, a comparison between the SAR derived map and existing maps for the Araracuara area is made. Accuracies for the forest structural, forest type and flooding maps are presented for different levels of speckle when using fully polarimetric data. Also data is presented before and after the application of the ICM method. In addition accuracies of the mentioned maps are presented for different bands and combinations of bands according to existing or coming radar systems. The effect of P-band is specially analysed.

In Chapter 7 a summary of the thesis and general conclusions on the use of polarimetric radar for tropical forest classification and mapping are presented.

2. LAND COVER TYPE AND BIOMASS CLASSIFICATION USING AirSAR DATA FOR EVALUATION OF MONITORING SCENARIOS IN THE COLOMBIAN AMAZON.

2.1. INTRODUCTION

Tropical rain forests cover large parts of the Earth's land surface. The significance of these forests, and the need for information, can be seen from several perspectives:

- (a) Tropical rain forests play an essential role in global hydrological, biochemical and energy cycles and, thus, in the Earth's climate;
- (b) Tropical rain forests are among the Earth's most complex ecosystems and have large biodiversity. The functioning of this ecosystem and the significance of its genetic resources are still not well understood;
- (c) Tropical rain forests are of large economic value as a major source of timber and other products, and as a source of land. Large areas are converted into forest plantations, arable land and pastures.

An urgent need exists for accurate data on the actual forest extent, deforestation, forest structure and composition. These data serve several purposes. They are needed as input for climate studies, for selection and monitoring of forest reserves (with or without sustainable use) and monitoring of environmentally sensitive areas, the latter related to mining and selective logging activities in areas under sustainable management. In new settlement or colonisation areas data on land cover (change) and land degradation processes are needed for land use planning and development of sustainable land use management. Hence, the availability of accurate land cover maps, and the possibility to update these maps frequently, is of great importance.

In this paper an attempt is made to assess the potential role of a spaceborne SAR component within a dedicated global forest monitoring system [Hoekman, 1997], by analysing experimental data from NASA's AirSAR airborne radar. Making an assessment of specific information needs that can be fulfilled by such a system is not a straightforward procedure in a period of time where the relevant technologies are advancing fast and new policies for sustainable forest management and nature conservation are under development. Tentatively, it may be assumed that, at map scales of 1:100,000 and smaller, accurate and up-to-date maps are required to fulfil several types of information needs. Processes of deforestation, conversion of forests to other types of land cover, secondary forest extent and land degradation will be some of the important types of land cover dynamics under consideration. Though spaceborne SAR may well be capable of providing relevant information in the near future, it is not yet clear how such a SAR should be designed in terms of, for example, wave parameters and resolutions. Clearly the optimal design will depend on specific priorities in information needs. On the other hand, the need to develop new dedicated spaceborne SAR systems will not be very high when sensors already planned for new spaceborne SAR missions, such as the C-band ASAR on

ENVISAT, RADARSAT-2 or the proposed polarimetric L-band 'LightSAR' of NASA, can satisfy the information needs cost-effectively. The use of P-band SAR has been proposed for its supposedly superior capabilities for biomass assessment and deforestation mapping. Most study results to date relate to temperate forests and indicate P-band's capability, notably the HV-polarisation, to estimate biomass levels up to 150-200 ton/ha [Le Toan *et al.*, 1992, Dobson *et al.*, 1992, Ranson and Sun, 1994, Kasischke *et al.*, 1995, Ranson and Sun, 1997]. By combining P-band data with L- and/or C-band data even higher biomass levels may be reached for certain forest types [Ranson and Sun, 1994, Kasischke *et al.*, 1995]. For tropical forests far less studies have been conducted. Imhoff [Imhoff, 1995], studied broadleaf evergreen forests in Hawaii and temperate coniferous forests and indicates saturation levels for biomass, for both types of forests, of 100 ton/ha in P-band and 40 ton/ha in L-band. Rignot *et al.* [Rignot *et al.*, 1995] conducted a study in the Amazon forest of Peru and show P-band's capability to differentiate biomass classes in excess of 200 ton/ha.

Technical problems make the use of P-band questionable: P-band radiation is subject to Faraday rotation in the ionosphere, there is no International Telecommunications Union (ITU) frequency band allocation (as yet) for radar remote sensing at P-band and band width limitations will prevent acquisition of data with both high radiometric and spatial resolution.

The results of research conducted at a well surveyed test site of the 'Tropenbos' foundation in Guaviare, a colonisation area at the edge of the Colombian Amazon, may provide some insight into the above issues. In May 1993, the AirSAR collected fully polarimetric C-, L- and P- band data [NASA, 1993] in this area, thus enabling evaluation of the utility of different wave parameters for different types of information needs. In this paper the results of an analysis of land cover type and biomass classification capabilities for a single frequency band (polarimetric or single/multi-polarisation) and for combinations of frequency-bands (polarimetric and/or single/multi-polarisation) are presented. Theoretical distributions describing single-point statistical polarimetric backscatter behaviour are proposed and fitted against experimental data using Kolmogorov-Smirnov tests of fit (section 2.4). The results are discussed in the context of an evaluation of the appropriateness of certain mission characteristics to meet current or foreseen information needs, considering the presently operational and proposed satellite radar systems. In this context the word scenario is adopted for a critical set of mission characteristics and approaches in relation to a set of predefined information needs to be met (section 2.5). Both as an example and as a validation of the overall approach, a land cover map resulting from AirSAR data classification is presented. In addition some direct applications of the results, such as a biomass class map, are discussed (section 2.6).

2.2. BRIEF DESCRIPTION OF THE GUAVIARE TEST SITE

The study area is located in the Colombian district of Guaviare (2.5°N, 72.5°W), south of the Guaviare river corresponding to the natural boundary between the

Amazon rain forest and the savannahs of the Llanos Orientales to the north (Fig.2.1). The total annual rainfall fluctuates around 2600 mm with a maximum in May and a dry period from December to March. The natural land cover mainly consisted of tropical rain forests and edaphic savannahs, but due to the process of colonisation, extensive parts of the primary forest have been cut and converted into cropland, pastures or secondary re-growth (fallow). Part of the remaining forest is affected by human influence, meaning that valuable trees have been extracted and that the original structure of some of the forest fragments has been affected. Pasture for cattle breeding is the dominant land use. After cutting and burning of primary or secondary forests, annual and perennial crops (mainly maize, cassava, plantain) and, subsequently, forage grasses (mainly *Brachiaria decumbens*) are grown. Pastures may seriously degrade and are sometimes left to bush fallow for a certain period. The processes of deforestation and land cover change are still going on, resulting in a continuous forest fragmentation, which makes this area very interesting for monitoring studies.

The most important vegetation cover types in the study area are (1) primary forest, (2) secondary forest re-growth, (3) recently deforested (burnt) areas and (4) pastures. Recently deforested areas are areas where forest has been recently cut and the remnants have been burnt after a short period of drying. Usually crops are planted shortly after burning, while big branches, trunks and stumps of big trees remain present for some time. In addition some natural savannahs (5) and bush lands (6) occur in the westernmost part of the test area. The location and extent of these two classes are known, and are not subject to significant change over time. The latter two classes are excluded from the results presented in this paper since the first four classes mentioned above suffice to evaluate monitoring scenarios.

2.3. DATABASE

Five AirSAR images [van Zyl *et al.*, 1992] have been processed, covering a strip of 8 x 40 km of flat to gently undulating terrain. These are in 16-look Stokes scattering operator matrix format with a slant range pixel spacing of 6.66 m in range and around 8.20 m in azimuth. The incidence angle (θ_i) varies from about 20° to 60°. For the identification and description of the land cover types, field observations on vegetation and terrain characteristics were made at 123 locations in the 45°-60° incidence angle range. With the help of the land cover map [Andrade and Etter, 1987], aerial photography acquired in 1990, airborne radar data acquired during the SAREX campaign of ESA in 1992 [Hoekman and van der Sanden, 1993, Wooding and Attema, 1993] and terrain knowledge, a total of 778 areas of at least 50 pixels could be delineated, covering the four land cover classes in a 25°-60° range of incidence angles.



Figure 2.1 The study area is located near the town San José del Guaviare in the Colombian district Guaviare, south of the Guaviare river corresponding to the natural boundary between the Amazon rain forest to the south and the savannahs of the Llanos Orientales to the north

Detailed measurements of structural and physiognomic characteristics were made for 13 plots of primary forest and 10 plots of secondary forest, each 1,000 m² in size. In addition, vegetation characteristics were collected for 5 plots of grassland with varying degrees of bush invasion. An allometric equation calibrated for the (Colombian) Amazon [PRORADAM, 1979] was applied to estimate (total above-ground wet) biomass of the plots of primary forest and secondary forest, using trunk diameter and height to the first living branch. The biomass of the pasture plots was estimated by cutting and weighing all vegetation within some small sample areas within these plots.

A database of plot averaged Stokes scattering operator matrix elements was created, which forms the basis for the analysis in this paper.

2.4. APPROACH

The usefulness of certain combinations of frequency bands and polarisation, polarimetry, the effect of incidence angle θ_i and the effect of speckle have to be evaluated for different types of information needs. This was done in several steps, which will be described briefly.

2.4.1. Variation with incidence angle

In this data set the incidence angle dependence of the backscatter parameter γ ($\gamma = \sigma^0 / \cos(\theta_i)$; σ^0 is the differential radar cross section) is low for the 35°-60° incidence angle range, for all land cover classes and frequency bands. It was decided, arbitrarily, to develop a classifier using field averaged radar data for all fields in the 45°-50° incidence angle range (table 2.1) and apply selected classifiers on AirSAR image data in the 35°-60° incidence angle for validation (section 2.6). Figure 2.2 shows the L-band HV-polarised backscatter as an example of the low incidence angle dependence. When, for example, the averaged backscatter in the 50°-60° incidence angle range is subtracted from the 35°-45° range, the difference is less than 1 dB for all four main land cover types (of table 2.1) and all eleven backscatter channels (of table 2.2) used, with only three exceptions. These are all for P-band primary forest data: with HV-polarisation (-1.5 dB) and circular polarisation (-2 dB).

Table 2. 1 Number of plots per vegetation cover class and selected incidence angle ranges .

Cover type	25°-60°	45°-50°
Primary Forest	233	34
Secondary Forest	227	25
Recently cut	93	24
Pastures	225	22
Total	778	105

2.4.2. Statistical description of data

A statistical description of full polarimetric data can be made in several ways. A mathematically straightforward approach would be to describe the cross-products of the elements of the scattering matrix S , i.e. the elements of the covariance matrix. Another way would be to describe the data in terms of backscatter γ , polarimetric phase difference ϕ and polarimetric correlation $|\rho|$. Though mathematically more complex, the latter approach was selected here because it allows better interpretation in terms of physical mechanisms of backscatter and, hence, physical understanding.

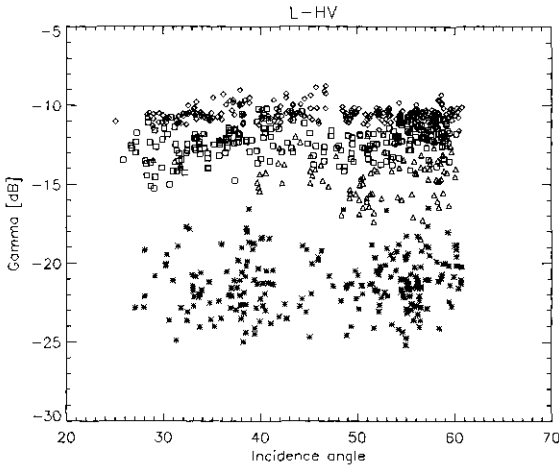


Figure 2.2 L-band HV-polarised field averaged backscatter levels as a function of incidence angle for the four main land cover types: primary forest (\diamond), secondary forest (\square), recently cut forest (Δ) and pasture ($*$).

The complex correlation between the HH- (i.e. horizontal linear receive and horizontal linear transmit) and VV-returns can be computed from elements of the Stokes scattering operator as:

$$\rho = |\rho| \exp(i\phi) = \frac{\langle S_{hh} S_{vv}^* \rangle}{\sqrt{\langle S_{hh} S_{hh}^* \rangle \langle S_{vv} S_{vv}^* \rangle}} \quad (2.1)$$

For a homogeneous area i , characterised by a spatially uniform differential cross section, phase difference *and* correlation, and a Gaussian probability density function (pdf) for the complex electric field vector, as measured by both antennae, multi-look pdf's of the observation can be described by the number of looks N (per pixel) and the underlying values for backscatter γ_i , phase difference ϕ_i and correlation $|\rho_i|$. The theoretical pdf for multi-look backscatter intensity is the well-known gamma function:

$$P_\gamma(\gamma | \gamma_i) = \frac{1}{\Gamma(N)} \left(\frac{N}{\gamma_i} \right)^N \gamma^{N-1} e^{-N\gamma/\gamma_i} \quad (2.2)$$

For phase difference and correlation marginal distributions are given by [Tough *et al.*, 1995]:

$$P_{\phi}(\phi | \phi_i, |\rho_i|) = \frac{(1 - |\rho_i|^2)^N}{2\pi} \left\{ \frac{(2N-2)!}{[(N-1)!]^2 2^{2(N-1)}} \left[\frac{(2N-1)\beta \arccos(-\beta)}{(-\beta^2)^{N+1/2}} + \frac{1}{(-\beta^2)^N} \right] + \right. \quad (2.3)$$

$$\left. \frac{1}{2(N-1)} \sum_{r=0}^{N-2} \frac{\Gamma(N-1/2)}{\Gamma(N-1/2-r)} \frac{\Gamma(N-1-r)}{\Gamma(N-1)} \frac{1+(2r+1)\beta^2}{(-\beta^2)^{r+2}} \right\}$$

where the last term is 0 for $N=1$ and $\beta = |\rho_i| \cos(\phi - \phi_i)$, and

$$P_{|\rho|}(|\rho| | \rho_i) = 2|\rho| (N-1) (1 - |\rho_i|^2)^N (1 - |\rho|^2)^{N-2} {}_2F_1(N, N, 1; |\rho|^2 | \rho_i|^2), \quad (2.4)$$

where ${}_2F_1(\cdot)$ is the Gaussian hypergeometric function.

For a classification procedure statistical descriptions are needed for pixels belonging to a certain class, rather than belonging to a certain homogeneous area. Such distributions do not follow directly from theoretical considerations. Assumptions should be made, which have to be carefully verified with experimental data. Here, it is assumed that pdf's are well described by Gaussian distributions for the parameter γ_i (in dB),

$$N(\gamma_i | \gamma_c, \sigma_c) = \frac{1}{\sigma_c \sqrt{2\pi}} \exp\left(-\frac{(\gamma_i - \gamma_c)^2}{2\sigma_c^2}\right), \quad (2.5)$$

with γ_c (in dB) as the mean of the mean field values of class c and σ_c as the standard deviation of γ_c , and by circular Gaussian distributions for the phase differences:

$$C(\phi_i | \phi_c, |\rho_c|) = \frac{1 - |\rho_c|^2}{2\pi(1 - \beta^2)} \left\{ 1 + \frac{\beta \arccos(-\beta)}{\sqrt{1 - \beta^2}} \right\}, \quad (2.6)$$

with $\beta = |\rho_c| \cos(\phi_i - \phi_c)$, $-\pi < \phi_i \leq \pi$, where ϕ_c = the "effective" mean phase difference for class c and $|\rho_c|$ is the "effective" mean correlation for class c . Note that (2.6) follows from (2.3) for $N=1$, but describes classes instead of single homogeneous areas.

Gaussian distributions are 'natural' distributions, which follow from application of Jaynes' maximum entropy principle [Jaynes, 1957]. For a continuous random variate varying over the (0, 1) interval, application of this principle results in the Beta function. Hence, phase correlations may be assumed to be properly described by Beta distributions:

$$B(|\rho_i| | a, b) = \frac{\Gamma(a+b)}{\Gamma(a)\Gamma(b)} |\rho_i|^{a-1} (1-|\rho_i|)^{b-1}, \quad 0 < |\rho_i| < 1, \quad (2.7)$$

where a and b are regression parameters.

The field averaged Stokes scattering element data of the database are used to calculate field averaged values for backscatter, phase differences and correlation. The accuracy of the estimation of field averaged values depends on the total number of independent looks. Inspection of the single-point statistics and the range and azimuth autocorrelation functions of large homogeneous pastures in these AirSAR images revealed an effective number of approximately 14 looks per pixel for all bands. Spatial correlation would decrease this number further by approximately 30% for C- and L-band and 60% for P-band.

In the 45°-50° incidence angle range subset studied each field has at least 100 pixels, except for recently cut areas, which cover at least 60 pixels. This would result in a minimum of 588 (60 x 14 x 0.7) independent looks in C- and L- band and, in case some of the smaller recently cut areas are ignored, at least 560 (100 x 14 x 0.4) independent looks in P- band. For this large number of 560 independent looks N , for homogeneous fields these averages can be regarded as accurate estimations of the underlying values. The standard deviation of the backscatter follows from [Hoekman, 1991; eq.27] and is less than 0.184 dB for $N > 560$. The standard deviation of the phase difference depends on $|\rho_i|$ and follows from [15;eq.69]. It is less than 2.97° for $|\rho_i| = 0.5$ and $N > 560$. The standard deviation of the correlation follows from application of the Cramer-Rao bound [Seymour and Cumming 1994; eq.20] and is less than 0.022 for $|\rho_i| = 0.5$ and $N > 560$.

It is assumed that the objects display azimuthal symmetry and, consequently, that only the correlation and phase difference distributions for HH-VV polarisation is important, and that for HH-HV and HV-VV polarisation these can be ignored [Nghiem *et al.*, 1992].

The appropriateness of the Gaussian distribution for field averaged gamma values in dB (2.5), the circular Gaussian distribution (2.6) for the field averaged HH-VV phase differences and the Beta distribution (2.7) for field averaged HH-VV phase correlation can be studied using these accurate estimations of field averaged values. This was done using a Kolmogorov-Smirnov (K-S) test of fit to determine the significance Q of the null hypothesis stating that the observed field averaged values are drawn from the corresponding theoretical distributions [Press *et al.*, 1994]. Results show that for all four cover types, for all three bands and for all five parameters tested (i.e. γ_i for HH-, VV- and HV-polarisation and ϕ_i and $|\rho_i|$ for the HH-VV polarimetric phase difference) the null hypothesis could not be rejected. Possible exceptions are only L-band γ_i values for primary forests and C-band phase

(ϕ_i and $|\rho_i|$) values, also for primary forest. Some examples of cumulative pdf's showing the generally good correspondence between theory and data are shown in Fig. 2.3. It is noted that the Gaussian distribution gives a poor fit when γ_i is not expressed in dB's.

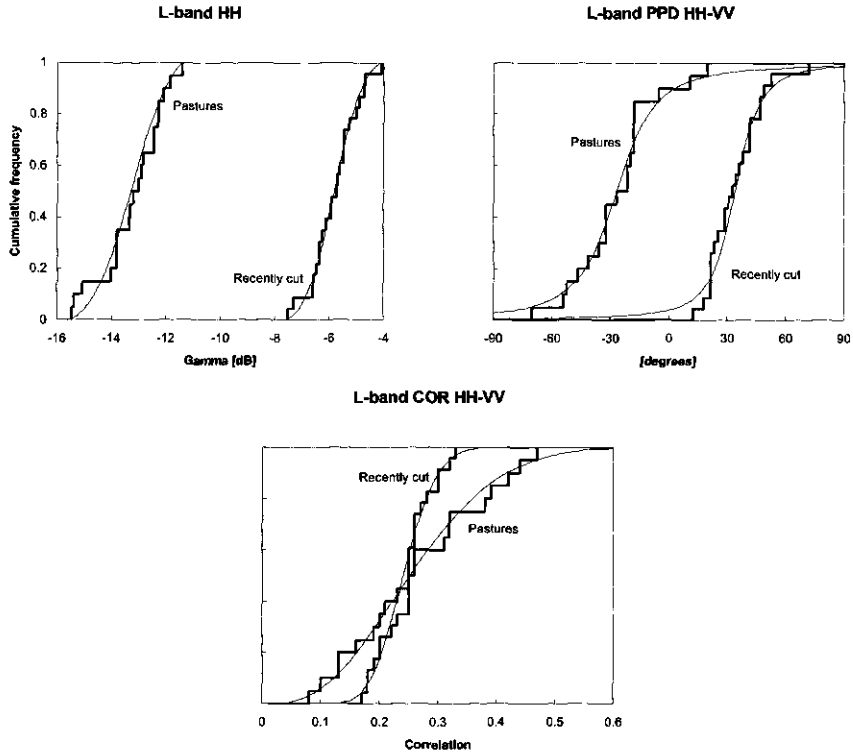


Figure 2.3 Theoretical cumulative probability density distributions of L-band HH-polarised backscatter, HH-VV phase difference and correlation, respectively, compared with experimental observation (step-functions). For recently cut areas the K-S fit significances Q are 0.9995, 0.81 and 0.85, respectively, and for pastures 0.96, 0.82 and 0.9996, respectively

2.4.3. Simulation of pixel classification

For classification several approaches can be followed. The most simple approach is to classify multi-look pixels. To reduce the effect of speckle box averaging or segmentation into homogeneous areas can be applied first. The resulting number of independent looks is usually too small to ignore the effect of speckle on the estimation of the underlying values of γ_i , ϕ_i and $|\rho_i|$. The effect of speckle can be simulated by using these field-averaged values to draw randomly from the distributions given by (2.2), (2.3) and (2.4). Here this was done 100 times for each field, thus raising the number of samples to be classified from 105 (table 2.1) to 10,500. The resulting distributions are wider because of the effect of speckle. The

shape of the resulting distributions can be modelled in two different ways. In case the distributions given by (2.5), (2.6) and (2.7) would have given a perfect match with the observed mean values, the result would follow by straightforward combination with (2.2), (2.3) and (2.4), respectively. However, the number of observed mean values per class is not large enough to be able to make such a decisive conclusion. The second approach would be to test whether (2.5), (2.6) and (2.7) still hold after adding speckle. Since the distributions become wider it simply means that the values of regression parameters $\gamma_c, \sigma_c, \phi_c, |\rho_c|, a$ and b change. Since these distributions are 'natural' distributions, meaning they are a result of several independent processes, it is not a contradiction to assume they still may hold when including an additional independent process, i.e. speckle. K-S tests of fit confirm the validity of the second approach. In this case deviations from the model may be detected by evaluating the K-S statistic D , which is defined as the maximum distance between the cumulative pdf of theoretical functions and observations (see also Fig. 2.3) and [20]. At the '1 dB' level (i.e. $N=20$) for only a few of the 36 γ_i distributions tested D is larger than 0.03, and for only a few of the 24 ϕ_i and $|\rho_i|$ distributions tested D is larger than 0.06. At the '2 dB' level (i.e. $N=5$) the fits are even slightly better.

The likelihood for an (polarimetric) observation vector to be classified as class c is modelled as the product of the joint Gaussian distribution of the backscatter values multiplied by the likelihoods of the phase difference values and the likelihoods of the correlation values. It is assumed, therefore, that values for phase difference and correlation are independent from each other and independent from backscatter level. It is noted that this assumption is not well validated, and, consequently, classification results may be underestimated.

A Kappa statistic (\hat{K}) can be computed to evaluate significant differences between any pair of classification results, cf. [Lillesand and Kiefer, 1994]. A test statistic $\Delta\hat{K}$ can be introduced as:

$$\Delta\hat{K} = \frac{|\hat{K}_1 - \hat{K}_2|}{\sqrt{\hat{\sigma}_\infty^2[\hat{K}_1] + \hat{\sigma}_\infty^2[\hat{K}_2]}}, \quad (2.8)$$

where $\hat{\sigma}_\infty^2[\hat{K}]$ is the approximate large sample variance of \hat{K} . At the 95% confidence level two results may be considered significantly different if $\Delta\hat{K} > 1.96$ [Benson and DeGloria, 1985].

For clarity the approach introduced here may be summarised as follows. On the basis of experimental data and theoretical considerations probability density distributions of backscatter, polarimetric phase difference and polarimetric phase coherence can be simulated for a number of land cover types for three frequency

bands, polarisation and speckle level. These distributions can be used to simulate classification results, using the same experimental data extracted from 105 well defined training areas in the 45° - 50° incidence angle range. Such an exercise is useful for comparison of capabilities of selected sensor parameters (see section 2.5), it is not meant to derive accurate quantitative predictions. As an example and as a validation of the overall approach a large area covering the 35° - 60° incidence angle is classified using regression parameters for the selected speckle level (out of the set of $\gamma_c, \sigma_c, \phi_c, |\rho_c|, a$ and b , for all classes c and all frequency bands) derived from the training areas (see section 2.6).

2.5. RESULTS

2.5.1. Land cover type classification

In the Total Power C-, L- and P-band AirSAR image (Fig. 2.8a) grasslands show up in very dark tones, primary forest in bright tones, secondary vegetation in blue and green, depending on age, and recently cut areas in red. Recently cut areas, characterised here by the presence of some trunk remnants in a low biomass and mostly bare area, have high P-band backscatter levels, while for C-band the backscatter is low. Primary and secondary forests both have a high (saturated) level of backscatter in C-band, while for P-band the primary forest backscatter level is clearly higher. As a result these main four land cover types can be separated well (Fig. 2.4).

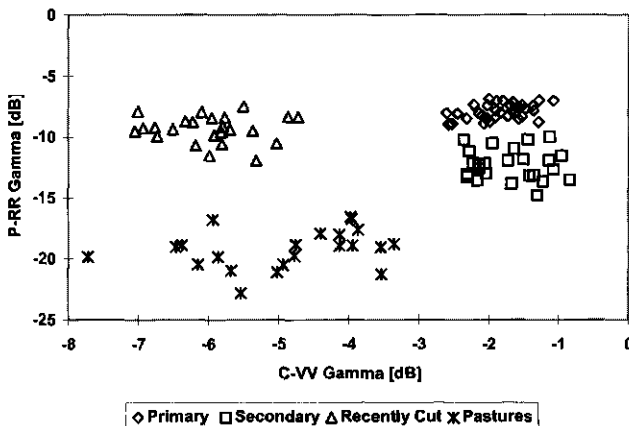


Figure 2.4. Scatter plot of the C-VV and P-RR field averaged backscatter levels for all 105 fields in the 45° - 50° incidence angle range, for the four main land cover types

The simulated classification results for the four main land cover types using a single channel configuration are shown in Table 2.2 It also includes results for LL- (i.e. left circular receive and left circular transmit) and RR-circular polarisation since these

(and only these!) are not affected by Faraday rotation in P-band as can be deduced from [Bickle and Bates, 1965]. Note that in this case the circular polarisation would be provided by a circular antenna feed, not from polarisation synthesis. At the '1 dB' level (i.e. 20-look data) only L-band with HV-polarisation (Lhv) and P-band with HV-polarisation (Phv) show reasonable results (80%).

Table 2.2. Overall Maximum Likelihood (ML) classification accuracy (expressed in percentages) at the 95% level of confidence for the 45°-50° incidence angle range using a single channel, for speckle levels of 0, 1 and 2 dB, (i.e. $N > 560$, $N = 20$, $N = 5$, respectively) for all AirSAR channels studied and for 4 land cover types. The bold numbers indicate the best result plus the results that are not significantly different from the best result at the 95% level of confidence. The numbers in the shaded boxes indicate the worst result plus the results that are not significantly different from the worst result at the 95% level of confidence

Channel	'0 dB'	'1 dB'	'2 dB'
Chh	59.0	45.4	36.0
Chv	71.4	56.7	42.3
Cvv	67.6	53.0	40.6
Lhh	69.5	60.1	52.8
Lhv	91.4	79.4	65.4
Lvv	82.9	66.2	53.0
Phh	81.9	73.0	60.4
Phv	88.6	80.3	67.5
Pvv	79.0	70.4	57.4
Prr	81.0	74.0	62.5
Pll	78.1	72.2	62.3

Table 2.3 shows that at the '1 dB' level many combinations of 2 channels reach results over 90%. There are many combinations of Lhv with C- or P-band and combinations of C- and P-band that are successful. Single frequency combinations are inferior to many of the best double frequency combinations. The effect of speckle can be studied in many ways. Fig. 2.5 shows results for some combinations as a function of speckle level. It clearly illustrates that for some of the better combinations results do not improve considerably anymore after 20 looks. Using three or more channels does not improve results considerably as can be seen in table 2.4. This table also includes results for polarimetric systems. Also fully polarimetric P-band (Ppol) systems are considered since these can be corrected for the effects of Faraday rotation relatively easily [Freeman *et al.*, sub]. It is noted that the simulated classification results given in tables 2.2, 2.3 and 2.4 and in Fig. 2.5 are generated at the 95% level of confidence. Consequently, roughly 5% of the data is expected to be classified as the class "unknown" and results in excess of 95% are unlikely. The bold numbers in these tables indicate the best result plus the results that are not significantly different from the best result at the 95% level of confidence, using the Kappa statistic (2.8). The numbers in the shaded boxes indicate the worst result plus the results that are not significantly different from the worst result at the 95% level of confidence.

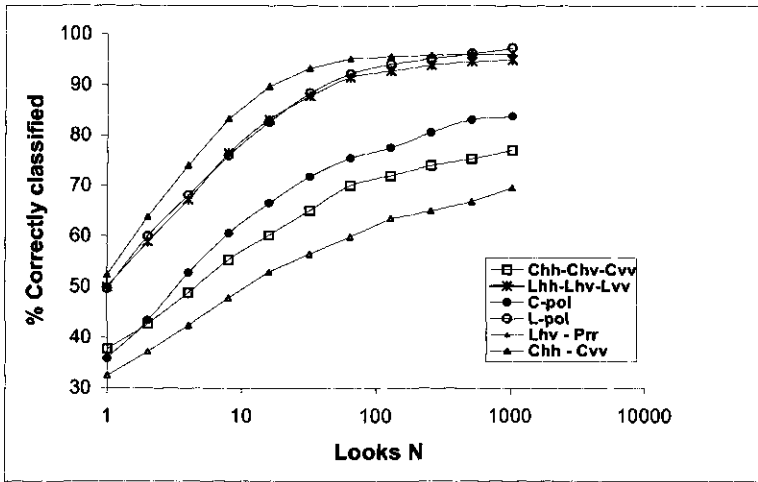


Figure 2.5. Overall Maximum Likelihood (ML) classification accuracy (expressed in percentages) at the 95% level of confidence for the 45°-50° incidence angle range for several combinations as function of the speckle level expressed in number of looks .

Table 2.3. Overall Maximum Likelihood (ML) classification accuracy (expressed in percentages) at the 95% level of confidence for the 45°-50° incidence angle range using 55 combinations of two channels, for a speckle level of '1 dB' and for 4 land (vegetation) cover types. The bold numbers indicate the best result plus the results that are not significantly different from the best result at the 95% level of confidence. The numbers in the shaded boxes indicate the worst result plus the results that are not significantly different from the worst result at the 95% level of confidence

	Chv	Cvv	Lhh	Lhv	Lvv	Phh	Phv	Pvv	Prr	Pll
Chh	58.5	54.0	75.7	83.7	74.8	85.3	88.7	83.6	86.5	86.8
Chv		61.0	81.7	86.9	80.6	90.3	92.9	89.1	92.2	92.0
Cvv			81.1	86.1	78.7	90.3	93.1	89.1	92.3	91.9
Lhh				83.1	74.6	72.7	78.8	71.8	73.3	72.5
Lhv					80.4	91.4	91.2	87.5	91.0	91.2
Lvv						86.1	85.3	80.8	84.3	84.7
Phh							84.3	80.1	79.9	78.0
Phv								80.0	80.8	81.3
Pvv									76.3	77.1
Prr										76.4

In table 2.5 the confusion between any pair of land cover classes for a number of wave parameter combinations is shown. Depending on specific application needs, certain combinations can be preferred, even when they yield lower overall results. For example, for monitoring the decrease of forest area it may be important to discriminate forest (primary and secondary) from pastures. L-band with HH-polarisation would be well suitable. For this particular configuration the confusion with recently cut areas would be large and also primary and secondary forests would be confused to a large extent.

Table 2.4. Overall Maximum Likelihood (ML) classification accuracy (expressed in percentages) at the 95% level of confidence for the 45°-50° incidence angle range for a selection of combinations at the '1 dB speckle level', the statistic \hat{K} and its large sample variance $\hat{\sigma}_{\infty}^2[\hat{K}]$. The bold numbers indicate the best result plus the results that are not significantly different from the best result at the 95% level of confidence. The numbers in the shaded boxes indicate the worst result plus the results that are not significantly different from the worst result at the 95% level of confidence.

Channel	result	\hat{K}	$\hat{\sigma}_{\infty}^2[\hat{K}]$
Cpol, Lpol, Ppol	94.7	0.931016	0.000768
Chv, Phv, Prr	94.0	0.921145	0.000885
Cpol, Prr	93.1	0.909599	0.001018
Phv, Cvv	93.1	0.908934	0.001032
Cvv, Chh, Chv, Prr	92.6	0.902984	0.001077
Lpol, Prr	91.9	0.893512	0.001174
Lhv, Prr	91.2	0.883844	0.001275
Cpol, Lpol	90.4	0.873539	0.001365
Lpol, Cvv	89.5	0.862657	0.001479
Ppol	87.1	0.829398	0.001803
Pvv, Phh, Phv	86.1	0.816590	0.001904
Lpol	85.8	0.813185	0.001926
Lvv, Lhh, Lhv	85.0	0.803859	0.001996
Lhh, Cvv	81.1	0.751464	0.002492
Lhh, Prr	73.3	0.647533	0.003142
Cpol	68.4	0.581294	0.003612
Cvv, Chh, Chv	61.9	0.497471	0.003859
Lhh	60.1	0.465214	0.003928
Cvv, Chh	54.0	0.393662	0.004008
Cvv	53.0	0.373692	0.004144
Chh	45.4	0.275277	0.004154

Some dual-frequency systems give excellent results, for example: a C-or L-band polarimetric system in combination with P-band in RR-polarisation.

2.5.2. Biomass classes

The potential for biomass class mapping was studied by evaluating the backscatter for all 5 fields of pasture, 10 fields of secondary forest re-growth and 13 fields of primary forest for which biomass (directly or indirectly) was estimated. For these fields the above ground fresh biomass was found to vary over the range of 2.9-10 ton per hectare (1 ton = 1,000 kg; 1 ha = 10,000 m²) for pastures, 6-159 ton/ha for secondary forest and 137-297 ton/ha for primary forest. Since biomass varies over several orders of magnitude γ_i values (in dB) were fitted to the logarithm of biomass (x) using a log-log functional relationship of the form γ_i [dB]= $a \exp(bx) + c$. The main results are summarised in table2.6.

Table 2.5. Percentage of confusion between land cover type pairs for the 45 °-50° incidence angle range at the 1 dB speckle level ($N=20$) for a selection of combinations. Each entry gives the result as the percentage of the sum of class *a* samples classified as *b* and class *b* samples classified as *a* from the sum of class *a* and class *b* samples, in the absence of other classes (i.e. absence of class *c*, etc., and the absence of the class 'unknown'). The expected value for maximum confusion therefore is 50%.

Bands and polarisation		Chh	Cvv	Cvv Chh	Lhh	Cvv Chh Chv	Lhh Cvv
Loss of forests	Primary-Pastures 1-4	20.1	10.6	9.1	0.5	7.7	0.4
	Secondary-Pastures 2-4	18.6	10.3	8.0	1.9	7.5	1.5
Newly deforested areas	Primary-Recently cut 1-3	12.6	3.3	1.8	40.9	0.4	3.0
	Secondary-Recently cut 2-3	11.3	3.2	1.6	30.8	0.3	2.2
	Pastures - Recently cut 3-4	38.6	32.3	32.2	1.1	16.8	0.8
Forest stages	Primary-Secondary 1-2	46.0	46.9	45.3	23.8	43.1	24.4

Bands and polarisation (continued)		Prr Lhv	Cpo l	Lpol	Lpol Cvv	Lpol Prr	Cpol Prr	Ppol	Cpol Lpol	Cpol Lpol Ppol
	1-4	0.0	4.0	0.0	0.0	0.0	0.0	0.0	0.0	0.0
	2-4	0.3	4.3	0.1	0.0	0.0	0.5	0.6	0.1	0.0
	1-3	2.9	0.5	2.2	0.5	2.2	0.4	10.2	0.1	0.1
	2-3	4.6	0.6	9.0	1.4	3.6	0.2	9.3	0.1	0.1
	3-4	0.1	12.3	0.9	0.7	0.1	0.1	0.0	0.0	0.0
	1-2	4.3	40.0	11.1	10.8	4.0	5.8	2.0	10.1	1.2

For the C-band the correlation is not very high. The maximum value for r^2 is 0.66 and was found for the VV-polarisation. For L-band with HV-polarisation and for P-band high values are found (Fig. 2.6). However there are some differences: L-band with HV-polarisation has a high correlation but the signal tends to saturate at high biomass levels. For P-band the saturation appears at higher biomass levels, however the *SEE* (Standard Error of Estimate) is higher. The combination of these bands can be used to improve overall results for the whole biomass range under study. Averaging backscatter of P-band with RR-polarisation and L-band with HV-polarisation, for example, results in a slightly higher correlation (r^2 is 0.94) and a considerably lower *SEE*. The ratio of the total range of backscatter and the *SEE* for this particular combination is high, namely 13.2. This number may be interpreted as 6.7 times 1.96 standard deviations or, in other words, at least 6 classes of biomass may be distinguished at the 95% confidence level (this should be interpreted as the confidence level for the real class being not more than one class away from the estimated class, see also next section). Also, since biomass values of the savannah, beyond the lower end of the range shown here, and biomass values of higher biomass primary forest (at other test sites) beyond the higher end of the range shown here, seem to obey this functional relationship well, it is believed that up to 8 biomass classes may be discerned using this particular combination. Further analysis, of additional biomass values of other areas in the Amazon, may permit

further elaboration of such relationships and may yield more insight into the saturation effect found for higher biomass values.

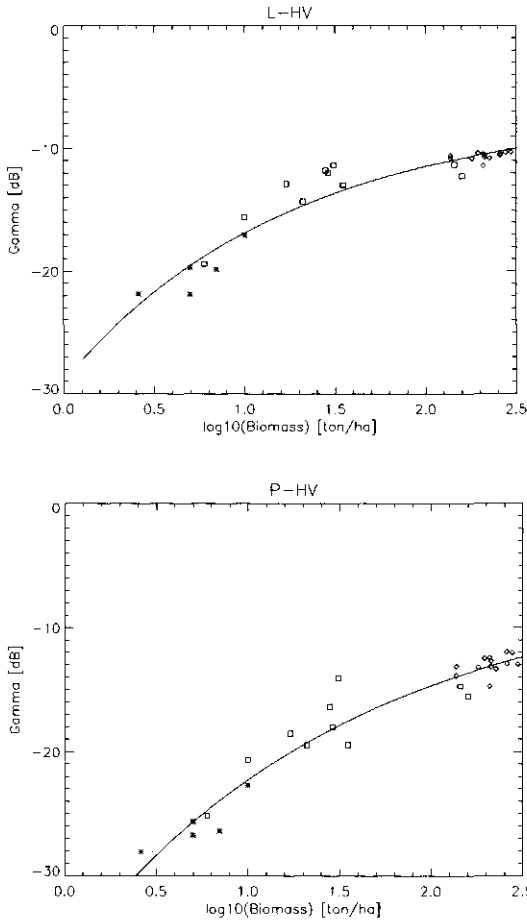


Figure. 2.6. L- and P-band backscatter with HV-polarisation as function of biomass. The biomass is the fresh weight above ground biomass (in ton/ha) on the logarithmic scale (i.e. 1.0 is 10 ton/ha, 1.5 is 31.6 ton/ha, etc.). Experimental data for primary forest (\diamond), secondary forest (\square) and pasture ($*$) are fitted to a curve of the form γ_i [dB] = $a \exp(bx) + c$, where x is the logarithm of the biomass.

2.5.3. Comparison with other results

Most studies of land cover and biomass in tropical forest areas to date relate to SIR-C (L- and C-band) data of the Brazilian Amazon. The results seem to be fairly consistent with the findings presented in this paper for the C- and L-band AirSAR data of the Colombian Amazon. Luckman *et al.* [Luckman *et al.*, 1997] conclude that L-band with HV polarisation is the best for biomass estimation and indicates a saturation level of 60 ton/ha. Foody *et al.* [Foody *et al.*, 1997] do not find significant

correlation with biomass, however, when using the C_{vv}/L_{vv} ratio a fair correlation with biomass of *Cecropia* dominated re-growth was found up to the level of 120 ton/ha. Yanasse *et al.* [Yanasse *et al.* 1997] also report the problem to separate regeneration stages: Lhv is the best channel, however, only useful up to an age of 9 years. The lack of sensitivity to secondary re-growth biomass variation of C- and L-band also affects classification results. Confusion between secondary re-growth of 5-8 years, i.e. around 100 ton/ha, and primary forest [Rignot *et al.*, 1997], confusion between old secondary forest and primary forest [Saatchi *et al.*, 1997] and between pastures and young secondary forest [Saatchi *et al.*, 1997] are reported as major problems. It is also noted that data of the wet season, i.e. during wet soil conditions, are less suitable for accurate classification [Rignot *et al.*, 1997, Saatchi *et al.*, 1997].

Table 2.6. Relationship between backscatter, expressed as γ_i [dB], and biomass expressed as \log_{10} of the above ground fresh biomass in ton/ha, for several frequency and polarisation combinations. The correlation coefficient r^2 , the standard error of estimate (*SEE*), the total range of γ_i of the experimental data and the ratio of range and *SEE* are shown

	r^2	<i>SEE</i> [dB]	range [dB]	range/ <i>SEE</i> [dB]
C-HH	0.32	0.41	3.2	8.0
C-HV	0.62	0.33	3.2	9.6
C-VV	0.66	0.51	4.8	9.5
L-HH	0.81	1.07	9.3	8.7
L-HV	0.93	1.05	11.6	11.0
L-VV	0.78	0.83	7.7	9.3
P-HH	0.90	1.39	11.1	8.0
P-HV	0.94	1.70	16.1	9.5
P-VV	0.91	0.82	9.6	11.6
P-RR	0.93	1.23	13.2	10.7
L-HV+P-RR	0.94	0.93	12.3	13.2

2.6. APPLICATION OF RESULTS

On the basis of the previous results a system configuration may be selected. As an example the combination Lhv and Prr may be chosen since it shows good overall classification results (table 2.4), even for a low number of looks (Fig. 2.5), little confusion between any pair of land cover classes (table 2.5) and useful information on biomass over a large range of values (table 2.6). To validate the appropriateness of the selected configuration the AirSAR data are classified in the 35°-60° incidence angle range using the statistics derived for the 45°-50° incidence angle range (section 2.4). The pixels within the first angular range and within the 778 ground truth plots can be used for validation. The results are very good and are shown in table 2.7 and illustrated in Fig. 2.8b. It is noted that no confidence level for the classification was applied and, thus, all pixels are classified as one of the four land cover classes (i.e. there is no class 'unknown'). The resulting values thus can be better than the ones given in the previous section. In this case they appear to be considerably higher with an overall result of 98.6%. It is noted that the validation set is large but limited to areas delineated within fields. For the scene as a whole, border

effects, such as mixed pixels, shadowing and layover, may cause a considerable additional error, depending on the scale used.

Table 7. Confusion matrix for the total sample area within the classified image, for the combination of Lhv with Prr. The results are expressed in % of pixels. The land cover types are encoded as: (1) Primary forest, (2) Secondary forest, (3) Recently cut areas, and (4) Pastures.

Lhv - Prr	1	2	3	4	
1	98.6	1.2	0.2	0.0	
2	1.8	97.2	0.9	0.0	
3	0.5	0.5	99.0	0.0	
4	0.0	0.1	0.0	99.9	
Total					98.6

It is noted that the previous classification was done on a 2 x 2 pixel averaged basis. High-resolution radar data can show single-point statistics that may deviate considerable from the gamma pdf (2) and equations (3) and (4) for multi-look phase difference and coherence [Oliver and Quegan, 1998]. The consequence is that classification results for high-resolution data, such as single pixel AirSAR data, may not be predicted well by the model introduced in section 4. Deviations from the model may be detected by evaluating the K-S statistic *D*. Here a comparison was made with the theoretical models describing 14-look data of extended homogeneous areas. The statistic *D* is relatively large (0.13) for backscatter in C-band of primary forests, and to a lesser extent for L-band and for secondary forests in C-band. This may be a result of the large size of trees resulting in image texture. The statistic *D* is also relatively large for backscatter of recently cut areas in C-band (0.14) and L-band (0.12). This may be an effect of field heterogeneity. For pastures the statistic *D* is relatively large in P-band and to a lesser extent in L-band. This may be an effect of a relatively low number of scatterers causing a transition from a gamma distribution into a K-distribution [Oliver and Quegan, 1998, Quegan and Rhodes, 1995]. No large deviations were found for the phase difference and coherence distributions. The first effect (i.e. texture) and third effect (i.e. non-Gaussian behaviour complex electric field vector) vanish when the spatial resolution gets smaller. The second effect, heterogeneity, may appear at several scales, depending on the scene's complexity. Averaging 2 x 2 pixels, as was done here, improves the classification result considerably, especially when C-band is used. This improvement is only partly a result of the reduced effect of speckle. It mainly appears to be a consequence of the strong reduction of image texture, and, of course, the fact that texture is not used as a classifier here.

Using the functional relationships between biomass and the average backscatter of the Lhv and Prr bands a map of biomass classes can be created. This was done for eight arbitrarily chosen biomass classes, namely: (1) ≤ 3.42 , (2) 3.42-4.72, (3) 4.72-6.85, (4) 6.85-10.7, (5) 10.7-18.5, (6) 18.5-38.1, (7) 38.1-109 and (8) > 109 (in ton/ha). Classes 2 until 7 correspond to equidistant values of backscatter separated at

1.96 standard deviation intervals as indicated in Fig. 2.7. Since the relationship does not hold for the class of recently cut areas, these areas have been excluded from the biomass classification as illustrated in Fig. 2.8c. It is difficult to validate the accuracy of these results since acquiring a sufficient number of additional biomass values is a huge task. The consistency between biomass classification and land cover type classification can be checked, however. Table 2.8 shows for each land cover class (excluding recently cut areas) the distribution of biomass classes as a percentage of the total area. The agreement with expected biomass ranges is high for all three-land cover types.

Table 2.8. Percentages of areas corresponding to the classification of the four main land cover types and the eight biomass classes. The land cover types are encoded as: (1) Primary forest, (2) Secondary forest, (3) Recently cut areas, and (4) Pastures. Shaded boxes in the first column may indicate areas of forest degradation, while shaded boxes in the last column may indicate areas of land degradation

Biomass classes (ton/ha)	1	2	3	4
Masked	0	0	100	0
0-3.42	0	0	0	16
3.42-4.72	0	0	0	18
4.72-6.85	0	1	0	23
6.85-10.7	0	3	0	20
10.7-18.5	1	12	0	12
18.5-38.1	2	28	0	6
38.1-109.	12	40	0	3
>109.	84	14	0	1

Very low values of biomass (≤ 3.42 ton/ha) were classified in areas corresponding to the natural savannahs (in the westernmost part of the area), which is in agreement with field observations.

The same low range was found for some pasture areas (east of the savannahs), indicating low biomass values which may be associated with recent pasture burning or pasture land degradation. The first possibility is less likely since burning of the pastures usually takes place during the dry season while the images were recorded in the middle of the rainy period. However, though no degradation data are available to support such a hypothesis firmly, the tendency for more lower biomass pastures to be found in the older settlement areas corresponds with expectation. Pastures in the higher biomass range (3.42–10.7 ton/ha) were found to correspond to areas where tall grasses and a high proportion of bushes and small palms occurred, as recorded in the field. Both the secondary and primary forest classes show a distribution over several biomass classes in the middle and higher ranges.

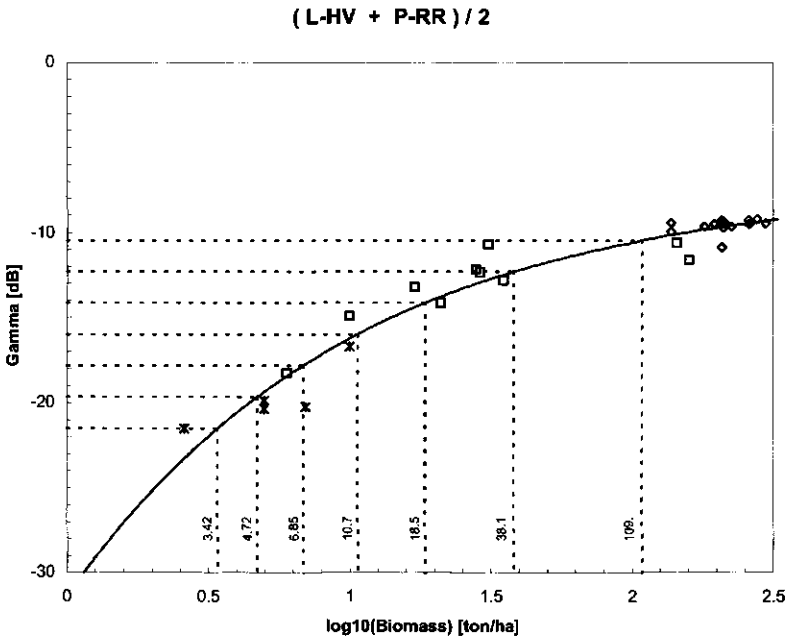


Figure 2.7. Experimental relationship between biomass and the average backscatter of the Lhv and Pr channels. Eight arbitrarily chosen biomass classes are indicated corresponding to equidistant values of backscatter separated at 1.96 standard deviation intervals.

It should be noted that the biomass class map shows broad biomass classes over several orders of magnitude and, thus, is useful for assessment of spatial patterns associated with land and forest degradation and secondary regrowth processes. It does not show accurate biomass value estimations and, thus, is of limited value for, say, foresters who want to assess parameters such as timber volume.

2.7. CONCLUSIONS AND RECOMMENDATIONS

A statistical description of full polarimetric data in terms of backscatter, polarimetric phase difference and polarimetric correlation was made. Theoretical distributions of field or segment averaged (multi-look) values for all four land cover types and all three frequency bands were shown to be in good agreement with observation. Classification results could be simulated for certain combinations of frequency bands and polarisation as a function of speckle level.

The results presented in this paper give insight into the problem of optimum wave parameter selection for operational systems, the utility of polarimetry, how this relates to certain applications (in tropical rain forest areas) and to the accuracy that can be obtained. Different scenarios may be used to evaluate these results. Within each scenario the appropriateness of a certain system configuration for a certain application is investigated.

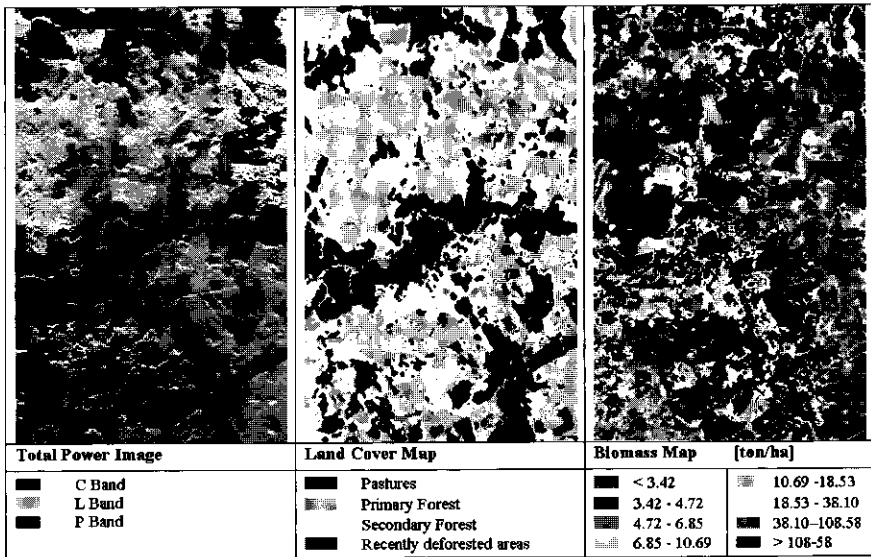


Figure 2.8 (a) AirSAR Total Power image, (b) Land Cover map and (c) Biomass map for a 4 x 7 km² area in Guaviare. In the biomass map the areas of recently cut forest are masked (black) (see colour plate 1).

The usefulness of these systems for land cover monitoring depend on, among other things, the type of information (land cover classes, biomass classes), the scale and accuracy of this information and the temporal frequency at which this information can be obtained. Depending on the specific information needs, land cover monitoring systems should have the capability to (1) differentiate between forested and non-forested areas, (2) to detect new areas of deforestation, (3) to differentiate between primary and secondary forest (e.g. to study regeneration), and/or (4) to provide some data on biomass (e.g. to study degradation or carbon budgets). Other issues such as costs and timeliness are beyond the scope of this paper.

In summary one may conclude that C-band is useful for monitoring deforestation, especially when the observation frequency is high. The very poor capability to differentiate primary and secondary forest may pose problems since the latter may develop very fast after clearing, and sometimes even before clearing of the original forest is complete. In L-band with HH- or VV-polarisation monitoring deforestation is also not without problems since recently cut areas are not well differentiated from the forested areas. Adding HV-polarisation would solve this problem to a large

extent. P-band has the same problem to a larger extent and for all polarisations although P-band's capability in differentiating pastures, secondary forest and primary forest are superior. P-band and L-band with HV-polarisation are suitable for biomass mapping. P-band, however, saturates at a much higher level of biomass and seems to cover the 10-200 ton/ha range well, which is of special interest for forest secondary regrowth monitoring.

Results would greatly improve if a dedicated system could be developed using two frequencies. Combinations of C- and L-band or C- and P-band would give good overall results, although there is still some confusion between primary, secondary and recently cut forest (table 2.5). The combination of L- and P-band would be even better. The combination of good land cover type and good biomass classification may be particularly useful, as was illustrated in section 2.6. Because the relation between backscatter and biomass depends on land cover type, it may even be a necessity for accurate biomass assessment to be preceded by a good land cover type classification.

Accurate field observations and measurements play a crucial role in analysis and validation. Though an extensive good quality data set was available the importance of repeating the experiment in other areas of the Amazon, and in different seasons, should be emphasised. For example, soil moisture variation, depending on wavelength and polarisation, may have a significant effect on the results. Also local variation in physical characterisation of the land cover types, related to factors like variation in floristic composition, physiognomy, forest structure and management practice, may have important effects.

From a practical point of view one may conclude that, as long as P-band with a reasonable bandwidth is not allowed for spaceborne SAR operation, the combination of C- and L-band is the best choice. Of course, high quality airborne inventory using P-band SAR may still be a viable option. Tables 2.4 and 2.5 show, for example, that C-band with VV-polarisation in combination with polarimetric L-band is a good choice. The only problem seems to be the relatively poor discrimination of primary forest and secondary forest. However, since primary forest can be differentiated well from pastures and recently cut areas, and the main problem is discrimination between primary and the older secondary forest, this problem may be circumvented in a monitoring system when using frequent observation and knowledge of deforestation in the past. The need for frequent observation (for timely detection of illegal clear-cut for example) and, likely, the need to cover different seasons (because results probably depend on season or can be improved by combining seasons) may translate into a maximum of 3 to 4 coverages per year. Hence, a swath width of 40 km could be sufficient. To achieve the same accuracy as indicated in tables 4 and 5 20-look data are required. For a scale of 1:100,000, pixels corresponding to a 20x20 m area would be required, which would translate into roughly 4-5 m resolution. Such a system is a technically viable option and may cover many information needs with high accuracy (monitoring land cover type change, deforestation and land degradation). The lack of P-band means that

applications like monitoring secondary re-growth (in the higher biomass range) and primary forest degradation could not be done accurately by spaceborne SAR. There may be no reason to assume that accuracy degrades significantly when observations at different bands are made a few days apart, except for incidental large soil moisture variations or flooding events. Hence, in the near future, combinations of single band SAR systems may appear to be a good alternative.

3. BIOPHYSICAL FOREST TYPE CHARACTERIZATION IN THE COLOMBIAN AMAZON BY AIRBORNE POLARIMETRIC SAR

3.1. INTRODUCTION

Primary and secondary tropical forests are on the agenda of scientists, politicians and land managers for different important reasons. (1) They comprise a major part of the planet's plant and animal biodiversity. (2) They have an important role in the global hydrological and biochemical cycles. (3) They are considered to be an important sink of atmospheric carbon. (4) They cover a large part of the tropical areas and are an important source of agricultural land. (5) The knowledge on the spatial distribution of its resources is limited.

During the past decade research activities on the development of the application of synthetic aperture radar (SAR) for monitoring ecosystem processes has grown significantly. Its potential use can be categorised broadly as follows: (a) classification and detection of change in land cover; (b) estimation of woody biomass; (c) monitoring the extent and duration of inundation; and (d) monitoring other temporally-dynamic processes [Kasischke *et al.*, 1997].

To fulfil information needs, accurate mapping and monitoring is required at different scales. Severe cloud cover often prevents the acquisition of optical remote sensing data, thus making the (additional) use of satellite radar remote sensing necessary for monitoring applications. At the other hand, radar data may provide different or additional information, thus making (the additional use of) radar data (both spaceborne and airborne) an interesting choice, also for less timeliness-demanding applications such as inventory [Hoekman, 2001].

In recent years many research activities focused on the use of SAR to study tropical rain forest. At continental scale mosaics of all tropical rain forests have been created using JERS-1 SAR images [Siqueira *et al.*, 2000; Rosenqvist *et al.*, 2000] and, for Africa, using ERS-1 [De Grandi *et al.*, 1999]. At a larger scale researchers have focused their studies on the development of inversion algorithms, segmentation and classification techniques for polarimetric and interferometric SAR images and created a variety of types of tropical rain forest classifications [Oliver, 2000; Hoekman and Quiñones, 2000; Hoekman and Varekamp, 2001; Varekamp and Hoekman, 2001]. In addition new models for the decomposition of polarimetric signals of forest vegetation were developed [Freeman and Durden, 1998]. An overview of decomposition theories was presented by [Cloude and Pottier, 1996].

In this paper the utility of multi-band polarimetric airborne SAR for tropical forest inventory is evaluated by analysing experimental data collected by NASA's AirSAR airborne radar system. Tentatively, it may be assumed that such a system may fulfil information needs related to the mapping of forest types and the assessment of biophysical characteristics at a scale of 1: 50,000 or larger.

Research conducted at the well-surveyed *Araracuara* test site of the '*Tropenbos*' foundation, a forest reserve in the Colombian Amazon, may provide new insight into radar inventory methodologies and capabilities. The first maps of this area were made in 1979 using X-band radar data acquired during the PRORADAM campaign [PRORADAM, 1979]. ERS-1 SAR image time series (1992) and data of high resolution airborne SAR were collected during the ESA-SAREX (1992) campaign [Hoekman, 1997]. In May 1993, the AirSAR system collected fully polarimetric C-, L- and P- band data [NASA, 1993]. These studies were facilitated by detailed inventory and extensive field observations in the period 1986-1991 resulting in a very detailed ecological landscape unit map [Duivenvoorden and Lips, 1991], which is described in the next section. Moreover, additional experience with analysis of (1993) AirSAR data was obtained at another *Tropenbos* test site, a colonisation area at the border of Colombian Amazon in the district *Guaviare* [Hoekman and Quiñones, 2000]. The methodology presented in this paper is largely based on the latter experience.

In this paper the polarimetric classification technique introduced in [Hoekman and Quiñones, 2000] is exploited to assess AirSAR's potential for forest structural type mapping, forest flooding mapping and forest biophysical characterisation. After the description of test site (section 3.2) and radar data acquisition experiment (section 3.3), field observations are discussed (section 3.4). The latter observations were made to obtain additional quantitative descriptions on forest structure and ground surface conditions, but also for assessment of the suitability of map legends utilised in the landscape ecological map. It will be shown that for classifications produced with SAR a new type of legend, based on a physical description of the wave-object interaction, leads to better interpretable results in terms of biophysical characterisation (section 3.5). The next step is the step from legend to classification. Problems related to radar data, such as speckle, texture and relief, and to classification aggregation, including drainage patterns, forest gradients and complexes, are discussed. A method based on iterated conditional modes [Besag, 1986] is introduced and is shown to yield radar-derived classifications with a high level of agreement with the landscape ecological map, as well as with ground observations (section 3.6). The third and final step discussed in this paper is the assessment of the relation between physical forest structure and polarimetric signal properties. Polarimetric decomposition techniques are briefly reviewed. A new method is introduced based on decomposition of polarimetric coherence, instead of power. It will be shown that various physical relations between polarimetric signal and forest structure can be revealed (section 3.7).

3.2. TEST SITE DESCRIPTION

The Araracuara study area is located in the administrative districts Amazonas and Caquetá in the South East of Colombia. The centred co-ordinates of the study area are $0^{\circ}40'S$, $72^{\circ}15'W$ (Figure 3.1). The general physiography of the region is fairly uniform with little variation in altitude (100 m - 300 m). Landscape-ecological maps of the area (scale 1:100.000), integrating geomorphologic, soil and vegetation characteristics, provide detailed information on the defined landscape units and on forest biophysical characteristics [Duivenvoorden and Lips, 1991].

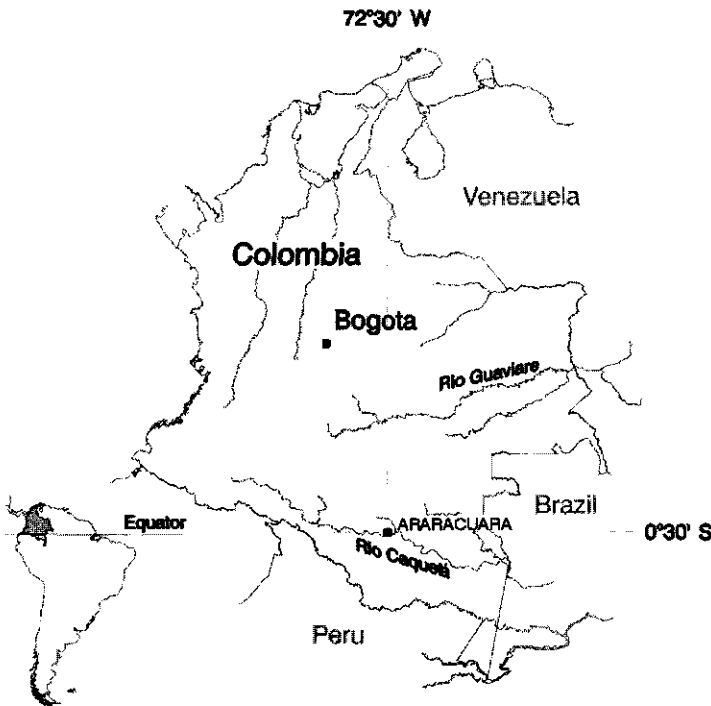


Figure 3.1. The study area is located in the Colombian Amazon, along the Caquetá river, downstream the village Araracuara. The position of this village is indicated.

These maps indicate three main geomorphologic units; the alluvial plain of the Caquetá river, the alluvial plains of Amazonian rivers and sedimentary plains. These units are subdivided into land systems. For example, frequently inundated flood plains, rarely inundated flood plains, low terraces and high terraces are land systems of the alluvial plain of the Caquetá. These land systems are subdivided in land units which are characterised by flooding condition, soil type and forest type cover (Table 3.1). Furthermore, the map summarises forest types with their structural and

physiognomic characterisation (Table 3.2). The vegetation is characterised as a tropical humid forest. High rain forests that can be found on the upland (or *tierra firme*) and on the alluvial terraces and floodplains have a complex structure with emergent trees exceeding 40 m in height and 40 cm in diameter. Terraces and floodplains comprise areas of permanent swampy forest types of varying height and structure and areas that are only seasonally inundated or never flooded. The maximum monthly precipitation occurs in April. The maximum height of the flooding occurs somewhat later, roughly coinciding with the time of image acquisition at the end of May 1993. Yearly river water level fluctuations are in the range of 6-9 m.

Table 3.1. Geomorphological units (underlined), land systems (*italic*), landscape ecological units (**bold**) and vegetation types (in brackets). It is noted that *treelets* are defined as small trees, higher than 2 m, but with a *dbh* smaller than 10 cm. (source: [Duivenvoorden and Lips, 1991]).

<u>Alluvial plain of the Caquetá river</u>		
<i>Frequently inundated flood plain</i>		
Ac	Palm swamp forest of relatively low palm density (low parts) and High forest of high to intermediate biomass and low tree density (high parts)	(P1) (H2)
<i>Rarely inundated flood plain</i>		
Ec	Palm swamp forest of relatively high palm density (low parts) and High forest of high biomass (high parts)	(P2) (H1)
Eb1	Palm Swamp forest of relatively high palm density	(P2)
Eb2	Very low forest of high treelet density	(L3)
Eb3	Open, very low forest with scattered palms	(P4)
<i>Low terraces</i>		
Tp	High forest of high biomass and high forest of intermediate biomass	(H1, H3)
Tb1	Palm swamp forest of relatively high palm density	(P2)
Tb2	Very low forest of high treelet density	(L3)
Tb3	Open, very low forest with scattered palms	(P4)
<i>High terraces</i>		
Hp1	High forest of high biomass and high forest of intermediate biomass	(H1, H3)
Hp2	Very low forest of high treelet density	(L3)
Hp3	Very low forest of high treelet density	(L3)
<u>Alluvial plain of Amazonian rivers</u>		
Cc	High forest of high biomass and high forest of intermediate biomass	(H1, H3)
Ce	High forest of intermediate biomass	(H3)
Cm2	Low forest of very high tree density	(L2)
Dp	High forest of high biomass	(H1)
<u>Sedimentary plains</u>		
Sv	high forest of high biomass and high forest of intermediate biomass	(H1, H3)
Si	high forest of high biomass	(H1)

3.3. RADAR EXPERIMENT

Five AirSAR images [Van Zyl *et al.*, 1992] acquired at 31 May 1993 have been processed, covering an 8 km wide and 40 km long stretch along the Caquetá river. These are in 16-look Stokes scattering operator matrix format with a slant range pixel spacing of 6.66 m in range and around 8.20 m in azimuth. The incidence angle (θ_i) varies from about 20° to 60°.

Detailed field observations were made at 23 plots in the 27°-60° incidence angle range. With the help of the landscape ecological map [Duivenvoorden and Lips, 1991], aerial photography acquired in 1987 and terrain knowledge, a total of 878 additional areas could be delineated, representing 15 classes (see table 3.3, last two columns). These well represent all main forest types and the variation in flooding, drainage and soil characteristics in a 24°-61° range of incidence angles. A database of plot averaged Stokes scattering operator matrix elements was created, which forms the basis for the analysis presented in section 5.

Table 3.2. Biophysical and structural characteristics of vegetation types. H = high forest; L = low forest; P = palm forest. Biomass includes only individuals with a *dbh* ≥ 10 cm (source: [Duivenvoorden and Lips, 1991]).

	Height (m) upper canopy	biomass (tons/ha)	basal area (m ² /ha)	Density(no. / 0.1 ha)			
				treelets	trees	palms	Species
high forests							
(H1)	26	340	36	640	71	4	39
(H2)	22	240	26	570	44	3	26
(H3)	20	190	25	650	71	7	32
low forests							
(L1)	14	130	27	680	117	7	14
(L3)	8	20	7	1700	40	3	10
palm swamp forests							
(P1)	20	250	34	620	92	9	17
(P2)	21	200	29	490	89	27	26
(P4)	6	50	8	1420	12	9	4

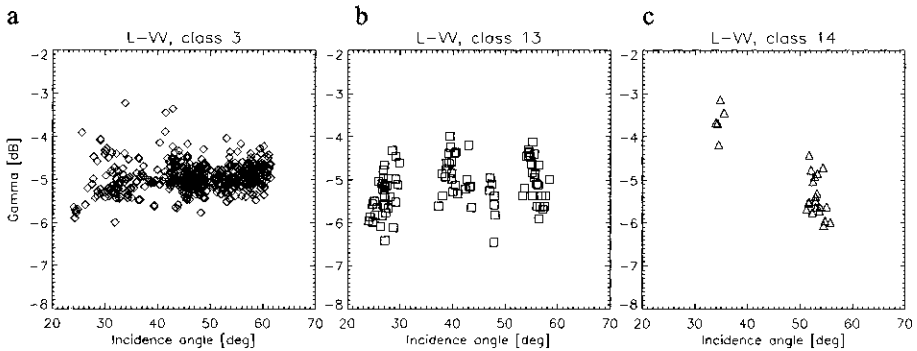


Figure 3.2. L-band VV-polarized plot averaged backscatter as a function of incidence angle, for three examples. a) class 3, b) class 13 and c) class 14.

The incidence angle dependence of the backscatter parameter γ ($\gamma = \sigma^0 / \cos(\theta_i)$; σ^0 is the differential radar cross section) can not be studied well with this data set.

For the dominant forest class (H), a high dense forest on non-flooded terrain, the incidence angle dependence is low for the 25°-60° incidence angle range, for all frequency bands and for HH-, HV- and VV-polarisation. When, for example, the averaged backscatter in the 50°-60° incidence angle range is subtracted from the averaged backscatter in the 25°-40° range, the difference is less than 0.6 dB in all cases. Figure 3.2 shows the L-band HH-polarised backscatter as an example of the low incidence angle dependence for this dominant class. For most of the other classes it is much harder to make firm statements since their areas do not cover a wide incidence angle range. The only exceptions are class 13 and 14 (see table 3.3) for which the backscatter parameter γ decreases considerably in P-band, notably for HH- and VV-polarisation, while for class 14 this seems also the case in the L-band. In these cases, when subtracting the average backscatter of the 50°-60° range from the 25°-40° range the difference is 1.7 dB or more. These signatures are also shown in figure 3.2.

Another point of concern has to be mentioned. For P-band the analysis has been done on modified data. The original data showed a range dependence of the intensity level, which may have resulted from poor calibration for antenna pattern. The same pattern showed up in the Guaviare forest data, collected nearby on the same day, but is far less pronounced. The strong increase of backscatter parameter γ with incidence angle found in P-band Araracuara data, therefore, seems to be an artefact. A range dependent intensity correction function was derived from the angular dependency for the forest on average, excluding the river and some large areas of flooded forest with very high backscatter, thus flattening the P-band angular dependence for the dominant classes considerably. It is noted that this step does not affect polarimetric phase difference and coherence, or influences the classification results which are to be discussed later.

The field averaged Stokes scattering element data of the database are used to calculate unbiased field averaged values for backscatter, phase differences and correlation. The complex correlation between the HH- and VV-returns can be computed from elements of the Stokes scattering operator as:

$$\rho = |\rho| \exp(i\phi) = \frac{\langle S_{hh} S_{vv}^* \rangle}{\sqrt{\langle S_{hh} S_{hh}^* \rangle \langle S_{vv} S_{vv}^* \rangle}} \quad (3.1)$$

This complex correlation (or coherence) ρ can be written as the sum of a real part and an imaginary part (e.g. see figure 3.6) or can be described with an amplitude $|\rho|$ and a phase ϕ , which are also known, respectively, as coherence magnitude and polarisation phase difference (PPD). For a homogeneous area i the averaged polarimetric (hh-vv phase difference) coherence magnitude is denoted here as $|\rho_i|$.

The accuracy of the estimation of field averaged values depends on the total number of independent looks N . Inspection of the single-point statistics and the range and azimuth auto-correlation functions of large homogeneous pastures in AirSAR images (of the Guaviare site) revealed an effective number of approximately 14 looks per pixel for all bands. Spatial correlation would decrease this number further by approximately 30% for C- and L-band and 60% for P-band.

The number of pixels for plots in the Araracuara data set varies considerably as a result of the necessity to include a fair number of small plots to represent rare forest types adequately. For the 23 field-work plots, all are in excess of 50 pixels and 10 are in excess of 100 pixels. For the 878 additional areas, 856 are in excess of 50 pixels and 729 in excess of 100 pixels. For none of the classes a significant fraction of the plots is less than 50 pixels. For 100 pixels the number of independent looks N is 980 ($100 \times 14 \times 0.7$) in C- and L-band and 560 ($100 \times 14 \times 0.4$) in P-band. For 50 pixels these numbers are 490 and 280, respectively.

For such large numbers of independent looks N , for homogeneous fields these averages can be regarded as accurate estimations of the underlying values. The standard deviation of the backscatter follows from [Hoekman, 1991; eq.27] and is less than 0.260 dB for $N > 280$. The standard deviation of the phase difference decreases with $|\rho_i|$ and follows from [Tough *et al.*, 1995; eq.69]. It is less than 4.19° for $|\rho_i| = 0.5$ and $N > 280$. The standard deviation of the coherence decreases with $|\rho_i|$ and follows from [Touzi *et al.*, 1999; eq.26]. It is less than 0.051 for $|\rho_i| = 0.5$ and $N > 280$. The estimation of $|\rho_i|$ is biased, however is negligibly small for such large values of N .

To the authors' best knowledge an analytical expression for the joint distribution of phase and coherence magnitude can not be found in literature. A numerical approach was taken to calculate confidence intervals for the complex coherence, based on the complex Wishart distribution. Confidence intervals of 50% and 90% are graphically shown in Figure 3.3 for 14-look and 280-look samples, for a phase difference of 45° , and $|\rho_i|$ values of 0.1, 0.5 and 0.9. Note that this figure clearly illustrates the above-mentioned: estimation of coherence magnitude and, notably, phase, is harder for low values of $|\rho_i|$.

3.4. FIELDWORK AND LEGEND

Additional fieldwork for this research was made in early 1998. Since the test area is primary forest in steady state, and no major disturbances occurred since 1993, changes can be assumed to be negligible in a statistical sense. The fieldwork was designed to capture the variation found in the landscape ecological map as well as in

the radar data. Consequently, selected plot locations cover a wide range of forest structure and flooding conditions. Detailed measurements of structural and physiognomic characteristics were made at 23 plots of primary forest, each 1,000 m² in size. In each plot two different transects were measured. Within the first transect of 100 m x 10 m all trees with a diameter at breast height (*dbh*) in excess of 10 cm were included, and measurements were made, among others, on the *dbh*, tree height, height to the first living branch, life form (tree, palm or liana), leaf size etc. Within the second transect, located inside the first transect and 50 m x 2 m in size, all plants with a *dbh* less than 10 cm and a height larger than 2 m were included. By measuring both types of transects the variation in the canopy as well as in the undergrowth is well sampled. Graphical illustrations are shown in Section 3.7. For each of these plots, but also along tracks from the river to the plots, observations were made of flooding condition, drainage and soil type.

The radar images show a lot of thematic variation, however this variation is not always reflected well in the variation shown on the landscape ecological map. Partly this is a consequence of the aggregation level of the map. For example, small units (mostly units of rare types) are not shown and complexes of long small structures with different forest types in the floodplain, the so-called 'bar complexes' are shown as separate aggregated classes. Within a single mapping unit, differentiation in the radar image can occur because of flooding (at the time of image acquisition) or soil type. The latter, for example, related to the depth of the peat layer. On the other hand, mapping units, which are clearly distinct, floristically or geologically, but are not distinct in terms of biophysical characterization, are not discernible on the radar images.

Eventually a new legend could be developed which appeared to be suitable for radar image classification and which can be linked to the units of the landscape ecological map. This legend is shown in table 3.3 and is a result of trial-and-error using the classification simulation technique introduced in [Hoekman and Quiñones, 2000] as an exploratory tool. The proposed legend for AirSAR data derived classifications is divided in three parts. The central part is a column showing landscape ecological units (see also table 1). At the right the associated forest types (Classification level 7) are shown (see also tables 3.1 and 3.2). The left part is a hierarchical division in associated biophysical parameters. In the legend proposed here the flooding state is the most dominant classification level (Level 1), followed by drainage type (Level 2), soil type (Level 3), cover type (major vegetation type) and structural type (Level 6) (refined level vegetation type). Though this hierarchical division is closely linked to the physics of radar scattering, this may not always be very obvious. To give an example. P-band backscatter level is related to biomass but relations are non-linear and big trees (i.e. large *dbh*) relatively contribute more. Thick peat layers are too soft to support big trees. Consequently there is a relation between peat layer thickness and backscatter level, even in case biomass levels not differ much, which is mediated by the absence of big trees. It is apparent from the table that there is no unique one-to-one relationship between the landscape units of the map and the 'radar' legend. Levels 1, 2 and 3 can be aggregated from Level 6 or can be made

directly. Also Level 7 (the forest types: 8 classes) may be aggregated from Level 6 (the 'radar' structural types: 15 classes), however some confusion between the high forest types (H1, H2 and H3) will remain.

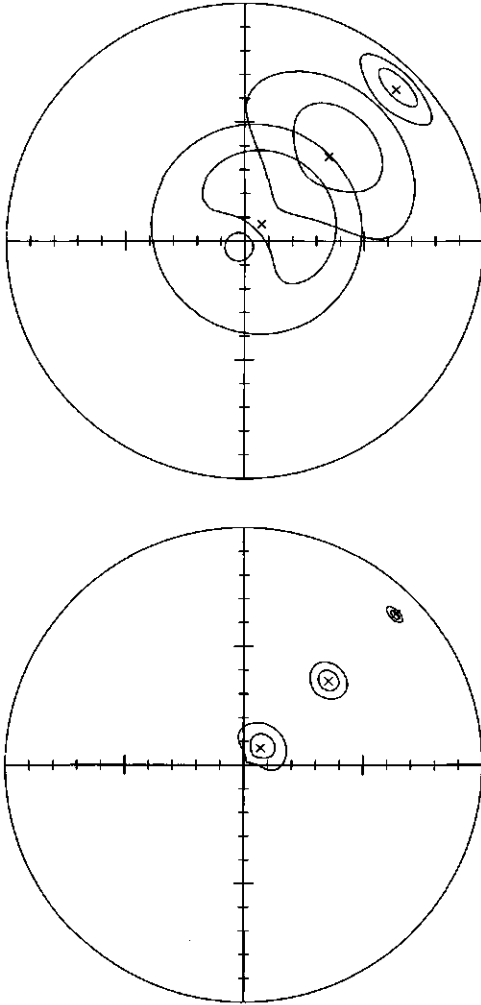


Figure 3.3. Confidence intervals for the complex coherence at 50% and 90% for (left) 14-look and (right) 280-look samples, for a phase difference of 45° , and $|\rho_i|$ values of 0.1, 0.5 and 0.9. The intervals are drawn within the unit circle of the complex plane

Table 3.3. Proposed legend for classification levels 1, 2, 3, 6 and 7 for classification of AirSAR polarimetric data in the study area, the number of training areas (*N*) for each of the classes of Level 6, and the class Code number. (see colour plate 6).

	Flooding	Soil	Cover type	Structural type	Land- scape unit	Forest type		
Level 1 2 classes	Level 2 3 classes	Level 3 8 classes		Level 6 15 classes		Level 7 8 classes	<i>N</i>	Code
Flooded	Permanently flooded or wet	Peat	Palm forest (peat)	P2 (peat)	Ec, (Eb1)	P2	36	11
				P4 (peat)	Tb3, (Eb3)	P4	22	12
			Low forest (peat)	L3 (peat)	Tb2, (Eb2)	L3	89	13
		Thin organic deposit	Palm forest	P2	Cb1	P2	36	14
		Thin organic deposit and peat	Palm forest	P2	Tb1	P2	36	7
		Thick H horizon	Low forest	L3	Hp2, Hp3	L3	18	15
		Hydrous and thin organic deposits	Palm forest (flooded)	P1 (flooded)	Ac	P1	10	6
		Hydrous organic deposits	Palm forest (flooded)	P4 (flooded)	Eb3	P4	18	8
				Low forest (flooded)	L3 (flooded)	Eb2	L3	9
			L2 (flooded)	L2 (flooded)	Cm2	L2	18	10
	Sporadically flooded			Thin H horizon	High forest (flooded)	H3 (flooded)	Ce	
		H2 (flooded)	H2 (flooded)		Ac, Ec		-	
		H1, H3 (flooded)	H1, H3 (flooded)		Cc		20	16
	Non-flooded	Never flooded	Thin and thick H horizon	Primary high forest	H2, (or H1, H3)	Ac, Ec	H2, (H1, H3)	114
H3					Ce	H3	11	2
H1, (or H3)					Hp1, Tp, Dp, Sv	H1, (H3)	431	3

3.5. CLASSIFICATION SIMULATION

The accuracy of classification results can be simulated as a function of the number of independent looks using the techniques introduced in a previous paper [Hoekman and Quiñones, 2000]. This previous paper describes a fully polarimetric multi-band approach to classification and introduces probability density functions (pdf) for multi-look samples of a certain class, for intensity, phase difference as well as coherence magnitude. Since the theoretical pdf's introduced were shown to be in good agreement with the experimental data, and the same type of data is used here (same sensor, same flight and nearby forest), it is assumed that the same method can be applied without need for modification.

The database of averaged Stokes scattering elements introduced in section 3 contains data for 878 delineated areas. These areas can be grouped according the legend introduced in section 3.4. In this way five levels are defined. Level 1 is the 'flooding' level and has 2 classes, Level 2 is the 'drainage' level and has 3 classes, etc. When, for example, a classification simulation for the Level 6 legend is made for samples of 144 looks the confusion matrix given in table 3.4 results. The overall result is 71.8%. When this is done for all five classification levels, at speckle levels corresponding to 64 looks, 144 looks and a very large number of looks, the overall results given in the top section of table 5 are found.

Table 3.4. Confusion matrix for classification of the Structural Type Classification (Level 6) using a 95% confidence interval for classification (class UC contains the unclassified pixels) and using the 144-looks simulated data set. Results are shown in percentages, and only in case these are larger than 2%.

	11	12	13	14	7	15	6	8	9	10	17	16	1	2	3
UC	7.7	10.9	4.6	3.6	4.2	3.9	3.0		4.0	7.2	2.0	4	2.6	3.6	6.5
11	57.2	5.0	5.1	5.6	11.9		8.0						2.2		
12		44.5		2.5											
13		4.5	72.4										4.8		
14	6.4	13.6	4.3	58.6		2.8							10.9		
7	4.7	12.3			70.0			5.6			6.0				
15				2.5		89.4									
6	10.6			2.8			86.0				3.0				
8		2.3			3.3			92.2							
9				5.8					89.0					7.3	
10				2.2	2.8					88.3	10.0	2.5			
17	4.2			3.6			2.0				70.0				
16										3.3	7.0	88.0			
1	4.2	3.2	6.3	7.8					4.0				64.9	3.6	7.1
2													2.0	83.6	9.6
3	2.2			2.2								4.5	4.6	7.3	73.4

The overall classification result of 71.8% is shown in the top section of table 3.5, where it is compared with the overall values for the other classification levels. These values are often higher, which is not surprising considering the lower number of classes. Of course the results are better when no speckle is present and are worse for

the 64 looks case. Another way of looking at the results is shown in the middle section of this table. Here the averaged confusion between pairs of classes is shown. This measure is defined as (see also [Hoekman and Quiñones, 2000]) the average confusion of all class pairs. The confusion of a class pair (*a*, *b*) is the number of samples of class *a* classified as class *b* plus the number of samples of class *b* classified as class *a*, classified in the absence of other classes, as a percentage of the total number of class *a* and *b* samples. The expected value for maximum confusion therefore is 50%. This measure is independent of the number of classes and gives a better impression of the suitability of a certain legend. For example, when there are 100 samples of class *a* and 200 samples of class *b* this could result in 60 samples of class *a* classified as *a* and 40 wrongly classified as *b*. Of the 200 samples of class *b*, 180 could be classified as *b* and 20 wrongly as *a*. In this numerical example the confusion of pair (*a*,*b*) would thus become (40+20)/(100+200) or 20%. For Level 6 the average confusion is clearly lower than for the other levels. Given the hierarchical structure of the levels it could be beneficial to aggregate all other classification levels from Level 6 instead of creating them directly. The lower section of the table illustrates this for the case of 144 looks data. In all cases the overall results improve, notably for Level 2 and 3.

Table 3. 5. Simulated overall classification results in percentages for all classification levels using a 95% confidence interval. Results are shown at three speckle levels: 64-looks, 144-looks and 'no speckle' (top section of table). The average confusion between two classes is shown in the middle part of this table and the overall classification results after aggregation from Level 6 is shown in the lower part.

	Level 1	Level 2	Level 3	Level 6	Level 7
Overall classification result					
64 looks	84.3	79.7	72.6	63.8	66.0
144 looks	85.0	81.2	76.7	71.8	71.6
no speckle	84.2	82.5	82.9	84.3	81.3
Average confusion in absence of other classes					
64 looks	9.7	9.1	7.8	4.5	5.8
144 looks	8.2	7.8	6.1	3.1	4.3
no speckle	6.7	6.4	3.2	1.2	2.4
	Level 1	Level 2	Level 3	Level 6	Level 7
Overall classification result aggregated from Level 6					
144 looks	87.6	86.7	82.0	71.8	73.4

3.6. IMAGE CLASSIFICATION, VALIDATION AND AGGREGATION

The creation of a classified image as well as the evaluation of the classification results, in general, are not very straightforward tasks. This may be particularly true for the complex structure of the tropical rain forest. Some points of consideration are the occurrence of many rare types of forests (table 3.6), absence of well-defined boundaries and presence of gradients between forest types, presence of complexes of forest types (section 3.4) and presence of *chagras*, small areas of shifting cultivation along the river. In the previous two chapters it was shown that 15 classes can be

defined on the basis of carefully selected training areas. Moreover, theoretically, pure samples of these 15 classes can be differentiated well, even at speckle levels of 144 looks (table 3.5). In real images the presence of speckle, texture, relief and drainage patterns may have a strong influence on the classification results. When not accounted for, the results can be significantly lower than for these theoretical cases. For example, when 3x3 pixels are aggregated to create samples of 95 (C- and L-band) and 66 (P-band) looks the overall result is only 50.5%, while a simulated result of 63.8% for 64 looks was obtained (table 3.5).

Table 3.6. The estimated relative occurrence of units in percentages of the total study area. These numbers can serve as an additional prior in the extended ICM method.

Classes	Rel. Occ.
1-2	10%
3	60%
6-15	1%
16-17	5%

To mitigate such 'averse' conditions encountered in real images, or to utilize these as potential sources of additional information, image processing techniques can be applied. However, because of the complexity of the scene, it was found that many of the commonly applied techniques fail to a large extent. For example, image segmentation techniques [Oliver and Quegan, 1998] are not very appropriate because of the absence of well-defined boundaries between many forest types. Texture analysis seems only partly useful because of the limited image resolution of approximately 10 m. Almost all types have a 'medium' type of roughness, while only the high forest type H2 along the river (class 1) has a 'rougher' texture, most likely caused by the presence of *chagras*. Also the relief poses problems resulting in many classification errors in the sedimentary plain. Application of relief detecting algorithms such as the ones proposed by Shuler *et al.* [1996, 1998] seem to capture most of the relief, however, also confuse the rough forest structure caused by *chagras* in the flat floodplain with the strong relief areas of the sedimentary plain. In the next part of this section the Iterated Conditional Modes (ICM) method [Besag, 1986] will be briefly introduced. It will be shown that a new approach, combining ICM with several types of *a priori* information, can yield very good classification results.

In [Hoekman and Quiñones, 2000] the likelihood of a pixel i belonging to class c , $li_{i,c}$, is based on the (multi-frequency) radar signal properties in terms of intensities, phases and coherences. The classification of a pixel simply is the selection of the class for which $li_{i,c}$ is the highest (the Maximum Likelihood or ML solution). In the ICM method the likelihood $li_{i,c}$ is modified to $mli_{i,c}$ by multiplication with a conditional probability $\exp(\beta u_{i,c})$, where $u_{i,c}$ is the current number of neighbours of pixel i having class c , and β is a parameter determining the relative importance of neighbourhood information. In the approach adopted here the eight surrounding pixels form the neighbourhood. Now the classification of a pixel is changed by

selecting the class for which the modified likelihood $mli_{i,c}$ is the highest (the ICM(1)-solution). Usually a number of cycles of ICM is required to reach a stable solution, and usually it is better to start with a lower value of β . By relaxing the value of β to the final value, more and more neighbourhood information is used. Note that the process is reversible, i.e. as soon as β would be set to zero again the initial ML-solution is recovered. The logarithmic version of the modified likelihood $mli_{i,c}$ for ICM-cycle n is denoted as

$$\ln(mli_{i,c,n}) = \ln(li_{i,c}) + \beta u_{i,c,n-1} \quad (3.2)$$

For appropriately chosen values of β , the number of cycles and the relaxation scheme, usually determined by trial-and-error, this approach is found to yield major improvements for the classification results. Evaluation of the remaining misclassifications revealed that most of the remaining error is induced by the relief or can be related to the rough texture of the *chagras*. Moreover, the overall accuracy can be increased further by taking the dominance of certain cover types into account. This knowledge can be included by adding additional priors to the (logarithmic version of the) modified likelihood as

$$\ln(mli_{i,c,n}) = \ln(li_{i,c}) + \beta_1 u_{i,c,n-1} + \beta_2 \ln(P_c) + \beta_3 \ln(R_{i,c}) - \beta_4 T_{i,c} \quad (3.3)$$

with

$$T_{i,c} = \text{Min} \left\{ \frac{(t_i - Tm_c)^2}{2Tv_c}, \beta_T \right\}$$

where P_c is the relative occurrence of class c (table 6),
 $R_{i,c}$ is the relief factor for pixel i and class c ,
 $T_{i,c}$ is the texture factor for pixel i and class c ,
 $\beta_2, \beta_3, \beta_4$ are factors defining the relative influence of *a priori* information,
 β_T is a factor defining a threshold for the influence of texture information,
 t_i is the (logarithmic version of) the coefficient of variation (CV) and
 Tm_c, Tv_c are the mean and variance of the CV for class c .

The (logarithm of the) relief factor is set to non-zero only for class 3 pixels in the sedimentary plain. The sedimentary plain (hilly area) was delineated on the radar images by a human interpreter. In future classification exercises this task may be easily automated when InSAR derived DEM's become available. The CV simply is

the standard deviation of the backscatter intensity (in dB) in the C-band Total Power image calculated over a 7x7 pixel window. The factor β_T was arbitrarily set at 1.5 outside the sedimentary plain and at 0 within the sedimentary plain.

Table 3.7a. Confusion matrix for the pixels of the training areas (in %) for the 15 classes of Level 6 after applying 30 cycles of the extended ICM approach. Only values larger than 2% are shown.

	11	12	13	14	7	15	6	8	9	10	17	16	1	2	3
11	70.1		3.4	4.8	10.5		65.1	4.7			3.5		3.5	2.1	
12	7.9	81.9		9.7	2.2	3.7		2.7							
13			92.2	5.4	2.8				30.9				21.6	32.4	3.0
14	2.6		2.5	63.5					14.5						
7	5.8				82.4		4.6								
15						89.3									
6							19.3								
8								91.0							
9									20.9						
10										79.4	2.7				
17				2.7			5.5				77.0				
16				2.2			3.7			20.6	13.3	96.9			
1	7.5			3.7					32.7				72.8	5.5	2.9
2														28.3	
3	3.7	7.9		7.0		5.9					3.5	3.1		31.0	93.7

Table 3.7b. Confusion matrix for the pixels of the validation (fieldwork) areas (in %) for the 15 classes of Level 6 after applying 30 cycles of the extended ICM approach. Only values larger than 2% are shown.

	11	12	13	14	7	15	6	8	9	10	17	16	1	2	3
11	12.8				12.9	---	---								
12		100.			29.0	---	---								
13	7.7		100.	50.0	3.2	---	---						13.6		3.7
14	23.1			0.0		---	---								
7					45.2	---	---								
15						---	---								
6							---								
8	23.1							100.							
9	20.5								---						
10										100.			9.1		
17											---				
16				50.0								100.			
1	12.8				3.2	---	---						77.3		13.4
2						---	---							0.0	
3					6.5	---	---							100.	82.9

It may be concluded that the approach chosen is highly heuristic. Moreover, as yet, it is not clear how the values for the influence factors ($\beta_1, \beta_2, \beta_3, \beta_4$), their relaxation schemes and other factors can be optimised. However, it can be shown that this approach yields major improvements in classification. Because of the limited ground truth available this is done in two ways. First the large set of 878 training areas is used to check the classification results, secondly the small set of 23 fieldwork plots is used for validation. With a set of empirically derived suitable

values for factors (of eq.3.3) and relaxation schemes, the following results were obtained. Table 3.7a is the confusion matrix in percentages resulting after completion of 30 cycles of the extended ICM method. In general good results are obtained, superior to the ones presented for simulation with 144-look data (table 3.5) and with a larger overall result, namely 88.8% (table 3.8) versus 71.8% for the simulation case (table 3.5). Figure 3.4 shows how results develop from cycle to

Table 3.8. Overall classification results for training areas and validation areas for Level 6, and for the other classification levels after aggregation from Level 6, after applying 30 cycles of the extended ICM approach.

	Level 1	Level 2	Level 3	Level 6	Level 7
Overall classification result aggregated from Level 6					
training areas	93.6%	93.2%	88.8%	88.8%	89.0%
validation areas	94.1%	92.6%	76.3%	68.9%	73.7%

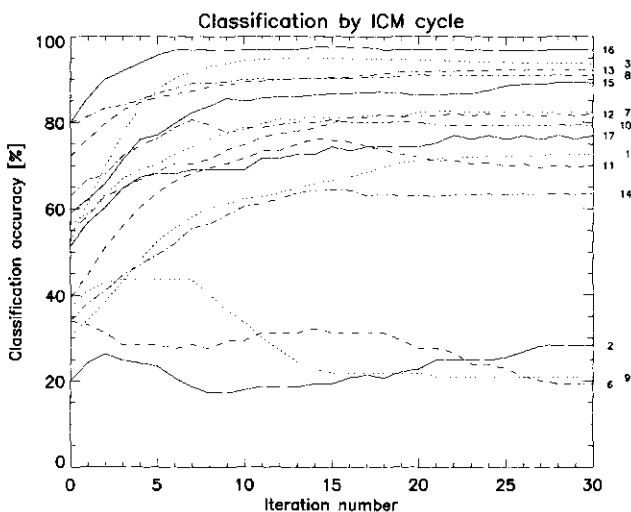
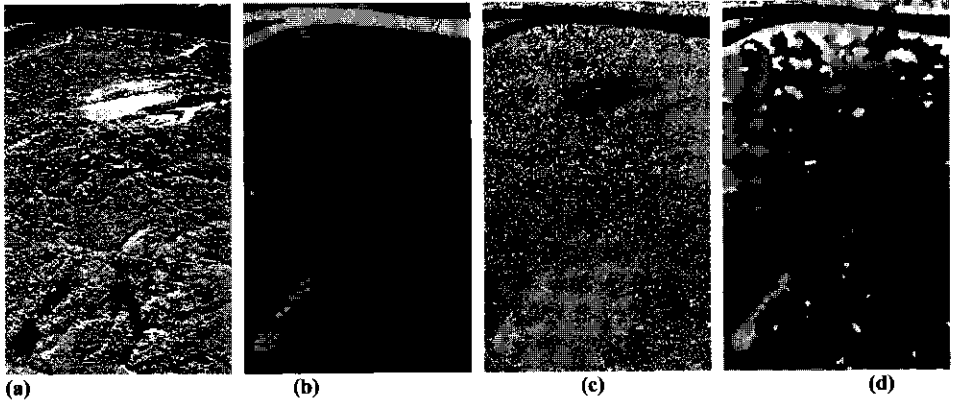


Figure 3.4. Evolution of the percentage well-classified pixels of the training areas for all 30 cycles of the extended ICM approach. The starting value is the ML-solution (denoted as cycle 0).

cycle for each individual class. The starting value is the ML-solution (denoted as cycle 0), with an overall accuracy of 50.5%. For most classes the results improve significantly during the first 10-15 cycles. Table 3.7b is the confusion matrix for the 23 validation areas. Out of the 11 classes 7 show good results (> 77%). Class 2 is completely misclassified as class 3, which has a very similar biophysical characterization. It should also be noted that the landscape ecological map is not free of error and that forest areas which can be very distinct in biophysical characterization are sometimes mapped in the same legend unit. For example for the

plots 14, 15 and 16, all belonging to the class of palm forest on peat soil (class 11) according the landscape ecological map, forest heights of 23, 28 and 28 m and biomass levels of 84, 133 and 172 ton/ha were found, respectively. The overall accuracy is 68.9% (table 3.8). The latter table also shows figures for other classification levels, aggregated from Level 6. These other levels have less classes and, consequently, higher accuracy. As an illustration Figure 3.5 shows a small section of the area as total power image, training areas derived from the landscape ecological map, the ML-classification and the ICM-classification.



Permanently Wet	Peat	Palm Forest	P2	
			P4	
		Low forest	L3	
	Thin organic deposit	Palm Forest	P2	
	Thin organic deposit and peat	Palm Forest	P2	
	Thick H horizon	Low Forest	L3	
	Hydrous and thin organic deposit	Palm Forest	P1	
	Hydrous organic deposit	Palm Forest	P4	
Low Forest		L3		
		L2		
Sporadically flooded	Thin H horizon	High Forest	H3	
			H1, H3	
Never flooded	Thin and thick H horizon	High Forest	H2	
			H3	
			H1	

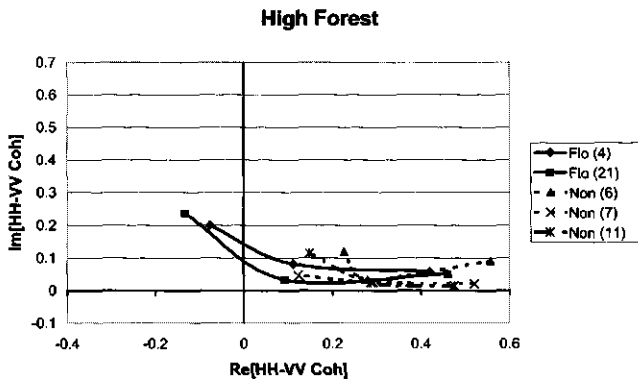
Figure 3.5. A 4.4 km x 5.8 km section of the Araracuara test area showing: (a) total power C-band (blue), L-band (green) and P-band (red), (b) training areas derived from [Duijvenvoorden and Lips, 1991], (c) ML-classification and (d) ICM(30)-classification. The Level 6 colour-codes for (b), (c) and (d) are shown in the legend. (see colour plate 3).

3.7. POLARIMETRIC MODELLING

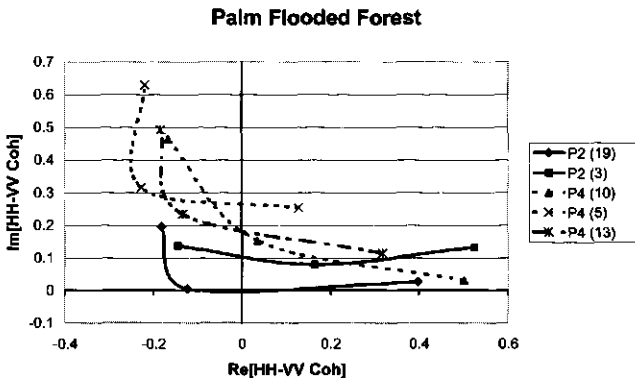
The frequency dependence of the complex coherence shows some characteristic features which may be strongly related to forest structure and which may be described well with existing physical backscatter models. To illustrate this, the

complex coherence values of a selection of the 23 field plots are divided in three groups as shown in Figures 3.6a-c. The curves connect the C-band coherence (in these examples always the right-most point), with the L-band and the P-band value (at the other end of the curve). Figure 3.6a shows high forests on flooded and non-flooded terrain. For the non-flooded cases, with increasing wavelength, the coherence magnitude decreases and the polarisation phase difference (PPD) increases from low values to values typically around 45° . For the two flooded cases the coherence magnitude increases again when moving to P-band and the phase increases to values around 120° . The second set of curves, shown in figure 3.6b, shows the behaviour of flooded palm forests. There is a clear distinction between the palm forest types P2 and P4. In all cases the coherence magnitude increases again when moving to P-band and the phase in P-band is always larger than 90° . The third set of curves, shown in figure 3.6c, shows the behaviour of low forest. Again the flooded and non-flooded behave differently and the coherence magnitude for the flooded plots increase when moving from L- to P-band.

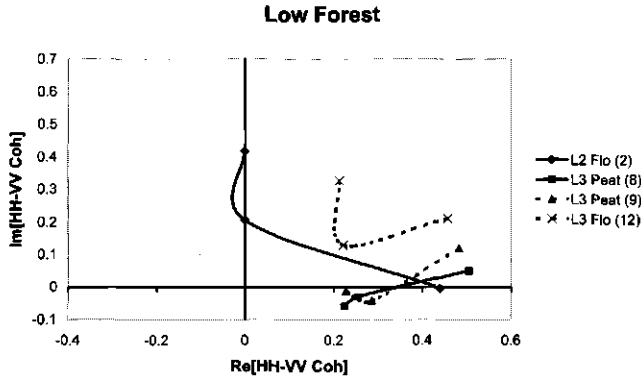
a



b



c



d

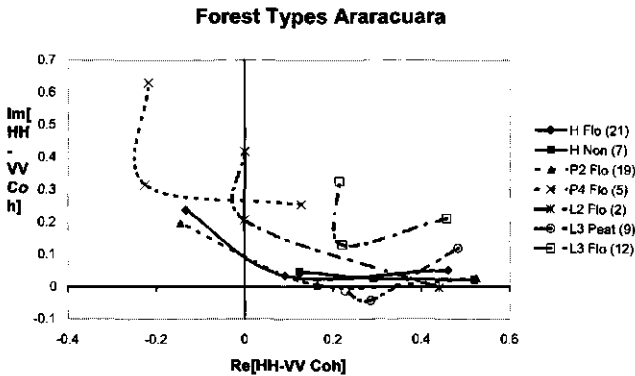


Figure 3.6. Multi-frequency complex coherence curves for (a) high forest, (b) flooded palm forest, (c) low forest and (d) different forest types (see also Figure 7). The curves connect the C-band coherence (in these examples always the right-most point), with the L-band and the P-band value (at the other end of the curve). In the legends plot numbers are shown within brackets, furthermore, H= High forest, P= Palm forest, L= Low forest, Flo= flooded, Non= non-flooded.

The non-flooded low forests, in contrast to the non-flooded high forests, show a general decrease of the phase difference with wavelength. This behavior, given in these examples, is not well described in literature. Figure 3.6d gives an overview for different forest types and Figure 3.7 shows structural drawings for these types.

Ulaby *et al.* (1987) describes the behaviour of the polarisation phase difference in L-band for several agricultural crops. It is hypothesised that the phase difference results from a combination of (1) propagation delay, (2) forward scatter by the soil surface and (3) specular bistatic reflection by the stalks (of corn). Ulaby *et al.* (1987) show that the (phase of the) second term is negligibly small. The first and third term are modelled for a layer of vertical stalks. Rao *et al.* (1995) discuss a very similar model, also for corn, and describe its frequency behaviour for P-, L- and C-band AirSAR data. Neither of these studies includes a description of the coherence of the

phase difference and simply model the total PPD as the sum of the PPD of these three components. A more complete description of the complex coherence will be introduced next.

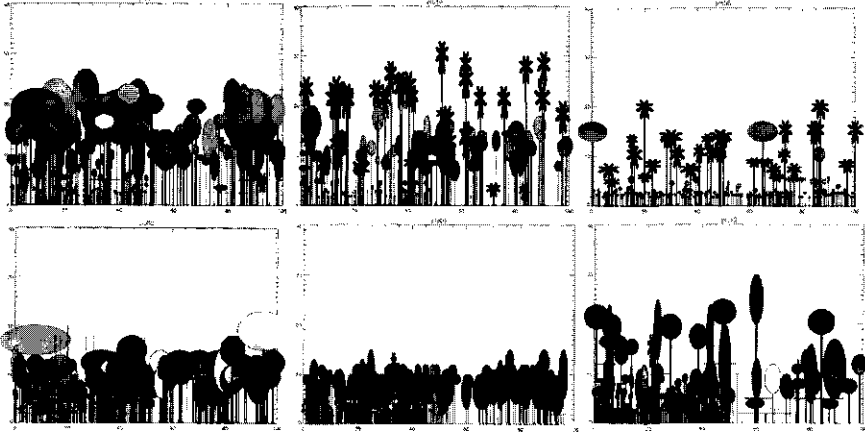


Figure 3.7. Transect drawing of primary forest plot in Araracuara, using a symbolic representation for the structural elements. The spatial units are in meters. Examples are given for plot 7 (H non-flooded), 19 (P2 flooded), 5 (P4 flooded), 2 (L2 flooded), 9 (L3 peat) and 12 (L3 flooded), respectively (compare with Figure 3.6d).

In many backscatter models, notably radiative transfer models, the backscatter is thought of as composed of three incoherent contributions [Ulaby *et al.* 1986, Fung, 1994]. These are (1) the direct backscattering from the vegetation layer, (2) the direct backscattering from the ground attenuated by the vegetation cover and (3) the backscattering originating from the ground-trunk interaction attenuated by the vegetation cover. These are sometimes referred to as the diffuse term, the single-bounce term and the double-bounce term, respectively [Van Zyl, 1989].

Suppose the received electric field can be thought of as composed of these three incoherent terms. Then, for H-polarisation:

$$E_{h,tot} = E_h = E_{h,1} + E_{h,2} + E_{h,3} \quad (3.4)$$

and the estimation of the HV cross-product follows as:

$$\begin{aligned} \langle E_h E_v^* \rangle &= \langle (E_{h,1} + E_{h,2} + E_{h,3}) (E_{v,1}^* + E_{v,2}^* + E_{v,3}^*) \rangle \\ &= \langle E_{h,1} E_{v,1}^* \rangle + \langle E_{h,2} E_{v,2}^* \rangle + \langle E_{h,3} E_{v,3}^* \rangle \end{aligned} \quad (3.5)$$

Similarly,

$$\langle E_h E_h^* \rangle = \langle E_{h,1} E_{h,1}^* \rangle + \langle E_{h,2} E_{h,2}^* \rangle + \langle E_{h,3} E_{h,3}^* \rangle \quad (3.6)$$

The following (power or backscatter) fractions can be introduced

$$h_1 = \frac{\langle E_{h,1} E_{h,1}^* \rangle}{\langle E_h E_h^* \rangle}, \quad h_2 = \frac{\langle E_{h,2} E_{h,2}^* \rangle}{\langle E_h E_h^* \rangle} \quad \text{and} \quad h_3 = \frac{\langle E_{h,3} E_{h,3}^* \rangle}{\langle E_h E_h^* \rangle}. \quad (3.7a,b,c)$$

Note that $h_1 = \frac{\sigma_{hh,1}^0}{\sigma_{hh}^0}$ and that similar expressions can be given for h_2 and h_3 and

for the V polarisation as v_1 , v_2 and v_3 . The polarimetric coherence ρ_{hhvv} of the HH and VV signals follows as:

$$\frac{\langle E_h E_v^* \rangle}{\sqrt{\langle E_h E_h^* \rangle \langle E_v E_v^* \rangle}} = \frac{\langle E_{h,1} E_{v,1}^* \rangle + \langle E_{h,2} E_{v,2}^* \rangle + \langle E_{h,3} E_{v,3}^* \rangle}{\sqrt{\langle E_h E_h^* \rangle \langle E_v E_v^* \rangle}}, \quad (3.8)$$

which will be denoted as

$$\rho_{hhvv} = \rho_{hhvv,1} + \rho_{hhvv,2} + \rho_{hhvv,3} \quad (3.9)$$

The first component can be written as

$$\rho_{hhvv,1} = \frac{\sqrt{\langle E_{h,1} E_{h,1}^* \rangle \langle E_{v,1} E_{v,1}^* \rangle}}{\sqrt{\langle E_h E_h^* \rangle \langle E_v E_v^* \rangle}} \frac{\langle E_{h,1} E_{v,1}^* \rangle}{\sqrt{\langle E_{h,1} E_{h,1}^* \rangle \langle E_{v,1} E_{v,1}^* \rangle}} = f_1 r_1 \exp(i\phi_1) \quad (3.10)$$

where

f_1 = the relative strength of the vegetation layer. Note that

$$f_1 = \sqrt{h_1 v_1} = \sqrt{\frac{\sigma_{hh,1}^0}{\sigma_{hh}^0} \frac{\sigma_{vv,1}^0}{\sigma_{vv}^0}}$$

r_1 = the HHVV coherence magnitude of the vegetation layer

ϕ_1 = the HHVV coherence phase of the vegetation layer

Similarly

$$\rho_{hhvv,2} = \alpha f_2 r_2 \exp(i\phi_2)$$

Polarimetric Data for Tropical Forest Monitoring

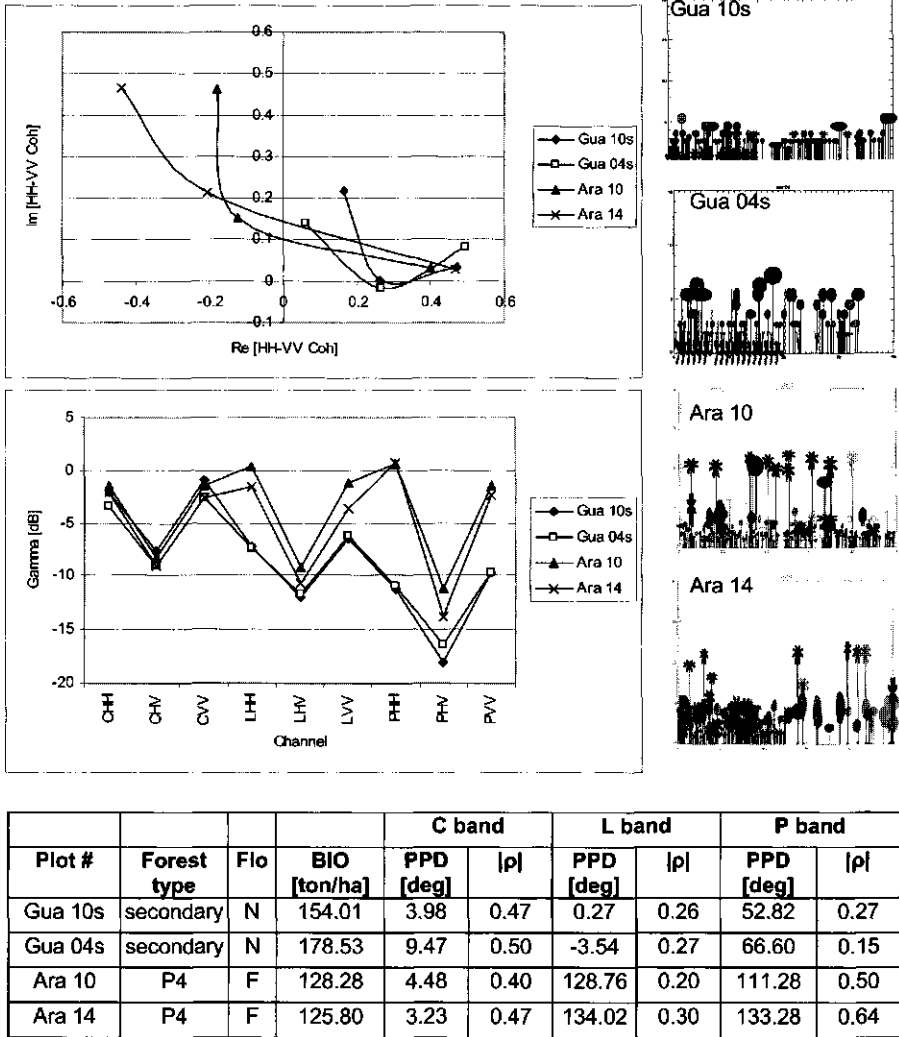


Figure 4.2. Multi-frequency complex coherence signatures and intensity signatures for low biomass non-flooded secondary forest plots (Gua 10s and Gua 04s) and low biomass flooded palm forest P4 (Ara 10 and Ara 14). The table in the figure presents information on the plot number, forest type, flooding condition (F = Flooded, N = Non-flooded, P = Peat), biomass estimated from field data, polarimetric phase difference (PPD) and polarimetric coherence magnitude $|\rho|$ of C, L and P-bands. Structural profiles illustrate the forest types. Vertical scale of the profiles is 0 to 40 m. Horizontal scale is 0 to 100 m.

Another example of plots with similar structure and flooding conditions are presented in Figure 4.2. In this case the plots of Guaviare correspond to non-flooded low-biomass secondary re-growth areas and the Araracuara plots correspond to flooded palm low-biomass forest (P4). The signatures of the plots of similar structure have the same pattern. The biomass levels between the sites are not exactly the same but it is noticeable that, as expected, the intensity signatures of the

Araracuara flooded plots for the L and P-band are much higher than the signatures registered for the non-flooded plots of Guaviare. In the Guaviare plots PPD increases with the wavelength but not exceeds 60° and the $|\rho|$ values are below 0.5. For the Araracuara plots the PPD increases with the wavelength and $|\rho|$ is much higher for P band.

For an effective comparison between the complex coherence signatures between plots and sites, it would be ideal to calculate the confidence interval of the complex coherence of the three bands for each plot for a certain number of independent looks as explained in Section 3.3 of [Hoekman and Quiñones, 2001]. Such calculations are out of the scope of this paper. Here it is intended to analyse tendencies and not to prove differences between classes. It is expected to derive some preliminary conclusions that will serve in the future as the base for a more detailed study, especially concerning the physical explanation of the different interactions.

4.5. RESULTS

4.5.1. Direct approach using empirical relationship with backscatter

The potential for biomass class mapping was studied by evaluating the backscatter for 5 fields of pasture, 10 fields of secondary forest re-growth and 13 fields of primary forest for which biomass was estimated. For these fields the above ground fresh biomass was found to vary over the range of 2.9-10 ton per hectare (1 ton = 1,000 kg; 1 ha = 10,000 m²) for pastures, 6-159 ton/ha for secondary forest and 137-297 ton/ha for primary forest. Since biomass varies over several orders of magnitude, radar intensity values γ_i (in dB) were fitted to the logarithm of biomass (x) using a log-log functional relationship of the form γ_i [dB] = $a \exp(bx) + c$. The main results are summarised in Table 4.2. For the C-band the correlation is not very high. The maximum value for r^2 is 0.66 and was found for the VV-polarisation. For L-band with HV-polarisation and for P-band high values are found. However there are some differences: L-band with HV-polarisation has a high correlation but the signal tends to saturate at high biomass levels. For P-band the saturation appears at higher biomass levels, however the *SEE* (Standard Error of Estimate) is higher. The combination of these bands can be used to improve overall results for the whole biomass range under study. Averaging backscatter of P-band with RR-polarisation and L-band with HV-polarisation, for example, results in a slightly higher correlation (r^2 is 0.94) and a considerably lower *SEE*. The ratio of the total range of backscatter and the *SEE* for this particular combination is high, namely 13.2. This number may be interpreted as 6.7 times 1.96 standard deviations or, in other words, at least 6 classes of biomass may be distinguished at the 95% confidence level. (This should be interpreted as the confidence level for the real class being not more than one class away from the estimated class). Also, since biomass values of the savannah, beyond the lower end of the range shown here, and biomass values of higher biomass primary forest (at other test sites) beyond the higher end of the

range shown here, seem to obey this functional relationship well, it is believed that up to 8 biomass classes may be discerned using this particular approach.

Table 4.2. Relationship between backscatter, expressed as γ_i [dB], and biomass expressed as log10 of the above ground fresh biomass in ton/ha, for several frequency and polarisation combinations. The correlation coefficient r^2 , the standard error of estimate (*SEE*), the total range of γ_i of the experimental data and the ratio of range and *SEE* are shown for the field measured plots in the two study sites.

Guaviare	r^2	SEE [dB]	range [dB]	Range [dB]/SEE [dB]
C-HH	0.32	0.41	3.2	8.0
C-HV	0.62	0.33	3.2	9.6
C-VV	0.66	0.51	4.8	9.5
L-HH	0.81	1.07	9.3	8.7
L-HV	0.93	1.05	11.6	11.0
L-VV	0.78	0.83	7.7	9.3
P-HH	0.90	1.39	11.1	8.0
P-HV	0.94	1.70	16.1	9.5
P-VV	0.91	0.82	9.6	11.6
P-RR	0.93	1.23	13.2	10.7
(L-HV+P-RR)/2	0.94	0.93	12.3	13.2
Araracuara				
C-HH	0.07	1.21	7.4	6.1
C-HV	0.09	0.92	3.6	3.9
C-VV	0.03	1.06	5.0	4.7
L-HH	0.20	1.92	13.8	7.2
L-HV	0.60	1.04	10.3	9.8
L-VV	0.16	1.67	11.9	7.2
P-HH	0.25	2.98	20.3	6.8
P-HV	0.69	1.53	13.9	9.1
P-VV	0.19	2.20	14.2	6.5
(LHV+PRR)/2	0.36	1.67	13.2	7.9

Using the functional relationships between biomass and the average backscatter of the L-HV and P-RR bands a map of biomass classes can be created. This was done for eight arbitrarily chosen biomass classes, namely: (1) ≤ 3.42 , (2) 3.42-4.72, (3) 4.72-6.85, (4) 6.85-10.7, (5) 10.7-18.5, (6) 18.5-38.1, (7) 38.1-109 and (8) > 109 (in ton/ha). Classes 2 until 7 correspond to equidistant values of backscatter separated at 1.96 standard deviation intervals as indicated in Figure 4.3.

It is difficult to validate the accuracy of these results since acquiring a sufficient number of additional biomass values is a huge task. The consistency between biomass classification and land cover type classification can be checked, however. Table 4.3 shows for each land cover class (excluding recently cut areas) the distribution of biomass classes as a percentage of the total area. The agreement with expected biomass ranges is high for all three land cover types.

For the Araracuara site the correlation coefficients are much lower in general than for Guaviare (Table 4.2). The maximum value of r^2 is only 0.69 and is found for P-

HV. All other values are lower than 0.6, including the (L-HV + P-RR) sum which was the best for the Guaviare site and was used for biomass mapping of this site [Hoekman and Quiñones, 2000].

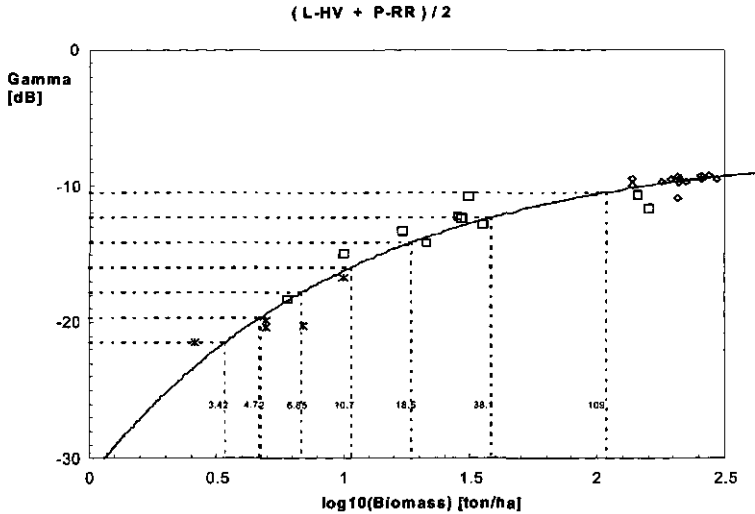


Figure 4.3. (PRR+L HV/2)-polarisation average as function of biomass for the Guaviare site. The biomass is the fresh weight above ground biomass (in tons/ha) at the logarithmic scale (i.e. 1.0 is 10 ton/ha, 1.5 is 31.6 ton/ha, etc.). Experimental data for primary forest (\diamond), secondary forest (\square) and pasture (*) are fitted to a curve of the form $y[\text{dB}] = a + b(1 - \exp(-cx))$, where x is the logarithm of the biomass.

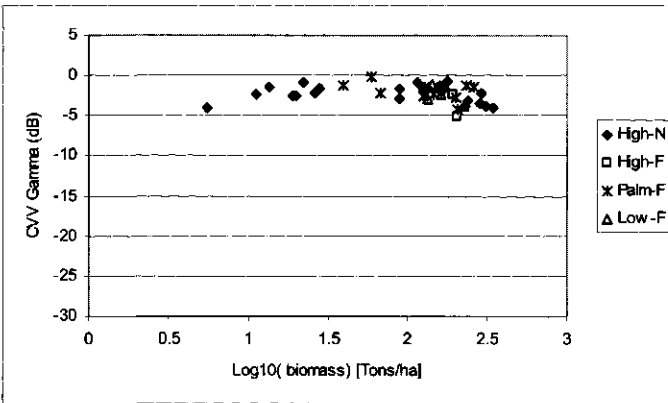
In addition the range/SEE ratio values for Araracuara are much lower than for Guaviare. Apparently this approach, which was successful for the Guaviare site, leads to poor results for the Araracuara site. Scatter plots for Araracuara showing the relation between biomass, radar signal (for several bands and polarisation) and main cover type reveal the underlying causes for these poor results (Figure 4.4).

Figures 4.4a-d show results for C-VV, L-HH, P-VV and P-HV, respectively. A distinction is made between high non-flooded forests (H1, H3), high flooded forests (H2), palm flooded forests (P1, P2, P4) and low flooded peat forests (L2, L3). For C-VV (Figure 4a) the correlation and the range/SEE ratio are very low (see Table 2). Not any clear relationship can be observed. For L-HH (Figure 4.4b) these numbers are higher: the ratio is 7.2 and the correlation is 0.20. In this case there is a slight relation with biomass, however there is also a clear dispersion between samples of different forest types and flooding conditions. For the P-VV (Figure 4.4c) the ratio is 6.5 and the correlation is 0.19. In this case the dispersion between samples of different forest types and flooding conditions is even higher than for the L-HH case. For P-HV (Figure 4.4d) the best results are found with a ratio of 9.1 and a correlation of 0.69. Although less dispersion of the data is observed, the saturation is reached very early, around 1.5 (or 31.6 ton/ha).

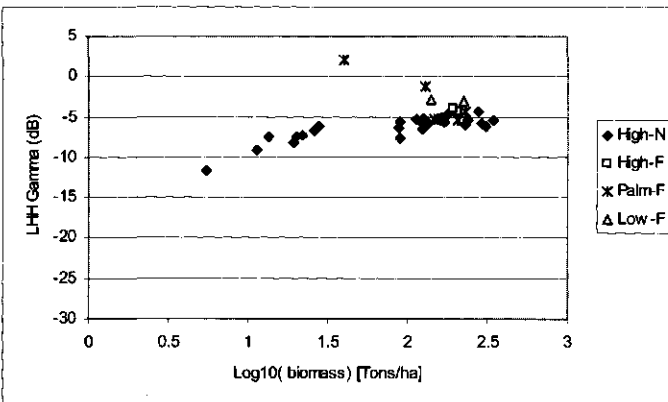
Table 4.3. Percentages of areas corresponding to the classification of the four main land cover types and the eight biomass classes. The land cover types are encoded as: (1) Primary forest, (2) Secondary forest, and (3) Pastures.

Biomass (ton/ha)	Cover types		
	1	2	3
0-3.42	0	0	16
3.42-4.72	0	0	18
4.72-6.85	0	1	23
6.85-10.7	0	3	20
10.7-18.5	1	12	12
18.5-38.1	2	28	6
38.1-109.	12	40	3
>109.	84	14	1

a



b



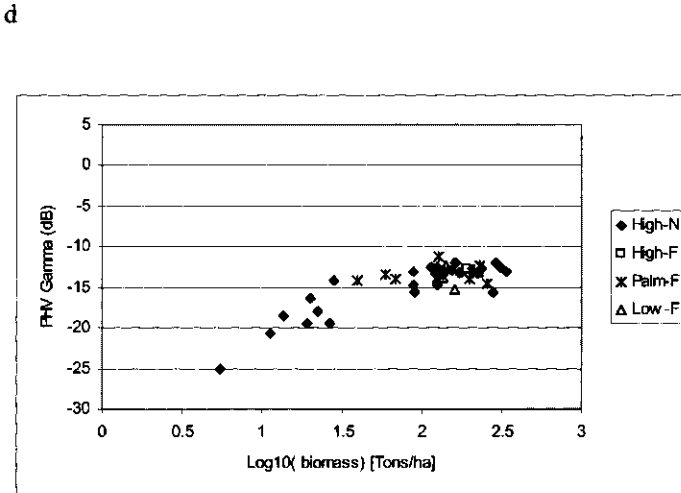
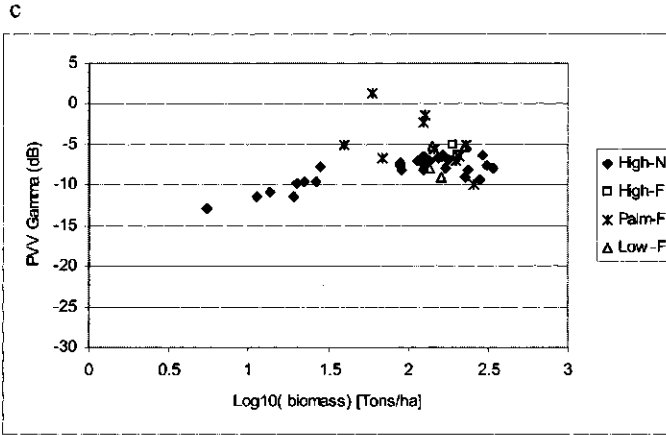


Figure 4.4: Scatter plots between the estimated biomass in plots of different structure and the corresponding intensity value expressed in Gamma (dB). The biomass is the fresh weight above ground biomass (in ton/ha) at the logarithmic scale (i.e. 1.0 is 10 ton/ha, 1.5 is 31.6 ton/ha, etc.). Experimental data for different forest structures according to Table 1: High N= High non flooded forest (H1, H3), High F = High flooded forest (H2), Palm F= Palm flooded forest (P1, P2, P3, P4), Low F = Low flooded or peat forest (L2, L3).

The fact that different forest types of very low biomass (P4 and L3) can be confused with high biomass forest types due to the early saturation of the backscatter intensity level will certainly have large effects on the accuracy of the biomass map, in case such a simple relation is applied. For that reason the possibility of using the structural forest type map, already available for the Araracuara site [Hoekman and Quiñones, 2001], to create a biomass map, was considered as a possible solution to

overcome the saturation and the confusion produced by the effect of forest structure and flooding condition.

4.5.2. Indirect approach using forest structural type classification

In the previous paper [Hoekman and Quiñones, 2001] it was shown that the radar classification of 15 structural forest type classes has a high level of agreement with the landscape ecological map [Duivenvoorden and Lips, 1991] maps and the ground data. When the 878 reference areas from the landscape ecological map are used for deriving training samples and a fully polarimetric maximum likelihood classification (of the C, L and P-band data) is followed by the technique of iterated conditional modes [Besag, 1986] an accuracy of 88.8 % is obtained. An independent validation for the 23 ground data collection areas yielded an accuracy of 68.9%, which is still very high for 15 classes. Of course, when these 15 forest structural classes are aggregated into 8 biomass classes even higher accuracy can be expected. The C, L and P-band total power image, the forest structural type map and the resulting biomass map and the legends were produced for the 5 scenes available for the Araracuara site.

In this paper an analysis is made of the possibilities for biomass mapping for reduced radar data sets, for example for single frequency band data. To this aim the technique of classification simulation is used as introduced in [Hoekman and Quiñones, 2000]. This technique predicts classification accuracy as a function of combinations of frequency bands, polarisation and speckle level. From the analysis presented in [Hoekman and Quiñones, 2001] it can be concluded that realistic predictions can be made solely on the basis of the averaged values of the elements of the Stokes scattering operator for these 878 reference areas.

Table 4.4. Defined biomass classes in ton/ ha for the area of Araracuara (see also Table 1)

Biomass class [ton/ha]	Forest Type
20	L3
50	P4
140	L2
190	H3
200	P2
240	H2
250	P1
340	H1

Through re-labelling and aggregation of the 15 forest structural type classes into 8 biomass classes (Table 4.1 and 4.4) and by comparing the thus predicted biomass level with the biomass level shown on the landscape ecological map a confusion matrix results. Such a confusion matrix is shown in graphical form in Figure 6a. Here each column shows the relative confusion (in %) of one biomass class (or level) with the other 7 classes (or levels). Classifications percentages are represented in the figure by the surface size of the circles. The average value for results on the diagonal (the correct classifications) is 94.6% (Table 5). Consequently, the simulated accuracy for biomass mapping using the complete full polarimetric C, L and P-band data set is very high, and higher, as expected, than the number of 88.8% found for the mapping of the 15 forest structural classes (of [Hoekman and Quiñones, 2001]). In this case the SEE between the estimated and the real biomass class of the training areas is calculated to be 32.6 tons (Table 4.5).

Table 4.5. Overall accuracy of biomass classification for different combinations of bands and polarisation. Results are presented as the averaged percentage of correct classification of a biomass class. The standard error of estimate (SEE) is calculated as the estimated biomass level and the biomass level as shown on the landscape ecological map. Using Kappa statistics and stating that combination (2) is the best spaceborne option for forest structural type classification, then only combination (3) is not significantly worse at the 95% level of confidence than combination (2). Stating that combination (12) is the worst spaceborne option for forest structural type classification, then only combination (11) is not significantly better at the 95% level of confidence than combination (12).

	Bands	Radar System	Biomass Map	
			% of well classified classes	SEE (ton/ha)
1	C pol, L pol, P pol	AirSAR	94.6	32.6
2	C pol, P pol	RADARSAT-2 + P pol	84.7	53.0
3	L pol, P pol	ALOS PALSAR + P pol	79.0	62.7
4	C pol, L pol	RADARSAT -2 +ALOS PALSAR	82.0	67.7
5	C intensity, L pol	ENVISAT+ALOS PALSAR	78.7	73.3
6	P pol	P pol	75.4	68.0
7	P intensity		78.9	70.9
8	L pol	ALOS PALSAR	60.5	91.7
9	L intensity		59.9	92.1
10	C pol	RADARSAT -2	52.3	119.1
11	L-HH	JERS-1	37.0	121.4
12	C intensity	ENVISAT	39.5	126.4

These figures can be computed for any subset of the radar data in terms of frequency band and polarisation. Table 4.5 gives an overview of the results. The central column links the result with spaceborne radar systems and combinations of systems. Of course this link should be interpreted with care because of differences in spatial resolution, incidence angle or other system or terrain related characteristics.

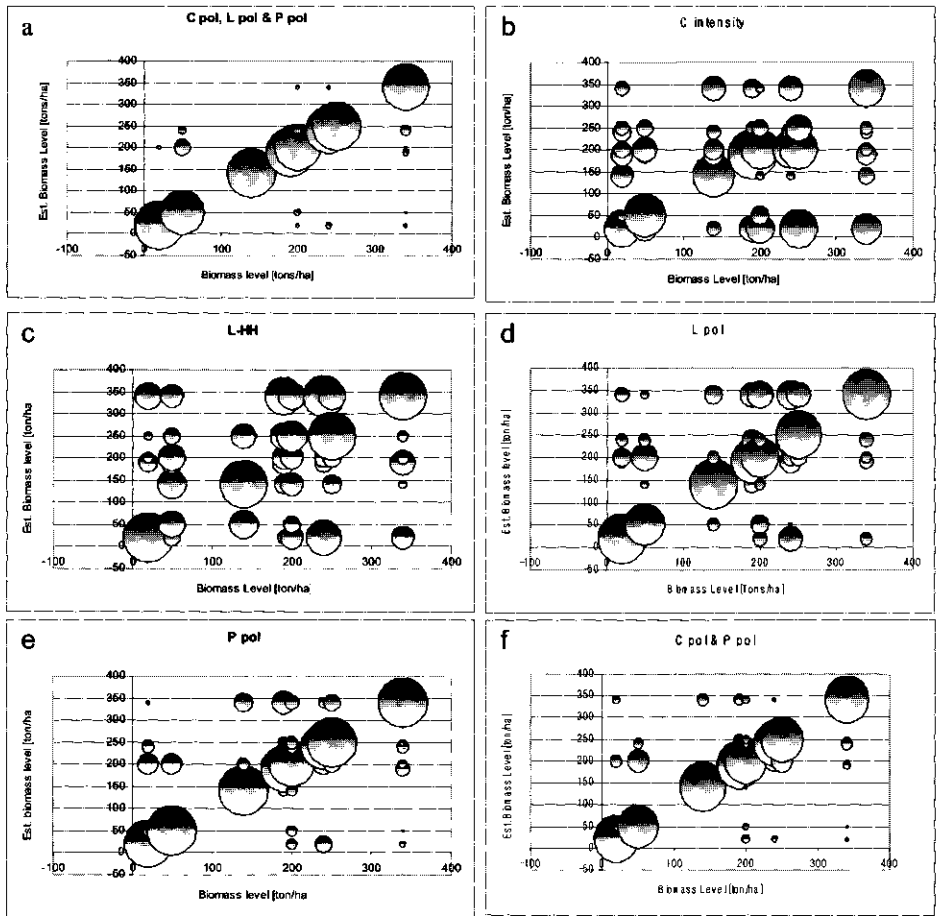


Figure 4.5: Confusion in percentages between biomass levels derived from landscape ecological map and the estimated biomass from the structural classification. Percentages in the diagonal correspond to samples classified in the correct biomass class. Graphs presented for different polarisation-band combinations. C pol = C-band polarimetric data, C intensity = C-HH, C-HV and C-VV intensities.

Excluding the C, L and P-band polarimetric combination (of the AirSAR), the best combinations are C and P- band polarimetric (Figure 4.5.f) and L and P-band polarimetric with results of 84.7% and 79.0% accuracy, and SEE values of 53.0 ton/ha and 62.7 ton/ha, respectively. For the underlying forest structural type classification (from which the presented results are aggregated) these results are not significantly different at the 95% level of confidence (using Kappa statistics, see also [Hoekman and Quiñones, 2000]). The worst combinations are C band intensities (i.e. for HH, VV and HV polarisation) (Figure 4.5b) and L-HH (Figure 4.5c) with results of 39.5% and 37.0% accuracy, and SEE values of 126.4 and 121.4 ton/ha, respectively. For the underlying forest structural type classification these results are not significantly different at the 95% level of confidence.

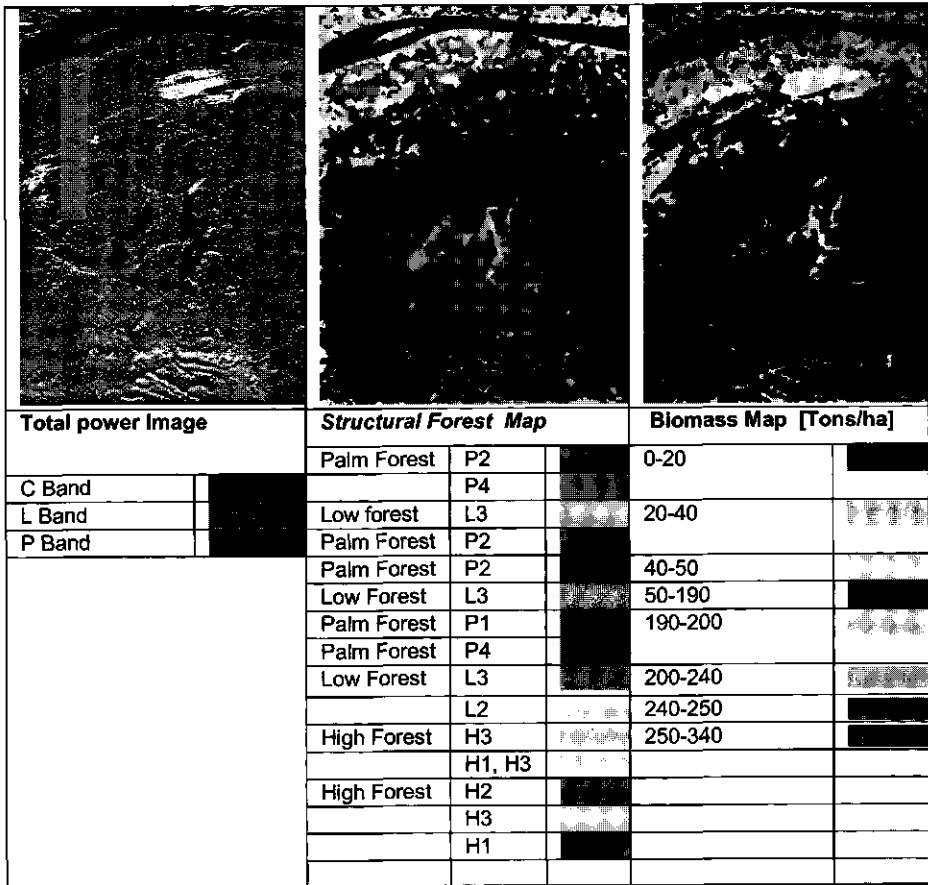


Figure 4.6. AirSAR 336-b scene covering a 5 x 8 km along the Caquetá river in the Araracuara study area. (left) Total power C, L, P-band image, (middle) Forest structural type map (15 classes) and (right) Biomass map (8 classes) (see colour plate 4)

Figures 4.5d and 4.5e illustrate the confusion that could exist if only using L-band polarimetric (ALOS PALSAR) or P-band polarimetric data (recently proposed to ESA for an EEOM biomass monitoring mission). The P-band would perform much better than the L-band. However, combining the P-band with either C or L-band (polarimetric) would even give a still better performance. The classified forest structural map using C L and P band polarimetric data and the corresponding reclassified biomass map is shown in figure 4.6 for one of the scenes of the Araracuara area.

4.5.3. Field data analysis

For better physical understanding of the effects of some terrain characteristics (such as flooding, forest structure and biomass level) on the radar return the multi-frequency linear polarisation signature and the multi-frequency complex coherence signature of the field plot areas were studied. Several specific cases are considered in order to elucidate the direct effect of the parameter on the radar return signal. The effect of flooding is analysed by comparing plots of the same biomass levels and canopy structural conditions in flooded and non-flooded areas (namely plots 11, 7, 4, 21 for high biomass levels and plots 8, 9, 12, 14 for low biomass level). The effect of canopy structure was analysed by studying plots with the same biomass level and flooding conditions with different canopy structure (plots 19, 2, 3, 4 for flooded high biomass areas and plots 12, 14 for flooded low biomass areas). The effect of biomass was studied by analysing plots with similar structure and flooding conditions but with different biomass levels (plots 6, 11, 7, 20 for close canopy high non-flooded forest and 19, 10, 14, 13 for open canopy palm flooded forest).

Changes in intensity are expected to occur as described in the literature, i.e. higher backscatter values where more scatterers of certain size (in relation to wavelength) occur, and higher backscatter in flooded terrain [Hess et al., 1995; Pope et al, 1997]. For the physical understanding of the interaction between the forest and the radar waves, a model of scattering mechanisms (single bounce, double bounce and diffuse scattering) was introduced in the past and image classification of the dominant scattering mechanisms were made [Van Zyl, 1989]. The dominance of a certain scattering mechanism could in some case be related to certain vegetation structures. In a previous paper [Hoekman and Quiñones, 2001] a model is introduced in which values of complex coherence are described as the combined effect of such scattering mechanisms. Pure scattering mechanisms as described by [Van Zyl, 1989] can be located in the complex coherence plane as points or, when including the effect of speckle, as small areas (see also [Hoekman and Quiñones, 2001]). For the complex structure of the tropical forest, pure scattering mechanisms are not expected to occur but it is expected that some patterns in the signatures can be related to specific forest structural characteristics. The intention of this analysis is not to derive definite conclusions but to relate qualitatively the changes in the radar signatures to the influence of specific terrain characteristics.

Effect of flooding

To analyse the effect of flooding two different cases are analysed. The first one compares high mature forest plots (H1, H2, H3) with a similar biomass level that are either flooded or non-flooded (Figure 4.7). In this case the intensity of the flooded plots is 2 dB higher for the L-HH and L-VV intensity and 3 dB higher for the P-HH and P-VV intensity. The PPD for flooded and non-flooded plots show an increase with the wavelength that is stronger for the flooded plots. Consequently it is shown that the signatures of forests with the same biomass level and the same structure can be significantly affected by the flooding of the terrain. Another example is given in Figure 4.8. In this case the same type of forest (L3) is under different terrain conditions. Plots 8 and 9 are located in areas with peat and plot 12 is flooded. In these three plots there is a high density of treelets of small diameter at breast height (*dbh*). In plot 12 there are some larger trees than in the other two plots but statistically and ecologically is still considered a low forest (L3).

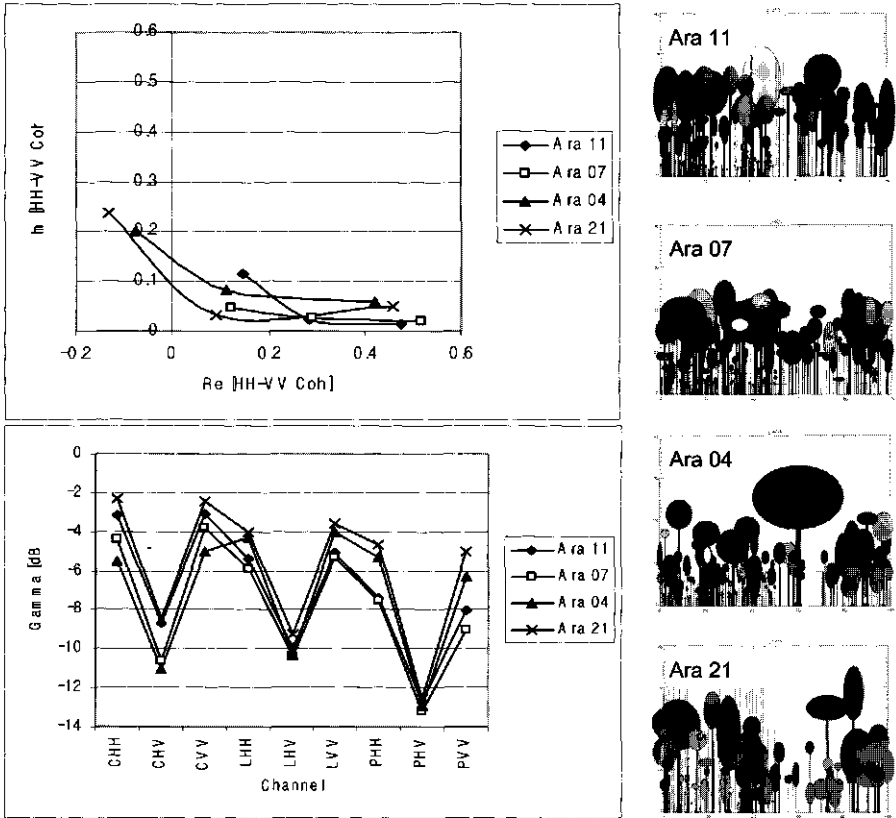
The two plots with peat show lower radar intensity values, especially in the L-HH (3 dB lower) and P-HH channels (5 dB lower). An increase of the PPD for plot 12 can be noticed for all three radar bands and may be related to the flooding condition. It is interesting to note that for the plots with peat there is a decrease of the PPD with increasing wavelength, thus leading to a very characteristic signature. This particular behaviour of the complex coherence signature has never been reported in literature and may be of great importance for mapping and monitoring of tropical peat swamp forest areas, which, even on a global level, are known as important carbon sinks.

Effect of forest structure

To analyse the effect of forest structure for identical biomass levels and flooding conditions two different cases are analysed. Plots 19 (P2) and 2 (L2) both have high biomass levels and are located in flooded terrain (Figure 4.9). Plot 19 has an open discontinuous canopy and many palm trees, which contrasts with the continuous closed canopy without palms of plot 2. The C-HH and C-VV intensities of the open canopy are higher than for the closed canopy forest. The PPD also differs between these plots. For plot 19 the PPD is low for C and L-Band (3° and 2°, respectively) and increased for P band (to 127°). For plot 2 the PPD increases from 0° in the C band to 90° in the L and P-band. It is interesting to notice that for this low forest (plot 2), mainly composed of small *dbh* trees, when changing from L to P-band, the PPD stays the same while the coherence magnitude $|\rho|$ increases. This may indicate that probably both L and P-band penetrate to the forest floor.

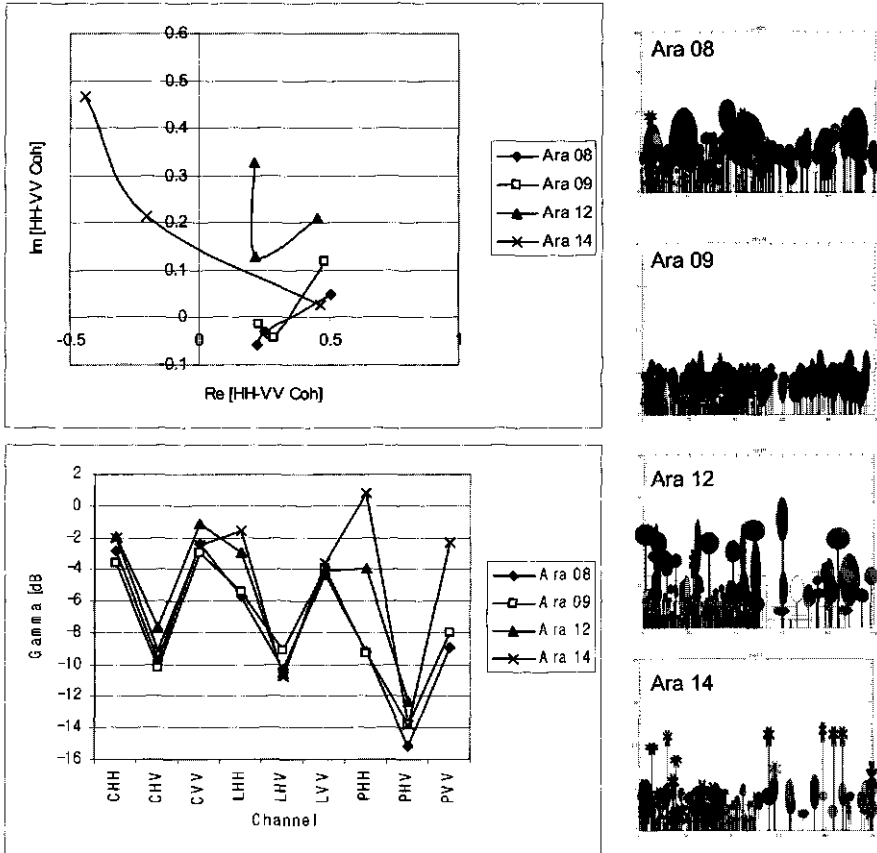
Plots 3 and 4 can also be used to study the effect of structure (Figure 4.9). Both areas have the same biomass level and are flooded. Plot 3 corresponds to a palm forest (P2) with an open discontinuous canopy and plot 4 to a high forest (H3). In the intensity signature the values of both forests are very similar with the exception of the P-HH intensity for which the palm forest exceeds the high forest with roughly 2 dB. In all bands the PPD of the palm forest exceeds the PPD of the high forest. For the C and L-band these almost have the double value, while for the P-band also the palm forest has a much higher PPD value. This may be related to differences in

penetration depth depending on the structural differences of the canopy. In both cases scatter mechanisms like the double bounce are likely to occur. The $|\rho|$ values for L and P-band are low in both cases, which may indicate that diffuse scattering is also an important constituent of the return signal for these bands.



Plot #	Forest type	Flo	BIO [ton/ha]	C band		L band		P band	
				PPD [deg]	$ \rho $	PPD [deg]	$ \rho $	PPD [deg]	$ \rho $
Ara 11	H1-H3	N	237.34	1.69	0.48	4.88	0.29	37.74	0.19
Ara 07	H1-H3	N	227.72	2.33	0.52	4.95	0.29	20.72	0.13
Ara 04	H1-H3	F	205.06	7.82	0.42	36.17	0.14	110.93	0.21
Ara 21	H2	F	192.11	6.33	0.46	20.18	0.10	119.29	0.27

Figure 4.7. Multi-frequency complex coherence signatures and intensity signatures for high forest (H1, H3) in non-flooded terrain (Ara 11 and Ara 07) and flooded terrain (Ara 04 and Ara 21). The table in the figure presents information on the plot number, forest type, flooding condition (F = Flooded, N = Non-flooded), biomass estimated from field data, polarimetric phase difference (PPD) and polarimetric coherence magnitude $|\rho|$ of C, L and P-bands. Structural profiles illustrate the forest types. Vertical scale of the profiles is 0 to 40 m. Horizontal scale is 0 to 100 m.



Plot #	Forest type	Flo	BIO [ton/ha]	C band		L band		P band	
				PPD [deg]	$ \rho $	PPD [deg]	$ \rho $	PPD [deg]	$ \rho $
Ara 08	L3	P	161.38	5.69	0.51	-6.66	0.26	-14.45	0.23
Ara 09	L3	P	135.10	13.91	0.50	-8.38	0.29	-3.27	0.23
Ara 12	L3	F	141.86	24.79	0.50	30.35	0.26	56.97	0.39
Ara 14	P2, (P3)	F	125.80	3.23	0.47	134.02	0.30	133.28	0.64

Figure 4.8: Multi-frequency complex coherence signatures and intensity signatures for low forest (L3) on peat (Ara 08, Ara 09), low forest (L3), flooded forest (Ara 12) and flooded palm forest (P2) (Ara 14). The table in the figure presents information on the plot number, forest type, flooding condition (F = Flooded, N = Non-flooded, P = Peat), biomass estimated from field data, polarimetric phase difference (PPD) and polarimetric coherence magnitude $|\rho|$ of C, L and P-bands. Structural profiles illustrate the forest types. Vertical scale of the profiles is 0 to 40 m. Horizontal scale is 0 to 100 m.

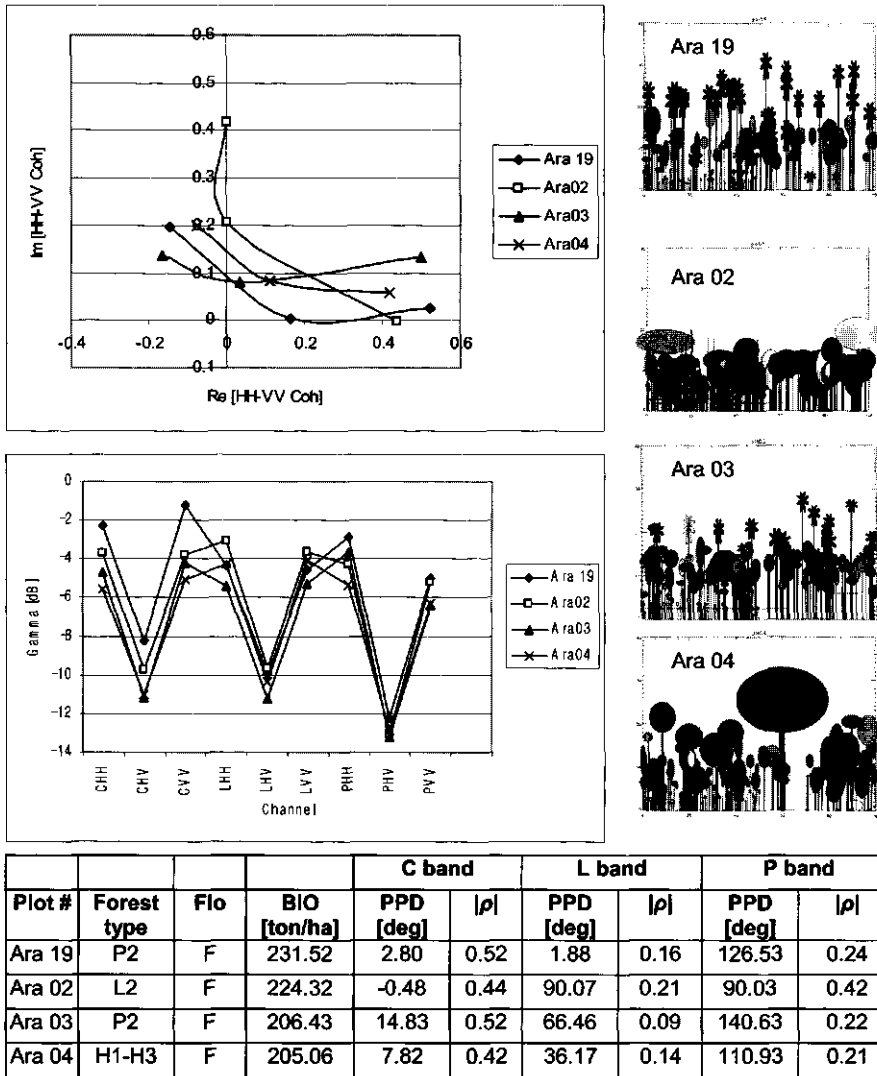
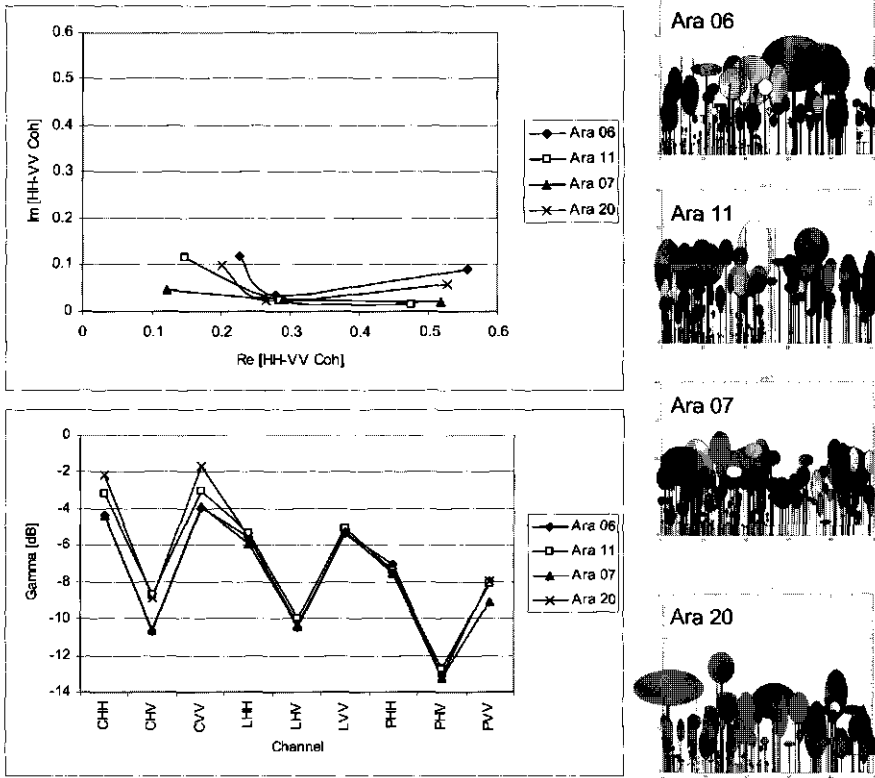


Figure 4.9. Multi-frequency complex coherence signatures and intensity signature for flooded palm forest (P2) in plots Ara 19 and Ara 03, low forest (L2) in plot Ara 02 and high flooded forest (H1, H3) in plot Ara 04. The table in the figure presents information on the plot number, forest type, flooding condition (F = Flooded, N = Non-flooded, P = Peat), biomass estimated from field data, polarimetric phase difference (PPD) and polarimetric coherence magnitude $|\rho|$ of C, L and P-bands. Structural profiles illustrate the forest types. Vertical scale of the profiles is 0 to 40 m. Horizontal scale is 0 to 100 m



Plot #	Forest type	Flo	BIO [ton/ha]	C band		L band		P band	
				PPD [deg]	$ \rho $	PPD [deg]	$ \rho $	PPD [deg]	$ \rho $
Ara 06	H3	N	341.06	9.27	0.57	6.88	0.28	27.81	0.26
Ara 11	H1- H3	N	237.34	1.69	0.48	4.88	0.29	37.74	0.19
Ara 07	H1- H3	N	227.72	2.33	0.52	4.95	0.29	20.72	0.13
Ara 20	H1- H2- H3	N	170.86	6.16	0.53	4.78	0.27	26.26	0.23

Figure 4.10. Multi-frequency complex coherence signature and intensity signature for high non-flooded forest (H1, H2 H3) in plots Ara 06, Ara 11, Ara 07 and Ara 20. The table in the figure presents information on the plot number, forest type, flooding condition (F = Flooded, N = Non-flooded), biomass estimated from field data, polarimetric phase difference (PPD) and polarimetric coherence magnitude $|\rho|$ of C, L and P-bands. Structural profiles illustrate the forest types. Vertical scale of the profiles is 0 to 40 m. Horizontal scale is 0 to 100 m.

Effect of biomass

The effect of the different biomass levels for similar forest types under identical flooding conditions is evaluated with two cases. In the first case four plots of high forest (H1-H3) with closed canopy on non-flooded terrain and with different biomass levels are compared (Figure 4.10). Differences in the L and P-band

intensities are not significant for the studied levels of biomass (i.e. in the 171-341 ton/ha range). The PPD increases with the wavelength for all the plots and no significant differences between these four plots can be noticed.

The second case studies the effect of the biomass level in open palm flooded forest (Figure 4.11). The relative biomass range in this case is much higher than for the previous case (i.e. 40-232 ton/ha) and the effects are noticeable. In the intensity signature the differences in the different band-polarisation combinations are not clearly associated with the biomass level. In the complex coherence plane it is clearly noticeable that the PPD increases with wavelength for all four plots. Also biomass effects are noticeable. In C-band the plot with the lowest biomass has a much larger PPD. In L-band the plot with the highest biomass has a much lower PPD. And in P-band the plot with the highest biomass has a much lower coherence magnitude.

As can be seen from these two examples the effect of biomass on the radar return signal varies with the structure. In a closed canopy forest biomass levels do not seem to have an effect on the signatures, at least within the studied biomass range. For open canopy forest the PDD and coherence magnitude of C, and P band are affected and related to biomass changes.

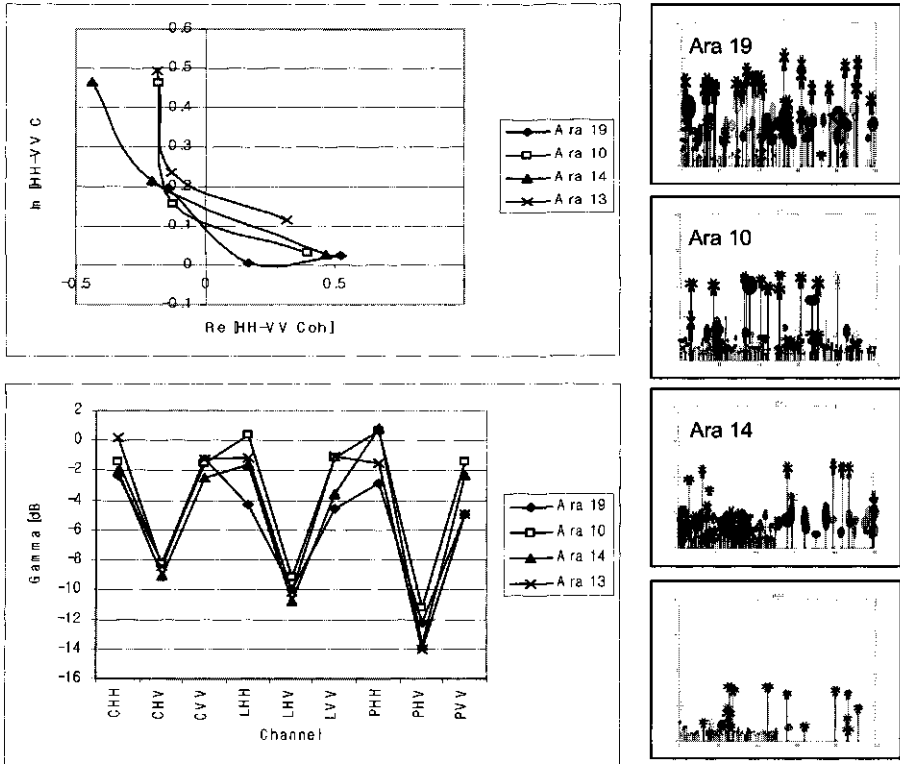
4.6. CONCLUSIONS AND RECOMMENDATIONS

Two algorithms for biomass mapping have been presented in this paper. In both cases the actual estimation of biomass is preceded by a classification step. There are fundamental differences though. The first algorithm, applied on the Guaviare test site, is a maximum likelihood classification followed by application of a single and relatively simple empirical relationship between biomass and backscatter intensity. In this case only two (P-RR and L-HV) band-polarisation combinations are used, which give a high correlation of 0.94, and the relation is applied on three of the four land cover classes (the recently cut areas are excluded).

The use of empirical relationships is constrained by the effect of radar saturation at a certain biomass level, limiting the number of biomass mapping classes. In this case 8 biomass classes could be mapped at a high level of confidence. To check the consistency of the results biomass classes were related to land cover classes. A good agreement was found between the biomass range measured in the field and the estimated biomass ranges for the three land cover classes (i.e. pasture, secondary re-growth, degraded primary forest).

The second algorithm, applied on the Araracuara test site, also includes classifications as a first step. In this case the full polarimetric data set was used for classification resulting in a forest structural type classification with 15 classes. Subsequently biomass levels were associated to each structural class, thus allowing estimation of biomass levels beyond the saturation level.

It should be noted that both biomass maps show broad biomass classes over several orders of magnitude and, thus, are useful for assessment of spatial patterns associated with land and forest degradation and secondary re-growth processes or variation in natural forests.



Plot #	Forest type	Flo	BIO [ton/ha]	C band		L band		P band	
				PPD [deg]	$ \rho $	PPD [deg]	$ \rho $	PPD [deg]	$ \rho $
Ara 19	P2	F	231.52	2.80	0.52	1.88	0.16	126.53	0.24
Ara 10	P2 (P3)	F	128.28	4.48	0.40	128.76	0.20	111.28	0.50
Ara 14	P2, (P3)	F	125.80	3.23	0.47	134.02	0.30	133.28	0.64
Ara 13	P4	F	39.63	19.85	0.34	119.48	0.27	110.40	0.53

Figure 4.11. Multi-frequency complex coherence signatures and intensity signatures for flooded palm forest (P2, P3, P4) for plots Ara 19, Ara 10, Ara 14 and Ara 13. The table in the figure presents information on the plot number, forest type, flooding condition (F = Flooded, N = Non-flooded), biomass estimated from field data, polarimetric phase difference (PPD) and polarimetric coherence magnitude $|\rho|$ of C, L and P-bands. Structural profiles illustrate the forest types. Vertical scale of the profiles is 0 to 40 m. Horizontal scale is 0 to 100 m.

To study the relative influence of different bands and polarisation classification simulation were made for a number of sub-sets of the radar data set. The best overall accuracy for the biomass map using a sub-set was obtained when using C-band polarimetric data combined with P-band polarimetric data. For this combination the percentages of well-classified classes was the highest. The combination of L-band polarimetric and P-band polarimetric data resulted in a lower percentage of well classified classes. In addition for the L and P-band combination the SEE in ton/ha increased with 10 ton/ha with respect to the C and P-band combination. These combinations may be relevant in the near future since they apply to RADARSAT-2 (C-band), ALOS PALSAR (L-band) and the recently proposed ESA EEOM P-band mission.

An analysis of field data appeared useful to increase understanding of specific effects of forest structure, flooding and biomass levels on the physical interaction with the waves. It was shown that forests with similar structures and biomass levels under identical flooding conditions generate similar radar signatures. (1) The effect of flooding depends on canopy structure and biomass level. Closed canopy forests have higher intensity values for HH and VV polarisation for L and P-band when flooded. Flooding also increases the PPD in all the bands but especially in L and P-band. The effect of flooding in open canopy forest strongly depends on biomass level. At lower biomass levels there is a considerable increase in the PPD in the L-band. Another important result is the specific coherence polarimetric signature produced by forest on peat terrain. The negative PPD values for L and P-band distinguishes this type of forest from all other forest types studied. (2) For closed canopy forest, flooded or non-flooded, the biomass level does not affect the radar signatures in a significant way, at least not for the biomass levels studied. For open canopy forest in flooded terrain changes in the complex coherence signature due to changes in biomass level are significant. The PPD increases with the wavelength and with the biomass level for C, L and P- band. For lower biomass levels, the increase in PPD from C to L-band was almost 100°, while for high biomass levels a significant increase of the PPD occurred from L to P-band. This may indicate large differences in canopy penetration depth, especially for the L-band, related to the biomass level.

The effect of forest structure on the radar signature depends on many factors like the height and openness of the canopy, the *dbh* distribution of the trees, the size of the crowns, the leaves, the distribution and size of the branches etc. These forest parameters determine the size and type of scatterers for the radar interaction. In this study forest types of open and closed canopy were compared under the same biomass level and flooding conditions. Other forest parameters are difficult to study experimentally simply because they can not be controlled at the moment of radar acquisition over natural areas. To study such parameters it is necessary to use a more theoretical approach like using backscattering models for specific and controlled forest conditions. This kind of research is being conducted at the moment by the

authors and it is expected to generate more specific data on the effect of the canopy structure, soil moisture and terrain roughness on the signatures of the radar data.

As shown in this paper the sensitivity of radar to forest structure and flooding conditions is large and allows the characterisation of vegetation in two different ways i.e. as vegetation cover types (Guaviare site: 4 classes) and as more detailed forest structural types (Araracuara site: 15 classes). Information needed nowadays for carbon dynamics and climate change studies can benefit from forest structural maps and flooding and peat maps, in which forest dynamics can be recorded. Biomass maps in addition can be created in association with these maps.

The study of the polarimetric radar signatures of different structural forest types in other study sites around the world may contribute to a knowledge based classification system, facilitating mapping of vegetation structures without additional field information. Extension of the actual database of tropical forest including areas in South-east Asia, Africa or Australia will be of great help in understanding the variations of radar signatures with structure and biomass. The creation of forest structural maps and flooding condition maps will be the first product in the classification procedure. Re-classification of the structural types will result in accurate biomass maps.

Biomass mapping may also benefit from additional information supplied by interferometric systems. Topographic mapping and possible forest height estimations will further increase the accuracy in biophysical characterisation.

5. THEORETICAL EXPLORATION OF PHYSICAL LIMITS FOR RADAR BIOMASS INVERSION

5.1. INTRODUCTION

Scientists and policy makers developed a strong interest in data on the amount and distribution of biomass over the earth surface. Most of the currently existing biomass maps may be of very poor quality, however [Houghton *et al.*, 2001]. At present, the largest single source of uncertainty in the global carbon budget, amounting to 1.3 Gigaton carbon per year, is due to terrestrial ecosystems [IPCC, 2001]. The study of the carbon cycle and its influence on processes related to climate change requires different sorts of earth surface observation (monitoring) in order to supply the necessary information on carbon flow dynamics [Quegan and Le Toan, 2002].

In many recent studies the use of radar for biomass mapping and estimation is investigated by applying direct empirical relationships between biomass and radar backscatter signal. However, in general, inversion of radar data for biomass estimation is limited by the variations of backscatter produced by vegetation canopy structural parameters and soil moisture (and terrain flooding) and limited to a certain maximum biomass level dependent on the structural class. Two main conclusions result from previous research. (1) The biomass dependency on radar backscatter varies with radar wavelength and polarisation. (2) The sensitivity of radar return values to biomass change saturates at certain biomass levels. In general it can be said that saturation points increase with wavelength and that HV polarisation is more sensitive to biomass changes [Kasischke *et al.*, 1995; Ranson and Sun, 1994; Rignot *et al.*, 1994]. Saturation level figures of up to 150 ton/ha for P-band and up to 100 ton/ha for L-band are mentioned. In addition theoretical studies have revealed that forest structure and soil moisture conditions affect the radar backscatter giving constraints for direct biomass estimations [Imhoff, 1995].

This paper focuses on the theoretical limits of biomass mapping and is a follow-on paper of three earlier publications focusing on land cover and forest type mapping in the Colombian Amazon [Hoekman and Quiñones, 2000, 2002] and experimental biomass mapping [Quiñones and Hoekman, 2002]. Experimental field and radar data were collected in the framework of NASA's 1993 South American Deployment [NASA, 1993; Van Zyl *et al.*, 1992] at two test sites, namely Guaviare and Araracuara. These test sites, radar data and field data collections were described extensively in these previous papers.

The development of robust radar inversion algorithms for biomass estimations, independent from study site, is still under investigation. Good theoretical modelling and good sets of ground observations are indispensable to further the understanding of the target-wave interaction. Radar is sensitive to the density, size and orientation of the wet above-ground components in a forest (leaves, branches, trunks and root parts). Attenuation along the paths of propagation in the forest canopy diminishes

the influence of components in lower layers (notably trunks) and the influence of the ground surface (notably its roughness and wetness). Furthermore, these effects are strongly dependent on wave parameters such as frequency and polarisation [Le Toan *et al.*, 2002]. It may be obvious from such theoretical considerations that the relationships between radar signals and above ground biomass are not direct. Most approaches developed to date inherently assume such a relationship exists however. An alternative approach, as proposed in [Quiñones and Hoekman, 2002] assumes that in case forest structure can be mapped accurately, as shown [Hoekman and Quiñones, 2000, 2002], an accurate biomass level can be deduced from this structure on the basis of (local) ecological knowledge. It was shown experimentally that all biomass levels present, for the Araracuara site up to 340 ton/ha, could be mapped accurately, and that the so-called 'saturation level' not poses a problem for this inversion approach.

In this paper the latter approach is studied in more depth using the UTARTCAN theoretical backscatter model [Karam *et al.*, 1992] by systematically examining the influence of forest structure, terrain roughness and wetness. This is done in three steps. Firstly, field observations are transformed into a structural description of the canopy using scatterer types, with different dimensions, orientations and densities, for several horizontal layers. A new approach is presented utilising the structural characteristics of different life forms (such as broad-leaved trees, palms, stem forbs, lianas, etc). For this purpose the so-called LIFEFORM interface model was developed, which achieves a fully automated transform (which is based on a large set of assumptions and rules) of field observation data into UTARTCAN input files (section 5.2 A, B, C). Secondly, the UTARTCAN model is validated, for all three-frequency bands of the AirSAR, both for intensity and the HH-VV coherence, using the experimental field data of all 45 plots available. This step will reveal certain weaknesses and limitations of the model, notably for heterogeneous palm swamp forests and certain types of young secondary forests (Section 5.3). For the theoretical exploration of biomass inversion limits only those structures that can be modelled well (by UTARTCAN) have been selected (Section 5.4). The third step is the systematic analysis of the multi-frequency polarimetric radar signatures simulated for a wide range of forest structures, terrain roughness and soil moisture level. Results are discussed in Section 5.5.

5.2. APPROACH

5.2.1. The UTARTCAN Backscatter Model

A polarimetric scattering model for layered vegetation, developed at the University of Texas at Arlington and known as UTARTCAN, was used to describe the microwave backscatter properties [Karam *et al.*, 1992]. This model is based on an iterative solution of the radiative transfer equation up to the second order for multiple scattering within the canopy and between the ground and the canopy. It covers a wide range of frequencies and is applicable to the C-, L- and P-band data of

the AirSAR. The model computes the full polarimetric backscatter coefficients (Mueller matrix), as well as the direct contributions of all scatter classes (branches, leaves and ground surface) and the canopy-ground interaction component to the total backscatter.

The vegetation canopy is described as a layered (up to three layers) random medium of discrete scatterers. Trunks and branches are modelled as cylinders, leaves as circular discs. Each layer contains a number of scatterer types and for each type a density, dielectric constant, dimensions and orientation distribution is specified. Tree trunks are represented as large cylinders with a preferred (vertical) orientation, branches of tree crowns or shrubs are mimicked as a collection of cylindrical shaped scatterer types (e.g. seven types) with different dimensions, densities and orientation distributions. The soil is described as a random rough surface. The soil backscatter properties are modelled using the Integral Equation Method [Fung *et al.*, 1992] and is also applicable over a wide range of frequencies. Soil and vegetation dielectric properties are described through dielectric mixing models [Wang and Schmugge, 1980; Ulaby and El-Rayes, 1987] which require data on soil texture, soil moisture and plant moisture as main input parameters.

For the purpose of this research the UTARTCAN model had to be adapted somewhat to be capable to properly describe the structural complexity of the vegetation for all AirSAR frequency bands. The allowed maximum number of scatterer types was increased from 1 to 10 for leaf type scatterers and from 7 to 20 for branch and trunk type scatterers. The LIFEFORM interface model developed at Wageningen University takes care of a proper translation of the ground truth into input files for the UTARTCAN model [Hoekman *et al.*, 1996]. To get an insight into the assumptions that have to be made in the LIFEFORM interface model the input data required for the UTARTCAN backscatter model will be discussed first in more detail.

The UTARTCAN model requires several types of input data. These are wave parameters, soil surface parameters and vegetation parameters. The soil surface is characterised by 5 parameters. These are, respectively, the rms height variation, the surface auto-correlation length, the volumetric soil moisture content fraction and the sand and clay fractions. The vegetation layer is determined by a number of scatterer classes, which can be distributed over three horizontal layers maximally. The scatterer classes are divided into two main categories: (1) the leaves (up to 10 classes) and (2) the branches and trunks (up to 20 classes). For each leaf scatterer class, information is provided on leaf radius (assuming circular elliptical shape), leaf half-height (a value that is around 1.5e-3 m, typically), leaf moisture content (a value that is around 0.55 for tropical trees, and up to 0.7 for green crops), the scatterer density per cubic meter, and the orientation distribution. Several standard distributions were used [Goel and Strelbel, 1984; Karam *et al.*, 1992]. Branch and trunk structure is modelled in the same way. For branch and trunk (skin) moisture content, typical values of 0.50 and 0.48 are used, respectively.

5.2.2. Field data for model validation

At the two study sites a total of 45 plots were available, with vegetation structures ranging from pastures to different types of tropical primary forest with different types of flooding condition. Slopes in the plots never exceeded 8%. These study sites and the ground data have been described in previous papers [Hoekman and Quiñones, 2000, 2002].

For each individual plant the height, the height of the first living branch, diameter at breast height (*dbh*), life form and leaf size were recorded. The life form description as proposed by Küchler [1988] was adapted for this study as shown in table 5.1. The leaf size was classified according the Raunkiaer-Webb [Webb, 1968] categories as presented by Givnish [1984], with a few minor adaptations in the area limits, as can be seen in table 5.2. Givnish follows Webb in the assumption that leaves are about twice as long as wide and have an area of roughly two-thirds of leaf length times width. In this study it is assumed that leaves have this length width ratio and an elliptical shape. In case of composite leaves (e.g. palms) the area of the leaflets is taken. It is not yet clear whether, in the description of the backscattering process, this is the best approach, and how this depends on radar wavelengths used.

A stratified sampling procedure was developed [Quiñones, 1995]. For most plots of primary forest three types of transects were defined as follows:

- Transect A: An area of 100 m x 10 m in size. In this area all trees with a diameter at breast-height (*dbh*) of at least 10 cm are measured.
- Transect B: An area of 50 m x 2 m in size, centred along the first half of the main axis of transect A. In this area all individuals with a *dbh* less than 10 cm and a height exceeding m are included.
- Transect C: An area of 20 m x 2 m in size, centred along the first 20 m of the main axis of transect A. In this area all individuals with a height less then 2 m are included. Measurements in this transect are limited to life form and leaf size class only.

For secondary forests and low biomass primary forest plots the procedure deviated somewhat. Transect A was not measured because of the low density or absence of trees with large trunk diameter. In case some large trunk diameter trees were present they were simply included in transect B. The size of transect B was changed from 50 m x 2 m into 33 m x 3 m.

To visualise these measurements a symbolic representation scheme was developed. It deviates considerably from the conventional approach to transect drawing as adopted by authors describing forest structure for other purposes [e.g. Oldeman, 1983] but serve the purposes of this study. Table 5.1 shows the symbols used to represent each life form. In the drawing all symbols have a variable height coinciding with the measured total height. The tree crown is drawn between the measured height of the first living branch and the total height. Crown width was

drawn proportional to *dbh*. The shades of grey used to fill the crowns and/or leaves correspond to leaf size class, i.e. the darker the shade of grey the larger the leaf size

Table 5.1. Life form classes adapted from Küchler [1988] with local names and symbolic graphical representation as used in the profile drawings generated by the LIFEFORM interface program. The gray level of the canopy component is an illustration of the corresponding leaf size for each life form , i.e. darker grey levels correspond to larger leaf sizes.

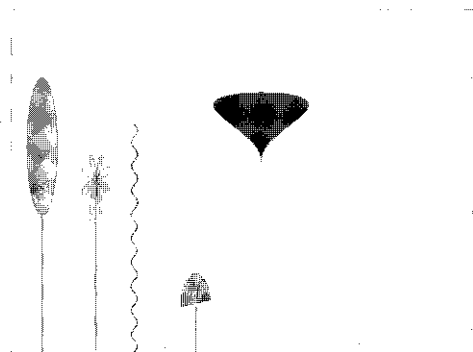


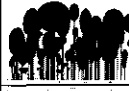
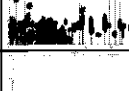
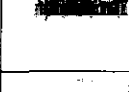
Table 5.2. Original Raunkiaer-Webb categories of leaf size [from Givnish, 1984] and the adapted limits used in this study assuming elliptical shape.

Leaf Raunkiaer-Webb category (code)	Adapted max surface area (cm ²)	Max length (cm)	Max width (cm)
Nanophyll (1)	2.26	2.4	1.2
Microphyll (2)	20.36	7.2	3.6
Notophyll (3)	45.80	10.8	5.4
Mesophyll (4)	183.22	21.6	10.8
Macrophyll (5)	1684.68	64.6	32.3
Megaphyll (6)	none	none	none

The diameter of trunks is indicated by line thickness. With the symbols introduced here transect drawings can be made, as shown in table 5.4.

Forest structural types were defined according to Duivenvoorden and Lips [1991]. Table 5.4 presents a summary of forest structural parameters, flooding conditions and examples of symbolic transect drawings for each forest type. Such drawings illustrate the differences in structure well and can give an indication of horizontal layering and the degree of (in-) homogeneity, in terms of parameters relevant to backscatter modelling.

Table 5.4. Forest types recorded for the measured plots of the studied areas according to the classification given by [Duivenvoorden and Lips, 1991]. An example of a symbolic forest profile as created by the LIFEFORM interface model is shown for each forest type. Treelets are trees with DBH <10 cm and height above 2m.

Forest types	Forest description	Forest profile	Field plot number	Flood condition	Height (m)	Bio (ton/ha)	Basal area (m ² /ha)	density (no. / 0.1 ha)		
								f	T	P
High Forest	(H1)		22, 23, 6	Flooded and non-flooded	26	340	36	640	71	4
	(H2)		1,21,11, 7	Flooded and non-flooded	22	240	26	570	44	3
	(H3)		4, 20, 17 Gua 2-13	Flooded and non-flooded	20	190	25	650	71	7
Low Forest	(L2)		2	Flooded and Peat	11	140	39	2100	246	0
	(L3)		8, 9, 12	Peat	8	20	7	1700	40	3
Palm Swamp Forest	(P1)		15, 16	Flooded	20	250	34	620	92	9
	(P2)		3, 19	Flooded	21	200	29	490	89	27
	(P3)		10, 14	Flooded	16	15	25	1280	99	14
	(P4)		5, 13, 18	Flooded	6	50	8	1420	12	9
Secondary Forest	Old secondary forest		Sec 03, Sec 07	Non-flooded	11	80	30	1720	-	-
	Young secondary forest		Sec 01, Sec 02, Sec 04, Sec 06, Sec 10, Sec 08	Non-flooded	8	25	10	1220	-	-
	Pastures		Sec 05, Sec 09	Non-flooded	2	5	2	190	-	-

5.2.3. The LIFEFORM interface model

To collect data for backscatter modelling three approaches may be followed. The classical approach is the most straightforward one and simply consists of measurements of all parameters used in the description of the microwave interaction process with sufficient statistical accuracy. This approach is common to modelling work of, for example, cultivated crops. For forest plantations this would be far more complicated because of the length of the growing cycle and management practices such as thinning. A practical solution is the use of a tree growth model. The model uses a description of the process of tree growth, under varying conditions, and a description of the tree architecture to generate automatically certain parameters relevant for backscatter modelling such as branch size and orientation distribution as a function of age [e.g. Woodhouse and Hoekman, 2000]. Such a model requires calibration for a certain tree species and climate zone.

For tropical rain forests neither of these two methods is practical. In the first place the complexity is too large. Secondly, i.e. in a statistical sense, the natural forest does not grow but is in a steady state on the scale of forest structural units [Oldeman, 1983]. This also implies that relevant structural information (including biomass) is not related to age. Hence, extraction of meaningful physical parameters for tropical forest characterization, additional to a qualitative classification of forest types, would require an appropriate description of this complex structure. In this study an attempt was made to group measurements in classes that are meaningful in backscatter models. The basic grouping is based on physiognomic appearance of plants in so-called life forms. This approach will be referred to as the LIFEFORM approach. In addition to classification of field measurements in life form classes it requires classification of leaf size and leaf orientation distribution, measurement of cover percentages for (horizontally layered) strata that can be recognised and measurement of trunk diameters. It also requires availability of a structural description of vegetation at the life form level. Of course these data should be collected with a sufficient statistical accuracy at representative plots of sufficient size and care should be taken to rule out the influence of possibly disturbing factors, such as relief, soil type and terrain drainage.

The LIFEFORM interface model uses tables of measured field data, as described in the previous sub-section, as input to generate four types of output: 1) biomass and basal area figures, 2) transect drawings, 3) vegetation statistics and 4) UTARTCAN model input files. To estimate (total aboveground wet) biomass, an allometric equation was applied, resulting in estimations for the biomass per plot. The equation uses the trunk diameter and total tree height as measured in the field and was calibrated with data from tropical rain forests in Central- and South-America, Africa and South-East. Asia [Brown *et al.*, 1989].

The transect symbolic drawings, as introduced in the previous chapter, are used to make a horizontal stratification of the canopy. UTARTCAN allows a maximum of three layers. This stratification is made by visual interpretation of the drawings. The

drawings also give an insight in the degree of spatial (horizontal) heterogeneity. UTARTCAN, like most other backscatter models, assumes a high degree of homogeneity. The effects of heterogeneity have been omitted in the present study.

The main task of the LIFEFORM interface is to solve the problem how scatterers should be divided over a limited number of scatterer classes for each of the layers. The approach is based on a set of assumptions, many of them being introduced in the remaining parts of this section. For leaves the approach is based on the rearrangement of the estimated cover percentages per stratum to cover percentages per layer. The first step is to relate cover to Leaf Area Index (*LAI*). This *LAI* is considered to be related to leaves uniformly distributed in the stratum. Then the *LAI* of a certain stratum can be divided proportionally to layers corresponding with the height range of this stratum. This can be done for all strata and these numbers can be added to determine a *LAI* figure per layer.

Biomass data for mixed forests in French Guiana, Guyana and Surinam indicate that the contributions of trunks, branches and leaves to the total amount of above ground dry biomass are in the order of, respectively 69%, 29.6% and 1.4%, with a moisture content of 39%, 41% and 55% [cited in: Van der Sanden, 1997]. For Colombian forests a figure for trunk moisture content of 25% is given [PRORADAM, 1979].

For the UTARTCAN model the trunks are always placed in the lower layer. The branches are placed in the layer which contains the center position of the crown, i.e. half-way the total height and the height of the first living branch. Also all leaves of an individual are assigned to this layer. The total branch biomass of a tree is divided over three to four branch classes with different scatterer dimensions and different orientation distributions, depending on its life form. The sizes of these scatterers are related to trunk diameter. The total *LAI* of a layer is divided over the individuals, which have its crown center position in that layer. For some life forms (notably broad-leaved trees and lianas) the division is proportional to the basal area of the individual, for other life forms fixed amounts per individual are taken. Also, different life forms have different leaf orientation distributions. Consequently, the *LAI* per layer can be subdivided in leaf size classes and orientation classes.

For the orientation distributions of trunk, leaf and branch type scatters a choice was made from a limited number of pre-defined standard probability density functions (pdf), depending on life form [Goel and Strelbel, 1984; Karam *et al.*, 1992].

The LIFEFORM interface generates statistics. Trunk statistics are compiled into four diameter classes. Branch statistics are generated for three layers and for six size-orientation combination classes (i.e. 18 types of scatterers). Leaf statistics are generated for three layers, for six size classes and four orientation classes (i.e. 72 types of scatterers). Within each class the number density and (for branches and trunks) the weighed-mean dimensions can be computed.

The final step is the generation of the UTARTCAN input files. Almost all information is available at this stage. Some parameter values are considered to be constant in this area, such as the leaf thickness (0.3 mm), leaf, branch and trunk moisture contents (0.55, 0.50 and 0.48), soil surface roughness (rms height is 1.2 cm, auto-correlation length is 24 cm) and the soil texture. Though the total number of branch plus trunk scatter classes is 22, in no case more than the maximum number of 20 occurred. For the leaves, omitting classes with a negligible amount of scatterers, the number of classes was often in excess of 10. To select the most important classes, for each class the fractional *LAI* (i.e. per layer, per orientation class and per size class) was computed and the 10 largest cases were retained.

5.2.4. Biomass inversion algorithm

In previous papers [Hoekman and Quiñones, 2002; Quiñones and Hoekman, 2002] biomass estimations were made on the basis of forest type classification. This indirect approach was shown to be appropriate for the Araracuara site where the natural vegetation types are in a steady-state and the relation between structure and biomass is known from empirical landscape-ecological data [Duivenvoorden and Lips, 1991]. Consequently, the ability to differentiate forest structures yields the capability to estimate biomass since biomass can be computed from structure in a straightforward way. Field experiments like the one described in this paper and the previous papers necessarily are limited to a certain number of classes under a limited range of environmental conditions. A model such as UTARTCAN, when valid, enables extrapolation of the empirical results to a wider range of structures and environmental conditions and thus, possibly, giving a better insight in the physical limitations of SAR biomass inversion.

The approach is straightforward. A wide range of 7 structures is chosen. The LIFEFORM interface is used to generate input files for UTARTCAN. For various levels of soil moisture and soil roughness the Mueller matrix is computed for all forest structure cases. Subsequently, speckle is added randomly a large number of times [cf. Hoekman and Quiñones, 2000], all simulated data are classified [also cf. Hoekman and Quiñones, 2000] and a large confusion matrix results. As a final step this large confusion matrix is aggregated to a limited number of classes, e.g. several biomass classes or several biomass and soil moisture combination classes. The results of different types of aggregation then can be evaluated and should give insight in the theoretical possibilities or limitations of biomass inversion.

5.3. UTARTCAN VALIDATION

To evaluate the performance of the UTARTCAN model with the LIFEFORM interface model, comparisons were made between the experimental AirSAR polarimetric data and the UTARTCAN simulated polarimetric data for all three frequency bands and all 45 plots measured in the field. For these plots the Stokes scattering operator (or, alternatively, the Mueller matrix) is averaged and unbiased

plot-averaged values for the HH-, HV- and VV-backscatter and the complex polarimetric HH-VV coherence ρ_i are derived. The plots vary in size but the number of independent looks N always exceeds 280 [Hoekman and Quiñones, 2000, 2002]. For homogeneous fields these averages can be regarded as accurate estimations of the underlying values. For $N > 280$ the standard deviation of the backscatter is less than 0.260 dB, the standard deviation of the (HH-VV) polarisation phase difference (the PPD or $\text{Arg}(\rho_i)$) depends on the coherence magnitude ($|\rho_i|$) and is less than 4.19° for a coherence magnitude $|\rho_i| = 0.5$, and the standard deviation of the coherence depends on the coherence magnitude and is less than 0.051 for $|\rho_i| = 0.5$. For further details see [Hoekman and Quiñones, 2000, 2002].

These accurate plot averaged values can be compared, in several ways, with the corresponding values simulated by UTARTCAN. The results of this validation are shown in Fig. 5.1 and table 5.3.

Fig. 5.1 shows the multi-frequency coherence signatures for experimental (M) and simulated (S) radar data for a selection of the field plots. Figs. 5.1a and 5.1b show signatures for high non-flooded forest (H2) (plot 07) and old secondary non-flooded forest (plot sec 07). In both cases the correspondence is good, notably for C- and P-band. For high flooded forest (H2) (plot 04) and forest with low palm density (P1) (plot 15) the simulated and the experimental coherence signatures are very similar (Figs. 1c and 1d). For flooded palm forests (P3) and (P4) (plots 14 and 18) the simulated and experimental signatures are very different (Figs. 1e and 1f). It can be noticed that in the first 4 cases the dominant life form in the plot is the broad-leaved tree while in the last two plots the palms are dominant and emergent, thus constituting the most important scatterers for these plots.

In table 5.3 section (a) the correlation coefficient (r) and standard error of estimate (SEE) are shown for the comparison of the individual band-polarisation combinations of the intensity measured experimentally with AirSAR data and the intensity simulated with UTARTCAN. Besides showing these numbers for all 45 plots, they are also shown for sub-sets of the data set namely for the plots of high forest in dry terrain (29 plots), plots of high forest in flooded terrain (3 plots), plots of palm forest in flooded terrain (9 plots) and plots of low forest on peat (4 plots).

In table 5.3 section (b) the experimental and simulated complex HH-VV coherences are compared for the same set and sub-sets of the data set using a complex correlation coefficient defined as:

$$r = \frac{\sum_{i=1}^{NF} \rho_{i,m} \rho_{i,p}^*}{\sqrt{\sum_{i=1}^{NF} (\rho_{i,m} \rho_{i,m}^*) \sum_{i=1}^{NF} (\rho_{i,p} \rho_{i,p}^*)}} \quad (5.1)$$

Table 3: Validation of UTARTCAN with 45 field plots. **(a)** Correlation coefficient (r) and standard error of estimate (SEE) calculated for the intensity data of the experimental AirSAR data and the UTARTCAN simulated radar intensity data for the field plots. Data is presented for all plots (All), plots of high forest in dry terrain (N), plots of high forest in flooded terrain (HF), plots of palm forest in flooded terrain (P) plots of low forest in peat terrain (L). Bold figures indicate values significantly different from the null-hypothesis at the 0.01 level of significance **(b)** Complex correlation coefficient (between measured and simulated values) for the HH-VV complex coherence for the same categories, expressed in magnitude $|r|$ and phase $\arg(r)$ (degrees). **(c)** Results for a selection of individual plots: biophysical characterization, correlation coefficient (r) and SEE for intensity values, complex correlation coefficient for the HH-VV complex coherence values expressed in magnitude $|r|$ and phase $\arg(r)$ (degrees). The best 5 results and the worst 4 results are shown (see text for details).

(a)										
type	All		N		HF		P		L	
n	45		29		3		9		4	
Intensity	r	SEE	r	SEE	r	SEE	r	SEE	r	SEE
HH-C	-0.27	1.19	-0.25	0.81	-0.93	0.99	-0.25	1.93	0.90	0.43
HV-C	-0.08	0.97	0.01	0.90	-0.88	0.98	-0.27	0.95	1.00	0.02
VV-C	-0.06	1.07	0.05	0.96	-0.98	0.40	-0.19	1.24	0.95	0.41
HH-L	0.53	1.94	0.30	1.47	0.83	0.56	0.41	2.92	-0.07	1.83
HV-L	0.72	1.24	0.83	1.12	1.00	0.08	-0.09	0.84	0.52	0.67
VV-L	0.52	1.65	-0.17	1.14	0.99	0.13	0.62	2.26	-0.63	0.30
HH-P	0.75	2.43	0.86	1.32	-0.95	0.52	0.49	3.34	0.01	3.61
HV-P	0.80	1.65	0.90	1.44	-0.38	0.20	0.03	1.09	-0.76	0.96
VV-P	0.71	1.81	0.65	1.36	-0.90	0.39	0.70	2.59	0.61	1.87

(b)											
Coherence	$ r $	$\arg(r)$									
C-band	0.53	7	0.70	7	0.96	14	0.26	-150	0.95	16	
L-band	0.60	-23	0.62	-28	0.83	9	0.62	-9	0.43	-25	
P-band	0.72	-24	0.69	-21	0.91	-8	0.80	-19	0.92	-58	

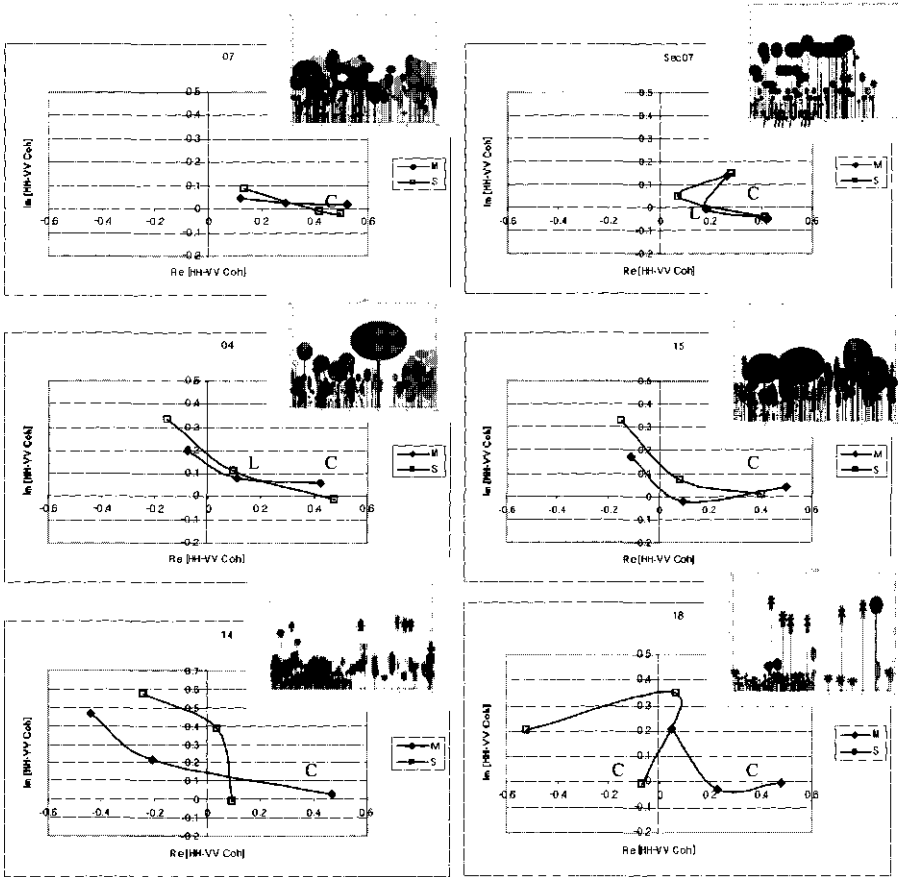
(c)										
plot	forest type	flooding	biomass	r intensity	SEE intensity	complex correlation				
			[ton/ha]			magnitude	phase			
'best 5 of 45'							$ r $	$\arg(r)$		
arat23	H1-H3	No	311.4	0.90	1.39	0.90	4			
ara04	H1- H3	Yes	205.1	0.88	1.69	0.97	4			
ara22	H1-H3	No	289.8	0.87	1.67	0.93	5			
ara07	H1- H3	No	227.7	0.86	1.78	0.98	4			
ara21	H2	Yes	192.1	0.83	2.08	0.92	3			
'worst 4 of 45'										
sec08	sec	No	13.6	0.80	3.41	0.60	-63			
ara18	P4	Yes	68.2	0.75	2.79	0.52	-93			
sec04	sec	No	20.1	0.74	3.10	0.44	-42			
pio02	H2	No	89.2	0.72	2.70	0.58	-22			

with	*	the complex conjugate operator
	NF	the number of fields
	$\rho_{i,m}$	the measured complex coherence of field i and
	$\rho_{i,p}$	the UTARTCAN predicted complex coherence of field i

In the table the amplitude $|r|$ and argument $\arg(r)$ (in degrees) of the results are shown. It is noted that when $|r|$ is close to unity and $\arg(r)$ close to zero the result is good. Further, the value of $\arg(r)$ is the mean offset in degrees between the measured PPD and the simulated PPD for a particular set of data.

In table 5.3 section (c) results are presented for individual plots using the correlation coefficient and the SEE of all nine band-polarisation combination intensity values and using the complex correlation coefficient for the HH-VV coherence of all three bands. The table shows the best 5 plots, which are the ones that have values for r , SEE, $|r|$ and $\arg(r)$ that are all within the best 50%. Also the worst 4 cases are shown, which are the ones for which all of these values fall within the worst 50%.

These results may be interpreted as follows. From the results shown in Fig. 1 it may be concluded that plots with a dominance of broad-leaved trees give much better results than plots dominated by palms. This notion is confirmed by the results given in table 3. When all plots are considered, or the sub-sets of high forest in dry or flooded terrain, then better results are obtained than for the sub-plots of palm forests or low forest on peat. Because of the lower number of plots this interpretation should be made with care. Two physical considerations may support this notion however. In the first place the UTARTCAN model was developed for broad-leaved plants. The completely different structure of palm leaves may not be accounted for well. Secondly the palm forests are very heterogeneous and have an open canopy, while UTARCAN assumes homogeneous horizontal layers. The large phase errors shown in table 5.3-section (b), notably in C-band for palm forests, may be a consequence. Double-bounce occurs in reality through the large gaps, while the homogeneous layering does not allow the C-band signal to penetrate unto the ground surface. It is noted that negative values for $\arg(r)$ reveal an underestimation of the phase difference, meaning an underestimation of the double-bounce effect. The results of table 5.3 section (c) confirm this notion in a different way. The best individual cases are all for high forests, the worst cases are for a palm forest and some low biomass (secondary) plots which have a large fraction of large leaf size individuals such as palm species, Cecropia species and stem forbs.



Plot name	Forest type	Flooding condition	Biomass [ton/ha]	Incidence angle	Terrain roughness	Soil moisture
07	H2	No	227.7	40.2	F	0.2
sec 07	Old sec	No	88.4	52.7	F	0.2
04	H3	Yes	205.1	40.4	F	0.9
15	P1	Yes	200.1	40.9	F	0.9
14	P3	Yes	125.8	37.5	F	0.9
18	P4	Yes	68.2	50.7	F	0.9

Figure 5.1. Polarimetric coherence signatures for experimental (M) and simulated (S) radar data for a selection of field plots. The corresponding symbolical forest structure drawings as created by the LIFEFORM interface model are also shown. The table shows some forest type characteristics. Further, values for incidence angle, terrain roughness (see table 6), and volumetric soil moisture as used for the simulation are shown.

Therefore, for the analysis with UTARTCAN in the remaining part of this paper, simulated forest plots consist solely of broad-leaved individuals, for which it is assumed that the simulations will yield fairly realistic results.

5.4. HYPOTHETICAL FOREST PLOTS

Hypothetical forest plots with varying density, height and biomass levels were created as the basis for the analysis of the effect of terrain conditions, such as soil surface roughness and moisture, on the radar signatures. For each hypothetical plot of 0.1 ha the life form, height, DBH and leaf size of the individuals were defined. To avoid variations due to life form and leaf size, only broad-leaved trees with leaf size 3 (Notophyll) were included. Structural variations between the plots were created in order to study the effects of DBH, tree density, height and layering.

Two different types of data sets were created. In the first set of data the density of trees is varied from 200 to 5 individuals per 0.1 ha and the height and DBH are kept at a constant level of 30 m and 15 cm, respectively. This data set will be referred to as the density data set (DD). In the second data set the height of the trees is varied from 50 to 2 m and the density and DBH are kept at a constant level of 100 individuals per 0.1 ha and 15 cm, respectively. This data set will be referred to as the height data set (HD-15). For these first two types of data sets input files for UTARTCAN and the biomass levels are computed by the LIFEFORM interface.

Table 5.5. Structural parameters calculated for the hypothetical plots: (a) Density Data set (DD) and (b) Height Data set (HD). Leaf size class is according table 2. DBH is the diameter at breast height.

a) DD plots	density [ind/0.1 ha]	height [m]	leaf size class	biomass [ton/ha] DBH=15 cm
Plot 01	200	30	3	236.1
Plot 02	100	30	3	118.0
Plot 03	50	30	3	59.0
Plot 04	20	30	3	24.0
Plot 05	5	30	3	6.0

b) HD plots	density [ind/0.1 ha]	height [m]	leaf size class	biomass [ton/ha] DBH=15	biomass [ton/ha] DBH=40	biomass [ton/ha] DBH=70	biomass [ton/ha] DBH=15
Data set name				HD-15	HD-40	HD-70	HD-L
Plot 01	100	50	3	245.5	1564.3	4499.3	223.2
Plot 02	100	35	3	175.3	1117.2	3213.1	152.6
Plot 03	100	25	3	127.6	813.2	2338.8	104.3
Plot 04	100	15	3	78.8	502.1	1444.1	54.7
Plot 05	100	6	3	63.8	406.7	1169.8	39.3
Plot 06	100	2	3	33.1	211.4	608.1	16.1

Three additional types of data sets were created by slight modifications of the UTARTCAN input files of the HD-15 data set. To analyse the effect of trunk DBH

in isolation the trunk diameter was changed from 15 cm to 40 cm and 70 cm, thus creating the data sets HD-40 and HD-70, respectively, out of the HD-15 data set. In this way the scatterer types and densities of leaves and branches and the density of trunks are kept constant and only the diameter of the trunk of the trees is changed. Furthermore, to study the effect of vegetation layering in isolation, 90% of the trees of the HD-15 data were re-located in a lower layer. In this way most trunk type scatterers were shortened and re-located in a lower vertical stratum, together with most of the branch and leaf type scatterers. This data set is called HD-L. A summary of these data set types is shown in table 5.5. All biomass levels were calculated using the allometric equation of [Brown *et al.*, 1989].

For all data sets shown in table 5.5 the soil moisture and terrain roughness parameters were varied in the corresponding UTARTCAN input files. The volumetric soil moisture fraction was varied from 0.1 to 0.9 in 0.1 intervals (9 classes). The soil surface roughness state is described using the rms height and auto-correlation length for three cases: flat (F), medium rough (M) and rough (R) (table 5.6). For soil texture a constant level of 0.15 and 0.6 for the sand and clay fractions, respectively, were selected.

Table 5.6: Terrain roughness parameters used for the tree terrain roughness cases selected for the analysis. RMS is the surface height variation and ACL is the surface auto-correlation length.

Terrain roughness	RMS (m)	ACL (m)
Flat (F)	1.2 e-3	2.4 e-1
Medium rough (M)	1.2 e-2	2.4 e-1
Rough (R)	5.0 e-2	1.0

Thus, for each vegetation structure, $3 \times 9 = 27$ soil moisture and terrain roughness cases were generated. This was done for the DD and HD-15 sets only. For the HD-40, HD-70 and HD-L data sets the soil surface roughness was not varied but fixed as flat terrain (F), thus generating only 9 cases for each vegetation structure. Since only plots with biomass levels not exceeding 1000 ton/ha were analysed the total number of cases (see also table 5.5), therefore, is $11 \times 27 + 11 \times 9 = 396$ (table 5.7). The incidence angle used for all the simulations is 45° . UTARTCAN was applied to generate Mueller matrices for each of these cases for C-, L- and P-band. Next, the intensities for HH-, VV- and HV-polarisation and the HH-VV polarimetric coherence data (PPD and $|\rho|$) were derived, which serve as the basis for further analysis. A detailed discussion of the statistical properties and physical information content of this coherence can be found in [Hoekman and Quiñones, 2002].

5.5. RESULTS

5.5.1. Effect of tree density

To evaluate the effect of tree density, plots of similar biomass level but with different tree densities were compared. Plots 1, 3 and 4 of the DD data sets were compared with plots 1, 5 and 6 of the HD-15 data sets to evaluate the effect on high,

intermediate and low biomass levels, respectively. In the DD data set the density of trees was changed and the height was kept at a constant level while in the HD data set the density was kept the same and the height of the trees was reduced in order to achieve similar biomass levels (table 5.4). For this first comparison plots with flat terrain (roughness case F) and a volumetric soil moisture fraction of 0.3 were used. The signatures are shown in figure 5.2.

Table 5.7. Description of the hypothetical forest data sets: DD= Density plots, HD= Height Plots. The table shows for each set the number of biomass classes (or plots), the terrain roughness classes (table 5), the number of moisture classes and the number of plots used for signature analysis and biomass inversion.

Data set name	# of biomass classes	terrain roughness type	# of soil moisture classes	total number of plots for signature analysis	total number of plots used for biomass inversion
DD	5	F, M & R (3)	9	135	135
HD- 15	6	F, M & R (3)	9	162	162
HD- 40	6	F (1)	9	54	36
HD- 70	6	F (1)	9	54	9
HD- L	6	F (1)	9	54	54
Total				459	396

In general, it can be observed that there are differences in the signatures for the two types of plots at the same biomass level. For the high biomass level the intensity and the polarimetric coherence signatures are almost identical, except for P-HH, for which the high-density plot (plot 1 of the DD set) is 2 dB higher. The phase difference (PPD) and coherence magnitude ($|\rho|$) values are only slightly different for these two plots. For the intermediate biomass level the intensity signature of the DD case (plot 3) is about 1-3 dB higher for L- and P-band, for HH- and VV-polarisation. The coherence signatures are only slightly different except for the C-band coherence magnitude. For the low biomass level the HD case (plot 6) is 2-5 dB lower for all the C-, L- and P-band polarisation. The polarimetric coherence signatures are different, notably for the C-band PPD.

When analysing the intensity signatures, for decreasing biomass, and for decreasing density or height, respectively, some interesting features can be observed. The C-HH and C-VV intensities increase noticeably with decreasing density, but not with decreasing height. The L-HH, L-VV, P-HH and P-VV intensities also increase noticeably with decreasing density, but decrease with decreasing height. L-HV and P-HV both decrease with lower biomass, either caused by decreasing density or decreasing height. The C-PPD is not affected much by decreasing density but increases with lower height. L-PPD and P-PPD increase both with decreasing density and decreasing height.

As can be seen from these results the same biomass level with the same soil moisture and terrain roughness conditions but with different structural parameters, in this case different density and different height, produces different signatures, especially at lower biomass levels.

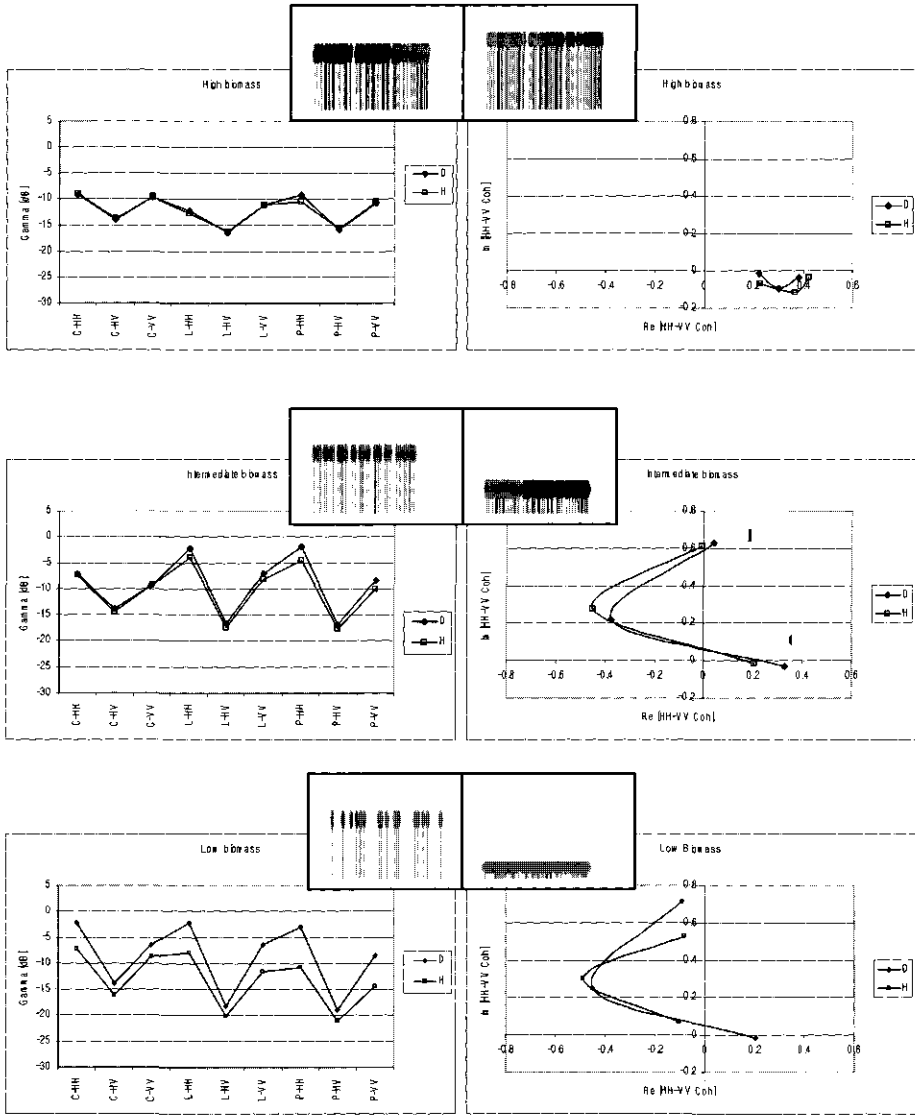


Figure 5.2. Comparison of signatures for two plots of similar biomass level from the DD (D) and the HD-15 (H) data sets, for three different biomass levels. For the high biomass level plot 1 from the DD and the HD-15 sets are compared. For the intermediate biomass level plot 3 (DD) and plot 5 (HD-15) and for the low biomass level plot 4 (DD) and plot 6 (HD-15) are compared. Profiles illustrating the structure of the compared plots are shown above the signature graphs. Biomass levels can be found in table 5.

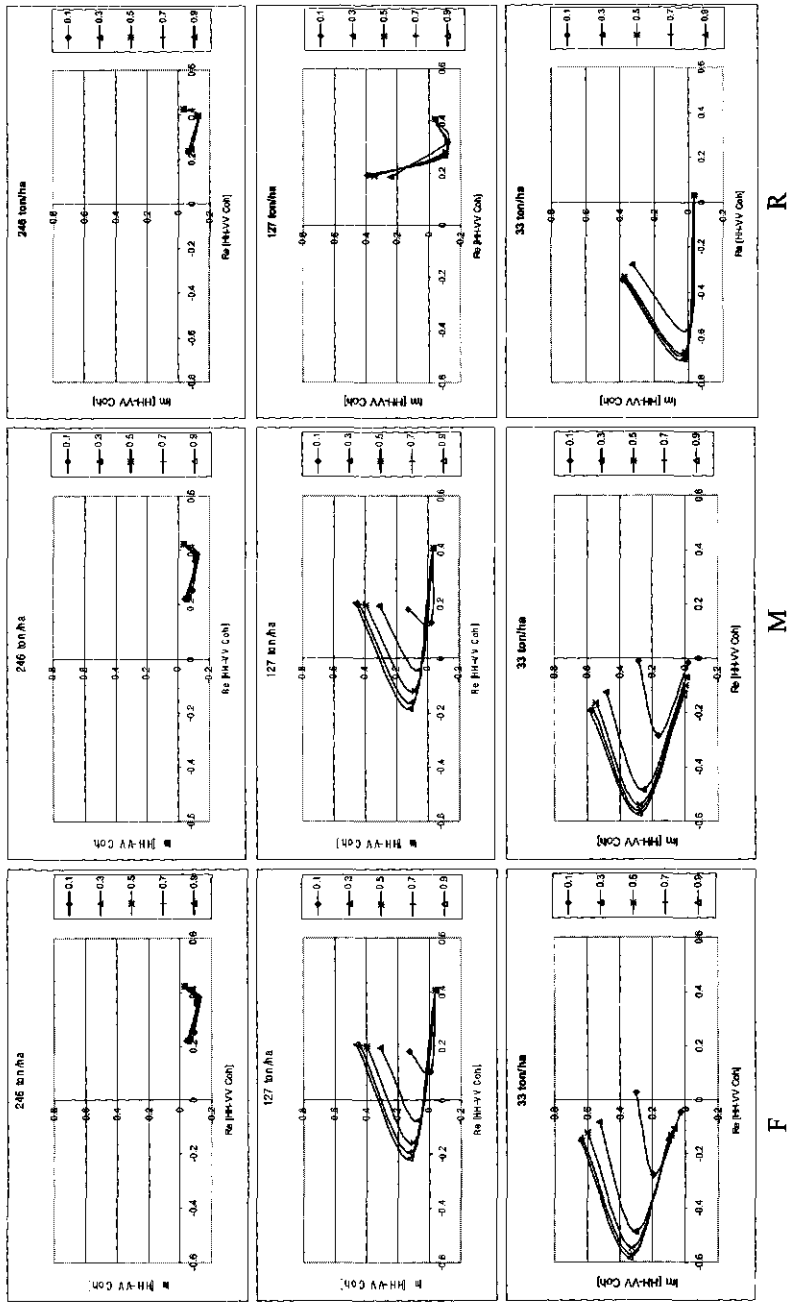


Figure 5.4. As figure 3, for the polarimetric coherence signatures

5.5.2. Effect of soil surface roughness and moisture

Soil surface roughness and moisture can be expected to have a significant influence on the signatures of the L- and P-band since the radar waves, as often is presumed, may reach the forest floor even under a closed canopy. To study such influences 3

plots (i.e. plot 1, 3 and 6) of the HD-15 data set are selected, which have biomass levels of 246, 127 and 33 ton/ha, respectively. For each plot the influence of the three terrain roughness cases and the nine soil moisture cases defined in section 5.4 were analysed. Results, sorted in nine graphs by increasing biomass and roughness levels, are shown in Figures 5.3 and 5.4.

The intensity signatures (Fig. 5.3) at a high biomass level (246 ton/ha) are saturated for the nine different soil moistures cases except for P-HH, for which there is a small range of 2 dB between the driest and the wettest soil. Hardly any differences can be observed between the three different roughness cases. When the biomass level decreases the effects of surface moisture content and roughness are more evident. At the intermediate biomass level (127 ton/ha), the intensity signal saturates for C-band, but large variation caused by soil moisture is present in L-HH, L-VV, P-HH and P-VV intensities for the flat surface. Differences for HH-polarisation (up to 5 dB) are larger than for VV-polarisation (2 dB) and disappear as terrain roughness increases. For rough terrain only a slight influence of soil moisture can be observed for P-HH (2 dB). For the low biomass level (33 ton/ha) and the flat surface the effect of soil moisture is evident for all bands and polarizations. In this case the difference between the driest and the wettest soil is the highest for the L-HH, L-VV, P-HH and P-VV intensities (up to 6 dB). With increasing terrain roughness the C-band saturates for the effect of soil moisture and for L-HH, L-VV and P-HH and P-VV the effect reduces slightly (up to 4 dB).

L-HV and P-HV levels are not affected much by soil moisture or roughness (up to 2 dB) and increase from the low to intermediate biomass level with approximately 5 dB for all cases while staying at the same level (i.e. saturates) for the high biomass level for all cases.

The polarimetric coherence signatures (Fig. 5.4) for the high biomass level (246 ton/ha) are almost identical for all terrain roughness and soil moisture cases. For the intermediate biomass level (127 ton/ha) and the low biomass level (33 ton/ha) the coherence signatures are strongly influenced by moisture level, notably for flat and medium rough terrain, and for L- and P-band. In general, for these levels of biomass and frequency bands, the coherence magnitude increases substantially with soil moisture content. For L-band, at the intermediate biomass level, there is a clear soil moisture dependent increase of the PPD with decreasing terrain roughness. For P-band, at the low biomass level, there is a clear decrease of the PPD with decreasing terrain roughness, however far less soil moisture dependent.

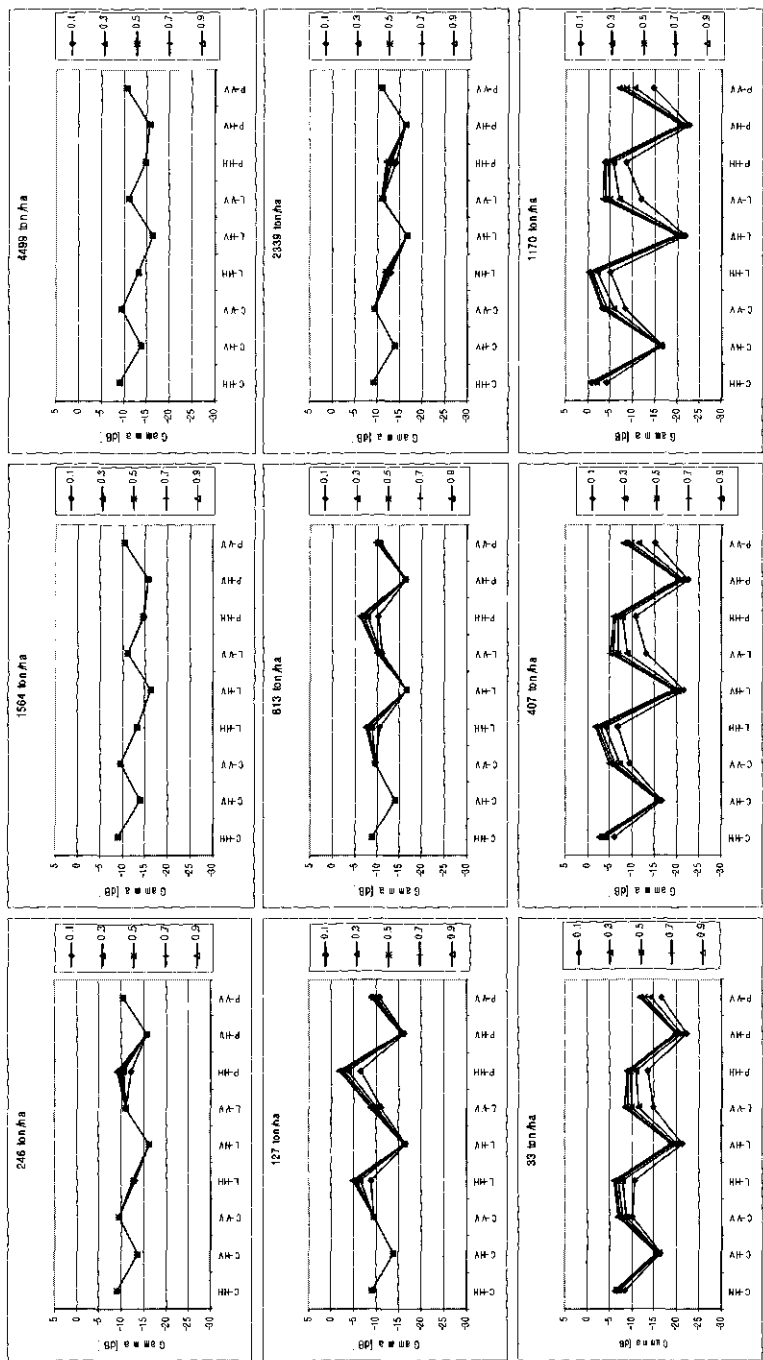
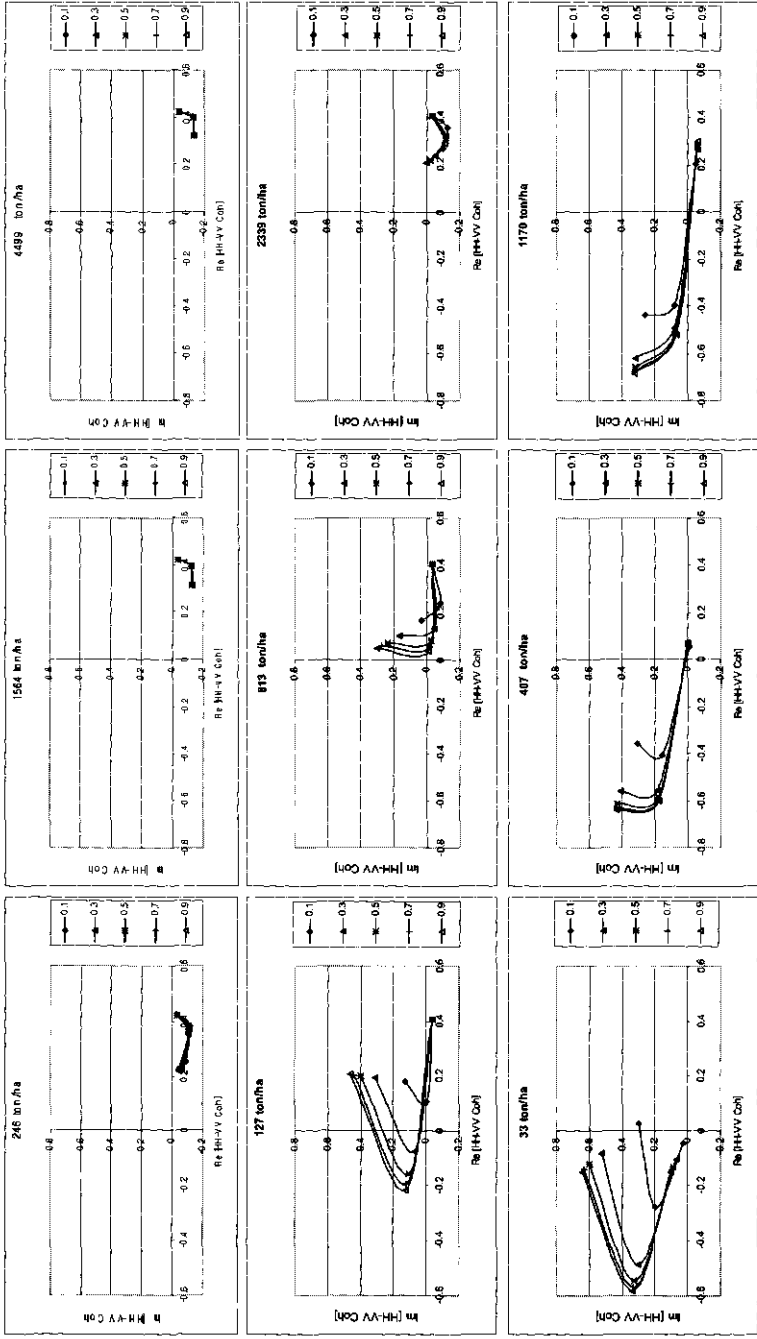


Figure 5.5. Effect of trunk DBH on the intensity signature of plots with different soil moisture levels for the HD-15, HD-40 and HD-70 data sets.



70 cm

40 cm

15 cm

Figure 5.6. As figure 5, for the polarimetric coherence signatures

In summary it may be concluded that at high biomass levels intensity and polarimetric coherence signatures tend to saturate with soil moisture and terrain roughness, except for the P-HH intensity. At intermediate biomass levels all L- and P-band signatures, except for the L-HV and P-HV intensity, are affected by terrain roughness and/or soil moisture, while at low biomass levels all signatures are affected by terrain roughness and/or soil moisture levels. The lowest influence is always found for the HV-polarisation intensity. It may be noted that in general when a signal is sensitive to biomass level it is also sensitive to terrain roughness and/or soil moisture.

5.5.3. Effect of DBH

To evaluate the isolated effect of DBH plots 1, 3 and 6 of the HD-15, HD-40 and HD-70 data sets are compared. For these plots the biomass levels change for the different data sets, as a consequence of the increase in DBH only, as can be seen in table 5.4. The density and type of the scatterers in the canopy stays the same for a certain plot number, only the scatterers representing the trunk have a different radius in the different sets. Results are shown in Figs. 5.5 and 5.6. Graphs are sorted by increasing biomass level and increasing DBH.

For high biomass level the intensity signal is saturated and no distinctions can be made between different soil moisture conditions except for the P-HH intensity (a 3 dB range of variation), in the HD-15 data set (i.e. DBH = 15 cm). For intermediate biomass levels the effect of DBH is more evident. For L- and P-band the HH and VV intensities decrease with increasing DBH, while the HV intensities are not affected. For low biomass levels the effect of the increasing DBH is opposite, i.e. for all bands the HH and VV intensities increase with increasing DBH, while the HV intensities are not affected. When studying the differences in the intensity signatures of the HD-70 set (i.e. DBH = 70 cm) an increase of HV and decrease of HH intensities with increasing biomass shows up. In all sets the intensities increase for the lower biomass values with the soil moisture and the sensitivity to soil moisture is much higher than for higher biomass values. This fact is particularly noteworthy because, for example, the low biomass level of the HD-70 set (608 ton/ha) is much higher than the high biomass level of the HD-15 set (246 ton/ha).

The polarimetric coherence signatures also change with increasing biomass and DBH. For high biomass levels there is hardly any influence of variation in soil moisture and DBH. For an intermediate biomass level the PPD for L- and P band decreases with increasing DBH. For the lower biomass levels there is an increase in the PPD with increasing DBH for P band.

5.5.4. Effect of layering

The effect of a different vertical distribution of the scatterers, by introducing a new layer in the forest canopy (see Fig. 5.7 and section 5.4), can be studied by comparing the signatures of the HD-15 (plots 1, 3 and 6) and HD-L (plots 1, 3 and 5) data sets. Note that the biomass levels differ slightly for these two sets and are 246, 127 and

33 ton/ha for the first and 223, 104 and 39 ton/ha for the latter set. The results for the intensity and coherence signatures are shown in Figs. 5.7 and 5.8, respectively. For a high biomass level, the intensity signatures are saturated, except for P-HH which shows sensitivity to soil moisture. For intermediate biomass levels the intensities for the L- and P-band are affected, in different ways for different polarizations. For the two-layer case the HH-polarized intensities are higher, the HV intensities seem hardly affected and the VV intensities show a soil moisture dependent increase or decrease. For low biomass level the C-band are not affected much but for L- and P-band intensities much lower levels are found in the two-layer case.

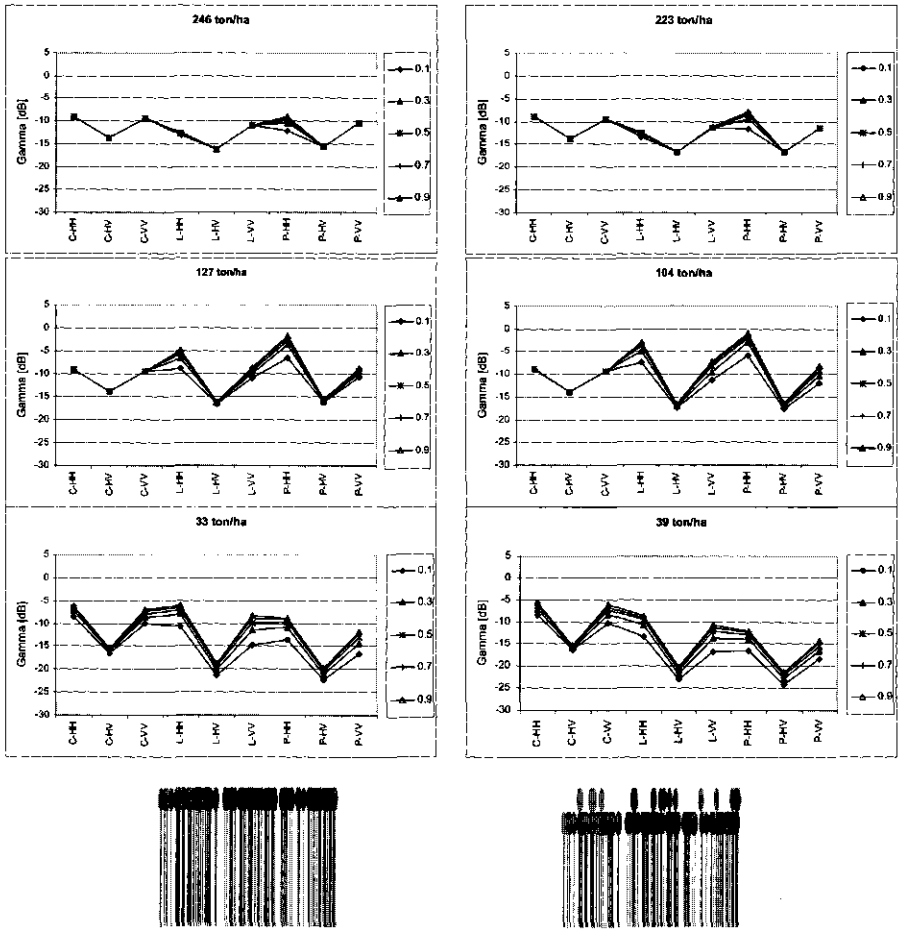


Figure 5.7. Effect of layering on the intensity signatures of plots with different soil moisture conditions for high, medium and low biomass levels selected from the HD-15 and HD-L data sets.

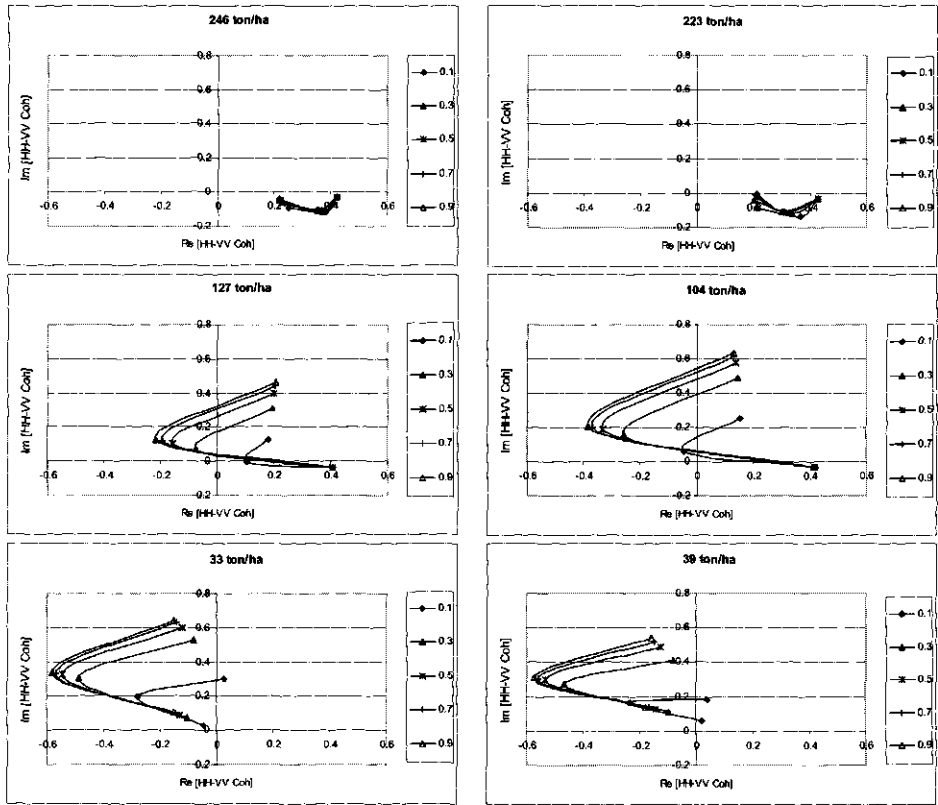


Figure 5.8. As figure 5.7, for the polarimetric coherence signatures.

The polarimetric coherence signature is also affected by the presence of layers in a forest (Fig. 5.8). For high biomass levels the signatures do not change much. For intermediate biomass levels the L- and P-band signatures change considerably, while for low biomass levels all signatures change.

5.5.5. Theoretical inversion results

The theoretical inversion of the radar data was done using the available hypothetical data sets (see section 5.2 D). Overall classification accuracy for different numbers of looks, as an indication of speckle level, are given in table 5.8.

The first inversion result is for all hypothetical plots, i.e. under 1000 ton/ha and including all terrain roughness and soil moisture cases. The overall accuracy for low numbers of looks is below 80%. For 64 and 100 looks 82.0% and 86.6% of accuracy are calculated, respectively. The confusion occurred mainly between the high biomass classes of the DD and HD data sets, which may be a logical consequence of the fact that the different soil moisture and terrain roughness cases can not be

separated (as was shown in section 5.5 B). To analyse the inversion result for the biomass level itself, all plots with the same biomass level, despite soil moisture or terrain roughness differences, were aggregated into the same class, resulting in 22 biomass classes. In this case an overall classification accuracy of 87.9% was obtained already for 16 looks. This case is very important because it shows that high percentages of biomass level accuracy can be reached even for a low number of looks and even when high biomass levels (up to 813 ton/ha, see table 5.4) are present.

Table 5.8. Overall classification accuracy after inversion of selected number of cases of the DD and HD data sets for different numbers of looks, as an indication of the speckle level.

Data sets	roughness classes	# of cases	4 looks	16 looks	32 looks	64 looks	100 looks
DD+ HD	F, M, R	396	25.4	57.0	71.2	82.0	86.6
DD+ HD	F, M, R	22 *)	56.9	87.9	95.8	99.0	99.7
DD	F, M, R	135	36.2	63.6	75.3	84.8	89.3
DD	F, R	90	41.4	71.4	83.2	91.9	95.5
DD	R	45	38.7	68.9	81.8	90.6	94.6
DD	F	45	49.4	75.5	85.9	93.5	96.8

*) aggregated to biomass levels

To avoid the confusion produced by the similarity in the biomass levels of the DD and HD data sets, the plots of the DD data set were inverted separately. The DD data set included plots of 5 biomass levels with tree different terrain roughness conditions and 9 soil moisture conditions (i.e. 135 cases). The overall classification accuracy increases to 84.8% and 89.3% for 64 and 100 looks, respectively. In this case most of the confusion occurred between the plots of the flat terrain (F) and the plots of the medium rough terrain (M). When leaving only extreme terrain conditions like flat and (F) and rough (R), then a classification accuracy of 83.2% is reached already for 32 looks. In this case most of the confusion between the classes occurred between the different soil moisture cases in terrain of similar roughness at high biomass levels and also between the high biomass plots of both terrain roughness cases. The inversion of the data set including only one terrain roughness state (i.e. either F or R) gives similar results. In general the overall classification is higher when including flat terrain roughness cases only.

5.6. CONCLUSIONS AND RECOMMENDATIONS

In this paper the LIFEFORM interface model is introduced as an innovative method to model the complex tropical forest structure for radar backscatter models through life form (table 5.1) dependent structural descriptions. For each individual plant, depending on its life form and other characteristics measured in the field, this model determines scatterer types and quantities and distributes them over vertically stratified layers. The output of this interface model comprises input files for the radar backscatter model and symbolic transect drawings for each plot measured in

the field. The latter drawings visualise structural differences between plots (as relevant for radar), vertical stratification (when present) and horizontal heterogeneity (which is not accounted for in most backscatter models). This refined description allows for better evaluation of the performance and possible limitations of current backscatter models for application in tropical forests.

Differences between radar signatures measured by the AirSAR and those predicted by the UTARTCAN backscatter model were studied for all 45 plots measured in the field (section 5.3). The results, evaluated both for intensity and HH-VV coherence, for all frequency bands, show that the model performs fairly well for high forests (on dry and flooded terrain), which have a dominance of broad-leaved tree species. The worst results are obtained for some (flooded) palm forests and some low biomass secondary forest plots which have a large fraction of large leaf size individuals, such as palm species, *Cecropia* species and stem forbs. Since the UTARTCAN model was developed for broad-leaved tree species and assumes horizontal uniformity such results may not come a surprise. Apparently the large leaves are not described well, either by LIFEFORM or by UTARTCAN. Secondly, UTARTCAN cannot account for the open structure (i.e. the horizontal heterogeneity) of the palm forests. The large HH-VV coherence phase difference errors, even in C-band, are a clear indication that UTARTCAN underestimates the relative importance of the double bounce interaction in this case.

Due to the limitation observed in UTARTCAN to describe the interaction with life forms such as palms, or open (i.e. horizontally heterogeneous) structures, like palm forests, hypothetical forest plots were designed with broad-leaved trees only. UTARTCAN input files were generated by the LIFEFORM model for a range of forest structures (from which the biomass level directly follows) with different soil surface roughness and soil moisture states. An extensive evaluation of the simulated radar signatures given in section 5.5 reveals complex relationships with forest structural parameters, including biomass, and the terrain conditions. Though results are hard to generalise it may be noted that, in general, when the radar is sensitive to biomass variation it is also sensitive to terrain roughness and soil moisture, and that this sensitivity is the lowest for the HV-polarisation. Further, large differences for forests with the same biomass level, and with the same terrain roughness and soil moisture level, may occur solely because of structural differences, such as differences in height versus density or differences caused by the presence or absence of layers. And, usually, these effects are much stronger for low biomass levels. When the radar backscatter intensity is sensitive for one or more of these parameters, the HH-VV coherence also shows large variation as a function of one or more parameters. It was noted though that these variations can be very different between L-band and P-band, suggesting these bands are both very important for forest observation.

The graphs of Fig. 5.9 may help to illustrate the most important differences between simulated signatures of the same biomass level, for different terrain roughness and soil moisture conditions. Signatures of six terrain roughness and soil moisture

condition combinations are shown for 3 different biomass levels. At low biomass levels differences in the intensity signatures can be very large, even up to 8 dB for L-HH. Also the coherence signatures vary a lot with soil moisture and terrain roughness for low and intermediate levels of biomass.

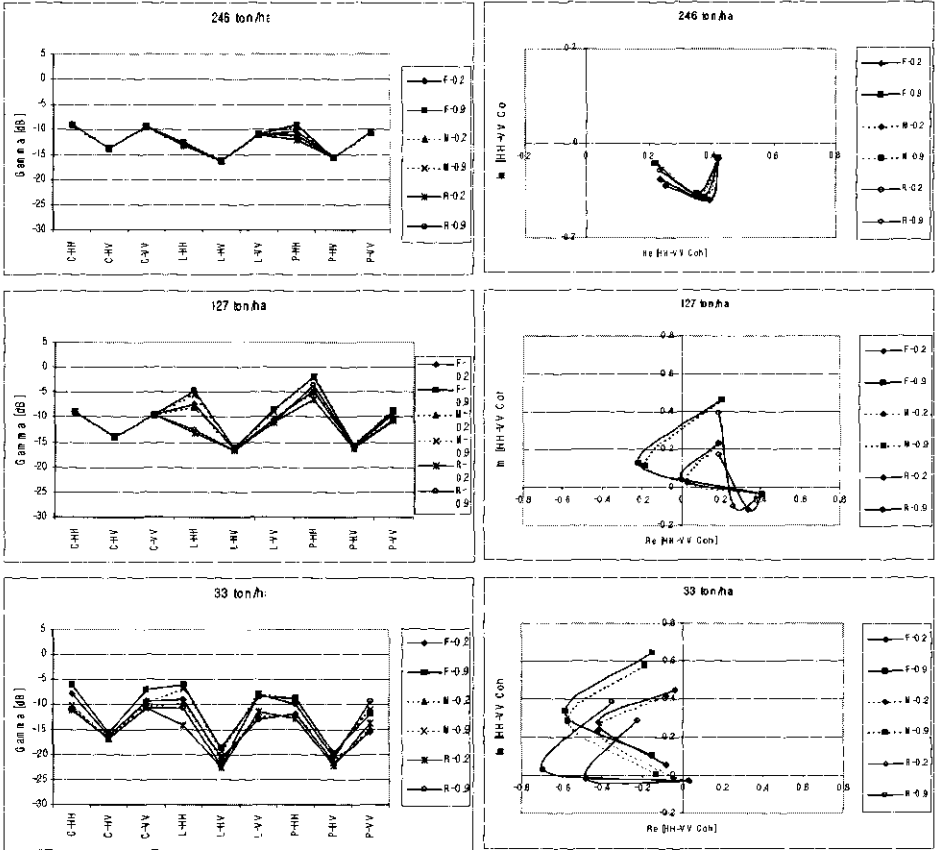


Figure 5.9. Intensity signatures and polarimetric coherence signatures for selected plots of the HD-15 data set, for high, intermediate and low biomass levels. Each plot presents signatures for 3 terrain roughness conditions (F, M, R) and two different extreme soil moisture conditions (0.2 and 0.9).

Since the radar signatures of (tropical) forests are influenced by many parameters and not only by the total volume of the scatterers (i.e. the biomass level) a direct inversion of the radar data into biomass values will result in a very inaccurate estimation. To study the effect of soil moisture, terrain roughness and forest structure on the classification of biomass levels, a theoretical inversion of different sets of plots was made for different levels of speckle. The results showed that the largest part of the confusion between classes was found for the high biomass levels, a logical consequence of the saturation of the radar signature levels for differences in

soil moisture and terrain roughness conditions. On the other hand low confusion occurred between low biomass plots with different soil moisture and terrain roughness conditions. This suggests that the application of direct inversion algorithms for biomass estimations can lead to large inaccuracies at low biomass levels.

Alternatively, the overall accuracy for the classifications were high for all of the inverted data sets. All overall accuracies were above 50% for 16 looks (1.1 dB of speckle) and above 70% for 32 looks. The high inversion results using the polarimetric inversion algorithm developed indicate that the polarimetric classification as presented by [Hoekman and Quiñones, 2000] is a powerful method able to combine the information contained in the different bands. As an example the radar data extracted from the AirSAR image for the field-measured plots was inverted using the same algorithm, for different levels of speckle (table 9). All the measured plots had a different structure that statistically could be grouped and used for the definition of the forest types, as presented in table 4. When assuming that all the 45 field plots were different the overall classification accuracy for 16 looks was 87.4% ! Furthermore, when the data of the plots are aggregated into forest types (as shown in table 4) the overall accuracy increases to 93.7% for the same number of looks. This means that the potential of multi-band full-polarimetric classification of tropical forest types is large and can be a good basis for accurate biomass classification.

Table 5.9. Overall classification accuracy in percentages after inversion of field plots for different number of looks, as an indication of the level of speckle. Results are presented (a) for all 45 plots individually and (b) after aggregation to forest types.

Data set	# classes	2 looks	4 looks	16 looks	32 looks	64 looks
All	45	28.9	47.8	87.4	96.6	99.3
By forest types	12	44.9	62.4	93.7	99.0	99.9

In summary, theoretically, direct biomass inversion is not accurate at low biomass levels because of many disturbing effects and is not accurate at high biomass levels because of saturation. The latter is reported in many papers (at levels up to 150 ton/ha for P-band) such as summarised in [Le Toan and Quegan, 2002; Quiñones and Hoekman, 2002]. The classification approach suggested in this paper, theoretically, can classify biomass levels accurately both at low and high biomass levels, even up to 800 ton/ha. The latter was experimentally confirmed by classification of the Araracuara forest test site biomass classes [Quiñones and Hoekman, 2002], which had levels up to 340 ton/ha. The latter level is much higher than the so-called saturation level for P-band.

In the future polarimetric data from different forest types all around the world could be compiled and used as the basis for the classification of new radar images by comparing the patterns of the new signatures with the available polarimetric database. In this way a biomass level could be assigned by relating it to a

corresponding forest type. Further research should focus on the possibilities of using this biomass classification algorithm when restricting the number of bands and polarisations, thus matching those available in the current and proposed satellite radar systems.

Regarding the development of theoretical backscatter modelling, it could be useful to use data from more test sites, pay more attention to absolute calibration issues, use several theoretical models instead of UTARTCAN only, and extend such models to include the effects of horizontal heterogeneity.

6. ASSESSMENT OF SUITABLE RADAR PARAMETERS FOR TROPICAL FOREST MAPPING APPLICATIONS.

6.1 INTRODUCTION

In the last ten years concern is growing over the state and changes in the tropical forest. Changes in cover are known to have an effect on the hydrological and bio-geo-chemical cycles and a significant impact on climate change and bio-diversity. Of special importance is the actual uncertainty in the carbon cycle, specially related to the differences on the biospheric sink calculations, which urged for the production of systematic accurate and consistent measurements of forest functions and structure and associated factors such as biomass [IPCC, 2000]. Some of the required systematic earth observations, can be obtained by remote sensing systems which, so far, have only been achieved by some optical remote sensing sensors (NOAA AVHRR, LANDSAT and MODIS), which are able to provide large regional coverage and acquisitions over long time. Nevertheless for tropical forest areas, optical remote sensing sensors are affected by cloud cover, influencing the temporal resolution, the accuracies of the products and the application of inversion algorithms for specific applications (i.e. for biomass assessment). Radar remote sensing on the other hand is free of the effect of clouds and the use of long wavelengths (P- and L-band) offers unique canopy penetrating observation capabilities that can be directly related to forest structure and biomass levels.

In these years, radar scientists have focused on the development of algorithms for the application of existing radar systems in different fields [Kasischke *et al.*, 1997]. In general it can be concluded that different bands and polarizations are sensitive to different parameters. For instance HH polarisation is more sensitive to flooding conditions [Hess *et al.*, 1990; 1995; Pope *et al.*, 1994, 1997] while HV polarisation is sensitive to biomass levels [Ranson *et al.*, 1997, Rignot *et al.*, 1994, 1995]. This implies that not all-available or coming radar systems are capable of producing accurate maps for all sort of applications. For instance the penetration and sensitivity of HH polarisation allowed the JERS L-HH to map flooding conditions in the Amazon basin [Hess *et al.*, 1995] while it was found to underestimate deforestation in the same region [Rignot *et al.*, 1997].

In addition the use of P-band for specific applications is still under investigation. The possibilities of a P-band satellite are being assessed specially in relation to biomass remote sensing. At that respect P-band is interesting because of the higher sensitivity to high biomass ranges, saturating at levels near 150-200 ton/ha while the saturation for L-band is being calculated at 50-100 ton/ha. [le Toan *et al.*, 1992; Dobson *et al.*, 1992; Beaudoin *et al.*, 1994; Israelsson *et al.*, 1994; Ranson *et al.*, 1994; Rignot *et al.*, 1994, 1995; Imhoff, 1995; Kasischke *et al.*, 1995; Hoekman and Quiñones, 2000]. The higher penetration capabilities of P-band into the forest canopy compared with C- and L-band are due to the larger wavelength allowing P-

band to "observe " big scatterers, related to forest structure and even to penetrate onto the forest floor to detect terrain characteristics.

An important technical inherent characteristic of a radar system is the image speckle. Speckle gives the images the so-called 'salt and pepper' or 'grainy' appearance and is caused by the interference among backscatter waves of the individual scattering elements (scatterers) that are present within one resolution cell. Interference between echoes produced by the scatterers can be constructive or destructive depending on the phase and the amplitude and therefore result in a higher or lower overall backscatter. In order to characterise objects with radar it is important that measurements are accurate estimates of either the mean power or the mean amplitude but the effect of speckle obstructs the measurements of a single resolution cell. The measurement of a single resolution cell is called a look. The accuracy of the radar measurements can be improved by the linear averaging of measurements corresponding to cells adjoining in the azimuth direction (direction of flight) which constitute a multi-look image. In general it can be said that multi-look images have less backscatter fluctuations and therefore the effect of speckle is less evident. The accuracy of the mean amplitude or power estimations will increase with an increase in the number of looks. A large number of looks reduce the fluctuations in the radar measurements and improves the radiometric resolution [Hoekman, 1990, 1991]. Speckle levels (i.e. different number of looks) is expected to have strong influences in classification accuracies, so far specific investigations on the effect of speckle on the accuracy of the classification for different types of applications has not been done. In this paper this specific issue is addressed.

In this paper we present a forest structural map, a flooding map and a forest type map created for a highly diverse area in the Colombian Amazon forest, using a polarimetric maximum likelihood classification algorithm developed for experimental AirSAR C-, L- P-band fully polarimetric data [Hoekman and Quiñones, 2000]. These maps bring insights into the forest structure, the biodiversity, the biomass levels and the flooding conditions and can be used as an example of the types of maps necessary to cover the information needs about the tropical forest. Overall accuracies of the resultant maps are presented before and after the application of a mapping algorithm, already introduced [Hoekman and Quiñones, 2002], to overcome the effect of speckle in the classification. In addition overall accuracies and confusion matrices can be simulated, for these three maps, when using only one or a combination of the available radar data bands as a function of the number of looks. That allows the partial assessment of new radar systems soon operational, like ENVISAT ASAR, (C-intensity satellite), the ALOS PALSAR (L-band polarimetric) and the RADARSAT-2 (C-band polarimetric), for the production of such maps. Simulation results are presented for the available systems and combination of them. The effect of P-band in the classification is evaluated. A comparison between legends of maps created for the same study area, in the past using other remote sensing techniques, is of interest to evaluate the new contributions of the actual systems.

6.2 STUDY AREA

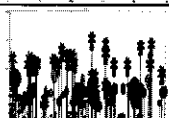
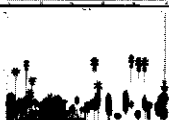
The Araracuara area corresponds to a pristine natural forest located in the Amazonas and Caquetá administrative districts of the Colombian Amazon (0°40', 72°15'). High diversity of landscapes, according to the Landscape Ecological Unit map (scale 1:100,000) are present in the area [Duivenvoorden and Lips, 1991].

Table 6.1. Legend of the Landscape Ecological Unit Map available for the Araracuara study site. Landscape ecological units (bold) and vegetation types (in brackets). Source: [Duivenvoorden and Lips, 1991]. Height above the Caquetá river level is indicated for each geomorphological unit in italic numbers. Note: Only landscape units occurring in the map in the area covered by the images are shown in this table.

Geomorphology	Landscape unit	Forest type
Alluvial plain of the Caquetá river	Frequently inundated floodplains <i>0-6</i>	Ac (P1) (H2)
	Rarely inundated flood plain <i>6-10</i>	Ec (P2) (H1)
		Eb1 (P2)
		Eb2 (L3)
		Eb3 (P4)
	Low terraces <i>10-15</i>	Tp (H1, H3)
		Tb1 (P2)
		Tb2 (L3)
		Tb3 (P4)
	High terraces <i>25-55</i>	Hp1 (H1, H3)
		Hp2 (L3)
		Hp3 (L3)
Alluvial plain of Amazonian rivers	Flood plains of clear water rivers <i>3-10</i>	Cc (H1, H3)
		Ce (H3)
		Cm2 (L2)
		Cb1 (P2)
	Terraces of Amazonian rivers <i>10-30</i>	Dp (H1)
Sedimentary plains	<i>40-70</i>	Sv (H1, H3)

The first geomorphology, soil and forest types maps of the Colombian Amazon region were published in 1979, as the result of the manual interpretation of the 1:200,000 images of the RADAM X-Band images (PRORADAM campaign, 1973). In 1991 the landscape ecological map (scale 1:100,000), based on interpretation of aerial photos was published for three areas of the Caquetá river [Duivenvoorden and Lips, 1991]. This map integrates information on geomorphology, flooding conditions, soil and vegetation structure, to characterise in detail each landscape unit. The hierarchical legend of the map divides the area in geomorphological units like the alluvial plains of the Caquetá river and the Amazonian rivers and the sedimentary plains of the Amazon basin. Each of these units is subdivided into land systems, which are defined according to the height relative to the Caquetá river and the frequency of inundation. Furthermore, each land system is divided into landscape units, which are characterised by a flooding condition, soil type and forest

Table 6.2. Forest types structural characteristics. Forest profiles as measured in the field to illustrate the structure (scale vertical axis 30 m, horizontal axis 100 m). Biomass estimation done including only individuals with diameter at breast height (dbh) >10 cm. Treelets are trees with dbh < 10 cm and higher than 2 m.

Forest types	Forest description	Forest profile	Flooding condition	Height upper canopy (m)	Bio-mass (ton/ha)	Basal area (m ² /ha)	Density (no. / 0.1 ha)		
							treelets	trees	palms
High Forest	(H1) High density, high biomass		Flooded and non-flooded	26	340	36	640	71	4
	(H2) Low tree density, intermediate biomass		Flooded and non-flooded	22	240	26	570	44	3
	(H3) High tree density, intermediate biomass.		Flooded and non-flooded	20	190	25	650	71	7
Low Forest	(L2) High tree density		Flooded and Peat	11	140	39	2100	246	0
	(L3) High treelet density		Peat	8	20	7	1700	40	3
Palm Swamp Forest	(P1) Low palm density		Flooded	20	250	34	620	92	9
	(P2) High palm density		Flooded	21	200	29	490	89	27
	(P3) High treelet density		Flooded	16	15	25	1280	99	14
	(P4) Very high treelet density and scattered palms		Flooded	6	50	8	1420	12	9

type (table 6.1) [Duivenvoorden and Lips, 1991]. The predominant life form, the biomass level, the density of the individuals and the height defines the forest types (table 6.2) [Duivenvoorden and Lips, 1991]. Forest profiles as measured in the field, are shown to illustrate the different forest structures. Maps like that can provide very relevant information on bio-diversity, and can be the base map to start monitoring activities on biomass changes and flooding condition variations.

6.3 DATABASE AND APPROACH

Five AirSAR fully polarimetric scenes were processed for the study site covering the same area as the landscape ecological map of 1991 [Duivenvoorden and Lips, 1991]. Images were acquired during high flood period (May 1993), covering a strip of 40 x 8 km, over the Caquetá river. Data is in 16-look, Stokes scattering operator format with a slant range pixel spacing of 6.66 m in range and about 8.2 m in azimuth [Van Zyl *et al.*, 1992]. Incidence angle (θ_i) varies from 20° to 60°. In this range the incidence angle dependence of the backscatter intensity parameter γ ($\gamma = \sigma^0 / \cos(\theta_i)$; σ^0 is the differential radar cross section) can be ignored [Hoekman and Quiñones, 2000, 2002].

When comparing the Total Power image of the AirSAR data with the existing landscape ecological map, it was evident that the polarimetric images have a great potential to generate a similar map. For that reason this map was selected as the basis for the interpretation of the images and for delineation of sample areas over the images. Each digitised polygon was labelled with the corresponding landscape ecological unit, the forest type and the flooding condition according to the landscape ecological map legend. In that way the same database could be sorted according to the desired parameter and used to study the classification capabilities of the polarimetric radar for flooding conditions (3 classes) and forest types (8 classes) independently from the landscape units (18 classes). The averaged Stokes parameters were extracted from the delineated areas and a data base was created from the extractions made over 878 sample areas. The averaged Stokes scattering element data of the database are used to calculate unbiased field averaged values for backscatter, phase differences and correlation from the delineated areas. Extractions cover at least 50 pixels, resulting in very accurate estimations of intensity, phase and coherence. The accuracy of the estimation of field averaged values depends on the total number of independent looks [Hoekman and Quiñones, 2000, 2002].

Classification results can be simulated as a function of independent looks using a technique introduced in a previous paper [Hoekman and Quiñones, 2000]. This previous paper describes a fully polarimetric multi-band approach to classification and introduces probability density functions (pdf) for multi-look samples of a certain class, for intensity, phase difference as well as coherence magnitude. Classification results could be simulated for a certain combination of frequency bands and

polarizations as a function of the speckle level, to give an insight into the optimum wave parameters for the different applications. The Kappa statistic is used to evaluate differences between any pair of classification results. A more detail explanation on this statistic can be found in [Hoekman and Quiñones, 2000].

The creation of a classified radar image and the evaluation of the results is not a straightforward process and can only be done properly after introducing the effect of the speckle, texture and relief into the classification and mapping procedure. A post-processing technique introduced in a previous paper [Hoekman and Quiñones, 2002] was used to mitigate those effects in the final result. The technique is a modification of the Iterated Conditional Modes (ICM) technique introduced by [Besag, 1986] by introducing new terms into the likelihood of the ICM method. The number of ICM cycles applied after the classification of the image has an effect on the overall classification result. An extensive and detailed explanation can be found in [Hoekman and Quiñones, 2002].

6.4. RESULTS

6.4.1. Maps and Legend

In this study three different types of maps could be created from the polarimetric classifications of the radar images with a relatively high overall accuracy. The radar data extracted from the 878 delineated areas over the images was used to investigate the capabilities of polarimetric radar to create a similar map. Initially all samples from the radar images were grouped in landscape units according to the existing map and assumed to be different. Some units could not be differentiated with the radar and therefore confusion between classes were found between them, forcing to derive a new legend appropriate to the differentiation capabilities of the radar. A SAR derived legend was created after a process of trial and error, using the classification simulation technique introduced by [Hoekman and Quiñones, 2000] as an exploratory tool.

In the original legend of the map, 18 landscape units occurred in the study area corresponding to 3 geomorphological units (Table 6.1). In the SAR derived legend units were grouped according to soil and flooding conditions which were parameters influencing the radar. In that way a new map with 15 different classes was created. Each class of the SAR derived map is a unique combination of soil and forest structure conditions and was named the structural type map. Table 6.3 presents the hierarchical SAR derived legend. The legend is divided in three parts. In the central grey column the landscape ecological units from the existing landscape map are shown. In that column the units that were not possible to be differentiated well can be observed, i.e., Hp1, Tp, Dp, Sv. At the right the corresponding forest types (8 classes) of the forest type map are shown. The left part is a hierarchical division of the units, according to the biophysical parameters associated to each unit. The main division is the flooding condition in which units under the same flooding regimes are

grouped (3 classes). Each flooding condition is subdivided into soil types and forest type as described in the map. This subdivision leads to the structural type map, in which 15 classes are separated. The flooding map and the forest type map can be created by class aggregation of the structural type map or by direct classification of the images using the radar averaged values associated with forest type and flooding [Hoekman and Quiñones, 2002]. For the calculation of the accuracies in this paper the database corresponding to each map was used in the simulation procedure.

Table 6.3. SAR derived legend for the flooding map, forest structural type map and forest type map, after the classification of AirSAR polarimetric data in the study area. *N* = number of training areas for each of the classes of the structural type map. The grey column corresponds to the land units as presented in the landscape ecological map. See Table 6.1. (see colour plate 6).

SAR derived Maps	Flooding Map		Cover type	Structural type map	Land-scape unit	Forest type Map		
2 classes	3 classes			15 classes		8 classes	<i>N</i>	
Flooded	Permanently flooded or wet	Peat	Palm forest (peat)	P2	Ec, (Eb1)	P2	36	
				P4	Tb3, (Eb3)	P4	22	
			Low forest (peat)	L3	Tb2, (Eb2)	L3	89	
		Thin organic deposit and peat	Palm forest	P2	Cb1	P2	36	
				P2	Tb1	P2	36	
		Thick H horizon	Low forest	L3	Hp2, Hp3	L3	18	
		Hydrous and thin organic deposits	Palm forest (flooded)	P1	Ac	P1	10	
				P4	Eb3	P4	18	
				L3	Eb2	L3	9	
		Sporadically flooded	Thin H horizon	High forest (flooded)	H3	Ce	H3	10
	H2				Ac, Ec		-	
	H1, H3				Cc	H1, H2	20	
	Non-flooded	Never flooded	Thin and thick H horizon	Primary high forest	H2, (or H1, H3)	Ac, Ec	H2, (H1, H3)	114
					H3	Ce	H3	11
H1, (or H3)					Hp1, Tp, Dp, Sv	H1, (H3)	431	

The overall classification accuracy was calculated independently for each of the maps using a 95% confidence interval for classification. Results were calculated using C-, L- and P- band fully polarimetric information (15 channels), as a function of the number of independent looks. The number of looks is an expression of the speckle level (i.e. 0.44-dB speckle level corresponds to 144 looks and 1 dB corresponds to 20 looks) [Hoekman, 1991]. Table 6.4 shows the overall classification in percentages and the average confusion between classes for different levels of speckle. In general the overall accuracy increased with the number of looks for the three maps. The simulation with an infinite number of looks (i.e. 0 dB level of speckle or absence of speckle) gave the best classification accuracy for all the maps. Percentages were higher than 80% and the confusion between classes was the lowest recorded for each map.

Table 6.4. Overall maximum likelihood classification accuracy (Over), expressed in percentages at the 95% level of confidence and the average confusion between classes (Conf) expressed in percentages. The confusion between classes is the percentage of the sum of class *a* samples classified as *b* and *b* samples classified as *a* from the sum of class *b* samples in the absence of other classes (i.e. absence of class *c* etc. and in the absence of class unknown). The expected value for maximum confusion therefore is 50%.

Type of data		Forest structural map		Flooding map		Forest type map	
# looks	ICM	Over %	Conf %	Over %	Conf %	Over %	Conf %
64	No	64.5	4.6	80.4	9.0	67.1	7.8
95	No	69.2	3.8	81.8	8.5	70.4	7.1
144	No	73.0	3.1	81.7	7.9	72.5	6.3
256	No	77.4	2.5	82.9	7.3	74.9	5.6
No	No	86.0	1.0	82.0	6.4	80.3	3.6
144	Yes	88.8	2.1	93.2	3.4	89.0	4.1

When applying the ICM mapping technique to a classified image, the accuracy of the maps increase. For instance for 144 looks (corresponding to 9 uncorrelated pixels of 16 independent looks, window of 3 x 3 pixels), the accuracy of the structural type map was calculated at 88.8% and the confusion between classes at 2.1%. These values are higher than the 73.0% and 3.1% calculated, respectively, for the same number of looks with no ICM. Furthermore the calculated overall accuracy with ICM is higher than the one calculated for no speckle level (Table 6.4).

To illustrate the effect of the post-processing ICM cycles, the classified scene of the study area, 336-b, is presented in figure 6.1, just after classification, and after 5, 10, 15 and 20 ICM cycles. The calculated overall accuracies and confusion between classes, after the application of the ICM cycles are also shown. After 20 cycles the accuracy and the confusion between classes did not improve further, in that case the map was supposed to achieve the maximum level of accuracy.

The final maps after 20 ICM cycles for the three SAR classified images can be seen in figure 6.2.. Colours of the maps correspond to the colours presented for the SAR derived legend of table 6.3.. For the mapping procedure of the flooding map and forest type map the classes from the structural type map were aggregated, saving a lot of computing time.

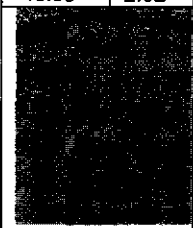
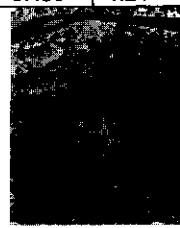
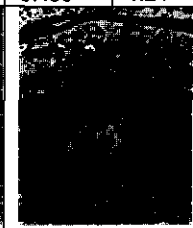
Classified image		5 cycles		10 cycles		15 cycles		20 cycles	
46.99	2.02	61.71	1.46	66.78	1.27	67.36	1.24	67.56	1.24
									

Figure 6.1. Effect of the ICM post processing algorithm over the scene 336-b of the Araracuara study site after the application of increasing number of post processing cycles. The classified image is the result of the classification algorithm (ML). For each example, the overall accuracy (expressed in percentages), and average confusion between classes (expressed in percentages). (see colour plate 8).

6.4.2. Simulation of map accuracy for different band and polarisation combinations.

Classification simulations were made as a function of the number of looks for different band and polarisation combinations corresponding to actual and soon available radar systems. In figure 6.3 the percentages of correctly classified samples as a function of number of looks, when using different band combinations, can be seen for each of the three maps. Classification clearly increases with the number of effective looks for all combinations and some combinations produce better results than others. For the tree maps the higher accuracies where achieved when using the combination of C-band polarimetric (C-pol), L-band polarimetric (L-pol) and P-band polarimetric (P-pol) data and the combination of C-band intensity (C-int), L-band intensity (L-int) and P-band intensity (P-int) data. The worst results for the three maps were found when using C-pol or C-int data alone. For L-pol and L-int results were higher than for C-band but much lower then when using only P-pol or P-int data. The combination of either C-pol or L-pol with P-pol results in higher accuracies, showing that the information contained in P-band has an important contribution to the classification.

In Table 6.5 the overall classification results, for each of the maps, using different combinations of bands can be seen for 64, 256 and an infinite number of looks as indicator of different levels of speckle (0.54 dB, 0.27 dB and 0 dB, respectively). For each map the accuracies coloured in light grey correspond to the best combinations within the three-selected speckle levels and are not significantly different from the best at the 95% level of confidence. The accuracies coloured with dark grey correspond to the worst result not significantly different from the worst result at the 95% level of confidence. The accuracies indicated in bold correspond to

the accuracies not significantly different from the best and the worst results within the same speckle level. In general the best results for the three maps are found when combining C-pol, L-pol and P-pol data or C-int, L-int and P-int data. The combination of C-pol with P-pol data also produces high non-significantly different accuracies.

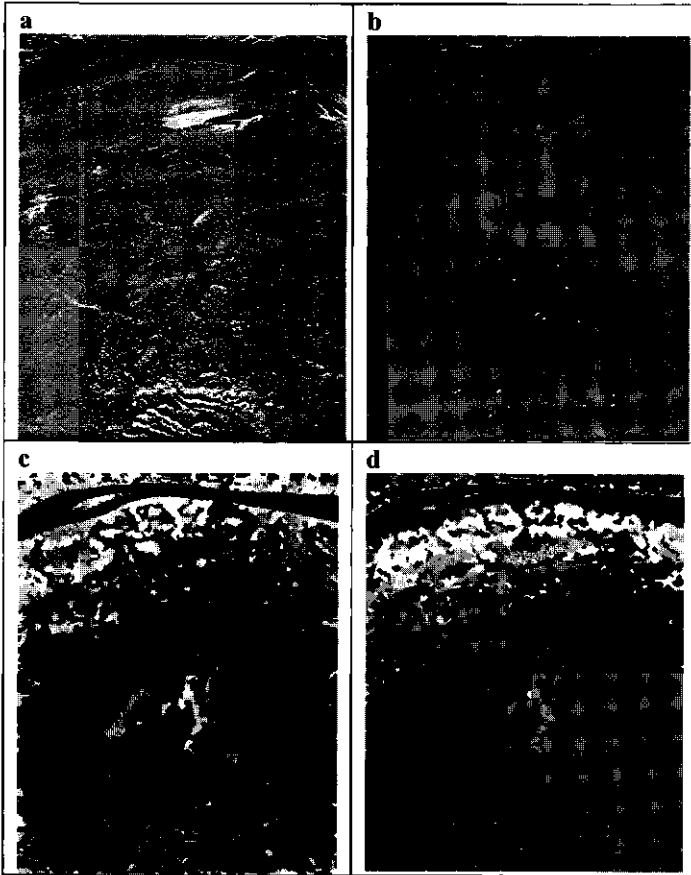
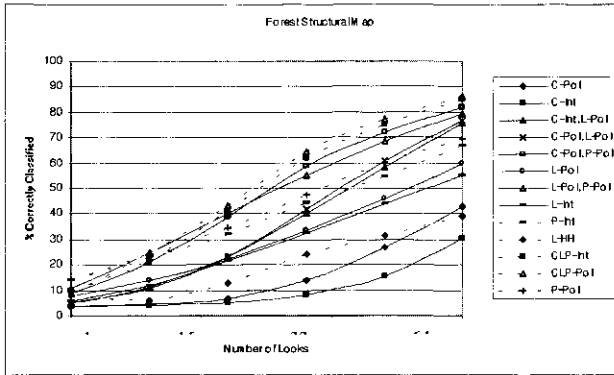


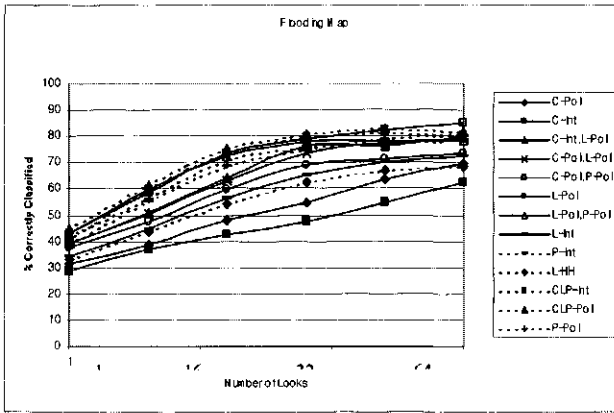
Figure 6.2: a) Total power image of AirSAR polarimetric System (C-band - blue, L-band - green and P-band -red). b) Flooding map, c) Structural type map and d) Forest type map. Colours of the maps correspond to the colours in legend (table6.3). (see colour plates 5, 9, 10, 11 respectively).

The relevance of P-band in the classification accuracy of the maps will be evaluated using the data for an infinite number of looks (0 dB speckle level). For the structural type map the use of C-pol or L-pol alone results in low accuracies (42.7% and 59.9%, respectively) while P-pol gives better results (69.7%). The combination of C-pol or L-pol with P-pol improves the accuracy to (81.8% and 79.5% respectively).

a



b



c

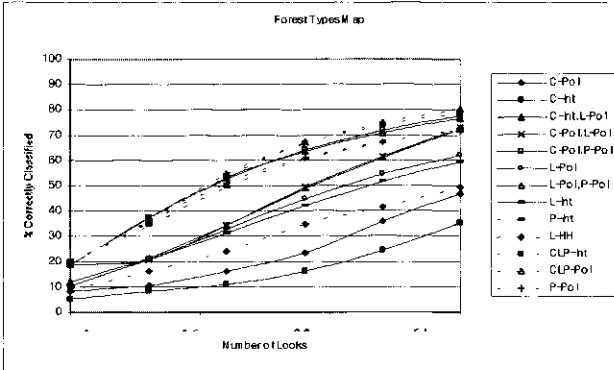


Figure 6.3. Overall maximum likelihood (ML) classification accuracy (expressed in percentages) at the 95% level of confidence for several combination of bands, as a function of the speckle level, expressed in number of looks for a) Structural Type Map, b) Flooding Map and c) Forest Type Map.

The combination of C-pol and L-pol data corresponding to the combination of actual systems results in a simulated accuracy of 76.6%. For the flooding map the accuracies produced by using a C-pol, L-pol or P-pol alone are relatively high (69.6%, 73.3% and 80.9%). Combining C-pol or L-pol with P-pol increases the accuracies to 85.1% and 78.3%, respectively.

It is interesting to notice that the accuracy of the combination of L-pol and P-pol is lower than the accuracy found when using only P-band. For the forest type map the accuracies of C-pol and L-pol are increased by adding P-pol data from 46.7% to 77.6% and from 61.8% to 76.5% respectively. The combination of C-pol and L-pol (72.7%) is similar to the results by using only P-pol data (72.0%).

For mapping purposes aggregations of pixels could be done in order to obtain a certain level of speckle (certain number of looks). If a map of a certain scale is necessary, the suitable combinations of bands for a specific number of looks must be analysed. For instance the best combination to create a flooding map scale 1:240,000 must be selected from the 64 looks column. In this case the accuracies in bold italic numbers are not significantly better. For this example the C-pol, L-pol and P-pol combination is the best but the accuracy produced by the combination of L-pol with P-pol is not significantly different from the best at 95% confidence level). With a radar system with one effective look per pixel and a spatial resolution of 12.5 m, maps at scales 1:240,000 and 1:600,000 can be created with 64 and 256 looks, respectively. Maps at those scales are supposed to fulfil the actual information needs.

To select the best combination of bands in order to create a map with a certain level of accuracy one can select the best overall accuracy and use that combination for the classification. Then the scale of the map can be calculated according to the final number of independent looks. The used number of ICM post-processing cycles improves the results to accuracies similar to the ones calculated for 0 dB of speckle.

6.5 CONCLUSIONS

The polarimetric classification of the AirSAR images, using a previously developed classification and mapping algorithm, allowed the creation of a new SAR derived legend. Three different maps were classified from AirSAR polarimetric images with a relatively high accuracy. The structural type map presents 15 classes defined according to the forest structure, soil and flooding conditions as presented in the existing landscape ecological map of the area. In the flooding map three flooding conditions can be distinguished and in the forest type map 8 different forest structures can be differentiated. The simulated accuracies for these maps when using the combination of C-pol, L-pol and P-pol data, in absence of speckle, are 86.0%, 82.0% and 80.3%, respectively.

Table 6.5. Overall maximum likelihood classification accuracy (expressed in percentages) at the 95% level of confidence for a selection of band combinations for different levels of speckle (0.54 dB = 64 looks, 0.27dB = 256 looks, 0 dB = ∞, infinite number of looks). Number under light grey shade indicate the best results plus the results that are not significantly different from the best at the 95% level of confidence, for the three levels of speckle per map. Numbers under dark grey shade indicate the worst results plus the results that are not significantly different from the worst at the 95% level of confidence, for the three levels of speckle per map. Bold italic numbers indicate the best and worst results and the numbers that are not significantly different from the best and worst result respectively, at the 95% level of confidence, for each level of speckle, for each map.

Bands	Radar system	Structural types			Flooding			Forest type			
		# of looks	64	256	∞	64	256	∞	64	256	∞
→											
C-pol, L-pol, P-pol	AirSAR	64.5	77.4	86.0	80.4	82.9	82.0	67.1	74.9	80.3	
C-int, L-int, P-int		61.7	75.2	84.9	79.6	81.4	80.3	66.7	73.9	78.6	
C-pol, P-pol	RADARSAT-2 + P pol	58.8	72.1	81.8	79.1	82.4	85.1	64.2	71.8	77.6	
L-pol, P-pol	ALOS PALSAR + P pol	55.2	68.6	79.5	77.9	78	78.3	63.6	70.6	76.5	
C-pol, L-pol	RADARSAT-2 +ALOS PALSAR	42	60.7	76.6	73.7	77.5	79.1	49.4	61.7	72.7	
C-int, L-pol	ENVISAT+ ALOS PALSAR	40.3	58.0	75.6	76.5	76.5	79.6	48.9	60.8	72.3	
P-pol	P pol	47.5	60.3	69.7	75.9	79.2	80.9	60.8	67.4	72	
P-int		44.4	54.5	67.2	75	77.5	78.7	60.3	67.4	72.4	
L-pol	ALOS PALSAR	33.3	46	59.9	68.8	71.2	73.3	44.7	54.6	61.8	
L-int		32.7	44	55.4	65.3	70.1	72.2	42.4	51.7	59.4	
C-pol	RADARSAT -2	■	26.7	42.7	■	63.4	69.6	■	36.0	46.7	
L-HH	JERS-1	■	31.5	39.0	62.5	66.6	68.5	34.8	41.6	49.3	
C-int	ENVISAT	■	■	30.6	■	■	62.4	■	■	■	

The new SAR derived legend of this map compiles information that can be compared to the landscape ecological map legend. The main difference between the legends is the main division of the geomorphological units. For the SAR derived map the main division is the flooding condition that is one of the parameters to which radar is sensitive and that compiles a large number of classes, allowing the development of a hierarchical legend. Geomorphological units can not be automatically classified with this specific sensor. One of the characteristics of the geomorphological units in the Amazon basin, besides the parental material and the geological age, is the height relative to the river basin. Differences in height can be from 3 to 50 m, which are possible to be mapped with interferometric radar. Nowadays many sensors are capable of creating digital elevation models with high level of accuracy such as the Dornier SAR, Aerosensing SAR and AirSAR TOPSAR. Some sensors can differentiate height differences in the terrain with an accuracy better than 3 m. The use of such a sensor in the study area will allow the

initial geomorphological mapping of the terrain previous to the polarimetric radar classification for structural types. If that will be the case a new and more detailed SAR derived legend could be created. Table 6.6 presents one possible legend that can be created when using interferometric and polarimetric data combined. This new possible legend is very similar to the landscape ecological unit map legend. In this case some landscape units that are not possible to be differentiated with polarimetric data can be first separated with interferometric data (i.e. Peat Eb3 and Tb3).

A comparison between all available maps for the study area is presented in Table 6.7, the area corresponding to the scene 336-b of the AirSAR data is selected to illustrate the differences. The first column refers to the first RADAR experiment in the Amazon basin, the PRORADAM campaign in 1973. These X-band images, scale 1:200,000, allowed the mapping of the whole Colombian Amazon for the first time. The images allow the manual interpretation of geomorphology, soil types and forest types at scale 1:500,000. For the same area covered by the scene 336-b the PRORADAM forest type map has only 3 different classes (column 2). The landscape ecological map, created from visual interpretation from aerial photos, scale 1:33,000, is shown in the third column. Fourteen classes were interpreted visually for the same area. The AirSAR total power image and the SAR derived structural types map can be seen in column 4 and 5. The classification of the map was done automatically using the classification and the mapping algorithm and allows the differentiation of 8 classes for the same scene. For this area the additional use of interferometric data will allow the differentiation of all landscape units with different flooding, soil and forest structure occurring at the same relative height (i.e. same geomorphological unit) for instance units like Hp1 and Dp or Eb2 and Tb2 will be possible to distinguish.

In this work it is shown that the developed algorithms can be used to produce accurate maps that can provide the information required for different applications. For instance the application of a system like the AirSAR to the Colombian Amazon will allow to map in a detail, similar to the landscape ecological map, the landscape units and therefore information on bio-diversity, flooding conditions and forest structure can be obtained with high accuracy. When biomass levels can be assigned to the mapped forest types a biomass map can also be created [Quiñones and Hoekman, 2002]. The analysis of radar data on the dry period will allow a more detailed study of the variations of the radar signature with the season and then the appropriate time for acquiring images in the future can be established. The algorithm developed to create these maps is now being tested in Indonesian tropical forest and in temperate forest, with satisfactory results [Rodriguez, 2002].

The analysis of the simulated accuracies produced by the combination of different bands and polarisations for the three produced maps, shows that in all cases the combination of C-pol, L-pol and P-pol data results in the best accuracies. In general the presence of P-pol data in the classification improved the accuracies. The importance of P-band in the classification of the images can be evaluated looking at the column of 'no speckle' level for the 3 maps (Table 6.5). For instance using only

C-pol data the simulated accuracy for the structural map is 42.7%. When adding the information contained in the P-band the classification in the structural map increases to 81.8%. The same occurs for the flooding and forests type maps

Table 6.6. Tentative SAR derived legend when integrating geomorphological information derived from interferometric systems.

Geomorphology		Flooding condition	Landscape unit	Forest type
Alluvial plain	Frequently and rarely inundated flood plains	Flooded	Ac-Ec	(P1) (P2)
			Ce	(H3)
			Cc	(H1, H3)
			Cm2	(L2)
			Eb2	(L3)
		Cb1	P2	
		Non-flooded	Ac-Ec	(H2) (H1)
			Ce	(H3)
		Peat	Eb1	(P2)
			Eb2	(L3)
	Eb3		(P4)	
	Low terraces	Flooded	Tb1	(P2)
		Non-flooded	Tp	(H1, H3)
		Peat	Tb2	(L3)
			Tb3	(P4)
High terraces	Non-flooded	Hp1-Dp	(H1, H3)	
	Peat	Hp2-Hp3	(L3)	
Sedimentary plain	Non-flooded	Sv	(H1, H3)	

Simulated data indicated that the L-pol system already planned for the coming ALOS PALSAR satellite radar when combined to the C-pol data of the RADARSAT-2 system can tentatively produce maps with high accuracy. In general it can be seen that this combination produced results higher than 75% for the three maps for 0 dB of speckle. Since these systems are not free from the effect of speckle, reduction of the accuracies can be expected. The application of post processing techniques, in this case the modified ICM algorithm, show to be very relevant in the mapping procedure after the classification of the image, to overcome the effect of the speckle in the classification.

One interesting aspect when comparing the accuracies of the maps with respect to the number of possible classified classes is that the accuracy of the structural type map (15 classes) is higher than the accuracy of the forest type map (8 classes). This can indicate that whenever the information concerning the soil and the flooding conditions is included in the definition of the classes, then the classes are better defined and can be separated with higher accuracy than when only structural parameters are defined. This implies that radar data (specially L-band and P-band) are sensitive to soil and terrain conditions and that indeed can be of great help in the definition of ecological units which are more specifically defined than a forest type unit in which only forest structure is considered.

Table 6.7. Maps and images available for the study area. (see colour plate 7)

PRORADAM Radar Image, 1973	Forest Type Map, 1979	Landscape Ecological Map, 1991	AirSAR Polarimetric Radar, 1993	Forest Structural Types Map, 2002
1 : 200,000	1 : 500,000	1:100,000	1:25,000	1:50,000
X-Band	PRORADAM Radar Image as source	Aerial Photos as source	C- L- and P-bands polarimetric	AirSAR radar image as source
	Visual interpretation	Visual interpretation	Total Power Image	Automatic classification
	Geomorphology in interpretation	Geomorphology in interpretation		Geomorphology not included in interpretation
	3 classes in this area	13 classes in this area		8 classes in this area



7. GENERAL DISCUSSION AND RECOMMENDATIONS

In this chapter an analysis of the previous 5 chapters is presented projected into the problems of using radar remote sensing for tropical forest monitoring. The evaluation is framed on technical and application aspects trying to answer some specific questions related to these issues and can be used as recommendations for the users and for future developments.

7.1 TECHNICAL DEVELOPMENTS

7.1.1. New developed classification algorithms

In the past decomposition algorithms for radar data have been related to specific wave-object interaction mechanisms and have been used for the unsupervised classification of the images. Algorithms are applied and the dominant scattering mechanism can be revealed in such a way that (vegetation) structures can associated to specific mechanisms. Algorithms are in general applied per frequency band and therefore there is always the impossibility of combining the information contained in the 3 bands. The Total Power data is a good exemption of combining multi-frequency incoherent data, but still coherent information is not incorporated. In this study the use of the total power image was essential for the initial interpretation of the images, but even the total power image was not able to reflect the structural variations as recorded in existing maps. Therefore deeper exploration of the polarimetric data was needed. The combination of the coherent information of the images was necessary for a complete assessment.

The classification algorithm developed in this thesis allows the combination of 15 channels of the AirSAR polarimetric system (C- L- and P-band with HH, HV and VV polarisations, polarimetric phase difference and polarimetric correlation for each band). The description of the radar data in terms of backscatter γ , polarimetric phase difference ϕ and polarimetric correlation $|\rho|$ was selected because it allows better interpretation in terms of physical mechanisms of backscatter and, hence, better physical understanding. The relevance of polarimetry and the effect of speckle level are studied by incorporating the (multi-look) pdf's of polarimetric phase differences and the polarimetric correlations. Kolmogorov-Smirnov tests of fit well confirm the agreement of theoretical pdf's used with experimental observations. The likelihood for an (polarimetric) observation vector to be classified as class c is modelled as the product of the joint distribution of the backscatter values multiplied by the likelihoods of the phase difference values and the likelihoods of the correlation values (Chapter 2).

The importance of combining the information contained in three bands i.e. on the three wavelengths lies in the differential detection of the forest elements relative to the size of the wavelength. In that way every band detects different scatterers. For

instance C- band can detect leaves and twigs that are transparent to P- band which interacts with bigger scatterers like trunks and branches. In addition the occurrence of dominant scattering mechanisms between the forest and the waves changes with the wavelength. For instance, in an open canopy double bounce can occur for the three bands while in a close canopy a double bounce will probably occur only for P-band that penetrates in the forest floor while C-band interactions will be basically of the single bounce or diffuse scattering type. In that way the combination of the three bands is complementary and give better insights into the interaction mechanisms that can be related to forest structure, flooding conditions or biomass levels.

In this study the selection of classes was done on the basis of field information and existing maps. Field campaigns were oriented to measure parameters to which radar could be sensitive. Forest structure, biomass, flooding conditions, terrain roughness and soil type were recorded in the two study sites. This procedure allowed the detailed study of the radar signatures for each class, i.e. different vegetation structures (Chapters 3 and 4). This step is considered of great importance for the evaluation of the data in these initial stages of the radar data analysis, because it helped to make the direct link between the radar data and the field parameters. Without the field information the interpretation of the signatures could not have been done properly or would have been incomplete. Features observed and measured in the field allowed the understanding of the separation capabilities of different classes by different bands. For instance, at the Araracuara site the presence of low backscatter values and low polarimetric phase differences in the P-band was associated with the presence of peat soil layers in the field. In this case the use of P-band was necessary for the differentiation of this specific class. This illustrates that observations on the field can be integrated into a knowledge based classifier in which all the special cases can be incorporated and used for the accurate classification of images under supervised or unsupervised regimes.

Another important aspect of this new classification algorithm is that it integrates the effect of speckle in the classification allowing the study of the effect of speckle in the accuracy of the classification. This aspect is considered of great importance in the assessment of a radar image.

The classification algorithm was also used to simulate classification accuracies for the different maps, when using only a combination of channels (Chapters, 2, 4 and 6). This capability allowed studying the use of simpler radar systems for classifying certain classes and creating different maps. This aspect is very relevant at this moment when many spaceborne radar systems are or will be taking images over the earth surface. It is important that the users assess the use of the different systems for the specific application needed. Not all the systems are useful for all sort of applications. In this thesis some examples of band combinations are studied for the created maps, this information can be used as a guide for the users to assess the actual systems. Nevertheless it is advised that before investing in a big mapping project the source images should be carefully assessed.

In this thesis the classification algorithm was used to create different types of maps. For the Guaviare site (Chapter 2), a land cover map (4 classes) was created with high accuracy (98.6%). In addition a biomass map (8 classes) could be derived using the empirical relationship between field biomass estimations and the radar values. For the Araracuara site (Chapter 3) a structural map (15 classes) was created with an accuracy of 82%. For this map the classification algorithm was used as an exploratory tool that allowed the study of the confusion between the classes for the definition of the final SAR derived legend. This is a very important aspect in the process of creating maps with radar images. An appropriate legend should present classes that are possible to distinguish with a certain level of accuracy. The overall accuracy of the classification will depend on the possibility of distinguishing the classes. This is an aspect that the users should consider carefully when assessing images for a specific product.

In the future the further developments of new decompositions based on *interferometric-polarimetry* and *interferometry* for forest structure may allow better structural classifications of the images. These new developments will probably bring new insights into the capabilities of radar systems for land survey applications.

7.1.2. New decomposition of polarimetric radar coherent elements in relation with forest structure

The tropical forest has a complex and variable structure. On one hand different forest types in general have different structure, resulting in different heights, canopy closure, DBH distributions, etc. On the other hand dynamical processes, like regeneration after gap formation or the floodplain dynamics or secondary re-growths after agricultural activities, create structural mosaics within the forest in which not well defined boundaries can be delineated.

The description of homogeneous areas within a radar image and the link with a specific forest structure could be made using for instance the decomposition of scattering mechanisms introduced in the past. Nevertheless for the Araracuara study site this decompositions were not sufficient to classify the vegetation structures occurring in the area. It is believed that the interactions of the radar with the forest is a combination of scattering mechanisms occurring at the same time and that that combination serves to characterise the structure of the forest instead of the dominant scattering mechanisms. In that way a new model based on the decomposition of the polarimetric coherence, instead of the power, is introduced in this thesis (Chapter 3).

The new approach is proposed to interpret multi-frequency coherence numbers in which the polarimetric coherence of the HH and VV signals for the three bands are decomposed. The attenuation, relative power, phase shift and coherence magnitude of the ground-surface interaction, the trunk- ground interaction, the vegetation layer interaction and the attenuation and phase shift due to the propagation through the vegetation layer are taken into account. In general it can be said that this decomposition gives insights into the scattering mechanisms occurring in a

homogenous area of an image. A detailed study of the multi-frequency polarimetric coherence in relation to field measured characteristics, allows the direct link of a certain signature to specific forest structures and terrain conditions. The effect of speckle is also considered, a large number of looks is required to enable a useful interpretation of the multi-frequency coherence. The accuracy of the complex coherence is made using the Wishart distribution

This new decomposition can be related to forest structural characteristics and terrain conditions and can be used for future applications on unsupervised forest type classifications. Still detailed analysis of this decomposition needs to be made for other study areas and forest types. Detailed study of these decompositions for polarimetric data sets all over the world can allow the study of the signatures in relation to forest structure and be useful to make interpretation of images that lack field information

7.1.3. Assessment of scattering models as tool for inversion

The scattering models are able to simulate radar values according to well-described wave-object interaction mechanisms. The description of the vegetation is made in terms of scatterers of different dimensions, orientation and water content. In this thesis the performance of the UTARTCAN scattering model is evaluated by comparing the simulated data versus experimental data of 45 field measured plots (Chapter 5). The new developed LIFEFORM interface model is being use to make a description of the tropical forest in terms of scatterer types, representing the structural characteristics of some of the life forms occurring in the tropical forest. As a conclusion of the analysis UTARTCAN performed fairly well for plots of high biomass where broad-leaved trees were the dominant life form. UTARTCAN failed to simulate radar signatures for forest types of low biomass where high proportions of palms occurred. Two main explanations can be given for such result. The first one is that UTARTCAN was developed for broad-leaved trees and the second reason is that it assumes horizontal uniformity, which is not the case for the open canopy structure of the palm forest.

From these observations it can be concluded that better descriptions of the wave-forest interactions need to be integrated to the scattering models. Perhaps the description of the life forms occurring in the tropical forest will give modellers a better idea of the type of scatterers that have to be modelled in the interactions. In addition the heterogeneity of the tropical forest canopy has to be included somehow into the models. Perhaps scatterers do not have to be distributed randomly into the layers allowing the possibilities of layers without scatterers, or perhaps the vertical distribution of scatterers can be modified according to the specific forest structures if a certain life form is dominant within one layer. The application of scattering models for the application of inversion algorithms for estimation of vegetation parameters is still not possible or applicable for tropical forest with diverse structure and terrain conditions.

Considering the limitations found for the UTARTCAN model, radar data was simulated for hypothetical forest plots of only broad-leaved trees as an exploratory tool. A systematic study of the effect of terrain and forest structure into the biomass estimations was made for high, intermediate and low biomass levels. In this case the use of UTARTCAN gave new interesting insights into the radar inversion for biomass estimation problems (Chapter 5).

With no doubt the use of models is of great importance in the study of the radar wave-object interactions, and it is expected that future improvements to actual models will be made. In addition it will be of interest to do the same type of analysis as made in Chapter 5 of this thesis, using other scattering models for comparisons, for deeper evaluation of the models.

7.1.4. New mapping techniques

The effect of texture, relief and speckle, typical of radar images, was observed to have a strong effect on the classification. To mitigate this adverse effect image-processing techniques could be used. In general traditional techniques such as image segmentation or texture and relief analysis algorithms fail to overcome these effects for different reasons as exposed in Chapter 3.

A new method based on Iterated Conditional Modes (ICM) is introduced in this thesis in order to yield radar-derived classifications with a high level of agreement with existing maps, as well as with the ground observations. In this new method the likelihood of a pixel is modified by a conditional probability on which the number of neighbours of a certain class determine the relative importance of the neighbourhood information for the classification.

This technique proved to have an important effect on the accuracy of the classification of the images in the Araracuara site (Chapters 3 and 6). The number of ICM cycles applied to a classified image increased the classification accuracy until reaching a maximum, in which a stable solution is found. Nevertheless research still needs to be done in order to optimise the use of the algorithm in other study areas. The appropriate selection of the parameters used in the neighbourhood operations and the number of appropriate cycles still has to be studied for different applications. Variations in the confusion between classes has to be carefully studied when applying this algorithm since classes occurring in small areas can easily disappear under the presence of more extended classes. In conclusion, the application of the ICM method is critical and detailed analysis of the classification results has to be done.

7.2 APPLICATIONS

7.2.1. Monitoring system

The usefulness of a radar system in a monitoring system will depend on the capacities of the system to create certain types of products that fulfil the information

needs. The type of information required, the scale and the accuracy required, and the temporal resolution, are important aspects to consider.

To monitor changes in the tropical forest a radar system should have the capacity for instance to:

- 1) Differentiate forest from non- forested land
- 2) Detect new deforested areas
- 3) Detect areas of secondary re-growth
- 4) Detect degradation processes
- 5) Detect flooding regimes
- 6) Detect differences in vegetation types

Some specific products, i.e. maps can be integrated in a monitoring system and be able to answer specific questions regarding the forest. For instance a land cover map of high accuracy can give information on the actual extension of the forested land. The information of this map when combined with multi-temporal biomass maps can give information on degradation or regeneration processes. Or when combined with flooding maps can give information for land use planning. For biodiversity assessment, for example, a map of vegetation types can be used as a base for the study of the spatial patters of species distribution or when combinations with a flooding and biomass map can be used for the study of the ecosystems.

In this thesis some specific types of maps where selected to be relevant for the monitoring of the tropical forest. Of course these maps are not the only ones that are possible to create using radar images, but for the purpose of this study were considered relevant for the establishment of a monitoring system. In the following section the feasibility of creating some maps with polarimetric radar images is summarised. For each map the accuracy when using the AirSAR system and actual radar systems is compared to accuracies simulated for other combinations of channels, the most suitable combination of bands for the map can be chosen according to the scale or speckle level of the maps. Limitations and problems encounter in the creation of these maps will be also discussed. The importance of P-band to increase the classification accuracy will be discussed.

7.2.2. Land cover map

A land cover type map was created for the Guaviare site, a colonisation area located at the edge of the Colombian Amazon. A map like this can be the base for monitoring deforestation activities, regeneration and degradation processes. Four land cover classes were selected to be interesting to monitor such changes. Classification accuracy for primary forest, secondary forest, recently deforested areas and pastures were studied to determine optimal wave parameter combinations, using an extensive database of 778 plots digitised over the AirSAR radar images. Kappa statistics were used to compare results for different combinations (Chapter 2).

In summary one may conclude that for instance for monitoring of deforestation using a single band system, the use of only C-band is useful especially when the observation frequency is high, nevertheless, the very poor capability to differentiate primary and secondary forest may pose problems. L-band with HH- or VV-polarisation for monitoring deforestation also has some problems since recently cut areas are not well differentiated from the forested areas. Adding HV-polarisation would solve this problem to a large extent. P-band has the same problem for all polarisations although P-band's capability in differentiating pastures, secondary forest and primary forest are superior.

Results would greatly improve by using a system using two frequencies. Combinations of C- and L-band or C- and P-band would give good overall results, although there is still some confusion between primary, secondary and recently cut forest (table 5, Chapter 2). The combination of L- and P-band would be even better. From a practical point of view one may conclude that, as long as P-band with a reasonable bandwidth is not allowed for spaceborne SAR operation, the combination of C- and L-band is the best choice. Tables 4 and 5 (Chapter 2) show, for example, that C-band with VV-polarisation in combination with polarimetric L-band is a good choice. The only problem seems to be the relatively poor discrimination of primary forest and secondary forest. However, since primary forest can be differentiated well from pastures and recently cut areas, and the main problem is discrimination between primary and the older secondary forest, this problem may be circumvented in a monitoring system when using frequent observation and knowledge of deforestation in the past.

Actual radar systems like JERS-1 (L-HH) will certainly not be able to distinguish all the possible classes. Primary and secondary forest could not be differentiated and both of them can not be distinguished from recently cut areas. New systems like RADARSAT-2 (C-polarimetric) will also have problems to differentiate primary from secondary forest and pastures from recently cut areas. L-polarimetric systems like the ALOS-PALSAR can improve results but still will give troubles to differentiate primary from secondary and secondary from recently cut. The combination of these two systems will increase the overall accuracy and increase the capacity to differentiate primary from secondary forest.

7.2.3. Structural type map:

The Araracuara site, a well-surveyed forest reserve in the centre of the Colombian Amazon, is characterised by a high diversity of forest types, soil types and flooding conditions. A landscape ecological map existing for the area was used for the definition of the classes. 878 delineated areas in the AirSAR images were used as the basis for the classification. Field observations were made at 23 0.1 ha plots to obtain additional quantitative descriptions on forest structure and ground surface conditions. The polarimetric classification algorithm was used to assess AirSAR's potential for landscape unit mapping as on the landscape ecological map, existing for the area. A map like this can be used as a base for bio-diversity assessment and for the study of the ecosystem dynamics. The suitability of the existing legend was

assessed for the SAR mapping process. It could be shown that a new type of legend should be derived from the SAR classification capabilities, that leads to physically better interpretable results (Chapter 3).

From this legend, the structural map (15 classes) combines information from flooding conditions, soil type and forest structure. In fact the aggregation of the structural map into different classes can lead to any of the other maps with high accuracy. C-, L- and P-band fully polarimetric data of the AirSAR system was necessary to create this map with low confusion between the classes. For a map like this the overall accuracy of the classification is very affected by the level of speckle (table 5, Chapter 6). Different levels of speckle are calculated when aggregating certain numbers of pixels in a classification procedure. For instance an aggregation of 2x2 pixels, with 16 independent looks per pixels, leads to a window with 64 independent looks (0.54 dB level of speckle). Classification accuracies can be simulated for different numbers of looks. Data is presented for different levels of speckle. In general classification accuracy increases with increasing number of looks, i.e. for the structural type map overall accuracy increases from 64.5% for 64 looks to 86.0% for an infinite number of looks (i.e. no speckle).

The effect of speckle can be overcome by reducing the scales in which the level of speckle can be increased by aggregating more pixels to increase the number of looks or by the application of post classification processing techniques, ICM (Chapters 3 and 6). The accuracy of the classification for each of the classes changes throughout the application of the ICM cycles. It is very important to analyse these changes to assess the accuracy of the map.

The overall classification accuracy was also simulated for other combination of channels. When considering the selected mapping process similar as a case free of speckle, then the best accuracy will be reached by the combination of C-pol (RADARSAT-2) with P-pol data (81.1%). The combination of L-pol (ALOS PALSAR) with P-band polarimetric (P-pol) also give good results 79.5%, affecting specially the differentiation of the high forest types. The combination of C-pol with L-pol can produce a map with 76.6 % of accuracy, but high degree of confusion occurs between the classes. This classification can be improved to a maximum of 86.0% when including P-pol data. C-pol or L-pol alone results in very low classification accuracies and high levels of confusion exist between many of the classes. The capabilities of that system to differentiate specific classes was not included in this study but can be studied in the future. In general it can be said that P-band is necessary to create a structural map with high level of accuracy, the classification accuracy when using only P-pol data is 69.7%. For C-pol data or L-pol data alone the simulated accuracies were of 42.7% and 59.9%, respectively, and is increased to 79.5% and 81.8% when adding P-pol data, respectively (Chapter 6).

7.2.4. Flooding map and forest type map

A flooding map and a forest type map are of great importance in the monitoring of a tropical forest. Water levels are related to the ecosystems and are of great importance in the maintenance of the water balance and biodiversity, in addition forest types are defined by structure, biomass levels and biodiversity.

For the Araracuara site the 878 delineated areas were also labelled according to the information on flooding condition (3 classes) and forest structure (8 classes), as defined by the landscape ecological map. The classification algorithm was used to simulate classification accuracies for this type of maps when using the AirSAR data or a combination of channels. A flooding map and forest type map were produced with high level of accuracy when using C-, L- and P-band polarimetric data without considering the effect of speckle (82.0% and 80.3%, respectively), (Chapter 6).

For the flooding map the simulated accuracies when using a single polarised band were calculated as 69.6%, 73.3% and 80.9% for C-, L- and P-band polarimetric, respectively. A very good classification is found when combining C-pol with P-pol data: 85.1%, indeed the best combination for this map. The combination of C-pol with L-pol will lead to a 79.1%, which is not significantly different from 80.9% calculated when using P-pol data alone. In this case P-band data can be important to improve the accuracy of the classification, but it is not necessary.

For the forest type map a high classification accuracy can be found when combining C-pol data with P-pol data, namely 77.6%, which is not significantly different from 80.3% calculated when using the combination of C-pol, L-pol and P-pol data. In this case the additional information given by P-band increases the accuracy calculated for L-pol alone from 61.8 % to 76.5%.

The use of RADARSAT-2 combined with ALOS PALSAR will result in accurate flooding and forest types maps, namely 79.1% and 72.7% respectively, which are high values considering the fact that they could be created with systems already available or soon available.

The designed hierarchical legend, derived from SAR classification capabilities, allows the creation of flooding and forest type maps by aggregation of classes from the forest structural map. This is a very important result since two new products can be created using the classification and computing time invested in only one map. The accuracies of the flooding map and forest type map after aggregation from the structural type map can be seen in table 5 of Chapter 3. In general accuracies are similar than the ones found for the map when no aggregation is made. The flooding map and the forest type map presented in this thesis are the result of the aggregation from the structural type map. In future mapping exercises the flooding and forest type maps will be created independently and the resultant maps could be compared.

7.2.5. Biomass map

The possibility to create biomass maps with multi-frequency polarimetric data was deeply investigated in this thesis. Chapters 2, 4 and 5 present different analysis into the problem. A biomass map is considered of great importance in a monitoring system. Biomass levels can be associated with forest types and variation throughout time can be an indicator of degradation and regeneration processes. In addition biomass is an important variable in the carbon cycle and plays an important role in the water cycle and in bio-geo-chemical processes. The distribution of biomass on the earth surface is being considered as an important question in the last years and is being one of the most important research subject for remote sensing scientists.

Studies on the relationship between biomass and radar backscatter have relied on field data to construct empirical relationships with radar backscatter that can be used for biomass estimations and mapping. In general inversion of radar data for biomass estimation is limited by the variation of backscatter caused by vegetation structural parameters and soil moisture or terrain flooding and limited to a certain maximum biomass level (roughly 150 ton/ha for P-band) dependent on the structural class.

In this thesis biomass maps are created for two study sites at the Colombian Amazon (Guaviare and Araracuara) by using results from a fully polarimetric classification algorithm that combines power, phase and coherence of C-, L- and P-band AirSAR data. Two different approaches are followed. For the Guaviare site, which is a flat and non-flooded area, land cover type classification is followed by application of an empirical relationship between biomass and backscatter intensity (using L-band HV and P-band RR polarisation) (Chapter 2). High consistency between biomass levels and land cover types are found. Saturation is around 150 ton/ha. For the Araracuara site (hilly and partly flooded) a biomass map is created by reclassifying an accurate biophysical forest structural map (15 classes) derived from a fully polarimetric SAR image classification. Each of these forest structural classes can be uniquely linked to a certain biomass level (8 classes) known from a landscape ecological map. In this case the saturation problem is avoided and biomass levels up to 340 ton/ha could be mapped accurately (Chapter 4).

Accuracy for the biomass maps are determined for subsets of the total radar data set available (Chapter 4). The best overall accuracy and the least confusion between classes are found when combining C-band polarimetric data with P-band polarimetric data (correlation 84.7%, SEE 53 ton/ha). Field data is used to validate maps and to study the behaviour of radar signatures in relation to different forest structures, flooding conditions and biomass levels. Relating the wave-object interaction to multi-frequency polarimetric coherence facilitates deeper physical understanding (Chapter 4). In addition hypothetical forest plots were created to simulate radar data using the UTARTCAN scattering model. The effect of soil moisture, terrain roughness and forest structure on the radar inversion for biomass estimations was investigated using simulated data (Chapter 5).

The simulated UTARTCAN radar data is used as input for an inversion algorithm which classified the samples after adding a certain level of speckle (expressed as number of looks) as belonging to a certain class. Results indicate that confusion between high biomass level plots of identical biomass is higher than between low biomass level plots, which means that at high biomass levels plots under different terrain roughness and soil moisture can not be differentiated. At low biomass level confusion is lower indicating that for a certain number of looks plots of different terrain and forest structure are classified as different classes.

These results indicate that direct biomass estimations from radar inversion will result in inaccuracies, but the approach proposed in this thesis allows accurate mapping of biomass, overcoming the limits imposed by the saturation effect. Multi-frequency polarimetric data can assess forest structure accurately and ecological relationships can link structures with biomass even for high biomass levels. In that way the effect of forest structure, flooding conditions and terrain roughness will have no effect on the biomass mapping accuracy.

A multi-frequency C-, L- and P-band polarimetric system like the AirSAR produces the biomass maps with higher accuracy (94.6%) with an SEE of 32 ton/ha. In the absence of this system, a combination of C-pol and P-pol data also results in accurate biomass classification (84.7%) with an SEE of 53 ton/ha and can be the most appropriate band combination since the combination of C-pol and L-pol results in 82% of accuracy but the SEE will increase to 67.7 ton/ha, almost twice the value calculated when using the AirSAR system..

7.3. AN IDEAL SYSTEM FOR TROPICAL FOREST MONITORING?

At this point of the research is still valid to ask if there is an ideal radar system configuration that can address the information needs. The need to P-band of course is always an important question since it has been widely discussed for the problems given by the band allocation and the inherent effect of Faraday rotation on the radar data.

In this thesis the potential role of a spaceborne SAR component within a dedicated global monitoring system for tropical rain forest areas was investigated. The need for frequent observation (for timely detection of illegal clear-cut for example) and, likely, the need to cover different seasons (because results probably depend on season or can be improved by combining seasons) may translate into a maximum of 3 to 4 coverages per year. Hence, a swath width of 40 km could be sufficient. To achieve accurate products it was shown that the radiometric resolution, i.e. number of looks, is an important factor. 20-look data (1 dB of speckle) can be suitable for mapping at scale of 1:100,000 for land cover maps. For structural types map, biomass map, flooding map and forest type map, a scale of 1:300,000 or 1:600,000 can be suitable. Pixels corresponding to a 30x30 m area would be required, which

would translate into roughly 6-8 m spatial resolution. Such a system is a technically viable option and may cover many information needs with high accuracy.

The possibilities of a P-band spaceborne system are still under investigation. If that system could be operational one day, the accuracy of the maps will certainly increase. In the mean time the synergism of the C-pol and L-pol systems has to be carefully investigated for the creation of the maps. The classification simulations that were done in this work indicate that multi-frequency C-, L- P-band polarimetric system is the best option to create accurate products. In the absence of such a system the combination of C-pol and P-pol data is the most suitable one to obtain accurate products.

7.4. FUTURE CAMPAIGNS?

After studying the AirSAR system, and observing that the classification of the multi-frequency polarimetric data results in the best accuracies for all the products created in this thesis, it is still a question of why not to make an extensive campaign covering the Amazon tropical forest using the AirSAR system? Very accurate airborne base maps could be created and further updating, for monitoring purposes, could be done using simpler spaceborne radar systems.

In addition new systems, like the AirSAR TOPSAR, will allow the integration of interferometric data into the classification benefiting the accuracy of, for example, biomass maps. At the moment very specific research on this system is being conducted at the Wageningen University and with no doubt results will have a big influence on the resolution, accuracy and type of information that can be derived from radar data. This thesis was a good exercise into the problem of using polarimetric radar for tropical forest monitoring, but certainly this is a science that is still new and innovative developments should be expected.

The PRORADAM campaigns over the Brazilian Amazon and the Colombian Amazon are good examples of the type of work that can be done for the mapping and investigation of the Amazon tropical forest. With the joint efforts of scientists, managers and policy makers the lack of information of the tropical forest can be a matter of the past and wise-appropriate decisions based on knowledge over the Amazon forest could be taken.

New research into the use of radar remote sensing in combination with optical systems in the monitoring of bio-diversity can be of great use in the design of natural parks for conservation purposes. As is presented in this thesis, multi-frequency polarimetric radar is well capable of landscape unit mapping, which can be a first step into the assessment of bio-diversity. New future radar campaigns the Colombian Amazon are expected to give

REFERENCES

1. Andrade, A and A. Etter, 1987, Levantamiento ecologico del área de colonización de San José del Guaviare, Corporación de Araracuara, *Proyecto DAINCO-CASAM*, Bogotá.
2. Beaudoin, A., T. le Toan, S. Goze, E. Nezry, A. Lopes, E. Mougin, C. C. Hsu, H. C. Han, J.A. Kong and R. T. Shin, 1992. Retrieval of forest biomass from SAR data. *International Journal of remote sensing*, 15, 2777-2796.
3. Beazley M., 1995, The Last Rain Forest, World Conservation Atlas. Gen. Edt. Marc Collins, Published in Association with World Conservation Union (IUCN). *Reed Books*, London.
4. Benson, A.S. and S.D. DeGloria, 1985. 'Interpretation of Landsat-4 Thematic Mapper and Multi-spectral Scanner data for forest surveys', *Photogrammetric Engineering and Remote Sensing*, vol.51, no.9, pp.1281-1289.
5. Besag, J., 1986, On the statistical analysis of dirty pictures, *Journal Royal Statistical Society B*, Vol.48, No.3, pp.259-302.
6. Bickel, S. H. and R.H.T. Bates, 1965, Effects of magneto-ionic propagation on the polarisation scattering matrix, *Proc. IRE*, 53, 8, 1089-1091, 1965.
7. Bijker, W., 1997, Radar for rain forest. A monitoring system for land cover change in the Colombian Amazon. *PhD thesis*. Wageningen Agricultural University, Sep, 1997.192 p.
8. Boerner, W. M., H. Mott, E. Luneburg, C. Livingstone, B. Brisco, R. J. Brown, J. S. Paterson. 1998. Polarimetry in Radar Remote Sensing:basic and Applied concepts. In *Principles and Applications of Imaging Radar, Manual of remote sensing* edited by Henderon F. M. and Lewis, A.J. Third Edition, Volume 2.
9. Brown, S., A.J.R. Gillespie and A.E. Lugo, 1989. Biomass Methods for Tropical Forest with applications to Forest Inventory Data. *Forest Science*. Vol. 35, No 4, pp881-992.
10. Cloude, S.R., and E. Pottier, 1996 a, A review of target decomposition theorems in radar polarimetry, *IEEE Transactions on Geoscience and Remote sensing* Vol.GE-34, pp. 498-518.
11. Cloude, S.R., and E. Pottier, 1997 b, An entropy based classification scheme for land applications of polarimetric SAR, *IEEE Transactions on Geoscience and Remote sensing*, Vol.GE-345 pp. 68-78.
12. De Grandi, G., J. P. Malingreau, and M. Leysen, 1999, The ERS-1 Central Africa Mosaic: a new perspective in radar remote sensing for the global monitoring of vegetation, *IEEE Transactions on Geoscience and Remote sensing*, Vol.37, pp. 1730-1746.
13. Dobson, M.C., F.T. Ulaby, T. Le Toan, A. Beaudoin, E.S. Kasischke and N. Christensen, 1992, Dependence of radar backscatter on conifer forest biomass, *IEEE Transactions on Geoscience and Remote Sensing* vol.30, pp.412-415.

14. Duivenvoorden, J. and H. Lips, 1991, *Mapa de Ecología del Paisaje del Medio Caquetá*, Tropenbos - Colombia, Bogotá, Colombia.
15. FAO, 2001, Global forest resources assessment 2000 Main report, ISSN 0258-6150, FAO Forestry paper 140.
16. Foody, G.M., R.M. Green, R.M. Lucas, P.J. Curran, M. Honzak and I. Do Amaral, 1997, Observations on the relationship between SIR-C radar backscatter and the biomass of regenerating tropical forests, *International Journal of Remote Sensing*, vol.18, pp.687-694.
17. Freeman, A. and S. L. Durden, 1998, A three-component scattering model for polarimetric data, *IEEE Transactions on Geoscience and Remote Sensing* vol.36, no.3, pp.963-973.
18. Freeman, A., Saatchi, S. S., Kuga, Y. and Ishimura, A., 1998. "Detection, Estimation and Correction of Faraday Rotation in Linearly Polarised SAR Backscatter Signatures", submitted to *Radio Science*, January 1998.
19. Fung, A.K., 1994, *Microwave Scattering and Emission Models and Their applications*, Artech House.
20. Fung, A.K., Z. Li and K.S. Chen, 1992, Backscattering from a randomly rough dielectric surface, *IEEE Transactions on Geoscience and Remote Sensing*, Vol.GE-30, pp.356-369.
21. Givnish, T.J., 1984, Leaf and canopy adaptations in tropical forests, in: E. Medina, H.A. Mooney and C. Vazquez-yanes (eds.): Proceedings of an international symposium on: Physiological ecology of plants of the wet tropics, Oxatepec / los Tuxtlas, Mexico, June 29- July 6 1983, pp.51-61.
22. Goel, N.S., and D.E. Strelbel, 1984, Simple beta distribution representation of leaf orientation in vegetation canopies, *Agronomy Journal*, Vol.76, pp.800-802.
23. Hess, L.L., J.M. Melack, S. Filoso and Y. Wang, 1995, Delineation of inundated area and vegetation along the Amazon floodplain with the SIR-C synthetic aperture Radar. *IEEE Transactions on Geoscience and Remote Sensing*, vol.33, pp 896-904.
24. Hess, L.L., J.M., Melack and D. S. Simonette, 1990, Radar detection of flooding beneath the forest canopy: a review. *International Journal of Remote Sensing*. Vol. 5 pp 1313-1325.
25. Hoekman, D. H. 1990, Radar remote sensing data for applications in forestry, *PhD thesis*, Wageningen Agricultural University. 277 p.
26. Hoekman, D. H. 1991, Speckle ensemble statistics of logarithmically scaled data. *IEEE Transactions on Geoscience and remote sensing* Vol 29, no.1, pp180-182.
27. Hoekman, D.H., 1997 a, ERS-1 observations of tropical rain forests in Araracuara, Colombia (LAM-6), *Proceedings TREES ERS-1 Study'94*, Ispra, 23-24 February 1995, JRC Report EUR 17286, pp.83-93.
28. Hoekman, D.H., 1997 b, Radar monitoring system for sustainable forest management in Indonesia, *Proc. IGARSS'97*, 3-8 August 1997, Singapore, pp.1731-1733.
29. Hoekman, D. H., 2001, Monitoring tropical forests using Synthetic Aperture Radar, *Proceedings of the International MOFEC-Tropenbos and NWO*

- Workshop: The balance between biodiversity conservation and sustainable use of tropical rain forests*, Balikpapan, Indonesia Dec. 6-8 1999..
30. Hoekman, D. H. and C. Verekamp, 2001, Observation of tropical rain forest trees by airborne high resolution interferometric radar, *IEEE Transactions on Geoscience and Remote Sensing*, Vol.39, No.3, pp.584-594.
 31. Hoekman, D. H. and J. J. van der Sanden, 1994, Results of the SAREX-92 campaign in Guyana and Colombia, *Workshop Proceedings SAREX-92 South American Radar Experiment*, ESA report WPP-76, Paris, 6-8 December 1993, pp.157-166.
 32. Hoekman, D. H. and M.J. Quiñones, 2000, Land cover type and biomass classification using AirSAR data for evaluation of monitoring scenarios in the Colombian Amazon, *IEEE Transactions on Geoscience and Remote Sensing* vol.38, pp.685-696.
 33. Hoekman D.H. and M.J. Quiñones. Biophysical Forest type Characterization in the Colombian Amazon by Airborne Polarimetric SAR. *Proceedings 3rd International Symposium on Retrieval of Bio-Geophysical Parameters from SAR Data for Land Applications. 11th-14th September 2001*. SCEOS, University of Sheffield UK, pp.19-23
 34. Hoekman, D. H. and M.J. Quiñones, 2002, Biophysical Forest Type Characterisation in the Colombian Amazon by Airborne polarimetric SAR. *IEEE Transactions on Geoscience and Remote Sensing* vol.40, No 6, pp. 1288-1300.
 35. Hoekman, D.H., J.J. van der Sanden and W. Bijker, 1996, Radar remote sensing of tropical rain forests: *The AIRSAR-93 campaign in Guyana and Colombia, National Remote Sensing Program report BCRS 96-02*.
 36. Houghton RA, KT Lawrence, JL Hackler and S. brown, 2001, "The spatial distribution of forest biomass in the Brazilian Amazon: a comparison of estimates. *Global Change Biology*, 7, 731-746
 37. Imhoff M.L., 1995 a, Radar Backscatter and Biomass Saturation : Ramifications for Global Biomass Inventory, *IEEE Transactions on Geoscience and Remote Sensing*, March 1995, No. 2, vol. 33, pp. 511-518.
 38. Imhoff, M.L., 1995 b, A theoretical Analysis of the effect of Forest Structure on Synthetic Aperture Radar backscatter and The Remote Sensing of Biomass. *IEEE Transactions on Geoscience and remote Sensing*, Vol.33, No.2, pp.341-353.
 39. IPCC 2000. Special Report, Land Use, Land use change and forestry, (Watson et al.), Cambridge University Press (2000) and (2001
 40. Israelsson H., J. Askne and R. Sylvander, Potential of SAR for bole Volume Estimations, *International Journal of remote sensing*, 1994, No 14, Vol. 15, 2809-2826.
 41. Jaynes, E.T., 1957, Information theory and statistical mechanics, *Physical Reviews*, Vol.106, pp.620-630.
 42. Karam, M. A., A. K. Fung, R. H. Lang and N.S. Chauhan, 1992. A microwave scattering model for layered vegetation, *IEEE Transactions on Geoscience and remote sensing*, Vol GE-30, pp.767-784.

43. Kasischke, E. S., J. M. Melack, and C. Dobson, 1997. The use of imaging radar for ecological applications – A review, *Remote Sensing of Environment*, Vol.59, pp.141-156.
44. Kasischke, E. S., N.L. Christensen, Jr. and L.L. Bourgeau-Chavez, 1995, Correlating radar backscatter with components of biomass in loblolly pine forest, *IEEE Transactions on Geoscience and Remote Sensing* Vol 33, pp.643-659.
45. Kùchler, A.W., 1988, Physiognomic and structural analysis of vegetation, in 'Handbook of vegetation science', edited by H. Lieth, Vol 10. of 'Vegetation mapping', edited by A.W. Kuckler and I.S. Zonneveld, Kluwer Academic Publishers, Dordrecht, 1988.
46. Le Toan, T., A. Beaudoin, J. Riom and D. Guyon, 1992, Relating forest biomass to SAR data, *IEEE Transactions on Geoscience and Remote Sensing* Vol. 30, pp.403-411.
47. Le Toan, T., G. Picard, J-M. Martinez, P. Melon, and M. Davidson, 2002, On the relationships between radar measurements and forest structure and biomass, ESA report SP-475 January 2002, *Proceedings of the Third International Symposium on Retrieval of Bio- and Geophysical Parameters from SAR Data for Land Applications*, 11-14 September 2001, University of Sheffield, UK, pp.3-12.
48. Lillesand T. M. and R. W. Kiefer, 1994. *Remote sensing and image interpretation*. N.Y (Jonh wiley & sons, Inc.) 3rd edition,750 p.
49. Luckman, A.J., J. Baker, T.M. Kuplich, C.C.F. Yanasse and A.C. Frery, 1997, A study of the relationship between radar backscatter and regenerating tropical forest biomass for spaceborne SAR instruments, *Remote Sensing of Environment*, vol.60, pp.1-13.
50. NASA, 1993, *AirSAR South American Deployment, Operation Plan 4.0*, Washington, DC.
51. Nghiem, S.V., S.H. Yueh, R. Kwok and F.K. Li, 1992, Symmetry properties in polarimetric remote sensing, *Radio Science*, Vol.27, pp.693-711.
52. Oldeman, R.A.A., 1983, Tropical rain forest, architecture, silvigenesis and diversity, *Tropical Rain Forest: Ecology and management*, pp.139-150, Blackwell Scientific Publications, Oxford.
53. Oliver, C. J., 2000, Rain forest classification based on SAR texture, *IEEE Transactions on Geoscience and Remote Sensing* Vol.38, pp.1095-1104.
54. Oliver, C and S. Quegan, 1998, *Understanding Synthetic Aperture Radar Images*, Artech House.
55. Pope, K.O., E. Rejmankova, J.F. Paris, and R. Woodruff. 1997. Detecting Seasonal Flooding Cycles in Marshes of the Yucatan Peninsula with SIR-C Polarimetric Radar Imagery. *Remote Sensing of Environment*.59:157-166.
56. Pope, K.O., J.M. Rey-Benayas and J.F. Paris, 1994, Radar remote sensing of forest and wetland ecosystems in the Central American tropics. *Remote Sensing of Environment*. Vol. 48 pp 205-219.
57. Press, W.H., B.P. Flannery, S.A. Teukolsky, S.A., and W.T. Vetterling, 1994, *Numerical Recipes in C*, Cambridge University Press.

58. PRORADAM, 1979, La Amazonia Colombiana y sus recursos. Proyecto Radargramétrico del Amazonas. República de Colombia, Bogotá.
59. Quegan, S., and I. Rhodes, 1995, Statistical models for polarimetric data: consequences, testing and validity, *International Journal of Remote Sensing*, Vol.16, pp.1183-1210.
60. Quegan, S., and T. Le Toan, 2002, Embedding remote sensing data in models for forest carbon dynamics, ESA report SP-475 January 2002, *Proceedings of the Third International Symposium on Retrieval of Bio- and Geophysical Parameters from SAR Data for Land Applications*, 11-14 September 2001, University of Sheffield, UK, pp.215-220.
61. Quiñones, M.J., 1995, Assessment of AIRSAR airborne polarimetric data for forested land recognition and tropical forest structure and physiognomic composition analysis, *M.Sc. Thesis*, ITC, Enschede, The Netherlands
62. Quiñones M. J. and D. H. Hoekman, a 2002, Biomass mapping using biophysical characterisation Of SAR Polarimetric Images. *Proc. 3rd. International Symposium, 'Retrieval of Bio- and Geophysical parameters from SAR Data for Land Applications'*, Sheffield, UK. 11-14 September 2001 (ESA SP-475, January 2002).
63. Quiñones M. J. and D. H. Hoekman, b 2002, Theoretical exploration of physical limits for radar biomass inversion. Submitted to *IEEE Transactions on Geoscience and Remote Sensing*, , July 2002
64. Ranson, K. J. and G. Sun, 1994, Mapping biomass of a northern forest using multi-frequency SAR data, *IEEE Transactions on Geoscience and Remote Sensing*, Vol. 32, pp.388-396.
65. Ranson, K. J. and G.Sun, 1997, An evaluation of AirSAR and SIR-C/X-SAR images for mapping northern forest attributes in Maine, USA, *Remote Sensing of Environment*, vol.59, pp.203-222.
66. Rao, K.S., Y.S. Rao, and J.R. Wang, 1995, Frequency dependence of polarization phase difference, *International Journal of Remote Sensing*, Vol.16, No.18, pp.3605-3617.
67. Rignot E. J., J Way, C. Williams, and L. Viereck., 1994 Radar Estimates of Aboveground Biomass in Boreal Forests of Interior Alaska, *IEEE Transactions on Geoscience and Remote Sensing*, No. 5, vol. 32, pp. 1117-1124.
68. Rignot, E., W. A. Salas, D.L. Skole. 1997. Mapping Deforestation and Secondary Growth in Rondonia, Brazil, Using Imaging Radar and Thematic Mapper Data. *Remote Sensing of Environment*. 59:167-179
69. Rignot, E.J, R. Zimmermann, J.J. van Zyl, 1995, Spaceborne applications of P band imaging radar for measuring forest biomass, *IEEE Transactions on Geoscience and Remote Sensing*, Vol 33, pp.1162-1169.
70. Rodriguez, Z.2002. Capabilities of POLSAR data for land cover classification in a tropical rain forest environment. East Kalimantan, Indonesia. 2002, *MSc. Thesis*, Wageningen University.
71. Rosenqvist, A., M. Shimada, B. Chapman, A. Freeman, G. De Grandi, S. Saatchi, Y. Rauste, 2000, The Global Rain Forest Mapping project - A review, *International Journal of Remote Sensing*, Vol.21, pp.1375-1387.

72. Saatchi, S.S., J.V. Soares and D.S. Alves, 1997, Mapping deforestation and land use in Amazon rainforest by using SIR-C imagery, *Remote Sensing of Environment*, vol.59, pp.191-202.
73. Schuler, D.L., J.S. Lee, and G. Degrandi, 1996, Measurement of topography using polarimetric SAR images, *IEEE Transactions on Geoscience and Remote Sensing*, Vol.34, pp.1266-1277.
74. Schuler, D.L., T.L. Ainsworth, J.S. Lee, and G. Degrandi, 1998, Topographic mapping using polarimetric SAR data, *International Journal of Remote Sensing*, Vol.19, pp. 141-160.
75. Seymour, M.S. and I.G. Cumming, 1994, Maximum likelihood estimation for SAR interferometry, *Proceedings IGARSS'94*, pp. 2272-2275.
76. Siqueira, P., S. Hensley, S. Shaffer, L. Hess, G McGarragh, B. Chapman, and A. Freeman, 2000, A continental-scale mosaic of the Amazon basin using JERS-1 SAR, *IEEE Transactions on Geoscience and Remote sensing* Vol.38, pp. 2638-2644.
77. Tough, R.J.A., D. Blacknell and S. Quegan, 1995, A statistical description of polarimetric and interferometric synthetic aperture radar data, *Proc. Royal Society London A*, Vol.449, pp.567-589.
78. Touzi, R., A. Lopes, J. Bruniquel, and P.W. Vachon, 1999, Coherence estimation for SAR imagery, *IEEE Transactions on Geoscience and Remote Sensing*, Vol.37, pp.135-149.
79. Ulaby, F. T., K. Sarabandi, K. McDonald, M. Whitt and M.C. Dobson, 1990, Michigan microwave canopy scattering model. *International Journal of remote sensing*, vol. 11, no.7, pp. 1223-1253.
80. Ulaby, F.T. and M.A. El-Rayes, 1987, Microwave dielectric spectrum of vegetation, Part II: Dual-dispersion model, *IEEE Transactions on Geoscience and Remote Sensing*, Vol.GE-25, pp.550-557.
81. Ulaby, F.T., D. Held, M.C. Dobson, K.C. McDonald, and T.B.A. Senior, 1987, Relating polarisation phase difference of SAR signals to scene properties, *IEEE Transactions on Geoscience and Remote sensing* Vol.GE-25, pp. 83-92.
82. Ulaby, F.T., R.K. Moore, and A.K. Fung, 1986, *Microwave Remote Sensing, Volume III: From Theory to Applications*, Artech House.
83. Van der Sanden, J. J., 1997. Radar Remote Sensing to Support Tropical Forest Management. *PhD thesis*. Wageningen Agricultural University, Dec 9.1997. 330 p.
84. Van Zyl, J.J., 1989, Unsupervised classification of scattering behavior using radar polarimetry data, *IEEE Transactions on Geoscience and Remote Sensing* vol.GE-27, no.1, pp.36-45.
85. Van Zyl, J.J., R. Carande, Y. Lou, T. Miller and K. Wheeler, 1992. 'The NASA/JPL three-frequency polarimetric airsar system'. In: *Proceedings of IGARSS'92; International Space Year: Space Remote Sensing*. Houston, May 26-29 1992, Volume I, pp.649-651.
86. Varekamp, C and D. H. Hoekman, 2001, Segmentation of high-resolution InSAR data of tropical forest using Fourier parameterised deformable models, *International Journal of Remote Sensing*, Vol. 22, No. 12, 2339-2350

87. Varekamp, C and D.H. Hoekman, 2001, Segmentation of high-resolution InSAR data of tropical forest using Fourier parameterised deformable models, *International Journal of Remote Sensing* (in press).
88. Wang, J.R. and T.J. Schmugge, 1980, An empirical model for the complex dielectric permittivity of soil as a function of water content, *IEEE Transactions on Geoscience and Remote Sensing*, Vol.GE-18, pp.288-295.
89. Webb, L.J., 1968, Environmental relationships of the structural types of Australian rain forest types, *Ecology*, Vol.49, No.2, pp.296-311.
90. Wismann, V., A. Cavanie, D. H. Hoekman, I. Woodhouse, K. Boenhke and C. Schnullius, 1996. Land Surface observations using the ERS-1 wind-scatterometer. Wedel (Institute for Applied Remote Sensing), *Final Report for ESA contract no. 11103/94/NL/CN*, 57 p.
91. Woodhouse, I.H. and D.H. Hoekman, 2000, Radar modelling of coniferous forest using a tree growth model, *International Journal of Remote Sensing*, Vol.21, pp.1725-1737.
92. Wooding, M. G. and E. P. W. Attema (eds.), 1994, *Workshop Proceedings SAREX-92 South American Radar Experiment*, ESA report WPP-76, Paris, 6-8 December 1993.
93. Yanasse, C.C.F., S.J.S. Sant'Anna, A.C. Frery, C.D. Rennó, J.V. Soares and A.J. Luckman, 1997, Exploratory study of the relationship between tropical forest regeneration stages and SIR-C L and C data, *Remote Sensing of Environment*, vol.59, pp.180-190.

SUMMARY

An urgent need exists for accurate data on the actual tropical forest extent, deforestation, forest structure, regeneration and diversity. The availability of accurate land cover maps and tropical forest type maps, and the possibility to update these maps frequently, is of great importance for the development and success of monitoring systems. For areas like the Amazon the use of optical remote sensing systems as the source of information, is impeded by the permanent presence of clouds that affects the interpretation and the accuracy of the algorithms for classification and map production. The capabilities of radar systems to acquire cloud free images and the penetration of the radar waves into the forest canopy make radar systems suitable for monitoring activities and provide additional and complementary data to optical remote sensing systems. Information regarding forest structure, forest biomass, vegetation cover and flooding can be associated with radar images because of the typical wave-object interaction properties of the radar systems.

In this thesis new algorithms for the classification of radar images and the production of accurate maps are presented. The production of specific maps is studied by applying the developed algorithms to two different study areas in the Colombian Amazon. The first site, San José del Guaviare, is a colonisation area with active deforestation activities and dynamic land cover change. The second, Araracuara, is a pristine natural forest with high diversity of landscapes.

In Chapter 2 the potential role of a spaceborne Synthetic Aperture Radar (SAR) component within a dedicated global monitoring system for tropical rain forest areas is investigated. Use is made of NASA's airborne radar system AirSAR, which acquired C-, L- and P-band polarimetric data of the study sites at the Colombian Amazon. Classification accuracy for primary forest, secondary forest, recently deforested areas and pastures are studied to determine optimal wave parameter combinations, using an extensive database of 778 plots. Kappa statistics are used to compare results for different combinations. The relevance of polarimetry and the effect of speckle level are studied by incorporating the (multi-look) pdf's (probability density functions) of polarimetric phase differences and the polarimetric correlations. Kolmogorov-Smirnov tests of fit well confirm the agreement of theoretical pdf's used and experimental observations. In addition possibilities for biomass estimation are studied using detailed vegetation structure measurements of bush invaded grasslands (5 plots), secondary forest (10 plots) and primary forest (13 plots). Accuracy for land cover type classification over 90% can only be obtained when two frequency bands are combined. L-band with HV polarisation and P-band showed the best possibilities for biomass estimation. After land cover type classification eight biomass classes can be differentiated at a high level of confidence. The results clearly indicate how SAR systems may be designed to accurately monitor processes of deforestation, land and forest degradation and

secondary forest re-growth. The effect of Faraday rotation on P-band data collected from spaceborne SAR is also taken into consideration.

In Chapter 3 a biophysical forest type characterisation is made by using fully polarimetric C-, L- and P- band AirSAR data of the *Araracuara* test site, a well-surveyed forest reserve in the centre of the Colombian Amazon. The area is characterised by a high diversity of forest types, soil types and flooding conditions. In this chapter a polarimetric classification technique is used to assess AirSAR's potential for forest structural type mapping and, indirectly, forest biophysical characterisation. Field observations were made at 23 0.1 ha plots to obtain additional quantitative descriptions on forest structure and ground surface conditions, but also to assess the suitability of existing map legends for SAR mapping. It could be shown that a new type of legend leads to physically better interpretable results. A method based on iterated conditional modes is introduced and is shown to yield radar-derived classifications with a high level of agreement with the landscape ecological map, as well as with the ground observations. The following results may indicate the high level of accuracy obtained: 15 classes can be differentiated, the average radar classification agreement ranges from 68-94% (depending on the type of classification and approach) and for only a few classes the agreement is less than 70%. The relation between physical forest structure and polarimetric signal properties is studied explicitly using polarimetric decomposition. A new method is introduced based on the decomposition of polarimetric coherence, instead of power. It is based on simple physical descriptions of the wave-object interaction. The accuracy of the complex coherence estimation is described using the complex Wishart distribution. Thus several interesting physical relations between polarimetric signal and forest structure can be revealed. The physical limitations of this technique and its relation with sample size are indicated.

In Chapter 4 biomass mapping using biophysical vegetation characterisation derived from SAR images is made by using results from a fully polarimetric classification algorithm that combines power, phase and coherence of C, L and P-band AirSAR data. For the two study sites Guaviare and Araracuara two different approaches are followed. For the Guaviare site, which is a flat and non-flooded area, land cover type classification is followed by application of an empirical relationship between biomass and backscatter intensity (using L-band HV and P-band RR polarisation). High consistency between biomass levels and land cover types are found. Saturation is around 150 ton/ha. For the Araracuara site (hilly and partly flooded) a biomass map is created by reclassifying an accurate biophysical forest structural map (15 classes) derived from a fully polarimetric SAR image classification. Each of these forest structural classes can be uniquely linked to a certain biomass level (8 classes) known from a landscape ecological map. In this case the saturation problem is avoided and biomass levels up to 340 ton/ha could be mapped accurately. Accuracy for the biomass maps are determined for subsets of the total radar data set available. The best overall accuracy and the least confusion between classes is found when combining C-band polarimetric data with P-band polarimetric data (correlation

84.7%, SEE 53 ton/ha). Field data is used to validate maps and to study the behaviour of radar signatures in relation to different forest structures, flooding conditions and biomass levels. Relating the wave-object interaction to multi-frequency polarimetric coherence facilitates deeper physical understanding.

In Chapter 5 a new and indirect radar inversion for biomass estimation is proposed. This new method may circumvent the problems given by signal saturation at medium biomass levels (roughly 150 ton/ha for P-band) and the effect forest structural differences, terrain roughness and soil moisture variation on the direct inversion of radar backscatter signals for forest biomass estimation. Using multi-frequency polarimetric radar the forest structure can be assessed accurately. Ecological relationships link these structures with biomass levels, even for high biomass levels. The LIFEFORM model is introduced as a new approach to transform field observations of the complex tropical forest into input files for the theoretical UTARTCAN polarimetric backscatter model. The validity of UTARTCAN for a wide range of forest structures is shown. UTARTCAN did not simulate correctly radar data of field plots with a high proportion of palms. In addition plots with discontinuous open canopy were also not well simulated, indicating that an horizontal variation in terms of scatters distribution should be included in scattering models. The systematic effect of the terrain conditions (forest structure, soil moisture and terrain roughness) on the radar signatures (backscatter and complex coherence signatures) for high, medium and low biomass levels is evaluated using simulated data of the UTARTCAN scattering model using 459 hypothetical forest plots. The results indicate that the mentioned parameters have an effect on the radar signatures, especially at low and intermediate biomass levels. At high biomass levels the signal seems to be saturated by the amount of forest scatterers and not very affected by the structural and terrain parameters. The variations on the low and intermediate biomass levels give restrictions to the direct biomass inversion. The simulated UTARTCAN radar data is used as input for an inversion algorithm, which classified the samples after adding certain levels of speckle (expressed as number of looks) as belonging to a certain class. Results indicate that confusion between high biomass level plots is higher than low biomass level plots, which means that at high biomass levels plots under different terrain roughness and soil moisture can not be differentiated. At low biomass level confusion is lower indicating that for a certain number of looks plots of different terrain and forest structure are classified as different classes. When inverting experimental field radar data, high classification accuracy (87.4%) can be found already for 16 looks when assuming that all plots have different structure and when aggregating plots by forest types according to existing forest type description, results increase to 93.7% for the same number of looks. This result indicates that structural grouping of the fields increases the classification accuracy of data. Backscatter simulations for a wide range of forest structures, terrain roughness and soil moisture clearly show the limitations of the direct inversion approach and the validity of the proposed indirect approach up to very high levels of biomass.

In Chapter 6 an assessment of suitable radar parameters is done for tropical forest mapping applications. AirSAR data is classified using the maximum likelihood polarimetric classification algorithm introduced in chapter 2. A forest structural map, flooding map and forest type map are produced with high level of accuracy when using C-, L- and P- band polarimetric data (86.0%, 82.0% and 80.3%, respectively). Different levels of speckle are calculated when aggregating certain numbers of pixels in a classification procedure. For instance an aggregation of 2×2 pixels, with 16 independent looks per pixel, leads to a window with 64 independent looks (0.54-dB level of speckle). Classification accuracies can be simulated for different numbers of looks. Data is presented for the three maps for different levels of speckle. In general classification accuracy increases with increasing number of looks, i.e. for the structural type map overall accuracy increases from 64.5% for 64 looks to 86.0% for an infinite number of looks (i.e. no speckle). Band combinations corresponding to actual or coming radar systems are assessed for the classification of the three maps. Kappa statistics are used to indicate accuracies not significantly different from others. The application of a mapping algorithm, introduced in chapter 3, to classified radar images has an effect on the overall accuracy reaching values similar as the ones calculated for data free of speckle. P-band polarimetric (P-pol) increases the overall classification of all maps, i.e. for the forest structural map (map that combines flooding and forest structure with 15 classes) the classification accuracy when using only C-pol and L-pol is increased from 76.6% to 86.0% when including P-pol data. For that same map the classification accuracy when using only P-pol data is 69.7% and is increased to 79.5% and 81.8% when adding L-pol and C-pol data, respectively. Combination of information of actual or to come radar systems will allow the creation of such maps, i.e. RADARSAT-2 or ENVISAT combined with ALOS PALSAR. If available, a P-band SAR system is expected to improve the accuracy.

The designed hierarchical legend, that includes the three maps, derived from SAR classification capabilities, allows the creation of maps by aggregation of classes. A SAR derived legend is expected to become very similar to the landscape ecological map existing for the Araracuara study area, when SAR interferometric data can be integrated. Interferometric data is expected to provide information of geomorphology for further classification of classes per gel.

RESUMEN

En la actualidad existe una urgente necesidad de información confiable y precisa sobre la extensión del bosque tropical, los procesos de deforestación y regeneración, la estructura del bosque y la distribución de la biodiversidad. La disponibilidad de mapas de cobertura de vegetación, de mapas de tipos de bosque y la posibilidad de actualizarlos es de gran importancia en el desarrollo de sistemas de monitoreo para el estudio continuo de los bosques. Para áreas como la Amazonia el uso de sistemas ópticos de sensores remotos como fuente de información es obstruido por la presencia casi permanente de nubes, afectando la interpretación, clasificación de las imágenes y así mismo la producción de mapas de alta confiabilidad. Por otro lado los sistemas de radar tienen la capacidad de adquirir imágenes libres de nubes y también pueden penetrar el dosel del bosque haciendo de estos dos tipos de sistemas, herramientas necesarias y complementarias en los procesos de mapeo y observación continua del bosque tropical. Información concerniente a estructura del bosque, biomasa, cobertura de vegetación e inundaciones puede ser asociada con los valores de las imágenes de radas debido a las propiedades de interacción de las ondas de radar y los objetos.

En esta tesis se presentan nuevos algoritmos para la clasificación de imágenes de radar y la producción de mapas de alta precisión. La producción de diversos tipos de mapas es estudiada a través de la aplicación de los algoritmos desarrollados en dos áreas de estudio en la Amazonia Colombiana. El primer sitio es *San José del Guaviare* un frente de colonización en el norte de la Amazonia en donde existe una dinámica de cambio en la cobertura de vegetación y ocurren procesos de deforestación. La segunda zona es el área de *Araracuara* donde hay una gran diversidad de unidades de paisaje y el bosque ha sido poco intervenido.

En el Capítulo 2 se investiga el uso potencial de un sistema de radar satelital de apertura sintética (SAR) en el marco de un sistema de monitoreo global del bosque húmedo tropical. Se hace uso del sistema aéreo experimental de la NASA, AirSAR, que adquirió imágenes polarimétricas, bandas C-, L- y P- sobre las áreas de estudio en 1993. La precisión en la clasificación de bosque primario, bosque secundario, pastos y zonas recién deforestadas, es estudiada para determinar la combinación apropiada de bandas y polarizaciones para un sistema de radar satelital óptimo. Para este propósito se utiliza una base de datos de 778 áreas de muestra. El estadístico Kappa, se utiliza para comparar los resultados de las diferentes clasificaciones. La importancia del uso de datos polarimétricos y el efecto del speckle en la precisión de la clasificación de las imágenes, son estudiados al introducir en la clasificación funciones de probabilidad (de varias observaciones) de la diferencia de fase polarimétrica y la correlación polarimétrica. El estadístico Kolmogorov-Smirnov es utilizado para confirmar la correspondencia de las funciones de probabilidad teóricas con las observadas en las imágenes. Adicionalmente se estudia la posibilidad de hacer estimativos de biomasa usando descripciones estructurales

detalladas de áreas de pastos (5 parcelas), bosque secundario (10 parcelas) y bosque primario (13 parcela). Precisiones de clasificación por encima de 90 % pueden ser obtenidas solo cuando se combinan dos o más bandas y polarizaciones. La banda L-HV combinada con las polarizaciones de la banda P mostraron las mejores posibilidades para la clasificación de tipos de cobertura y para realizar estimaciones de biomasa. La clasificación de ocho niveles de biomasa puede ser realizada con alta precisión al asociarlos con el mapa de cobertura de vegetación. Después de realizar una clasificación de los tipos de cobertura. Los resultados presentados en este capítulo ilustran claramente como un sistema SAR debe ser diseñado para lograr un monitoreo preciso y confiable de procesos de deforestación, degradación de bosques y regeneración de bosques secundarios. También es considerado el efecto Faraday de rotación, que afecta a las ondas de la banda P, si fueran emitidas desde el espacio.

En el capítulo 3 se hace una caracterización biofísica de tipos de bosque utilizando datos polarimétricos de las bandas C-, L- y P- del área de *Araracuara*. El área esta caracterizada por una alta diversidad de tipos de bosque, tipos de suelo y condiciones de inundación. En este capítulo la técnica de clasificación polarimétrica, desarrollada en el capítulo 2, es usada para evaluar el potencial de las imágenes AirSAR en la clasificación de tipos estructurales de bosque y la caracterización biofísica del bosque. Observaciones de campo, fueron realizadas sobre 23 parcelas de 0.1 ha, no solo con el propósito de obtener descripciones cuantitativas de la estructura del bosque y de hacer observaciones del terreno sino también para evaluar la aplicación de la leyenda del mapa de ecología de paisaje disponible para el área de estudio, en el mapa resultado de la clasificación de las imágenes de radar. Se pudo comprobar que el desarrollo de una nueva leyenda es necesario para una mejor interpretación en terminos físicos de los resultados de clasificación. Adicionalmente, un nuevo método de post-procesamiento de las imágenes clasificadas es introducido en este capítulo y se muestra que este post-procesamiento es relevante y necesario para lograr precisión y un alto nivel de correspondencia tanto con el mapa de ecología de paisaje como con las observaciones de campo. Los siguientes resultados son un indicativo del nivel de precisión encontrada: 15 tipos estructurales de bosque pueden ser diferenciados con niveles de precisión que van desde 68% hasta 94% (dependiendo del tipo de clasificación y de la metodología), menos clases pueden ser diferenciadas con un 70% de correspondencia. De gran importancia en el proceso de mapeo es el estudio de la relación entre las características estructurales del bosque y las propiedades polarimétricas de las ondas de radar que en este capítulo es estudiada explícitamente usando una nueva descomposición física de la información polarimétrica. Un nuevo método de descomposición de la señal se presenta, basado en la descomposición de la coherencia polarimétrica en vez de la normalmente utilizada descomposición del poder (nivel de energía) de la señal. La coherencia compleja esta basada en una descripción física simple entre la interacción de las ondas de radar y los objetos. La precisión de esta nueva descomposición se puede realizar utilizando la distribución de Wishart. De esta manera diversas relaciones físicas entre las señales polarimétricas y la estructura del bosque pueden ser observadas. Las limitaciones físicas en la aplicación de esta

nueva técnica y su relación con el tamaño de la muestra (numero de observaciones del radar) son indicadas.

En el capítulo 4 mapas de biomasa para las áreas de estudio se realizan utilizando la descripción biofísica estructural de la vegetación, derivada de la clasificación de las imágenes de radar. La clasificación se realiza utilizando el algoritmo de clasificación que combina la información de poder y la información polarimétrica de las bandas C-, L- y P- del sistema AirSAR. Para cada sitio de estudio se siguen diferentes metodologías. Para el área de Guaviare, cuyo terreno es plano y no-inundado, la clasificación de los tipos de cobertura es seguida por la aplicación de una relación empírica entre los valores de radar y su correspondiente valor de biomasa, según registros de campo (utilizando la combinación de polarizaciones L-HV y P-RR). Un alto nivel de consistencia es encontrado entre los niveles de biomasa y los tipos de cobertura. La saturación de la señal de radar esta alrededor de 150 Ton/ha de biomasa. Para el área de Araracuara (terreno ondulado y parcialmente inundado) el mapa de biomasa es creado a partir de la re-clasificación del mapa de tipos estructurales (15 clases) creado con la clasificación polarimétrica de las imágenes de radar. Cada una de estas clases estructurales puede ser ligada con un nivel específico de biomasa (8 niveles en este caso) según el mapa de ecología de paisaje. En este caso el efecto de saturación de la señal de radar no es relevante y se pueden lograr mapas de alta precisión, derivados de imágenes de radar con niveles de biomasa hasta de 340 Ton/ha. El mejor valor de clasificación con la menor confusión entre clases es obtenido cuando se combinan la información polarimétrica de la banda C con la información polarimétrica de la banda P (correlación de 84.7%, SEE 53 ton/ha). Los datos de campo son utilizados para validar los mapas y para estudiar las señales de poder y polarimétricas del radar en relación con la estructura de bosque y el nivel de inundación y su influencia en las estimaciones de biomasa. Al relacionar el tipo de interacción entre la onda de radar y los objetos con la descomposición polarimétrica se llega a una mayor comprensión física.

En el capítulo 5 se propone un nuevo método de inversión para estimaciones de biomasa. Este nuevo método evita los problemas dados por la saturación de la señal de radar en valores medios de biomasa (cerca de 150 Ton/ha para la banda P) y por el efecto de la estructura del bosque, las diferencias del terreno y las condiciones de inundación del suelo sobre la inversión directa de los valores de radar, para la estimación de valores de biomasa. Usando la clasificación polarimétrica la estructura del bosque puede ser mapeada con precisión. Relaciones ecológicas pueden ligar valores de biomasa con ciertos tipos estructurales hasta alto niveles de biomasa. El modelo LIFEFORM es introducido como un nuevo método para transformar las observaciones de campo de la compleja estructura del bosque tropical en archivos de entrada para modelos teóricos de simulación de datos de radar polarimétrico, tal como el modelo UTARTCAN. La validez de los resultados producidos por UTARTCAN se ilustra para una gama diversa de tipos estructurales de bosque, según los datos de campo. UTARTCAN simulo incorrectamente valores de radar para las parcelas con un alto porcentaje de palmas. Adicionalmente valores de radar para parcelas con un dosel discontinuo tampoco fueron simulados

correctamente, indicando que la variación horizontal en la distribución de los objetos de interacción con el radar es importante y debe ser incluida en los modelos de simulación. Adicionalmente se estudia el efecto sistemático de las condiciones del terreno (estructura de bosque, humedad de suelo y ondulación del terreno) en las señales del radar (señal de poder y señal polarimétrica) para valores de biomasa alta, media y baja. Para esto se hace uso del modelo UTARTCAN usando 459 parcelas hipotéticas de bosque en las que la estructura y las condiciones del terreno variaban. Los resultados indican que los parámetros arriba mencionados tienen un efecto sobre los valores de radar y por ende tienen un efecto en las estimaciones de biomasa a través de una inversión directa de los valores de radar, especialmente en los valores intermedios y bajos de biomasa. A niveles altos de biomasa la señal se satura y el efecto de la estructura y el terreno son imperceptibles. Las variaciones producidas por las características del terreno y la estructura en los valores simulados de radar, producidos por el modelo UTARTCAN, para diferentes tipos hipotéticos de estructura de bosques bajo diferentes regímenes de inundación y ondulación del terreno, son utilizados como entrada en un algoritmo de inversión que clasifica cada muestra después de agregar diferentes niveles de ruido (speckle), de acuerdo a una clase específica. Los resultados indican que la confusión entre clases es mayor entre parcelas de alta biomasa, lo cual significa que debido a la saturación, parcelas de vegetación de alta biomasa, localizadas bajo diferente terreno y bajo diferentes regímenes de inundación, no pueden ser diferenciadas con el radar. A niveles bajos de biomasa la confusión entre clases es menor, indicando que a estos niveles tipos de bosque con diferente estructura y condiciones de terreno pueden ser clasificados con diferentes niveles de precisión, dependiendo de la resolución radiometría del radar (numero de observaciones del radar). Para 16 observaciones de radar (looks) se puede obtener una precisión del 87.4% para parcelas de diferente estructura y terreno. Cuando las parcelas se agregan de acuerdo con el tipo de estructura la clasificación mejora hasta un 93.7 % para ese mismo numero de observaciones. Estos resultados indican que la nueva metodología de inversión de las imágenes de radar propuesta en este capítulo es la mas apropiada para las imágenes de radar hasta la fecha.

En el Capítulo 6 se hace una evaluación de las diferentes características de los sistemas de radar para las diversas aplicaciones en el bosque húmedo tropical. Las imágenes AirSAR disponibles para el área de Araracuara son clasificadas utilizando el algoritmo introducido en el capítulo 2. Usando la combinación de las bandas C-, L-, y P- se clasificaron las imágenes de acuerdo a tipos estructurales, condiciones de inundación y tipos de bosque, produciendo mapas con 86 %, 82.0% y 80.3 % de precisión respectivamente. Diferentes niveles de speckle (expresado en numero de observaciones de radar) fueron calculados agregando diferente numero de pixeles en un proceso de clasificación. Por ejemplo la agregación de 2x2 pixeles con 16 observaciones independientes por pixel, resulta en una ventana de 64 observaciones independientes (que es lo mismo que decir un nivel de speckle de 0.54 dB). Precisiones de clasificación pueden de esa manera ser simuladas para diferentes numero de observaciones (looks). En general la precisión de la clasificación

incremento con el número de observaciones. En este capítulo se presentan resultados de clasificación para los tres mapas, con diferentes niveles de speckle y diferentes combinaciones de bandas. Por ejemplo para el mapa de tipos estructurales la precisión varía de 64.5% para 64 observaciones hasta 86.0% para un número infinito de observaciones. Las combinaciones de bandas, correspondientes a sistemas de radar que actualmente son operativos o que serán en un futuro próximo operativos, son evaluadas para los mapas aquí producidos. El estadístico Kappa es utilizado para identificar diferencias significativas entre los resultados de clasificación. La aplicación del algoritmo de mapeo, introducido en el capítulo 3, para las imágenes de radar clasificadas, tiene un efecto positivo, sobre los estimativos de precisión de la clasificación: la precisión de clasificación aumenta hasta niveles semejantes a los simulados para imágenes sin speckle. Considerando este efecto se puede decir que la aplicación en la clasificación, de banda P polarimétrica (P-pol) aumenta la precisión de la clasificación. Por ejemplo para el mapa de tipos estructurales la precisión de clasificación usando solo P-pol combinado con L-pol aumenta de 76.6% a 86% si se incluye la información de P-pol. Para el mismo mapa la precisión de la clasificación usando solo P-pol es de 69.7% y aumenta a 79.5% y 81.8% si se combina con L-pol o con C-pol respectivamente. Combinación de sistemas de radar actuales con sistemas futuros permitirá la creación de mapas de alta precisión a niveles regionales a incluso globales. Los sistemas RADARSAT-2 o ENVISAT combinados con el futuro sistema ALOS PALSAR pueden generar la información requerida sobre el bosque húmedo tropical. En un futuro es probable que el satélite de banda P, hasta ahora no autorizado, pueda, mejorar la precisión de los mapas producidos por otros radares.

El desarrollo de tecnología tal y como la interferometría, podrá en un futuro ser aplicada en temas como el mapeo de las zonas de bosque tropical. Sin lugar a dudas la interferometría integraría un nuevo tipo de datos que podrían mejorar aun más la precisión de los mapas aquí creados.

SAMENVATTING

Er is een urgente behoefte aan een nauwkeurig bepaling van het huidige areaal tropisch bos, de ontbossing, de structuur van het bos, de regeneratie en de biodiversiteit. De beschikbaarheid van nauwkeurige kaarten van landbedekking en de soorten tropisch bos, en de mogelijkheid om deze kaarten regelmatig te actualiseren, is van groot belang voor de succesvolle ontwikkeling van monitoringsystemen. Voor gebieden zoals het Amazone gebied is het gebruik van optische remote sensing systemen als informatiebron sterk gelimiteerd door de bijna permanente aanwezige bewolking die de interpretatie bemoeilijkt en de nauwkeurigheid van de classificatie algoritmen negatief beïnvloed. De mogelijkheid om onder alle omstandigheden bewolkingsloze opnamen te maken en de mogelijkheid om met radargolven in de vegetatie door te dringen bewerkstelligen dat radarsystemen, in relatie tot optische remote sensing systemen, aanvullende en complementaire informatie kunnen leveren. Informatie betreffende de vegetatie structuur, biomassa, bedekking en overstromingscondities kan worden bepaald met behulp van radarbeelden door de specifieke eigenschappen van de interacties tussen radargolven en het meetobject.

In dit proefschrift worden nieuwe algoritmes voor de classificatie van radarbeelden en het maken van nauwkeurige kaarten gepresenteerd. Het maken van specifieke kaarten is bestudeerd door gebruik te maken van nieuw ontwikkelde algoritmes voor twee verschillende onderzoekslocaties in het Colombiaanse Amazone gebied. De eerste locatie, *San José del Guaviare*, is een gekoloniseerd gebied waar actieve ontbossing en dynamische landbedekkingsveranderingen plaatsvinden. De tweede locatie, *Araracuara*, is een ongerept natuurlijk bos met een grote diversiteit in landschapseenheden.

In Hoofdstuk 2 wordt de mogelijke rol van een in de ruimte gestationeerd SAR instrument binnen het kader van een mondiaal monitoringsysteem voor tropische regenwoud gebieden bestudeerd. Hier is gebruik gemaakt van C-, L- en P-band polarimetrische opnamen met het NASA vliegtuigradarsysteem AirSAR van een gekoloniseerd gebied aan de rand van het Colombiaanse Amazone gebied. De classificatie nauwkeurigheid voor primair bos, regeneratie bos, recent ontboste gebieden en grasvelden is bestudeerd om optimale combinaties van radargolfparameters te bepalen. Hierbij is gebruik gemaakt van een uitgebreide database met 778 meetlocaties. Een Kappa-statistiek analyse is gebruikt om de resultaten voor verschillende combinaties te vergelijken. Het belang van polarimetrie en het effect van het *speckle* niveau worden bestudeerd door de *multi-look* kansdichtheidsfuncties (*pdf*) van de polarimetrische faseverschillen en correlaties mee te nemen in de analyse. Kolmogorov-Smirnov tests bevestigen de overeenkomst tussen de theoretische *pdf*'s en experimentele metingen. Bovendien worden de mogelijkheden voor biomassa schattingen bestudeerd door gebruik te

maken van gedetailleerde vegetatiestructuurmetingen van grasvelden overwoekerd met struiken (5 plots), regeneratie bos (10 plots) en primair bos (13 plots). Een nauwkeurigheid voor de landbedekkingsclassificatie groter dan 90% kan alleen worden bereikt door het combineren van twee frequentiebanden. De L-band met HV polarisatie en P-band leverden de beste mogelijkheden op voor biomassa schattingen. Na de classificatie van de landbedekking kunnen acht biomassa klassen met een grote mate van zekerheid worden onderscheiden. De resultaten geven duidelijk aan hoe SAR systemen kunnen worden ontwikkeld om nauwkeurig ontbossingsprocessen, land- en bosdegradatie en de hergroei van regeneratie bos te meten. Het effect van de Faraday rotatie op de P-band data gemeten met een satelliet SAR systeem is ook meegenomen in de analyse.

In Hoofdstuk 3 wordt de biofysische karakterisering van bostypen afgeleid uit volledig polarimetrische C-, L-, en P-band AirSAR metingen van het *Araracuara* proefgebied, een goed onderzocht bosreservaat in het midden van het Colombiaanse Amazone gebied. Het gebied wordt gekenschetst door een grote diversiteit van bos- en bodemsoorten en overstromingscondities. In dit Hoofdstuk wordt een polarimetrische classificatietechniek gebruikt om de potentie van AirSAR data voor het bepalen van structureigenschappen en, indirect, de biofysische karakterisering. Er zijn metingen van 23 0.1 ha locaties gemaakt voor het verkrijgen van extra kwantitatieve beschrijvingen van de bosstructuur en bodemcondities, maar ook om de geschiktheid van bestaande legenda eenheden voor van SAR afgeleide kaarten vast te stellen. Het kon worden aangetoond dat een nieuwe soort legenda leidt tot een resultaat dat beter fysisch geïnterpreteerd kan worden.

Een methode gebaseerd op iteratieve conditionele toestanden (*iterative conditional modes, ICM*) is geïntroduceerd en het wordt aangetoond dat dit een op radar gebaseerde classificatie oplevert die goed overeenkomt met de bestaande landschap-ecologische kaart en tevens met de eigen veldwaarnemingen. De hierna volgende resultaten geven de hoge mate van nauwkeurigheid aan die bereikt is: 15 klassen kunnen worden onderscheiden, de gemiddelde overeenkomst tussen de bestaande kaart en de radarclassificatie varieert tussen 68-94% (afhankelijk van het vegetatietype en de benaderingsmethode). Slechts voor een klein aantal klassen is de overeenkomst minder dan 70%. De relatie tussen de fysische bosstructuur en de polarimetrische radarsignaaleigenschappen is expliciet bestudeerd door gebruik te maken van polarimetrische decompositie. Een nieuwe methode gebaseerd op de decompositie van polarimetrische coherentie in plaats van de *Total Power* wordt geïntroduceerd. Dit is gebaseerd op eenvoudige fysische beschrijvingen van de interactie tussen de radargolf en het meetobject. De nauwkeurigheid van de complexe coherentie schatting is beschreven door middel van de *complex Wishart* verdeling. Hierdoor kunnen enkele interessante fysische relaties tussen het polarimetrische signaal en de bosstructuur worden aangetoond. De fysische beperkingen van deze techniek en de afhankelijkheid met het aantal radar *looks* worden aangegeven.

In Hoofdstuk 4 wordt de kartering van biomassa, gebaseerd op de biofysische vegetatiekarakterisering en afgeleid van SAR beelden, uitgevoerd door gebruik te maken van de resultaten van een volledig polarimetrische classificatiealgoritme dat de intensiteit, faseverschil en coherentie van de C-, L-, en P-band AirSAR metingen combineert. Voor de twee proefgebieden *Guaviare* en *Araracuara* worden twee verschillende benaderingen toegepast. Voor de *Guaviare* locatie, een vlak en niet geïnundeerd terrein, wordt de toepassing van een empirische vergelijking tussen biomassa en de radarintensiteit (door gebruik te maken van L-band HV en P-band RR polarisatie) voorafgegaan door een classificatie van het landbedekkingstypen. Dit resulteert in een goede overeenkomst tussen de hoeveelheid biomassa en landbedekkingsklassen en het verzadigingsniveau ligt rond de 150 ton/ha. Een biomassakaart is gemaakt voor de *Araracuara* locatie (heuvelig en gedeeltelijk overstroomd) door een herclassificatie van een nauwkeurige kaart van de biofysische bosstructuur (15 klassen), afgeleid van een classificatie van een volledig polarimetrische SAR opname. Elk van deze bosstructuurklassen kunnen ondubbelzinnig worden gerelateerd aan een specifieke hoeveelheid biomassa (8 klassen) bepaald uit een landschap-ecologische kaart. OP deze wijze wordt het verzadigingsprobleem voorkomen en hoeveelheden biomassa tot 340 ton/ha kunnen nauwkeurig worden gekarteerd. De nauwkeurigheid van de biomassa kaarten wordt bepaald aan de hand van een deel van de beschikbare radardataset. De beste nauwkeurigheid en de laagste verwarring tussen klassen wordt bereikt door het combineren van C-band met P-band polarimetrische data (correlatie 84.7%, SEE 53ton/ha). Veldmetingen worden gebruikt om kaarten te valideren en om de veranderingen in radarsignalen als functie van verschillende bosstructuren, overstromingscondities en hoeveelheden biomassa te bestuderen. Het relateren van interacties tussen de radargolf en het meetobject en de multi-frequente polarimetrische coherentie verschaft een beter fysisch begrip.

In Hoofdstuk 5 wordt een nieuwe en indirecte afleiding van schattingen van biomassa met behulp van radar voorgesteld. Deze nieuwe methode kan de problemen van signaalverzadiging bij 'gemiddelde' biomassaniveaus (ongeveer 150 ton/ha voor de P-band) vermijden ongeacht het effect van de verschillen in boomstructuur, terreinruwheid en variaties in bodemvocht op het radarbackscattersignaal. De boomstructuur kan nauwkeurig wordt bepaald door gebruik te maken van multi-frequente polarimetrische radarbeelden. Ecologische relaties koppelen deze structuren aan de hoeveelheden biomassa, zelfs voor grote hoeveelheden. Het LIFEFORM model wordt geïntroduceerd als een nieuwe benadering voor het aanmaken van de invoergegevens voor het theoretische UTARTCAN polarimetrische backscatter model, gebaseerd op veldmetingen in tropisch bos. De toepasbaarheid van UTARTCAN voor een grote variatie van bosstructuren wordt gedemonstreerd. UTARTCAN is niet in staat om de radar data voor terrein met een hoge dichtheid van palmen realistisch te simuleren. Bovendien, locaties met een onderbroken open kronendak kunnen ook niet goed worden gesimuleerd wat aangeeft dat de horizontale variatie, uitgedrukt in de verdeling van de scatterers moet worden opgenomen in de verstrooiingsmodellen. Het systematische effect van de terreincondities (bosstructuur, bodemvocht en

terreinruwheid) op de radarsignatuur (intensiteit en complexe coherentie kenmerken) voor grote, gemiddelde en kleine hoeveelheden biomassa wordt geëvalueerd op basis van simulaties met het UTARTCAN verstrooiingsmodel dat 459 hypothetische bosstructuren gebruikt. De resultaten geven aan dat genoemde parameters een effect hebben op de radarkenmerken, speciaal voor lage en gemiddelde hoeveelheden biomassa. Voor grote hoeveelheden biomassa lijkt het signaal lijkt te verzadigen ten gevolge van het grote aantal verstrooiingselementen en wordt niet sterk beïnvloed door de bosstructuur- en terreinkarakteristieken. De variaties voor kleine en gemiddelde hoeveelheden biomassa beperkt de directe afleiding van hoeveelheden biomassa. De radar data gesimuleerd met UTARTCAN worden gebruikt als invoer voor een inversie-algoritme dat de hypothetische bosstructuren classificeert, na het toevoegen van een specifiek *speckle*-niveau (uitgedrukt in het aantal *looks*). De resultaten geven aan dat de verwarring tussen structuren met grote hoeveelheden biomassa groter is dan die voor kleine hoeveelheden biomassa. Dit betekent dat voor grote hoeveelheden biomassa er geen onderscheid kan worden gemaakt tussen locaties met verschillende terreinruwheden of bodemvochtniveaus. Voor kleine hoeveelheden biomassa is de verwarring kleiner wat aangeeft dat onder bepaalde omstandigheden verschillende terrein- en boomstructuren worden geclassificeerd. Met het inverteren van radarsimulaties van experimentele veldwaarnemingen wordt een hoge classificatienauwkeurigheid (87.4%) al bereikt voor 16 *looks* als wordt aangenomen dat alle locaties een verschillende structuur hebben. Aggregatie van de resultaten, afhankelijk van het type bos en gebaseerd op de bestaande beschrijving van het bos, resulteert in een toename van de nauwkeurigheid tot 93.7% voor hetzelfde aantal radar *looks*. De resultaten geven aan dat een structurele groepering van de locaties de classificatienauwkeurigheid vergroot. Simulaties van radarbackscatter voor een veelvoud aan bosstructuren, terreinruwheds- en bodemvochtklassen later duidelijk de beperkingen en de toepasbaarheid van de directe inversie benadering zien voor grote hoeveelheden biomassa.

In Hoofdstuk 6 wordt een studie uitgevoerd naar de geschiktheid van radarparameters voor de kartering van tropisch bossen. AirSAR data worden geclassificeerd gebruik makend van het *maximum likelihood* polarimetrische classificatie algoritme, beschreven in Hoofdstuk 2. Kaarten van de bosstructuur, overstromingscondities en type bos worden gemaakt met een hoge mate van nauwkeurigheid door verwerking van de C-, L- and P-band polarimetrische data (respectievelijk 86.0%, 82.0% and 80.3%). Aggregatie van specifieke aantallen pixels in de classificatieprocedure resulteert in verschillende niveaus van *speckle*. Bijvoorbeeld, aggregatie van 2 x 2 pixels met 16 onafhankelijke *looks* per pixel, resulteert in een venster met 64 onafhankelijke *looks* (0.54 dB *speckle* niveau). De classificatienauwkeurigheid kan worden gesimuleerd voor het verschillende aantallen *looks* te variëren. De resultaten worden beschreven voor de drie kaarten voor verschillende *speckle* niveaus. In het algemeen neemt de classificatienauwkeurigheid toe met het aantal *looks*. De totale nauwkeurigheid van de kaart van bosstructuur neemt bijvoorbeeld toe van 64.5% voor 64 opnames tot 86.0% voor een oneindig aantal *looks* (d.w.z. geen *speckle*). De combinaties van

golf lengtes, die overeenkomen met de actuele of de nog te ontwikkelen radar systemen, worden voor de classificatie van de objecten op deze drie kaarten geëvalueerd. Aan de hand van Kappa-statistieken worden niet significante verschillen in de nauwkeurigheden vastgesteld. Het gebruik van het *ICM* nabewerkings-algoritme, zoals beschreven in Hoofdstuk 3, op de geclassificeerde radarbeelden heeft een effect op de totale nauwkeurigheid zodanig dat de hoge waarden berekend voor data zonder *speckle* worden bereikt. Het toepassen van P-band polarimetrische data leidt tot een toename in de totale nauwkeurigheid van de classificatie voor alle kaarten. Bijvoorbeeld, de nauwkeurigheid van de bosstructuurkaart (waarin de overstromingscondities en bosstructuren in 15 klassen worden gecombineerd) neemt toe van 76.6%, wanneer alleen C- en L-band polarimetrische data worden gebruikt, tot 86.0%, als tevens P-band polarimetrische data worden gebruikt. Voor dezelfde kaart neemt de classificatienauwkeurigheid toe van 69.7%, wanneer alleen P-band polarimetrische data worden gebruikt, tot respectievelijk 79.5% en 81.8% als L-band of C-band polarimetrische data worden toegevoegd. Het combineren van de informatie van de huidige of toekomstige radarsystemen, zoals RADARSAT-2 of ENVISAT gecombineerd met ALOS PALSAR, maakt het mogelijk om dergelijke kaarten te produceren. Een eventueel beschikbaar P-band SAR systeem zal mogelijkerwijs een verbetering van de nauwkeurigheid opleveren.

De hier ontwikkelde hiërarchische legenda, die is gebaseerd op de mogelijkheden van classificatie met SAR, maakt het aanmaken van minder gedetailleerde kaarten door middel van aggregatie triviaal. De verwachting is dat, als SAR interferometrische data kunnen worden geïntegreerd met de polarimetrische, een legenda gebaseerd op SAR classificatiemogelijkheden zal ontstaan die vergelijkbaar is met die van de landschap-ecologische kaart van het *Araracuara* studiegebied. Interferometrische data kunnen informatie opleveren betreffende de geomorfologie en, aldus, verdere classificatie door opdeling in geomorfologische eenheden..

CURRICULUM VITAE

Marcela Quiñones received her BSc degree in Biology at Los Andes University in Bogotá in 1987. Since 1987, she has been involved mainly in research activities for tropical rain forest conservation and management. For one year she participated in research projects for re-establishment of iguana populations in central Panama, at the Iguana Management Project of the Smithsonian Institute. After that she was involved in research activities in the Amazon basin with the Institute of Natural Resources in Colombia, where she participated on land evaluation of forested land for the design of an international natural park in the Amazon. In 1990 she, together with other two biologists, started a research project in primate ecology and forest fruit production in the Colombian Amazon. Out of that research several publications in refereed journals were made and the final report was awarded with the national prize for sciences of the Alejandro Angel Escobar Foundation, in Bogota in 1993. In 1992 she started working with Remote Sensing and GIS for Forestry Applications and obtained her MSc degree in Remote Sensing in 1995, at the International Institute for Aerospace Survey (ITC), Enschede, The Netherlands. For one year she worked at Los Andes University as an associate researcher of the Ecology Laboratory integrating GIS in to the ecological research. Since 1996 she has been a guest researcher at the sub-department of Water Resources at Wageningen University, where she worked with AirSAR radar data for specific applications in monitoring and conservation of the Amazon region. Her main interest is the development of remote sensing algorithms for accurate data acquisition over tropical forest for management and conservation purposes.

List of publications on the research field.

Quiñones M.J., 1995, Assessment of AirSAR airborne polarimetric data for forested land recognition and tropical forest structure and physiognomic composition analysis, *MSc. Thesis, ITC. Enschede, The Netherlands.*

Hoekman D.H., F. Amar and M.J. Quiñones, 1995, Biomass and structure estimation of primary and secondary tropical rain forest using AirSAR data. *Proc. IGARSS'95 Symp.: Quant. Remote sensing Science Applicat.*, Firenze, Italy, pp.706-707.

Quiñones M.J., 1996, Uso de imágenes de radar AirSAR para el estudio de los bosques tropicales. 1996. In '*Sistemas de Información Geográfica para la Amazonía. El caso Guaviare*'. TROPENBOS, Colombia, Studies in the Colombian Amazon series, Number XIII.

Hoekman D H. and M.J. Quiñones. 1997. Land cover and forest biomass assessment in the Colombian Amazon. *IEEE International Geosceince and Remote Sensing Symposium Proceedings*. 03-08 August 1997, Singapore. pp 1728-1731.

Hoekman D.H. and M.J. Quiñones, 1998. Land cover type and biomass classification using AirSAR data for evaluation of monitoring scenarios in the Colombian Amazon. *Proc. 2nd Intl. Workshop on Retrieval of Bio-and Geophysical Parameters from SAR data for Land Applications*. 21-23 Oct.1998, ESA-ESTEC Noordwijk, The Netherlands. pp.215-223 .

Quiñones M.J. and Hoekman D.H. and, 1998 Forest type classification by airborne SAR in the Colombian Amazon. *Proc. 2nd Intl. Workshop on Retrieval of Bio-and Geophysical Parameters from SAR data for Land Applications*, 21-23 Oct.1998, ESA-ESTEC Noordwijk, The Netherlands. pp 225-231.

Hoekman D.H. and M.J. Quiñones, 1999, P-band SAR for tropical forest mapping and land cover change. *Earth Observation Quarterly*. EOQ N 61. pp 18-22.

Hoekman, D.H. and M.J. Quiñones, 2000, Land cover type and biomass classification using AirSAR data for evaluation of monitoring scenarios in the Colombian Amazon, *IEEE Transactions on Geoscience and Remote Sensing* Vol.38, pp.685-696.

Quiñones M, J. and D. H. Hoekman. 2001. Aplicaciones del radar polarimetrico para monitoreo de bosques tropicales. Estudios en la Amazonia Colombiana, *Internal report in Spanish*, TROPENBOS Colombia.

Hoekman D.H and M. J. Quiñones 2001. Biophysical forest type characterisation in the Colombian Amazon by airborne polarimetric SAR. *Proc. 3rd. International Symposium, 'Retrieval of Bio- and Geophysical parameters from SAR Data for Land Applications'*, Sheffield, UK. 11-14 September 2001 (ESA SP-475, January 2002). pp 19-25.

Quiñones M. J. and D. H. Hoekman, 2002 a, Biomass mapping using biophysical characterization of SAR polarimetric images. *Proc. 3rd. International Symposium, 'Retrieval of Bio- and Geophysical parameters from SAR Data for Land Applications'*, Sheffield, UK. 11-14 September 2001 (ESA SP-475, January 2002). pp 25-33..

Hoekman, D. H. and M. J. Quiñones, 2002, Biophysical forest type characterization in the Colombian Amazon by Airborne polarimetric SAR. *IEEE Transactions on Geoscience and Remote Sensing*, Vol.40, pp.1288-1300.

Quiñones M. J. and D. H. Hoekman, 2002 b, Biomass mapping using biophysical characterization derived from SAR images. Experimental analysis in the Colombian Amazon. Submitted to *IEEE Transactions on Geoscience and Remote Sensing* March 2002

Quiñones M. J. and D. H. Hoekman, 2002 c, Theoretical exploration of physical limits for radar biomass inversion. Submitted to *IEEE Transactions on Geoscience and Remote Sensing*, July 2002.

PUBLICATIONS IN ECOLOGICAL STUDIES

Stevenson, P. R., M. J. Quiñones and J. A. Ahumada, 1991. Relación entre la abundancia de frutos y la dieta de cuatro especies de primates en los bosques del Río Duda, Macarena. *Informe presentado al Banco de la República*. 1991.

Stevenson, P. R., M. J. Quiñones and J. A. Ahumada, 1993, Ecological strategies of the woolly monkey (*Lagothrix lagotrichia*) at Tinigua National Park, Colombia. *American Journal of Primatology* 32:123-140.

Stevenson, P. R., M. J. Quiñones, 1994, Vertical stratification of four new world primates at Tinigua National park, Colombia. *Studies of New World Primates, La Macarena Colombia*. 8:11-18.

Ahumada J., Stevenson, P. R., and M. J. Quiñones. 1997. Ecological response of spider monkeys to temporal variations in fruit abundance: Importance of flooded forest as a keystone habitat. *Primate Conservation. Conservation International- UICN*. 1997

Stevenson, P. R., M. J. Quiñones and J. A. Ahumada, 1998. Annual variation in fruiting patterns using two different methods in a lowland tropical forest Tinigua National Park, Colombia. *Biotropica* (1): 129-134.

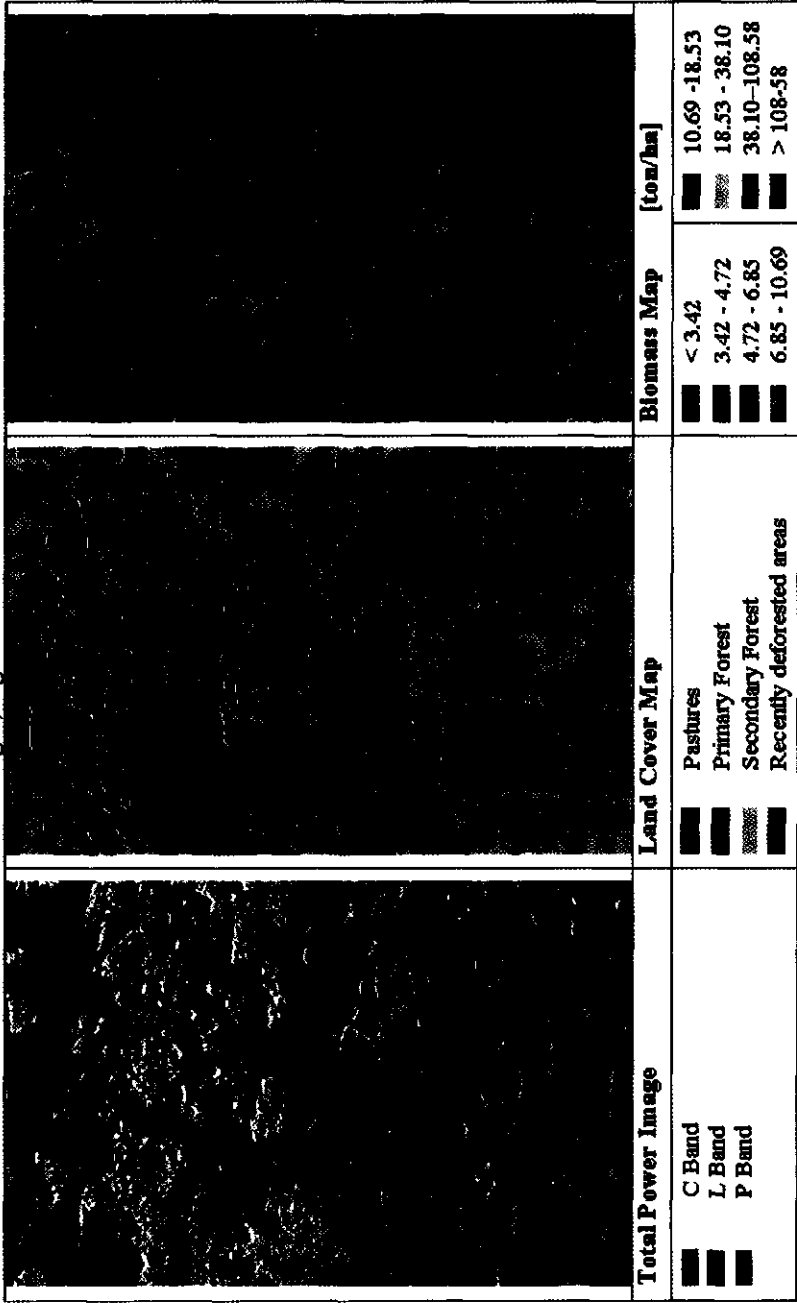
Stevenson, P. R., M. J. Quiñones and J. A. Ahumada, 1999 Effects of fruit patch availability on feeding sub-group size and spatial patterns in four primate species, at Tinigua national park, Colombia. *Int. J. Primatology*. 19 (2):3313-324.

Stevenson, P. R., M. J. Quiñones and J. A. Ahumada, 1999, Influence of Fruit availability on ecological overlap between four Neotropical Primates at Tinigua national park, Colombia. *Biotropica*.

Stevenson, P. R., M. J. Quiñones and M. C. Castellanos, 2000. Guia de frutos de los bosques del Río Duda. . IUCN, *Netherlands Fund and Association para la Defensa de la Macarena*.

1. San José del Guaviare – Colombia.

Detail of Scene 303-1c of the AirSAR images, Figure 2.8 in the text.



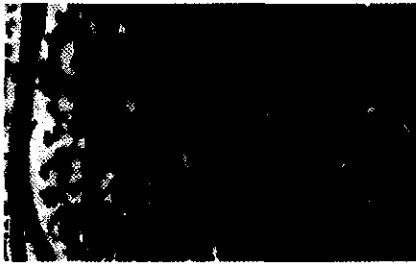
2. San José del Guaviare — Colombia

Mosaic of Land Cover and Biomass Map. 25 x 8 km² classified from 5 AirSAR Scenes. Legends as in plate 1.



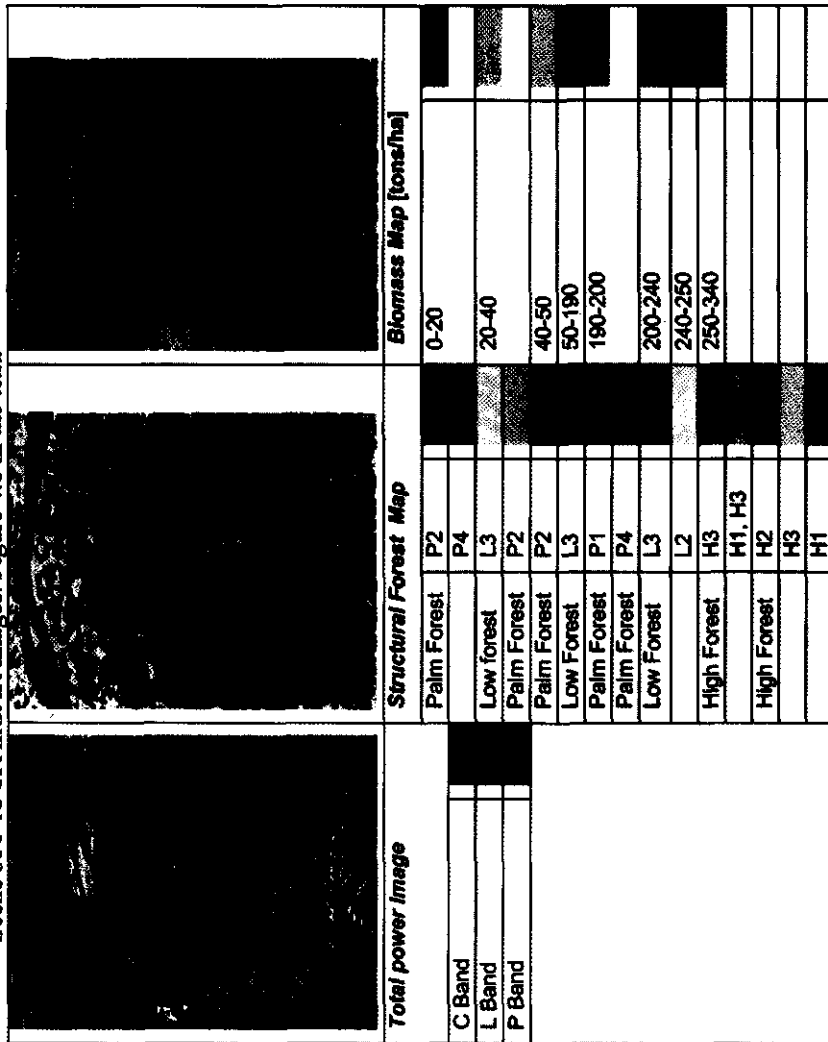
3. Araracuara – Colombia.

Detail of Scene 336-1b of the AirSar images. Figure 3.5 in the text.

				Peat	Palm Forest	P2
				Thin organic deposit	Low forest	P4
				Thin organic deposit and peat	Palm Forest	L3
				Thick H horizon	Palm Forest	P2
				Hydrous and thin organic deposit	Low Forest	L3
				Hydrous organic deposit	Palm Forest	P1
					Palm Forest	P4
					Low Forest	L3
					Low Forest	L2
					High Forest	H3
Sporadically flooded	Thin H horizon	High Forest	H1, H3			
Never flooded	Thin and thick H horizon	High Forest	H2			
			H3			
			H1			

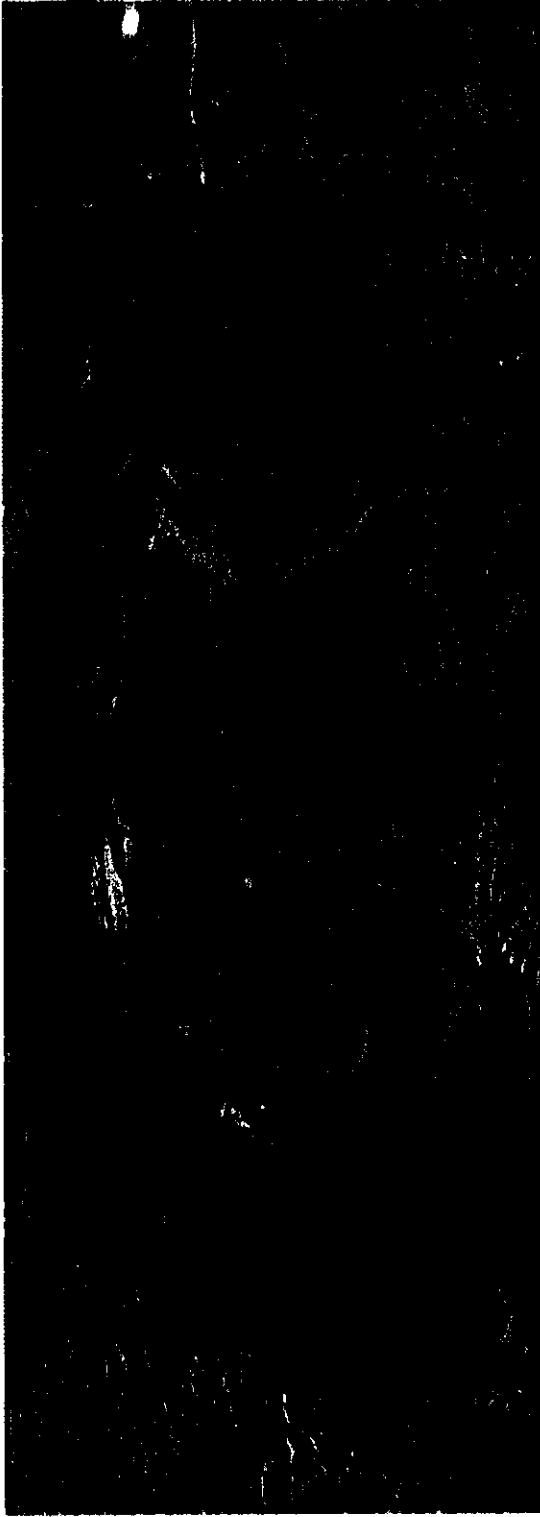
4. Araracuara – Colombia

Scene 336-1b of AirSAR images. Figure 4.6 in the text.



5. Araracuara – Colombia

Total Power mosaic 20 x 8 km² corresponding to 4 AirSAR scenes. C band, L Band and P Band. Figure 6.2-a.



6. Araracuara AirSAR derived maps legend.

Table 6.3 in text. This legend serves the interpretation of plates 7- 11.

SAR derived Maps	Flooding Map		Structural type map	Landscape unit	Forest type Map	N	
2 classes	3 classes		15 classes		8 classes		
Flooded	Permanently flooded or wet	Peat	P2	Palm forest (peat)	P2	36	
			P4		P4	22	
	Thin organic deposit and peat	Low forest (peat)	L3		Tb3, (Eb3)	L3	89
			P2	Palm forest	Cb1	P2	36
		Palm forest (Peat)	P2		Tb1	P2	36
			L3	Low forest	Hp2, Hp3	L3	18
	Thick H horizon	Hydrous and thin organic deposits	P1	Palm forest(flooded)	Ac	P1	10
			P4	Palm forest (flooded)	Eb3	P4	18
			L3	Low forest (flooded)	Eb2	L3	9
	Thin H horizon	Sporadically flooded	L2		Cm2	L2	18
H3			High forest (flooded)	Ce	H3	10	
H2				Ac, Ec		-	
H1, H3				Cc	H1, H2	20	
Non-flooded	Never flooded	Thin and thick H horizon	H2, (or H1, H3)	Ac, Ec	H2, (H1, H3)	114	
			H3	Ce	H3	11	
			H1, (or H3)	Hp1, Tp, Dp, Sv	H1, (H3)	431	

7. Existing Maps for the Araracuara area - Colombia.

Detail corresponding to the Scene 336-1b of the AirSAR images. Table 6.7 in the text.



PRORADAM Radar Image, 1973	Forest Type Map, 1979	Landscape Ecological Map, 1991	AirSAR Polarimetric Radar, 1993	Forest Structural Types Map, 2002
1 : 200,000	1 : 500,000	1:100,000	1:25,000	1:50,000
X-Band	PRORADAM Radar Image as source	Aerial Photos as source	C- L- and P-bands polarimetric	AirSAR radar image as source
	Visual interpretation	Visual interpretation	Total Power Image	Automatic classification
	Geomorphology in interpretation	Geomorphology in interpretation		Geomorphology not included in interpretation
	3 classes in this area	13 classes in this area		8 classes in this area

9. **Flooding map, Araracuara - Colombia**

Mosaic of 4 scenes of AirSAR classified images for flooding conditions. 20 x 8 km² corresponding to 4 AirSAR scenes Figure 6.2-b
Legend on plate 6.



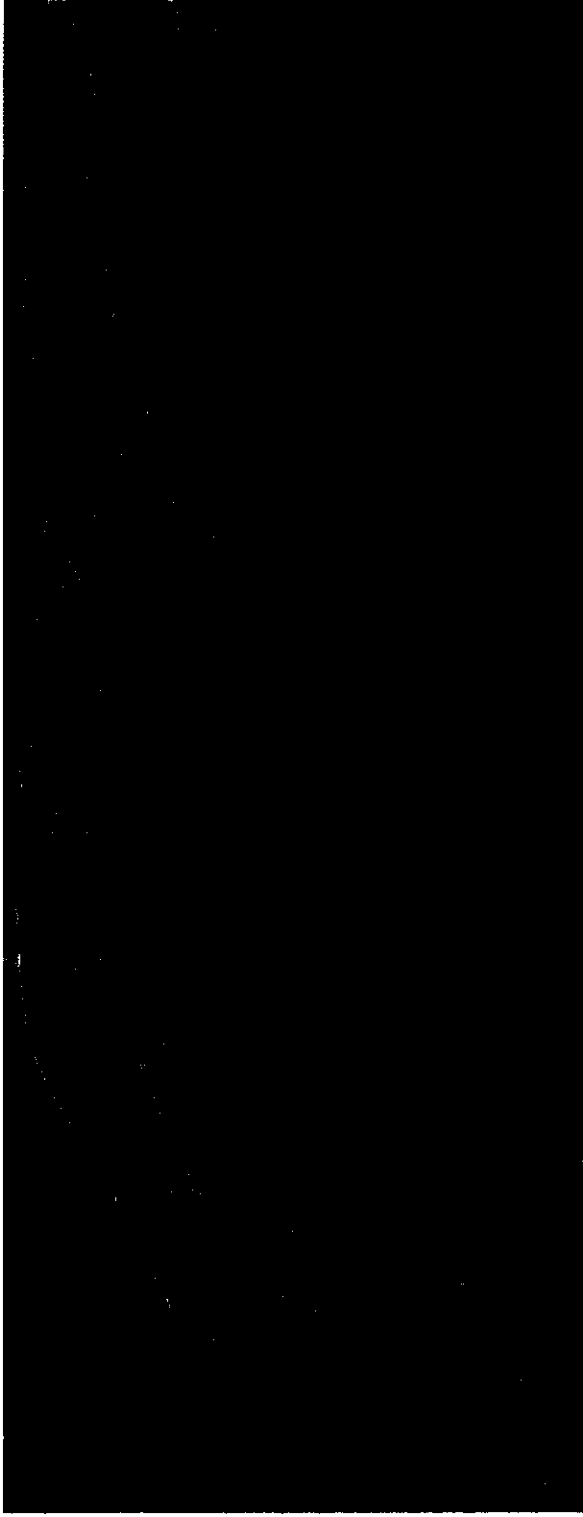
10. Structural type map, Araracuara - Colombia

Mosaic of 4 scenes of AirSAR classified images for structural types. 20 x 8 km² corresponding to 4 AirSAR scenes Figure 6.2-c
Legend on plate 6.



11. Forest type map, Araracuara - Colombia

Mosaic of 4 scenes of AirSAR classified images for forest types. 20 x 8 km² corresponding to 4 AirSAR scenes Figure 6.2-d Legend on plate 6..



12. Biomass map, Araracuara - Colombia

Mosaic of 4 scenes of AirSAR classified images for biomass classes. 20 x 8 km² corresponding to 4 AirSAR scenes Legend on plate

4

